Regulation of Na-K-2Cl cotransport by protein phosphorylation and protein-protein interactions

Karen Louise Hegney
BSc (Hons)

Thesis Submitted for the Degree of Doctor of Philosophy

The University of Edinburgh

2008

Declaration

I, Karen Louise Hegney, candidate for a PhD in Biomedical Sciences, declare that this thesis has been composed solely by me and that the work described is my own, except where indicated, and has not been submitted for any other degree or professional qualification.

Karen Hegney

BSc (Hons)

Acknowledgements

I would like to thank my supervisors, Dr Peter Flatman and Professor Alistair Aitken. In particular, Peter, for providing not only academic support but also a listening ear and encouraging advice.

To my Mum, for encouragement and financial support, both of which were extremely welcome. Thank you for believing that I would always achieve my goals.

To my Dad, though sadly he will not see this thesis, for instilling within me a desire to inquire about the world and a love of learning.

To Jimi, thank you for discussing my ideas with me and for being a constant support throughout all of this. It is so important to me that we can share our lives and our interests together.

To Anke and Jenny, for your company and support in the lab. You guys have been great motivators, especially when checking up on my progress with this thesis.

Last, but not least, to the Medical Research Council, for funding this degree.

Abstract

Na^+-K^+-Cl^- cotransporters (NKCC) are important membrane proteins involved in cell ion homeostasis and cell volume regulation. NKCC mediates electroneutral cotransport of $1Na^+$, $1K^+$ and $2Cl^-$ across cell membranes, followed by osmotically obligated water. The first aim of this thesis was to study the phosphorylation of NKCC found in ferret erythrocytes. Immunoprecipitation and subsequent western blotting using total phosphothreonine antibodies showed low levels of phosphorylation even when cotransport was not stimulated. This was reduced by ~40% when cotransport was inhibited by the use of kinase inhibitors or Mg^{2+} removal. When cells were stimulated by deoxygenation or calyculin A phosphorylation increased 2-3 fold. Although western blot evidence is presented that ferret erythrocytes express SPAK (Ste20-related proline alanine rich protein kinase) and phosphorylated SPAK, use of NKCC-P, an antibody that detects threonine residues on the cotransporter phosphorylated by SPAK/OSR1 (oxidative stress response kinase 1), showed no significant increase in cotransporter phosphorylation in response to deoxygenation. This suggests that SPAK/OSR1 do not phosphorylate the cotransporter in response to this potent cotransport stimulus. A second aim was to isolate the differently phosphorylated forms of NKCC. A proteomic approach was used, including standard 2-dimensional (2-D) gel electrophoresis. Improvements were made in the overall appearance of 2-D gels, but did not result in identification of the cotransporter itself. However, distinct spots were observed on western blots using phospho-specific NKCC antibodies indicating that this method could be of use for studying differentially phosphorylated NKCC proteins. Blue-native PAGE was employed to look at proteins that interact with NKCC. The cotransporter was found

to separate into two major complexes with apparent molecular masses of 250 and 440 kDa. Mass spectrometric methods identified the erythrocyte anion exchanger, Band 3, in complex with NKCC. This was confirmed by co-IP of Band 3 with NKCC, using an NKCC1 specific custom-made antibody. The third aim was to identify different isoforms of NKCC in erythrocytes. Although it has always been assumed that this isoform is NKCC1, evidence to support this has never been published. Using western blot and PCR techniques, this thesis provides evidence to suggest that not only is NKCC1 present in red blood cells, but that NKCC2 is also present. This has implications for the study of cotransport regulation in these cells.

Abbreviations

1-D/1-DE	One-dimensional gel electrophoresis
2-D/2-DE	Two-dimensional gel electrophoresis
AATYK1	Apoptosis-associated tyrosine kinase 1
BN-PAGE	Blue-native polyacrylamide gel electrophoresis
BSC	Bumetanide-sensitive cotransporter
CCC	Cation-coupled chloride cotransporter
CO-IP	Co-immunoprecipitation
ESI	Electrospray ionisation
FBM	Ferret basic medium
HEK-293	Human embryonic kidney cell line
HSP70	Heat shock protein 70 kDa isoform
IEF	Isoelectric focussing
IP	Immunoprecipitation
IPG	Immobilised pH gradient
KCC	K^+-Cl^- cotransporter
LC	Liquid chromatography
MALDI-TOF	Matrix-assisted laser desorption ionisation time-of-flight
MS	Mass spectrometry
MW	Molecular weight
NCC	Na^+-Cl^- cotransporter
NKCC/Na-K-Cl	Na^+-K^+-$2Cl^-$ cotransporter
OSR1	Oxidative stress-response kinase 1
pI	Isoelectric point
PP1	Protein phosphatase 1
PP1i	Src tyrosine kinase inhibitor, PP1
PrxII	Peroxiredoxin-2
RBC	Red blood cell
SDS-PAGE	Sodium dodecyl sulphate polyacrylamide gel electrophoresis
SPAK	Ste20-related proline alanine rich protein kinase
TAL	Thick ascending limb of the loop of Henle
Tm	Transmembrane domain
Y-2-H	Yeast-two-hybrid

Contents

Figures

Tables

Chapter 1

Introduction

Chapter 1 - Introduction

Cell ion homeostasis and the maintenance and regulation of cell volume are processes fundamental to all organisms. Amongst important membrane proteins involved in these processes are the Na^+-K^+-Cl^- cotransporters (NKCC). NKCCs mediate electroneutral cotransport of Na^+, K^+ and Cl^- ions across cell membranes (Geck *et al*, 1980), followed by osmotically obligated water (Haas, 1994). In order for cotransport to occur, all three ions must be present on the same side of the membrane (Russell, 2000). The third defining characteristic of NKCC is that it is bound and inhibited by the "loop" diuretics, which have been useful drugs in the study of the cotransporter. NKCC activity has been found in a wide variety of animal cells, and homologous proteins may also be present in prokaryotic organisms (Park and Saier, 1996). The stoichiometry of ion transport is 1 Na^+, 1 K^+ and 2Cl^- in all known cases, apart from the squid giant axon, which transports 2 Na^+, 1 K^+ and 3Cl^- (Russell, 2000). In mammals, two distinct isoforms of the cotransporter are known. NKCC1 is expressed in nearly all cell types, whereas NKCC2 is found only in the kidney. However, both isoforms share the same basic properties mentioned above. Cotransport via NKCC occurs in response to cell shrinkage, reduced intracellular Cl^- concentration, hormonal stimuli and hypoxia (Lytle, 2003; Haas and Forbush, 2000). How cells respond to such stimuli to produce the resultant Na^+-K^+-Cl^- cotransport, and how this system is regulated, are not well understood and represent important areas of research. This thesis presents evidence that cotransport is regulated in ferret erythrocytes by direct phosphorylation of NKCC and that this is altered in response to physiological and pharmacological stimuli.

1.1 - The Cation-Coupled Chloride Cotransporters

NKCCs are part of a larger family of cation-coupled chloride cotransporters (CCC), members of the solute carrier family 12 (*SLC12*). These proteins couple the movement of Na^+ and Cl^- (with or without K^+) or K^+ and Cl^- ions across cell membranes (Gamba, 2005; Russell, 2000; Mount *et al*, 1998). So far, nine proteins have been designated members of the *SLC12* family (Hebert *et al*, 2004). There are three transporters that move sodium with chloride. These are the Na-Cl (NCC) and Na-K-Cl cotransporters (NKCC1 and NKCC2). There are four K-Cl cotransporters (KCC1-4) and two orphan members, *SLC12*A8 and 9 (Gamba, 2005). *SLC12*A8 (CCC9) is not well understood, but appears to be a candidate gene for psoriasis pathogenesis (Hewett *et al*, 2002). *SLC12*A9 is known as the cation-chloride cotransporter interacting protein (CIP) due to evidence that human CIP (hCIP) is co-immunoprecipitated from cell lysates of HEK-293 cells (transfected with hCIP), with endogenous $hNKCC_{HEK}$. Although when expressed in *Xenopus* oocytes and HEK-293 cells this protein does not transport Na, K or Cl, it does appear to have inhibitory actions on NKCC cotransport (Caron *et al*, 2000). Figure 1.1 shows how these proteins relate to one another on the basis of amino acid sequence with percentage homologies shown between closely related members.

1.2 - Na-K-2Cl Cotransporter Isoforms

With the advent of molecular biology, full length clones of two NKCC isoforms have been isolated from a number of different species and tissues (Gamba, 2005). The proteins are coded for on different genes and the gene products are of different size. Human NKCC1 is coded for on chromosome 5q23.2 and the product is 1212 amino acids in length, whereas human NKCC2 is coded for on 15q15–q21.1 and is 1099

amino acids in length (Russell, 2000). The numbers of amino acids vary from species to species, but NKCC1 is the larger of the two. More detail about each isoform is given in the following sections.

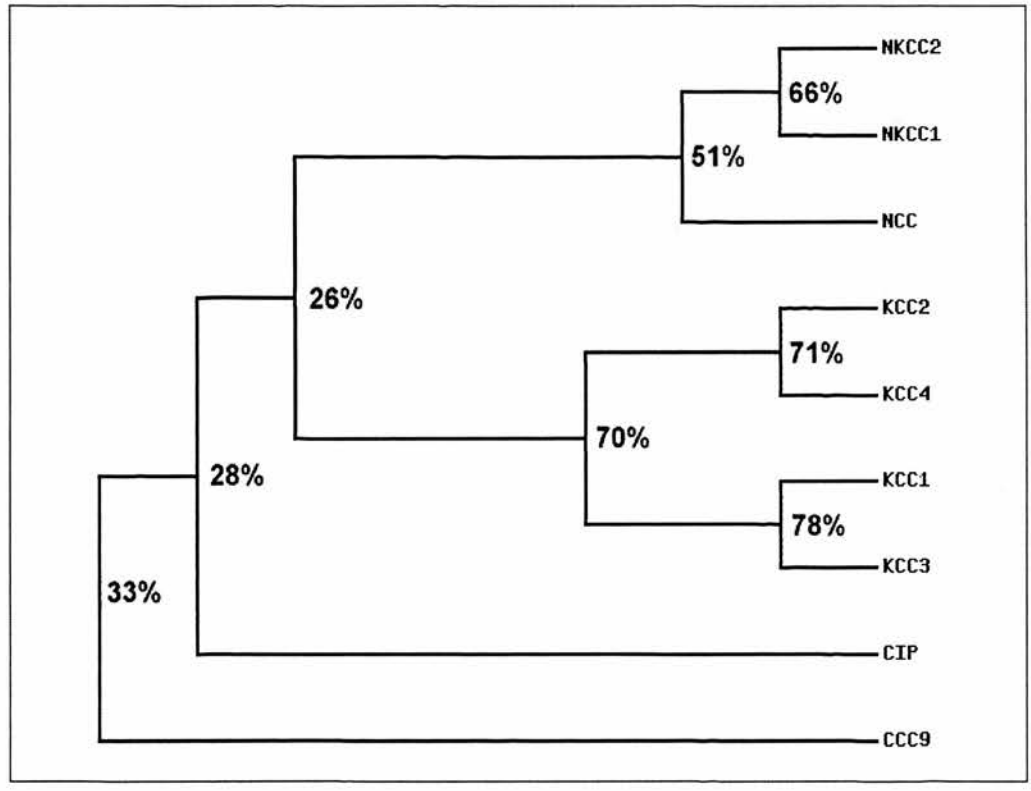

Figure 1.1 – Phylogenetic Tree Diagram of the SLC12 Cation-Chloride Cotransporter Family

All the proteins are human and the following sequences (accession numbers) used: NKCC1 (P55011), NKCC2 (Q13621), NCC (P55017), KCC1 (Q9UP95), KCC2 (Q9H2X9), KCC3 (Q9UHW9), KCC4 (Q9Y666), CCC9 (AAM73657), and CIP (AAF88060). These were aligned based on amino acid sequence identity using the CLUSTALW tool from www.ebi.ac.uk/clustalw/index.html and the resulting alignment used to create a tree diagram. This was achieved using the TreeTop phylogenetic tree prediction tool from www.genebee.msu.su/services/phtree_reduced.html. Sequence homology percentages were obtained from comparison of amino acid sequences in "Blast 2 Sequences" from www.ncbi.nlm.nih.gov/blast/bl2seq/wblast2.cgi.

1.2.1 - NKCC1

NKCC1 (BSC2; *SLC12*A2) is often referred to as the basolateral isoform, as it is present in the basolateral membranes of the cells of secretory tissues (Russell, 2000). This isoform was first cloned from shark rectal gland epithelium (Xu *et al*, 1994). Delpire *et al* (1994), show that this isoform is not solely specific to polarised cells such as secretory epithelia, but is found in non-polarised cells such as myocytes. It is known to be present in a wide variety of tissues and other cell types (Lytle *et al*, 1995; Haas and Forbush III, 1998; Xu *et al*, 1994), and is thought to be the isoform present in red blood cells (Lytle, 1997; Flatman, 1991; Pewitt *et al*, 1990). Due to its wide distribution this isoform has been referred to as the 'housekeeping' isoform, as well as the 'secretory' isoform when in relation to secretory epithelia (Russell, 2000). Two splice isoforms have been identified, in both mouse and human tissues. Randall *et al* (1997), using a PCR approach, found a form of mouse NKCC1 in brain and skeletal muscle, that was shorter than the full-length protein by 16 amino acids. Similarly, Vibat *et al* (2001) found an NKCC1 splice variant in human ocular trabecular meshwork cells that was analogous to the mouse variant. They named these NKCC1a and NKCC1b and upon further investigation it was revealed that these transcripts were present in a variety of human tissues. The most abundant expression of NKCC1a was in salivary gland, whereas NKCC1b was most prevalent in brain tissue. In both cases the NKCC1b form is missing a region within the C-terminus that contains a putative consensus site for phosphorylation by protein kinase A. As such, it has been speculated that these variants may have different affinities for ions or are regulated differently, however, the truth of this is not yet known. Moore-Hoon and Turner (2000) have demonstrated that NKCC1 exists as a

homodimer in the membrane of rat parotid gland cells, forming a complex of approximately 355 kDa. Yeast-2-hybrid (Y-2-H) mapping analysis narrowed the interaction of NKCC1 dimers to regions in the C-terminus (Simard *et al*, 2004a), and these were found to be able to interact within a single NKCC1 molecule. However, it appears from cross-linking studies that the cotransporter exists in an oligomeric state and that these regions are likely to interact with regions in other NKCC molecules rather than be solely self-interacting. Using chimeras, chemical cross-linking and co-immunoprecipitation (co-IP), Parvin *et al* (2007) further investigated the significance of these interactions. Chimeras with alternative C-termini, as well as C-terminal truncation mutants, are unable to form dimers with full-length NKCC1 and the important residues lie within region 751-998 of the rat cotransporter. This work also suggested that NKCC1 did not form heterodimers with NKCC2 or CIP and only a weak interaction was observed with NCC. Simard *et al* (2007) found that NKCC1 forms heterodimers with KCC4. These findings could represent an extra level of regulation to the functioning of the various CCC family members.

1.2.2 - NKCC2

Full-length clones of NKCC2 (or the bumetanide sensitive cotransporter (BSC1); *SLC12*A1) were first identified in rabbit kidney by Payne and Forbush (1994) and in rat kidney by Gamba *et al* (1994) by screening cDNA libraries from these tissues. Both showed Northern blot analyses suggesting that NKCC2 is expressed exclusively in the kidney. Immunocytochemical investigations and immunoelectron microscopy reveal that it is localised in apical membranes in the thick ascending limb (TAL) of the Loop of Henle and macula densa (Nielsen *et al*, 1998). Six main isoforms have been identified, comprising three splice variants combined with two

truncation variants. The splice isoforms are generated by splicing of cassette exons and the products of these events are termed A, B and F isoforms (Payne and Forbush, 1994). Yang *et al* (1996) cloned a variant from rat kidney that has both A and F exons (NKCC2AF), which was localised to the mTAL and Gagnon *et al* (2002) have found a similar situation from shark kidney. They are spatially distributed within the kidney and exhibit different affinities for Na^+, K^+ and Cl^- ions, as measured by their transport characteristics when cDNAs were expressed in *Xenopus* oocytes (Giménez *et al,* 2002). "Long" and "short" isoforms are generated by splicing at a polyadenylation site between exons 16 and 17 (Mount *et al*, 1999), as found in the gene for mouse NKCC2. The truncated "short" isoform loses the last 327 C-terminal amino acids, but ends with 55 amino acids unique to this form only. The functional characteristics of the "long" isoforms have been investigated, by measurement of ^{86}Rb transport under different ion concentrations, bumetanide inhibition and in response to cell swelling, after microinjection of *Xenopus* oocytes with the various murine A, B and F forms (Plata *et al*, 2002). They found that NKCC2-A exhibited the greatest transport capacity, but showed similar ion affinities with the B isoform. The F isoform had the lowest affinities for ions and bumetanide, but was most susceptible to inhibition by cell swelling. This group also found that although the "short" isoforms do not transport ions when expressed in *Xenopus* oocytes, co-injection with the longer forms exerts a dominant negative effect which is reversed by the activation of protein kinase A (Plata *et al*, 1999). The AF isoform does not appear to have cotransport capability (Gagnon *et al*, 2002). Figure 1.2 describes where the main splice variants are distributed within the kidney. The distribution of these different forms coincides with the reduced concentration of transported ions in

the lumen of the TAL and the functional significance of this will be described in section 1.4.2.

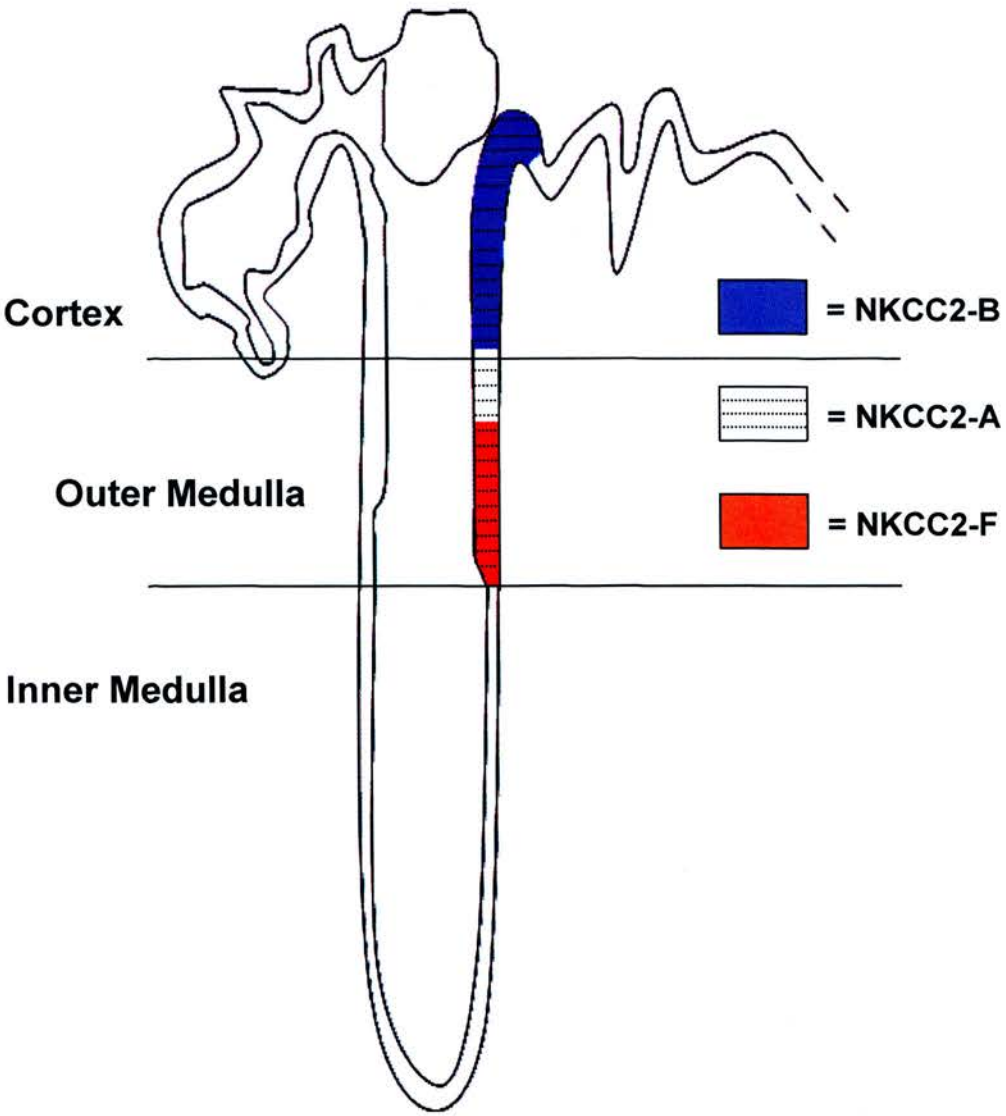

Figure 1.2 – Representation of NKCC2 splice isoform localisation within the kidney
This depicts the positions of the various splice isoforms of NKCC2 (BSC1) along the thick ascending limb of the Loop of Henle. This diagram was created from information sourced from Gamba (2005) and Plata *et al* (2002).

1.3 - Structural features of NKCCs

Based on hydropathy analysis of NKCC protein sequences it has been proposed that they have 12 transmembrane (TM) spanning regions with large cytoplasmic N and C termini (Russell, 2000; Haas, 1994; Xu *et al*, 1994). Park and Saier (1996) formed an average hydropathy plot from seven different animal NKCCs. They agree that a 12 –TM model for NKCC structure is likely, although they show membrane regions 9 and 10 (m9-m10), and 11 and 12 (m11-m12) appearing as one spanning unit each. Using an *in vitro* transcription and translation method (described in figure 1.3), Gerelsaikhan and Turner (2000) have provided experimental evidence that each of the proposed TM sections (from rat NKCC1) insert into canine pancreatic microsomes. They continued this work to look at the membrane insertion of larger sections of NKCC in intact mammalian cells (Gerelsaikhan *et al*, 2006). Again, they conclude that a 12 TM conformation is likely. More recent data from this group (Nagy and Turner, 2007) has shown that membrane domains m11-m12 form a tight hairpin with a very short extracellular linker, which they also suggest is true for m9-m10. They note that these features are generally missed in hydropathy analyses and are likely the reason why these sections are seen as single membrane spanning regions in various hydropathy plots. There are also several pieces of experimental evidence to support the idea that both N and C termini are intracellular. Again, hydropathy analyses suggest that overall these regions are hydrophilic and are therefore likely to be intra or extracellular (Park and Saier, 1996). Payne and Forbush (1995) produced a hypothetical model of human colonic NKCC1 showing that both termini are intracellular. Using antibodies specific to regions in the N and C termini of rat parotid NKCC1, Moore-Hoon and Turner (1998) showed that these

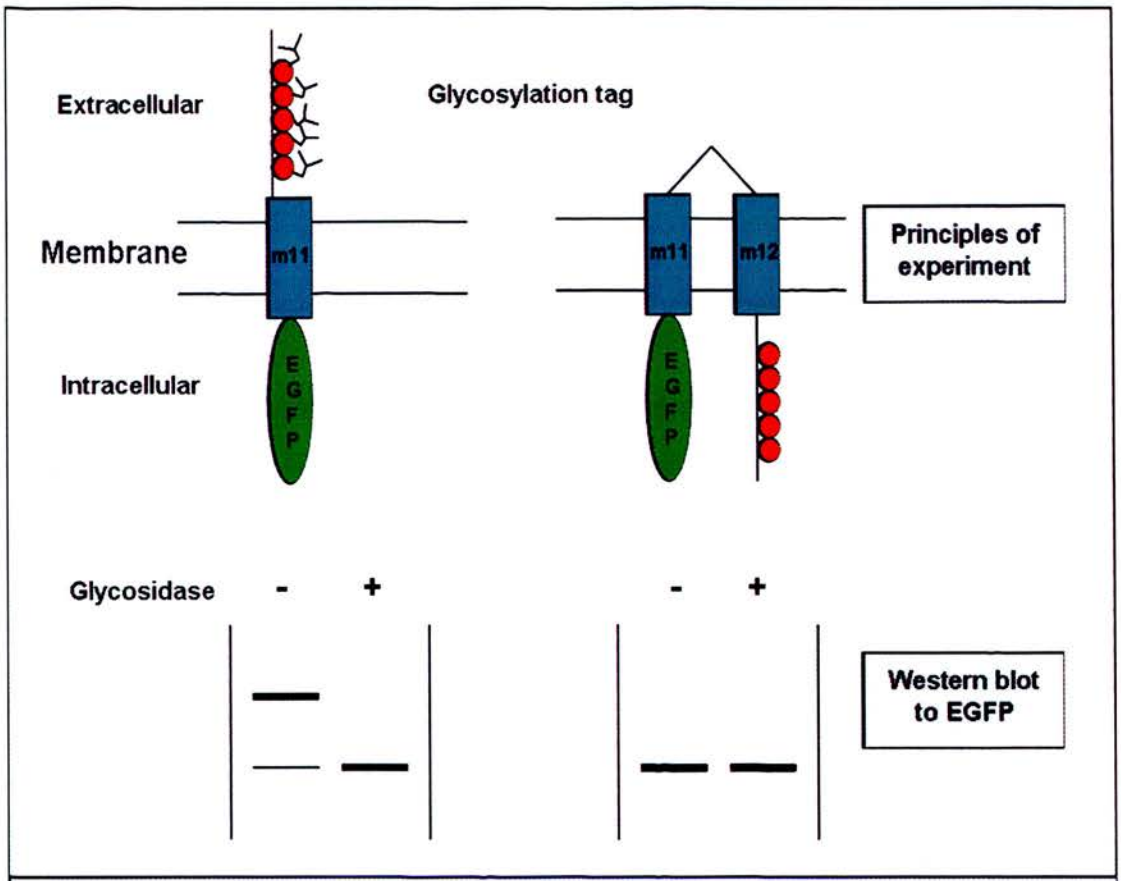

Figure 1.3 – Depiction of experiments that show membrane integration of NKCC Tm domains

Lysed cells or microsomes, that expressed the EGFP-NKCC-Tag fusion protein construct, were subjected to SDS-PAGE and western blotting. The sections of NKCC are coloured in blue and refer to membrane sections 11 and 12. EGFP has a strong signal for position within the cytoplasm. Depending on whether the parts of NKCC expressed as part of the construct span the membrane once or twice determines if the glycosylation tage is present extra- or intracellularly. If it is outside it can be glycosylated and produces a 14 kDa mass shift which is easily detected on western blots. This helps identify orientation of NKCC regions within the cell or membrane. This figure was created from data and ideas presented by Gerelsaikhan and Turner (2000), Gerelsaikhan *et al* (2006) and Nagy and Turner (2007).

antibodies were only detected by confocal immunofluorescence microscopy when the cells studied were permeabilised, suggesting that these regions are indeed intracellular. Both termini have sites for phosphorylation, which again provides evidence for their positions inside the cell (Darman and Forbush, 2002; Lytle, 1997).

The importance of the transmembrane domains to ion transport and bumetanide binding were demonstrated by the construction of chimeras of human and shark NKCC1 (Isenring and Forbush, 1997). These transporters exhibit different affinities for ions and bumetanide. Substitution of N- and/or C-termini in these chimeras, expression in HEK-293 cells and subsequent bumetanide-sensitive ^{86}Rb flux measurements were made. It was found that in all cases (six different chimeras in total) ion and bumetanide affinities corresponded to the species from which the central hydrophobic domain came from. Site-specific mutagenesis of another set of human-shark NKCC1 chimeras in HEK-293 cells implicated transmembrane domain 2 as playing an important role in cation transport (Isenring *et al*, 1998a). Further work by this group, utilising the same approach, gave a more complete map of the domains involved in ion transport and bumetanide binding (Isenring *et al*, 1998b). They found that mutations in transmembrane domains 4 and 7 altered the affinity for chloride ions and that bumetanide binding was altered by mutations in these regions, and others in transmembrane domains 11 and 12. The findings of this study, with relation to bumetanide binding, contradict earlier work suggesting that bumetanide binds at one of the cotransporter Cl sites. Haas and McManus (1983) suggested that their kinetic evidence showed that Cl and bumetanide compete for the same site on the cotransporter. This was based on evidence that higher concentrations of bumetanide were required for half maximal inhibition of cotransport when extracellular chloride concentrations were increased. It seems likely from these studies that the exact mechanisms by which bumetanide inhibits will be more complicated to elucidate. In the absence of crystal structures of the NKCC proteins it may well be far from being understood. The cotransporter has three potential sites

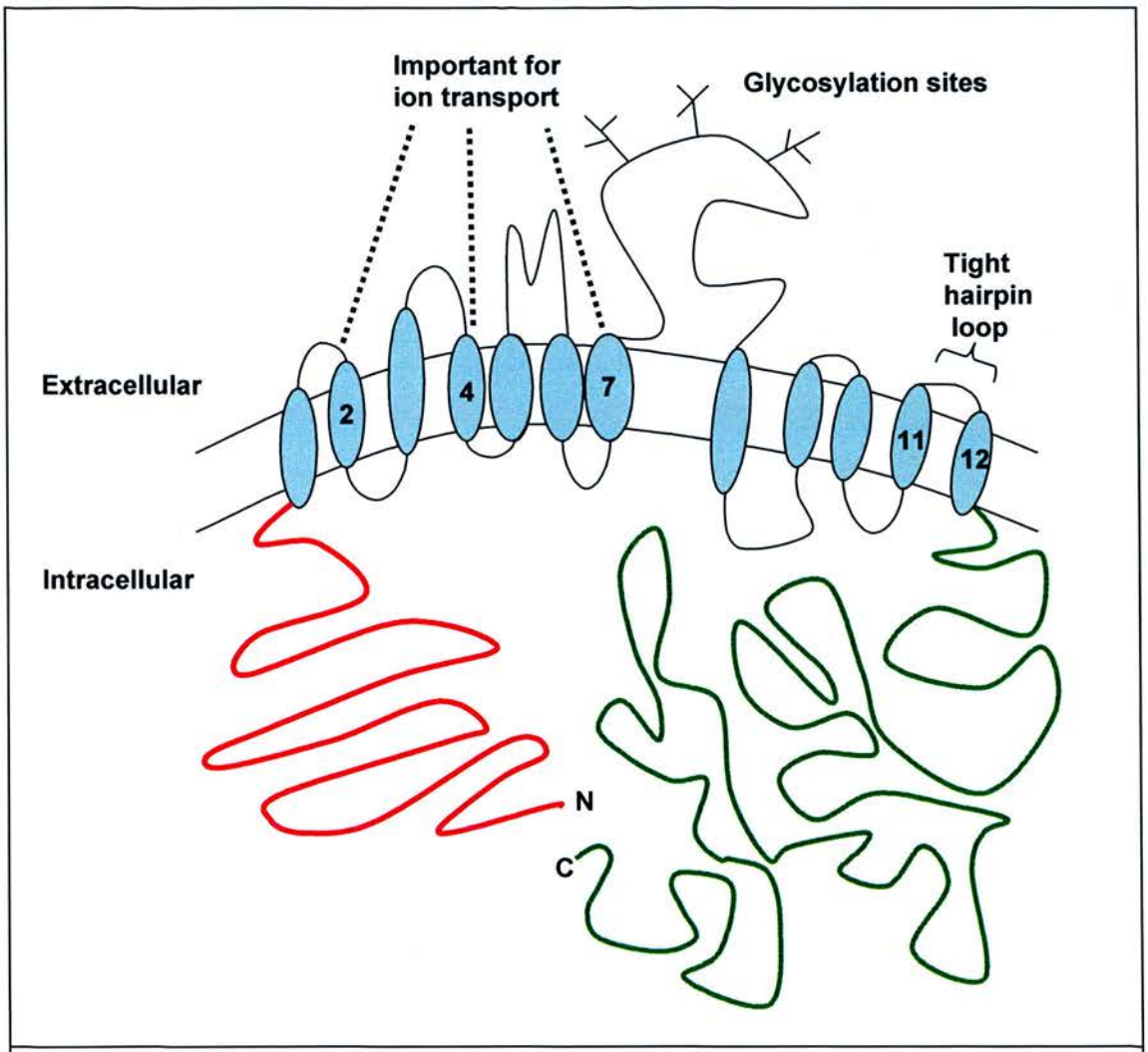

Figure 1.4 – Representation of major structural features of NKCC proteins
This cartoon depicts the major features of NKCCs and was compiled from all of the sources referred to in section 1.3. Transmembrane domains of known importance are numbered.

for N-linked glycosylation within the extracellular loop between transmembrane domains 7 and 8, as suggested by Xu *et al* (1994) during their study of the shark rectal gland cotransporter. The level of glycosylation on the cotransporter is not known, but is likely to vary between tissues and species. This is supported by data presented in this thesis as well as findings in Lytle *et al* (1995) showing that NKCC from different cell types migrate at similar positions on SDS-PAGE after enzymatic

deglycosylation, but not before. It is, as yet, unknown as to the functional significance of these oligosaccharides.

Figure 1.4 depicts a predicted two-dimensional structure of the NKCC protein, with the discussed features shown.

1.4 - Physiological Roles

1.4.1 – NKCC1

NKCC1, as well as the other members of the *SLC12* family, is involved in the regulation of cell volume. The transport of ions allows the cell to make changes to the osmolarity of its contents when exposed to altered extracellular osmolarity. NKCC1 is ubiquitously expressed and is responsible for the movement of ions, and therefore water, into or out of cells. For most cells, the gradients of potassium, sodium and chloride mean that NKCC1 transports ions into cells and as such this isoform is postulated to be a main player in regulatory volume increase (RVI) after cells have lost volume (Russell, 2000). O'Brien *et al* (1988) showed that inhibition of NKCC with the phorbol ester 12-0-tetradecanoylphorbol-13-acetate (TPA) reduced cell volume by 25%, whereas a Na-K-2Cl cotransport deficient mutant cell line showed no cell volume reduction in response to TPA. Prolonged exposure of Ehrlich ascites tumour cells to hypertonic medium results in increased expression of NKCC in the membrane (Jensen and Hoffmann, 1997) and the NKCC activity was increased. Due to the increased NKCC synthesis and membrane insertion an adaptive response to hypertonic media is implied, where NKCC plays an important role in Ehrlich cell maintenance.

NKCC1 also functions to set intracellular Cl^- concentration above electrochemical equilibrium. Some evidence for this comes from observations that dogfish rectal

gland cells exposed to external furosemide (an NKCC inhibitor) are seen to lose Cl^- (Greger *et al*, 1994) and lost intracellular Cl^- could not be recovered in frog dorsal root ganglion cells that were exposed to bumetanide (Alvarez-Leefmans *et al*, 1988). This function of NKCC1 appears to be of particular importance in the developing nervous system. In the mature central nervous system, the response to the neurotransmitter GABA (Gamma-aminobutyric acid) is inhibitory due to influx of chloride resulting in hyperpolarisation of post-synaptic membranes. However, there is high expression of NKCC1 in immature neurons, which causes chloride accumulation in cells. Schomberg *et al* (2003) demonstrate that activation of $GABA_A$ receptors causes Cl^- efflux and reduction of $[Cl^-]_i$ in immature cortical neurons. This Cl^- efflux produces a depolarizing effect and is excitatory. Throughout maturation, K-Cl cotransporters are expressed and NKCC1 levels are reduced giving the conditions for GABA to become inhibitory (Payne *et al*, 2003). However, there is some evidence that GABA still produces depolarising currents in mature sensory neurons. Cl^- accumulation in the dorsal root ganglion neurons is mediated by NKCC1, as knock-out mice show no chloride accumulation in these cells (Sung *et al*, 2000). These mice show an increased pain threshold, consistent with NKCC1 involvement in modulation of sensory input to the spinal cord.

In red blood cells the concentration of cell chloride is determined by the HCO_3^-/Cl^- anion exchanger 1 (Band 3), which is by far the most abundant erythrocyte membrane protein. The nature of the role of NKCC in the erythrocyte is not certain, but they are thermodynamically poised to allow either inward or outward flux depending on the concentrations of Na^+_i and K^+_i/K^+_o (Lytle, 2003). As such, it has

been speculated that red blood cell NKCC may function to buffer changes in plasma potassium.

In secretory epithelia, the NKCC1 isoform is polarised to the basolateral membrane. This provides Cl^- entry to the cell from the interstitium, which is secreted at the apical membrane by other transport proteins. Recycling of Na^+ and K^+ by the Na^+-K^+-ATPase maintains the driving force for the transport of ions via NKCC1 (Gamba, 2005). However, in epithelial cells of the choroid plexus, NKCC1 (and the Na^+-K^+-ATPase) are expressed apically (Praetorius and Nielsen, 2006; Wu *et al*, 1998; Keep *et al*, 1994) where it is proposed to reabsorb K^+ from the cerebrospinal fluid back to the blood. NKCC1-null mice show salivation impairment, growth retardation and reduced intestinal secretions. These result in death due to blockade and bleeding of the caecum and colon (Gamba, 2005). Inner ear dysfunction is evident, with deafness and balance impairement. This is thought to be due to the inability of epithelial cells to uptake K^+ basolaterally for secretion apically into the cochlear chamber (Flagella *et al*, 1999).

NKCC1 also appears to have a role in neurite outgrowth in response to nerve growth factor (NGF). RNAi-knockdown experiments showed that NGF-induced neurite growth of a cell line originating from adrenal medulla was significantly reduced, although the mechanisms underlying the importance of NKCC1 are as yet unknown (Nakajima *et al*, 2007).

NKCC1 has been found to play more of a role in the kidney than previously thought. Plasma renin levels were found to be significantly higher in NKCC-null mice, an effect that is also shown in wild-type mice treated with furosemide (Castrop *et al*, 2005). The NKCC1-deficient mice showed greater recruitment of granular cells to

afferent arterioles of the juxtaglomerular apparatus. Renin release from wild type and NKCC-null juxtaglomerular granule (JG) cells in culture was measured and showed that this was increased in wild type cells upon treatment with furosemide. Basal renin release in NKCC-null JG cells was higher than wild type and was not affected by furosemide. The authors suggest that NKCC1 suppresses basal release of renin and that the higher levels of renin seen upon administration of furosemide are due to NKCC1 inhibition. Also, mouse inner medullary collecting duct cells absorb NH_4^+ from the basolateral surface via NKCC1, a function that may be required for the deposition of NH_4^+ from the collecting duct to the urine (Glanville *et al*, 2001).

1.4.2 – NKCC2

NKCC2 is expressed in the apical membrane of epithelial cells of the TAL in the kidney. Inward absorption of Na^+, K^+ and Cl^- helps to recover water and salts from the glomerular ultrafiltrate resulting in more concentrated urine. As mentioned in section 1.2.2, there are six main forms of NKCC2. The A, B and F isoforms are expressed at different positions within the TAL (see figure 1.2) and are associated with different ion affinities and cotransport capacities (table 1.1 shows the ion binding capacities of these different isoforms). NKCC2F is present in the medullary TAL only where the concentration of transported ions is the highest. Of the three splice isoforms, NKCC2F has the lowest affinity for ions, but was found to be the most sensitive to changes in osmolarity (Plata *et al*, 2002). NKCC2A is found in both cortical and medullary TAL and has the highest capacity for cotransport. It has a higher affinity for ions than NKCC2F, but less than NKCC2B. This splice isoform is found solely in the cortical TAL, where the concentration of ions is lowest. The expression of these isoforms at different positions within the TAL allows for

maximal concentration of urine. As mentioned previously, Gagnon *et al* (2002) found that shark NKCC2AF was a non-functional cotransporter. Co-expression of this form with either A or F in *Xenopus* oocytes showed a reduction of cotransport from expression of A or F alone. This suggests that NKCC2AF can exert a dominant-negative effect on cotransport. This may be through interaction of the different isoforms as suggested by yeast-two-hybrid studies (Brunet *et al*, 2005).

	NKCC2F	NKCC2A	NKCC2B
Na^+	20.6 ± 7.2	5.0 ± 3.9	3.0 ± 0.6
K^+	1.54 ± 0.16	0.96 ± 0.16	0.76 ± 0.07
Cl^-	29.2 ± 2.1	22.2 ± 4.8	11.6 ± 0.7

Table 1.1 – Ion Binding Properties of the A, B and F NKCC2 Splice Isoforms
Data shown here was sourced from Gamba, 2005 and are the K_m values (in mM) from mouse NKCC2.

As well as the A, B and F splicing events, there are those that produce the short (BSC-S) and long (BSC-L) isoforms. Several lines of evidence suggest that the short isoform acts a regulatory molecule in order to modulate the function of the long isoform. In *Xenopus* oocytes, Plata *et al* (1999) show that the BSC-S exerts a dominant-negative effect on cotransport via the long isoform, a function that was halted when cAMP was raised. *In vivo* it appears that this effect is mediated by preventing delivery of the long isoform to the plasma membrane (Meade *et al*, 2003), as demonstrated by fluorescence confocal microscopy. The short isoform, in the mouse, is mostly found in the mTAL and may confer regulation of cotransport in response to cAMP-generating hormones such as vasopressin (Mount *et al*, 1999). The short form also has transporting properties, as shown by expression in *Xenopus* oocytes (Plata *et al*, 2001). The BSC-S is inhibitable by the "loop" diuretic furosemide, but unlike the longer isoform appears to only transport sodium and

chloride. The cotransport was inhibitable by raised cAMP and activated by inhibitors of PKA. Tubules isolated from mouse mTAL showed a shift from Na-Cl to Na-K-Cl cotransport when cAMP was raised after treatment with vasopressin (Sun *et al*, 1991). A model has been proposed for the actions of these forms in the mTAL. During periods of increased extracellular osmolarity or in the presence of vasopressin the long isoform is the predominant form cotransporting Na, K and Cl. However, in the converse situation, BSC-S provides apical Na and Cl cotransport as well as preventing expression of BSC-L at the apical membrane (Plata *et al*, 2002 and 1999).

1.5 - Regulation of cotransport

1.5.1 – Dependence of Cotransport on ATP

The transport of one sodium, one potassium and two chloride ions via the NKCC protein is an example of secondary active transport, where the movement of ions against the electrochemical gradient is coupled to the diffusion of ions down their chemical gradient (Russell, 2000). However, early on it was noted that ATP was required for cotransport of ions. Russell (1976) found that influx of ^{36}Cl into squid giant axons was reduced when the axons were dialysed with ATP-free solutions, a phenomenon which was reversible by repletion of ATP. Further evidence from study of the squid giant axon (Russell 1979) showed that a furosemide-sensitive coupled Na-Cl influx was dependent on the presence of ATP. The dependence of Na-K-Cl cotransport on ATP was described in the seminal paper by Geck *et al* (1980) and was then observed in a number of different species and cell types (Hall and Ellory, ferret erythrocytes (1985); Palfrey and Rao, avian erythrocytes (1983); Rindler *et al*, Madin-Derby Canine Kidney cells (1982)). The focus was then to identify whether ATP was required as an energy source to drive the transport of ions against their

electrochemical gradients, as an allosteric activator of cotransport by altering ion binding affinities, or as a phosphate donor for the phosphorylation of the cotransport protein. Flatman (1988) showed the importance of intracellular Mg^{2+} concentration to cotransport, where reduced internal magnesium slows cotransport rate and vice versa. However, an increase in intracellular Mg^{2+} concentration did not stimulate cotransport rate when cells were depleted of ATP (Flatman, 1991). This evidence implies that ATP and Mg^{2+} work in concert to influence cotransport rate, perhaps as necessary components of kinase activation of the cotransporter. In 1988, Altamirano *et al* conducted experiments to investigate whether the requirement of ATP was in phosphorylation of the protein responsible for cotransport or for driving the cotransport process by ATP hydrolysis. They found that dialysis of squid giant axon with vanadate or fluoride had little effect on Na-K-Cl cotransport. However, the treatments substantially reduced the rate of cotransport inactivation when ATP was depleted from the axon. They suggested that vanadate and fluoride must inhibit a phosphatase that is normally responsible for keeping the cotransporter dephosphorylated and inactive. Pewitt *et al* (1990) studied the effects of kinase inhibitors and the phosphatase inhibitor okadaic acid on cotransport in avian erythrocytes. Stimulation of ^{86}Rb flux by cpt-cAMP (a lipophilic cAMP analogue that activates cAMP-dependent kinases), hypertonicity and NaF was blocked by the kinase inhibitors K-252a and H-9. Also, okadaic acid was found to stimulate cotransport. This study also identified a protein of approximately 150 kDa that bound the photoaffinity probe BSTBA (a bumetanide analogue) and was phosphorylated (by ^{32}P measurement). These studies together gave strong evidence that phosphorylation and dephosphorylation events were important in the regulation

of Na-K-Cl cotransport. The next set of studies furthered these ideas. Palfrey and Pewitt (1993) took another look at the dependence of cotransport on ATP and Mg^{2+}, but from the viewpoint of protein phosphorylation. They tested whether a number of different cotransport activating stimuli were sensitive to ATP depletion by Antimycin A and to intracellular Mg^{2+} removal by the ionophore A23187 and EDTA. To monitor protein phosphorylation they examined ^{32}P changes in the avian erythrocyte membrane protein goblin (which is now thought to be ankyrin). Cotransport stimulated by cAMP was reversed by metabolic depletion, but not when the phosphatase inhibitor calyculin A was the stimulus. Likewise, goblin phosphorylation was reduced when cAMP stimulated cells were depleted of ATP or Mg^{2+}, but not in calyculin A stimulated cells. This work greatly supported the hypothesis that Mg^{2+} and ATP were required as kinase cofactors in the regulation of Na-K-Cl cotransport. Studies of cotransport in the shark rectal gland by Lytle and Forbush (1992) gave direct evidence that the cotransport protein itself was phosphorylated. Using antibodies directed against the shark cotransporter, they were able to immunopurify a 195 kDa protein which showed a 4-fold increase of ^{32}P under conditions of increased cotransport activity. By acid hydrolysis and subsequent thin layer chromatographic separation it was found that the active cotransport protein had increased radioactive phosphothreonine and phosphoserine present. They were able to sequence one of the phosphopeptides by Edman degradation and by relating this back to the shark cotransporter cDNA sequence identified residue Thr^{189} as phosphorylated under conditions of cotransport activation. Although the data for this are unpublished, Lytle and Forbush also claim to have identified Thr^{1114}, in the C-terminus of the cotransporter, as phosphorylated (Xu *et al*, 1994). Evidence from the

avian salt gland showed that this feature was not restricted to the shark rectal gland. A protein of 170 kDa that was detectable using the antibodies raised against shark cotransporter (from the study by Lytle and Forbush) showed increased phosphorylation in response to forskolin and vasoactive intestinal peptide (which can cause cAMP levels to rise and stimulate NKCC activity).

1.5.2 – Phosphorylation of NKCC

Once it became clear that phosphorylation of NKCC proteins was required for activating cotransport activity a great deal of work went into further understanding this process. Many studies showed that cotransport activating stimuli caused increases in cotransporter phosphorylation (Lytle (1997); Haas *et al* (1995); O'Donnell *et al* (1995)). Tanimura *et al* (1995) provided evidence for three phosphorylation sites on the rat parotid Na^+-K^+-Cl^- cotransporter. They digested ^{32}P-labelled pp175 (rat parotid NKCC) with V8 protease from acini treated with or without isoproterenol and separated the resultant peptides by gel electrophoresis. Autoradiography showed three peptides of different size, which were all recognised by a rabbit parotid NKCC antibody. Only one of these peptides showed increased phosphorylation in response to isoproterenol. Study of the cotransporter in the avian erythrocyte by Lytle (1997) showed increased cotransport activity and phosphorylation in response to four different stimuli (cell shrinkage, cAMP, fluoride and calyculin-A). Chemical cleavage (at tryptophan residues by *N*-chlorosuccinimide) of immunoprecipitated ^{32}P-cotransporter resulted in two phosphorylated fragments that were 82 and 41 kDa in size. Only the smaller fragment was recognised by a C-terminal NKCC antibody, indicating some phosphorylation of the cotransporter in this domain. As was found in the shark

cotransporter (Lytle and Forbush, 1992), only phosphothreonine and phosphoserine residues were present on avian erythrocyte NKCC under conditions of increased cotransport activity. Studies of NKCC recovered from shark rectal gland have identified three key threonine residues, in the cytoplasmic N-terminal region, that are phosphorylated when the cotransporter is active (Darman and Forbush, 2002). ^{32}P-labelled NKCC was immunoprecipitated from shark rectal gland tubules, which were treated with forskolin to activate cotransport, and then digested with trypsin. Radiolabelled peptides were separated by high-performance liquid chromatography and then subjected to MALDI-TOF mass spectrometry. Peptides observed to lose phosphate (by measuring peptide masses before and after treatment of samples with alkaline phosphatase) were sequenced by Edman degradation. By comparison with the complete sequence (obtained from cDNA) these residues were identified as Thr^{184}, Thr^{189} and Thr^{202}. Point mutants of these were expressed in HEK-293 cells and led to the discovery of several interesting features. Firstly, Thr^{189} phosphorylation is an absolute requirement for shark NKCC cotransport activity in response to low intracellular Cl^-. Secondly, Thr^{184} and Thr^{202} appeared to modulate this activity by increasing the rate of cotransport and the sensitivity to changes of Cl^- concentration and cell volume. Importantly, these residues are conserved among NKCC1, NKCC2 and NCC from a variety of species. The importance of these threonines has been demonstrated *in vivo* by Flemmer *et al* (2002), using immunofluorescent microscopy and an antibody raised to a diphosphorylated peptide from human NKCC1 (containing Thr^{212} and Thr^{217} which correspond to Thr^{184} and Thr^{189} from shark NKCC). This antibody (dubbed R5) was able to detect rises in cotransporter phosphorylation with cotransport activity and showed NKCC

phosphorylation in sections from shark rectal gland, rat colon, parotid gland and trachea. They are also phosphorylated on the actively transporting NKCC2 isoform (Giménez and Forbush, 2003). These three threonine residues are well conserved between NKCC1 and NKCC2 and also between different species, and as such it has been suggested that this cluster of threonines represent a universal regulatory locus for the activation of NKCC (Giménez and Forbush, 2003; Darman and Forbush, 2002). However, there may be other threonine or serine residues whose phosphorylation could modulate cotransporter function. Indeed, Lytle showed (by measurement of stoichiometry of ^{32}P incorporation) that activation of NKCC in duck erythrocytes causes the cotransporter to be phosphorylated at five sites within the N- and C-termini (Lytle, 1997). Although the discovery of the three threonine residues within the N-terminus was a great leap forward in understanding cotransport regulation, their identification did not implicate a cotransporter kinase, as they do not lie within consensus sites for any known kinases.

1.5.3 – Kinases and Phosphatases

A great many studies, involving the use of phosphatase and kinase inhibitors, have provided complementary evidence to show that in order to activate cotransport the protein must be phosphorylated and then dephosphorylated to inhibit cotransport. These studies have also suggested that such phosphorylation events may involve different kinases activated in response to differing stimuli. The main kinases and phosphatases that have been studied with reference to NKCC regulation are discussed here as well as some of the difficulties involved in using inhibitors to infer function of a particular kinase or phosphatase.

1.5.3.1 – Protein Kinase A and Protein Kinase C

Once the NKCC1 protein had been sequenced it became evident that it possessed consensus sites for phosphorylation by protein kinase A (PKA) and protein kinase C (PKC), as well as sites for casein kinase II (Russell, 2000). As yet, there is little evidence to suggest an involvement of casein kinase II, but there is to implicate PKA and PKC. PKA is known as cAMP-dependent kinase as it requires binding of the cyclic nucleotide in order for the catalytic subunits of the kinase to dissociate from the regulatory subunits and become active. Indeed, cAMP-generating agonists cause upregulation of NKCC cotransport in some cell types, including the avian erythrocyte (Lytle, 1997; Palfrey *et al*, 1980), avian salt gland cells (Torchia *et al*, 1992) and human colon adenocarcinoma HT29 cells (Turner *et* al, 1990). Interestingly, shark rectal gland cell NKCC activity is also stimulated by raised cellular cAMP even though this cotransporter does not contain the known PKA consensus phosphorylation site (Xu *et al*, 1994; Palfrey *et al*, 1984). The effects of PKA and cAMP on NKCC activity are also inhibitory in a great many cell types. In mature skeletal muscle inhibition of the cAMP-dependent protein kinase A (PKA) pathway stimulates NKCC activity during hyperosmotic challenge (Gosmanov and Thomason, 2003). They also found that in cultured rat skeletal muscle (L6) and intestinal epithelial (IEC-6) cells cotransport by NKCC was inhibited by isoproterenol and forskolin (cAMP-elevating substances). Direct inhibition of PKA (by H-89) produced an increase in NKCC activity. The inhibitory actions of cAMP-elevating substances have also been observed in cultured endothelial smooth muscle cells (Smith and Smith, 1987) and human fibroblasts (Owen and Prastein, 1985). Overall, it appears that the response to cAMP and the involvement of PKA in NKCC activation is cell specific and may be more likely due to the actions of these factors

on other cell transport systems and the resultant changes in cell ion levels (e.g. Cl^-). Indeed, evidence has been presented from giant squid axon (Breitwieser *et al*, 1990), shark rectal gland and canine tracheal epithelial cells (Lytle and Forbush, 1996; Haas *et al*, 1995) that low intracellular Cl^- concentration can stimulate cotransport in the absence of any other stimulus.

PKC is a serine/threonine protein kinase that can stimulate or inhibit NKCC activity depending on the cell type examined. For example, NKCC cotransport is inhibited in human pigmented ciliary epithelial cells by the PKC activator phorbol 12-myristate, 13-acetate (PMA) (Layne *et al*, 2001). In human tracheal epithelial cells shrinkage induced NKCC activation is dependent on the actions of PKC-δ (Liedtke and Cole, 2002) and elevated activity of this PKC isoform has been shown to stimulate NKCC1 activity in human airway epithelial cells (Liedtke *et al*, 2003). Like the situation for PKA, no direct phosphorylation of NKCC by PKC has yet been determined.

1.5.3.2 - Myosin Light Chain Kinase

Cell shrinkage induces raised activity of Na-K-Cl cotransport. O'Neill and Klein (1992) found that hypertonic cell shrinkage increased the bumetanide-sensitive influx of Na, K and Cl into bovine aortic endothelial cells, producing recovery of cell ion and water content. Myosin light chain (MLC) was identified as a protein that was phosphorylated in shrunken aortic endothelial cells by Klein and O' Neill (1995), which was reversed by cell swelling. ML-7, an inhibitor of myosin light chain kinase (MLCK), was found to prevent MLC phosphorylation and was able to reduce cotransport in shrunken cells. Krarup *et al* (1998) also found that inhibition of myosin light chain kinase by ML-7 resulted in reduced cotransport in response to hypertonic stimulation in Ehrlich cells. The ML-7-sensitive cotransport was 2-fold

greater during regulatory volume increase (RVI) than after stimulation of cotransport by treatment with calyculin A, suggesting a possible role for MLCK as a modulator of NKCC cotransport in response to cell shrinkage. Rho kinase plays a role in hypertonic MLC phosphorylation, and its activity is enhanced in response to cell shrinkage (Di Ciano-Oliveira *et al*, 2003). Inhibition of this kinase did not affect ^{86}Rb uptake under isosmotic conditions and only reduced hyperosmotic stimulation by around 10% in porcine aortic endothelial cells and kidney tubular epithelial cells, whereas, as shown previously, the MLCK inhibitor ML-7 reduced isosmotic activity and almost completely inhibited NKCC activation. However, recent data suggest that while ML-7 does inhibit Na-K-Cl cotransport, this is not via inhibition of MLCK and is not dependent on the phosphorylation of myosin light chain (Di Ciano-Oliveira *et al*, 2005). Another inhibitor of MLCK, K-252a, prevented the increase of MLCK phosphorylation seen on hypertonic stimulation. Whilst cotransport by hypertonic stimulation was reduced by 36%, K-252a did not prevent cotransport induced by Cl^- depletion. Flatman and Creanor (1999a) found that high concentrations of K-252a had only a modest effect on cotransport in ferret erythrocytes, reducing cotransport rate by around 20%. Expression of a non-phosphorylatable form of myosin light chain (MLC) in porcine kidney tubular LLC-PK1 cells exerted a dominant-negative effect on endogenous MLC phosphorylation. This mutant suppressed hyperosmotically induced phosphorylation of MLC, but did not prevent cotransport via NKCC. Also, a constitutively active MLC mutant was not itself an activator of cotransport in LLC-PK1 cells. These data suggest that MLC phosphorylation is neither required nor sufficient for the activation of Na-K-Cl cotransport in response to hypertonic stimulation (Di Ciano-Oliveira *et al*, 2005).

This group concluded that myosin ATPase activity was important after studying the effects of blebbistatin (inhibitor of myosin II ATPase) on hypertonic and Cl^- depletion-induced stimulation of Na-K-Cl cotransport. This inhibitor only affected hypertonic stimulation of cotransport. It has since been found that myosin II-depleted cytoplasts (plasma membrane vesicles) from Ehrlich ascites cells are insensitive to stimulation of NKCC by cell shrinkage, whilst still being responsive to stimulation of cotransport by calyculin A (Hoffmann and Pedersen, 2007). These data together suggest that MLCK could affect myosin ATPase activity independent of MLC phosphorylation in response to cell shrinkage and that these steps are important in activation of Na-K-Cl cotransport under hypertonic conditions.

1.5.3.3 – Stress-Activated and Mitogen-Activated Protein Kinases

The stress-activated protein kinases (SAPK) and mitogen-activated protein kinases (MAPK) are serine/threonine kinases that are activated in response to cellular stresses and extracellular mitogens. These kinases are structurally similar but are functionally distinct, resulting in downstream activation of different targets (Tibbles and Woodgett, 1999). There is evidence to suggest involvement of both kinase sets in NKCC regulation. Studying the effects of arsenite (an activator of SAPKs) in ferret red blood cells, Flatman and Creanor (1999b) found that it produced a large stimulation of cotransport. In combination with the phosphatase inhibitor calyculin A, which stimulates NKCC activity, the level of cotransport was higher than when either treatment was used alone and that this stimulation was prevented by prior removal of cell Mg^{2+}. The additive effects of these compounds indicated that there may be different pathways involved in this activation of cotransport in ferret erythrocytes. This study showed, however, only a very small decrease in cotransport

when inhibitors of p38 MAPK and p42/p44 MAPK (ERK) were applied (SB203580 and PD98059 respectively) and a general activator (anisomycin) of MAPKs and SAPKs had a mild but inhibitory effect on cotransport. Klein *et al* (1999) presented evidence using an in-gel kinase assay that stress-activated c-Jun NH_2-terminal kinase (JNK) was responsible for NKCC phosphorylation in shrunken aortic endothelial cells, but there is little other evidence to implicate this kinase *in vivo*. Other studies, however, show greater effects of MAPK inhibition on cotransport. Pre-treatment with PD98059 prevented stimulation of cotransport in skeletal muscle (Wong *et al*, 2001). The more potent MEK 1/2 inhibitor U-0126 completely abolished all cotransport in response to an activating stimulus. NKCC activity was found to be increased in rat skeletal muscle after exercise and that this activity was associated with an increase in ERK phosphorylation (Gosmanov *et al*, 2002). Phenylephrine induced α_1-adrenoceptor activation has been shown to increase NKCC activity in isolated rat cardiomyocytes and that this activation is linked to ERK-dependent phosphorylation of the cotransporter (Andersen *et al*, 2004). PD98059 was found to eliminate the NKCC response to phenylephrine.

1.5.3.4 – Tyrosine Kinases

Although it has been shown that the cotransporter is not phosphorylated on tyrosine, Flatman and Creanor (1999a) found that genistein, an inhibitor of tyrosine kinases, caused a 60% reduction of ^{86}Rb uptake in ferret erythrocytes. Likewise, the potent Src family tyrosine kinase inhibitor, PP1 (PP1i; 4-amino-5-(4-methylphenyl)-7-(*t*-butyl)pyrazolo[3,4-d]pyrimidine) reduced cotransport. Genistein inhibits the response of NKCC to hyperosmotic stress in L6 rat skeletal muscle cells, but isolated cotransporter under these conditions shows no tyrosine phosphorylation (Zhao *et al*,

2004). These data imply the involvement of tyrosine kinases at some stage of the activation of cotransport. However, a recent examination of a wide range of kinase inhibitors shows that what were once thought to be very selective inhibitors may not actually be so. Indeed, although more selective than many inhibitors, PP1i has been shown to inhibit some serine/threonine kinases (Bain *et al*, 2007; Bain *et al*, 2003). Whilst these studies have provided some insight into the proteins involved in regulating cotransporter function they do also highlight the difficulties when using inhibitors. Recent studies by Bain *et al* (2007 and 2003) have shown that many of the commonly used small-molecule inhibitors are far less specific than previously thought. For example, 20 μM ML7, used in the studies linked to MLCK, also inhibits mitogen- and stress-activated protein kinase 1 (MSK) by 50% *in vitro* (Bain *et al*, 2003). SB 203580, widely used to inhibit p38 MAPKs, inhibits other kinases with similar potency, such as casein kinase I. At a 1 μM concentration, SB 203580 inhibits p38 MAPK activity by about 90%, but was found to inhibit receptor-interacting protein 2 (RIP) kinase with even greater potency (Bain *et al*, 2007). Although these inhibitors can imply or rule out the activity of a particular kinase in cotransporter regulation users should be aware that any observed effects may result from inhibition of several targets, which complicates any findings.

1.5.3.5 – Serine/Threonine Protein Phosphatases

Calyculin A and okadaic acid are serine/threonine protein phosphatase inhibitors that inhibit PP1 and PP2A (Resjö *et al*, 1999; Ishihara *et al*, 1989). Okadaic acid is more specific at inhibiting PP2A, whereas calyculin A affects both phosphatases similarly. Both okadaic acid (Pewitt *et al*, 1990) and calyculin A (Palfrey and Pewitt, 1993) were stimulators of Na-K-Cl cotransport in duck red blood cells. Darman *et al*

(2001) showed that NKCC1 possesses a motif in its N-terminus that is a binding site for PP1 (RVxFxD), which when mutated caused changes to the activation of the cotransporter by intracellular Cl^- concentration. Microcystin binds very strongly to PP1 and has been used to isolate this phosphatase by affinity chromatography (Moorhead *et al*, 1995). Microcystin-conjugated beads have been used to co-precipitate PP1 and NKCC1 from HEK-293 cells (an action that was inhibited by pre-incubation of samples with free microcystin) indicating that the phosphatase interacts with the cotransporter. Matskevich *et al* (2005), using the same approach, showed that the greater the amount of phosphorylation on NKCC the more cotransporter was co-precipitated with PP1. However, Y-2-H experiments do not provide evidence that NKCC1 and PP1 directly interact (Gagnon *et al*, 2007b). Although false negatives are not unusual in Y-2-H, this issue requires further investigation. PP2A has been immunoprecipitated with NKCC1 from an airway epithelial cell line (Calu-3) and treatment of these cells with okadaic acid produced around 4-fold increases in flux via the cotransporter (Liedtke *et al*, 2005). Calyculin A did not produce any alteration to cotransport in these cells. Like the various kinases, it would appear that phosphatase activity may be cell type specific.

1.5.3.6 – SPAK, OSR1 and WNKs

The greatest leap forward in understanding Na-K-Cl cotransport regulation came with the discovery that the stress-related serine/threonine kinases, Ste20-related proline-alanine rich kinase (SPAK) and oxidative-stress response 1 (OSR1), interacted with the NKCCs. Y-2-H assays identified these proteins and their interactions with the NKCCs were confirmed by GST pull-down and co-immunoprecipitation experiments (Piechotta *et al*, 2002). SPAK and OSR1 are

similar in structure with the highest amino acid identity within the catalytic domain. The SPAK/OSR1 binding motif on the cotransporters was identified as (R/K)Fx(V/I) followed by a further five residues which show no clear consensus but without which the kinase did not bind in Y-2-H assays. In choroid plexus cells, both SPAK and NKCC1 localise to apical membranes, whereas in salivary gland cells both proteins were found to localise to basolateral membranes, as indicated by immunohistochemistry (Piechotta *et al*, 2002). Further work by this group found that expression of NKCC1 with point mutations within or deletions of one or both SPAK/OSR1 binding motifs (RFxV) in *Xenopus* oocytes did not affect $^{86}Rb^{+}$ uptake in response to hypertonicity and low $[Cl^{-}]_i$ and the authors therefore suggested another role for the SPAK/OSR1 interaction other than modulation of cotransporter function via direct phosphorylation (Piechotta *et al*, 2003). From these data it was inferred that SPAK may function as a scaffold to allow NKCC to interact with other proteins. On the other hand, Dowd and Forbush (2003) show that overexpression of a kinase-inactive dominant-negative SPAK mutant (referred to as PASK in this paper) caused dramatic inhibition of human and shark NKCC1 activity expressed in HEK-293 cells. A reduction of phosphorylation of Thr^{184} and Thr^{189} was also observed on western blots using the R5 antibody. Some of these issues were resolved with the discovery that SPAK and OSR1 require activation by other kinases before they themselves can activate the cotransporter. It was discovered that people with Gordon's syndrome (also known as Pseudohypoaldosteronism type II - a disease characterised by high blood pressure and hyperkalaemia) had mutations in genes that code for with-no-lysine kinases (WNK, K = lysine), in particular WNK1 and WNK4 (Wilson *et al*, 2001). These are large serine/threonine kinases without a

lysine within subdomain II of the enzyme, which is considered vital for the binding of ATP and catalysis in protein kinases. However, another lysine is located within subdomain I and when mutated in WNK1 rendered the enzyme inactive (Xu *et al*, 2000). There are four known WNK isoforms (1-4) and are coded for on different genes (Verissimo and Jordan, 2001). Piechotta *et al* (2003) showed that WNK4 interacted with SPAK. Vitari *et al* (2005) rationalised that these may be involved in cell ion regulation due to the nature of the symptoms of Gordon's syndrome and using anti-WNK1 antibodies for co-IP experiments, followed by protein identification with mass spectrometry, identified SPAK as an interacting protein. WNK1 and WNK4 (overexpressed N-termini in HEK-293 cells and *E. coli*) were able to phosphorylate SPAK and OSR1, whereas catalytically inactive mutants were not. This group also demonstrated that expression of WNK1/4, SPAK or OSR1 and the N-terminus of NKCC1 in *E. coli* led to phosphorylation of the NKCC molecule, whereas expression of these proteins individually (or kinase mutants) did not. Moriguchi *et al* (2005) demonstrated by Y-2-H assays and immunoprecipitation that SPAK could bind to WNK1. *In vitro* kinase assays showed that WNK1 was a direct activator of SPAK and OSR1 and that this was by phosphorylation of the kinases, as kinase dead WNK1 was ineffective at activating SPAK or OSR1. Gagnon *et al* (2006a) provided further evidence that WNKs are involved in the activation of SPAK and OSR1. Co-injection of OSR1 with WNK4 into *Xenopus* oocytes resulted in increased cotransport via NKCC1, whereas injection of OSR1 alone produced no significant change. By measurement of ^{32}P incorporation onto SPAK and the N-terminal of NKCC1 in the presence of different pharmacological agents several other features of were highlighted. K-252a and staurosporine both resulted in reduced

phosphorylation on NKCC1 and SPAK, whereas NEM and diamide had little effect. Arsenite had very little effect on phosphorylation even though this causes great NKCC cotransport in the ferret erythrocyte (Flatman and Creanor, 1999b). SPAK was also shown to be sensitive to changes in Cl^- concentration, where a reduction of cell Cl^- resulted in more autophosphorylation on SPAK. Further *Xenopus* oocyte co-injection experiments (Gagnon *et al*, 2006b) reinforced the fact that for NKCC activation, the presence of catalytically active WNK and SPAK are required. Y-2-H experiments showed that WNK4 and NKCC1 did not physically interact, placing SPAK as an intermediate between the WNK kinase and NKCC1. How these proteins interact with one another was investigated by Vitari *et al* (2006). *In vitro* kinase assays, where active SPAK or OSR1 were combined with an N-terminal fragment of NKCC1 (residues 1-260 from the shark protein), were conducted to determine which residues on the cotransporter were phosphorylated by the kinases. Trypsin digestion followed by liquid chromatography isolated those peptides that had ^{32}P incorporated. Edman sequencing identified a doubly phosphorylated peptide and a singly phosphorylated peptide, indicating phosphorylation on Thr^{175}, Thr^{179} and Thr^{184} (which correspond to threonines 203, 207 and 212 on human NKCC1 and 197, 201 and 206 on mouse NKCC1). Anselmo *et al* (2006) found that knock-down of WNK1 or OSR1 (with inhibitory RNA) in HeLa cells substantially reduced NKCC activity in sorbitol treated cells, as well as basal NKCC cotransport. They also found that OSR1 did not catalyse the incorporation of phosphate onto WNK1, but that WNK1 did phosphorylate OSR1 *in vitro*. These data again place the WNKs upstream of SPAK/OSR1. This group also demonstrated that after activation with WNK1, OSR1 could phosphorylate the N-terminus of NKCC2. Zagórska *et al*

(2007) found that WNK1 isolated from cells exposed to hyperosmotic stress would phosphorylate OSR1 more than kinase isolated from untreated cells and that this stimulation was dose dependent on the concentration of sorbitol, NaCl or KCl. Other stimuli, including calyculin A, failed to induce the activation of WNK1. Sorbitol treatment also increased phosphorylation of other residues including WNK1 on Ser^{382}, which results in activation of the kinase. Phosphorylation of the kinase on Ser^{1261}, adjacent to the SPAK binding domain, prevented its interaction with SPAK or OSR1. Using the same approach as Anselmo *et al* (2006), this group furthered the work of siRNA of WNK1 in HeLa cells. They found that the phosphorylation that is normally found on SPAK and OSR1 upon treatment with sorbitol was markedly reduced. They also observed that GFP-WNK1 had a striking relocalisation within HEK-293 cells upon stimulation with sorbitol. Normally, it was dispersed throughout the cytoplasm, but after treatment relocated to discrete intracellular structures which contained clathrin, the transcription factor AP-1 and TGN46 (a protein thought to regulate membrane traffic to and from the trans-Golgi network).

As mentioned, five sites for phosphorylation have been mapped in the N-terminus of NKCC1. These are threonines 175, 179, 184, 189 and 202 (Darman and Forbush, 2002; Vitari *et al*, 2006). These correspond to 197, 201, 206, 211 and 224 on mouse NKCC1 and each was mutated in turn in NKCC1 constructs. These were expressed in *Xenopus* oocytes and the functional consequence of each mutation assessed (Gagnon *et al*, 2007a). *In vitro* phosphorylation assays were conducted using wild-type SPAK with each NKCC1 mutant. Mutation of Thr^{197} or Thr^{206} resulted in 33% less phosphorylation on NKCC, with 66% less on the double mutant. Mutation of Thr^{201} had no effect on NKCC phosphorylation, but in combination with Thr^{197} and

Thr^{206}, ^{32}P incorporation into NKCC was reduced by 95% in comparison to wild type. Expression of NKCC1 with T206A or T211A mutations in *Xenopus* oocytes resulted in cotransporter that was non-functional. This study also investigated whether or not SPAK binding to NKCC was required for activation of cotransport, which follows on from their earlier work that suggested that binding was not required in response to hypertonicity (Piechotta *et al*, 2003). Deletion of one SPAK binding domain did not result in loss of cotransport. However, when both SPAK binding motifs were removed from NKCC, cotransport was ablated in response to hyperosmolarity. Point mutations (F79A and F135A) had the same effect on cotransport and *in vitro* phosphorylation assays showed that this mutation resulted in very little phosphorylation on NKCC. They concluded that only one motif was required for *in vivo* activation of cotransport by SPAK/WNK. There have been suggestions that hydrophobic residues flanking the specific site of substrate phosphorylation are important for NKCC and SPAK interaction. Gagnon *et al* (2007a) demonstrated that mutation of M212A (after Thr^{211} in mouse NKCC1) did not alter the ability of the cotransporter to function in the presence of SPAK and WNK4 (in *Xenopus* oocytes) or hyperosmotic conditions, whereas a F207A (following Thr^{206}) mutation on NKCC1 resulted in a non-functional transporter. As Thr^{211} is not a target of SPAK/OSR1, mutation did not affect the activity of NKCC1 under these conditions. Villa *et al* (2007) provide structural information about the interaction of SPAK/OSR1 with peptide containing the RFxV motif. Crystals of the conserved C-terminal (CCT) domain of OSR1 bound to a peptide from WNK4 (GRFQVT) were formed and X-ray diffraction data was collected and modelled. The structure of the CCT domain was considered unlike any other known protein

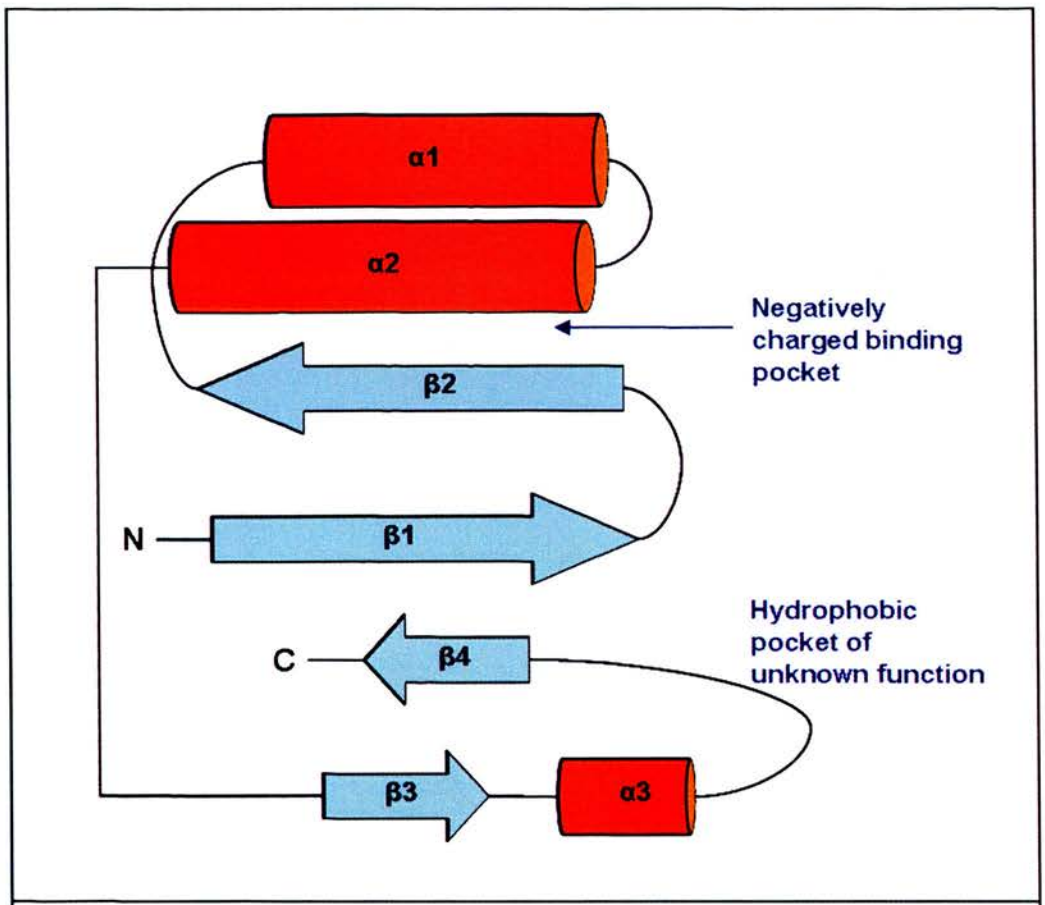

Figure 1.5 – SPOC Fold of OSR1
This diagram was constructed from information obtained from Villa *et al* (2007) and represents the novel SPOC fold observed in the conserved C-terminus of OSR1.

fold and was dubbed the SPOC fold (SPAK/OSR1 C terminus). It consists of four anti-parallel β-sheets that are packed against two large alpha-helices and a third smaller alpha-helical section (see figure 1.5 for a representation). The WNK4 peptide used possessed a terminal threonine residue, which when phosphorylated prevented its binding to the CCT of OSR1. The authors note that a serine or threonine following the RFxV motif appear to be conserved across species and as such the interaction between WNKs and SPAK/OSR1 substrates, such as NKCCs, may be regulated by the phosphorylation of these residues. Figure 1.6 describes a model of NKCC regulation based on the evidence compiled from the work of

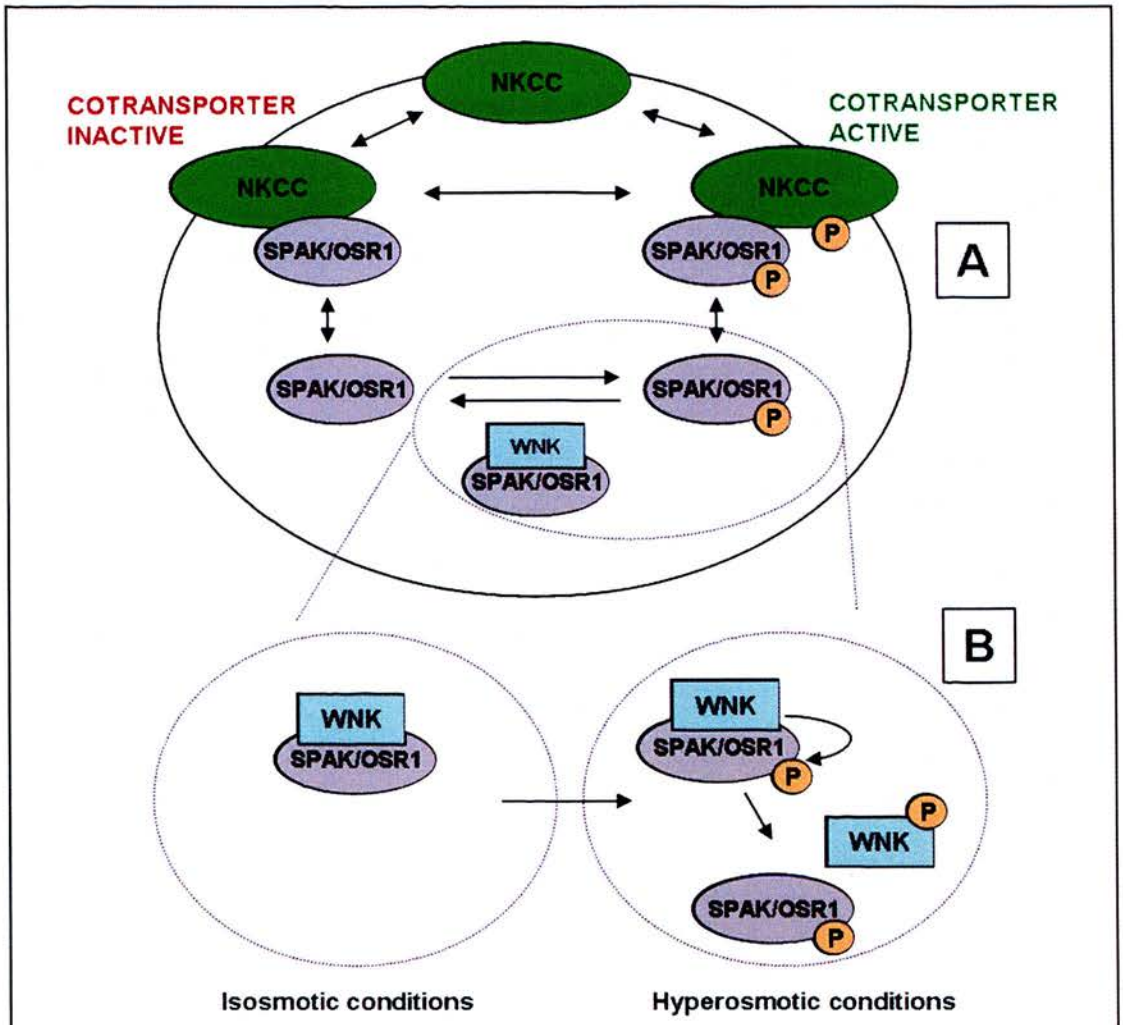

Figure 1.6 – Model of NKCC regulation via SPAK/OSR1 and the WNK kinases
SPAK/OSR1 docks on NKCC via one of its RFXV motifs. SPAK/OSR1 is phosphorylated by WNK in the cytosol under hyperosmotic conditions resulting in dissociation of the molecules. This allows active SPAK/OSR1 to bind and phosphorylate NKCC. Gagnon *et al* propose that a small proportion of NKCC binds active SPAK under isosmotic conditions which accounts for the basal activity seen in many cell types. Although in panel A SPAK is found associated with NKCC and free in the cytosol, Villa *et al* (panel B) propose that normally WNK and SPAK are bound together until stimulation causes phosphorylation of WNK (by an as yet unknown kinase) and WNK phosphorylation of SPAK, inducing dissociation allowing free active SPAK to dock on NKCC and activate it. This figure was compiled from models proposed by Gagnon *et al* (2007a – panel A) and Villa *et al* (2007 – panel B).

Gagnon *et al* (2007a) and Villa *et al* (2007). Y-2-H assays with SPAK as bait (Piechotta *et al*, 2003) found proteins other than WNKs and NKCC. Apoptosis-associated tyrosine kinase1 (AATYK1) was one of these and has since been further

investigated (Gagnon *et al*, 2007b). This protein contains two RFxV motifs and was found to interact with both SPAK and protein phosphatase 1 (PP1) in Y-2-H experiments. These proteins were also found to co-IP from HEK-293 cells transfected with SPAK, PP1 and AATYK1. Through more Y-2-H experiments these interactions were characterised further. NKCC1 did not interact with AATYK1 or PP1, whereas SPAK and PP1 both interacted with the regulatory domain of AATYK1. Mutation of the phenylalanine residue in either AATYK1 RFxV motif prevented interaction with SPAK as did a V1175A mutation in PP1 stop interaction with the tyrosine kinase. *Xenopus* oocyte co-injection experiments showed that AATYK1 inhibited cotransport even when non-catalytic AATYK1 was used. Mutations that prevent binding of AATYK1 to SPAK or PP1 remove or reduce the inhibitory effects of the kinase on cotransport and as such, the authors suggest that expression of AATYK1 acts to bind SPAK and PP1 removing them from acting upon the cotransporter. Furthermore, they postulate that this is not purely due to sequestration of these molecules, but that PP1 may actually dephosphorylate and therefore deactivate SPAK. A model for the role of AATYK1 is depicted in figure 1.7. As previously mentioned in section 1.5.3.3, there may be involvement of the SAPKs and MAPKs in cotransport regulation. Links have been made to several of these proteins and either SPAK or WNKs. Johnston *et al* (2000) found that SPAK was able to activate p38 kinase in rat pancreatic cells (catalytically inactive SPAK did not result in p38 phosphorylation of the substrate AF-2 *in vitro*). More recently (Piechotta *et al*, 2002), p38 MAPK has been found to co-IP with SPAK and NKCC1 from brain lysates. Zagórska *et al* (2007) found that sorbitol stimulated ERK1/2, p38 and JNK in HEK cells, a stimulus that activates NKCC cotransport. This study was

investigating the activation of WNK1. However, inhibition or activation of these SAPKs and MAPKs had no effect on the activation of WNK1. Again, it seems that the relationships of the various kinases may be cell specific and specific to certain stimuli.

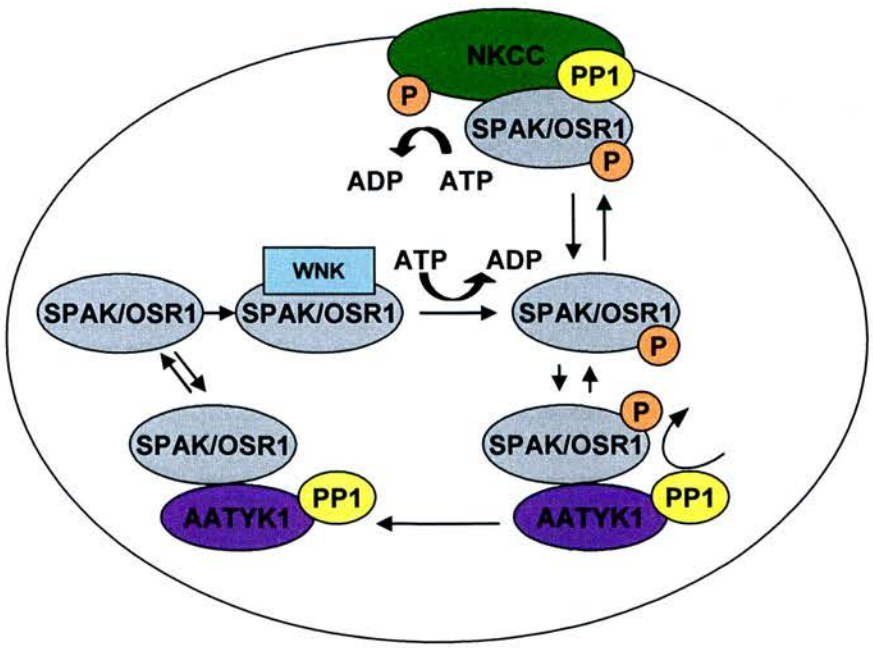

Figure 1.7 – Model for Regulation of NKCC Cotransport by AATYK1
This diagram was reworked from Gagnon *et al* (2007b) and demonstrates the idea that AATYK1 functions to scaffold SPAK/OSR1 and PP1. This model involves AATYK1 acting as a negative regulator of NKCC activity by binding of SPAK/OSR1 and dephosphorylation of these kinases by PP1.

1.5.3.7 – Phosphorylation of NKCC2

Study of the regulatory phosphorylation of the NKCC2 isoform has been minimal when compared to the wealth of studies that have been undertaken to understand regulation of NKCC1. However, useful studies have been conducted and show that some features of regulation may be common to both isoforms. NKCC2 has N-

terminal threonine residues in common with those involved in regulatory phosphorylation in the N-terminus of NKCC1, including the three known phosphoacceptor sites (shark NKCC1 T184, T189, and T202 correspond to rabbit NKCC2 T99, T104, and T117). Indeed, activation of mouse NKCC2 by the peptide hormone vasopressin resulted in phosphorylation of Thr^{99} and Thr^{104} residues, as detected by the R5 antibody (Giménez and Forbush, 2003). Further study showed that mutations to any one of the three phosphoacceptor sites had no effect on NKCC2 activity when expressed in *Xenopus* oocytes (Giménez and Forbush, 2005). Cotransport in response to hypertonicity was only affected when all three residues were mutated, but these mutations had little effect on cotransport under isotonic or hypotonic conditions. Flux of ^{86}Rb in NKCC2 mutants that lack the SPAK binding site was not affected, suggesting that this kinase is not required for phosphorylation of NKCC2 or that it is not required to bind the cotransporter to phosphorylate. WNK3 has been implicated in the regulation of NKCC2 function. This kinase is most abundantly expressed in the brain and kidney. Co-injection of WNK3 with NKCC2 resulted in a three-fold increase in ion cotransport (Rinehart *et al*, 2005). Measurement of phosphorylation with the R5 antibody showed increases on NKCC2, especially under hypertonic conditions. Kinase-dead WNK3 mutants did not produce the same effects on NKCC2 phosphorylation. This may suggest that SPAK, in conjunction with WNK3, is involved in NKCC2 phosphorylation. Recently, it has been observed that AMP-activated protein kinase (AMPK) phosphorylates mouse NKCC2 on Ser^{126} and that these two proteins co-IP from mouse macula densa-derived cells (Fraser *et al*, 2007). This serine residue was phosphorylated under non-stimulated conditions and appears to be responsible for the maintaining the basal

activity of NKCC2. This serine is conserved in NKCC1 and it may be of interest to examine the involvement of this residue and AMPK in NKCC1 regulation.

1.5.4 – Current Understanding of NKCC Phosphorylation

In the last few years, a great number of studies have produced a wealth of data to help us understand the regulation of NKCC cotransport by protein phosphorylation. These have highlighted several kinases that are required for activation of the cotransporter under hyperosmotic stress. We know that active WNK phosphorylates and activates SPAK and OSR1 kinases, which in turn can then phosphorylate and activate NKCC. However, these actions do not account for all phosphorylation seen on the cotransporter. Figure 1.8 demonstrates some of the knowledge acquired with respect to NKCC phosphorylation. This also indicates that there is still much to be identified. SPAK and OSR1 appear to only act upon certain residues. The kinases that are responsible for phosphorylation of the other known threonines have not yet

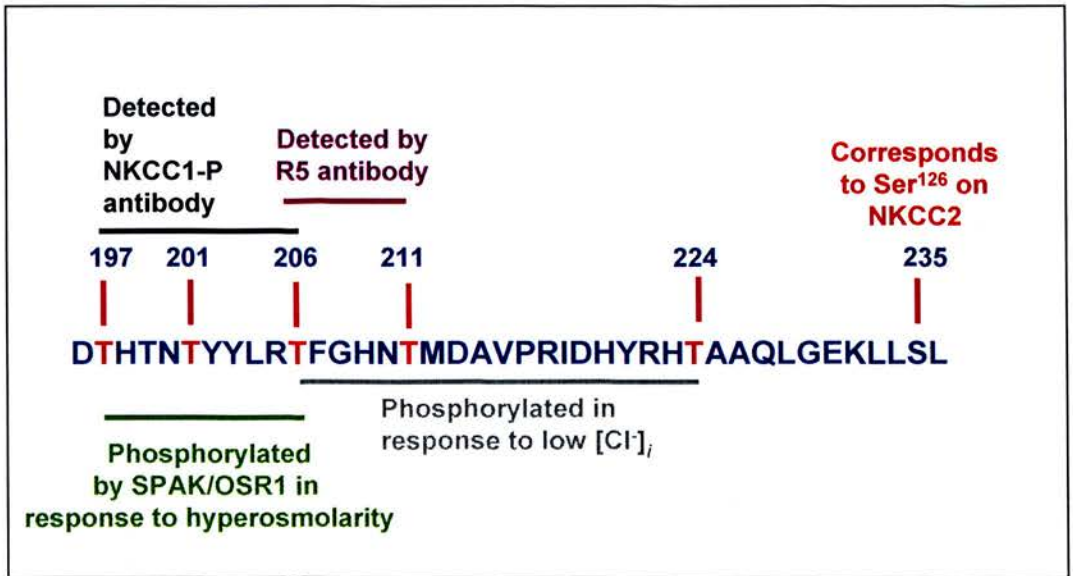

Figure 1.8 – Phosphorylation of NKCC at the N-terminal Regulatory Locus
This diagram summarises the information thus far obtained about phosphorylation at the N-terminus of NKCC. The numbering of amino acids is from mouse NKCC1 (accession NP_033220)

been identified. Total ^{32}P incorporation indicates phosphorylation on serine residues. Only one known serine residue on NKCC2 has been uncovered, but there may be others. Although a great deal of understanding has been made, there is still much to decipher, particularly in the response of NKCC to different cotransport stimuli.

1.6 - Implications to Health and Disease

1.6.1 – Loop Diuretics

Perhaps the most important link between NKCCs and medicine is through the use of "loop" diuretics as treatment to reduce fluid volume in the body. The most well known loop diuretics are furosemide, bumetanide and benzmetanide. They are used commonly in the USA to treat hypertension and furosemide is given to those with heart or renal failure (Padilla *et al*, 2007). Torasemide has been used to reduce the oedema that is associated with chronic congestive heart failure, renal disease, hepatic cirrhosis and for use in hypertension treatment (Dunn *et al*, 1995; Friedel and Buckley, 1991). This drug appears to be longer lasting than the other loop diuretics and lower doses are required. However, there are side effects associated with the use of these drugs. Among these are hyponatremia, hypokalemia, dehydration, tinnitus, hearing loss, and vertigo. Perhaps, with greater understanding of cotransport regulation, more specific anti-cotransport drugs could be developed, perhaps with fewer side effects.

1.6.2 - Bartter's syndrome

In the early 1960s, Bartter described a new syndrome characterised by hypokalaemia, alkalosis, hyperaldosteronism, polyuria, polydipsia, hypercalciuria, juxtaglomerular hyperplasia (on renal biopsy), and normal or low blood pressure (Bartter *et al*, 1998). Gill and Bartter (1978) noted that this defect was due to poor chloride reabsorption in

the loop of Henle and the effects of furosemide also resemble the syndrome (Unwin and Capasso, 2006). Healthy individuals who were administered furosemide showed increased urine output and this contained greater than normal levels of chloride (Köckerling *et al*, 1996). Like patients with Bartter's syndrome hyperaldosteronism and hypercalciuria were observed. Though it was clear that renal ion transport was likely to be involved in this disease, it wasn't until 1996 that Simon *et al* linked mutations in the gene for NKCC2 with Bartter's syndrome. However, other mutations that affect the ability of the TAL to absorb salts can also produce similar phenotypes (Gamba, 2005). For example, the apical inward rectifying K^+ channel (ROMK) and the basolateral chloride channel CLC-KB also result in Bartter's disease. Failure of K^+ recycling and intracellular Cl^- extrusion all function to prevent NKCC2 activity in the kidney, and thus mutations to ROMK and CLC-KB have the same effect as an NKCC2 mutation. NKCC2 knockout mice, generated by Takahashi *et al* (2000) were severely dehydrated and failed to thrive. However, when mice were treated with indomethacin those that survived showed features of the Bartter's phenotype such as polyuria, hypokalemia, metabolic alkalosis and hypercalciuria. Thus far, Bartter's syndrome is the only known human disease where a mutation of NKCC has been directly linked to illness.

1.6.3 – Blood Pressure

Both isoforms may have a role to play in the regulation of blood pressure. We know that inactivating mutations to NKCC2 can result in hypotension (from Bartter's syndrome and mouse knock-outs) and the converse, where activity of the cotransporter is increased, could feasibly contribute to hypertension (Gamba, 2005). Gordon's syndrome (Gordon, 1986), also named pseudohypoaldosteronism type II

(Schambelan *et* al, 1981), is characterised by hypertension, hyperkalemia, and metabolic hyperchloremic acidosis with normal glomerular filtration rate. It was suspected that Gordon's syndrome was due to a gain-of-function mutation to the NCC cotransporter, particularly as thiazide diuretics have been successfully used to treat this syndrome, but no mutations to this protein have been found in Gordon's patients (Gamba, 2005). However, mutations to WNK1 and WNK4 have been linked to the syndrome (Wilson *et al*, 2001). WNK4 is a negative regulator of NCC function and thus inactivating mutations would allow unchecked activity of NCC in the kidney, whereas WNK1 inhibits WNK4 in the kidney and activating mutations to this kinase would produce the same effect (Xie *et al*, 2006). Yang *et al* (2007) produced a knockin mouse model possessing a WNK4 mutation found in human Gordon's patients. These mice showed the characteristic symptoms of Gordon's syndrome and increased expression of NCC at the distal convoluted tubule was observed. The authors also found increased phosphorylation on SPAK/OSR1 and NCC and suggest that the pathogenesis observed is due to increased function of NCC via activation of this phosphorylation pathway. Stiefel *et al* (2000) made some interesting observations about NKCC activity in a patient with Gordon's syndrome. This group studied red blood cells rather than renal tubular cells and found increased NKCC activity in Gordon's syndrome compared with patients with essential hypertension. They suggest that kidney NKCC activity may be inferred from their results and that increased activity of this transporter may contribute to the pathology of the syndrome. Increased NKCC cotransport has also been observed in red cells from spontaneous hypertensive rats and patients with essential hypertension (Orlov *et al*, 1999; Righetti *et al*, 1995). Further studies have implicated NKCC1 activity

with hypertension, particularly with relation to vascular tone. Treatment of rats with bumetanide resulted in a decrease in blood pressure, an effect that was not affected by clamping of renal arteries (Garg *et al*, 2007). This, and evidence that the effect was not observed in NKCC1-null mice, suggest that the effects of bumetanide on blood pressure was due to inhibition of NKCC1. The contractile effect of phenylephrine on mesenteric arteries was reduced in the presence of bumetanide and the authors concluded that NKCC1 has a role on smooth muscle tone in resistance vessels. Importantly, hypertension caused by chronic phenylephrine administration was successfully treated with bumetanide in rats. Orlov (2007) suggests that a specific NKCC1 inhibitor could be useful for the treatment of hypertension.

1.6.4 - Inflammation

A number of studies now suggest that increased NKCC1 activity may be involved in the pathophysiology of inflammatory disorders. Levels of NKCC1 mRNA in human vascular endothelial cultured cells were raised in response to inflammatory cytokines (IL-1β and TNF-α) and *in vivo* in lung and kidney after administration of the bacterial endotoxin lipopolysaccharide (LPS) to mice (Topper *et al*, 1997). These authors also demonstrate that NKCC1 was upregulated *in vitro* in response to fluid mechanical stress. Using apparatus that mimics the type of environment that endothelial cells would be exposed to in the vasculature (i.e. blood flow), they identified that NKCC1 expression was highest under conditions of steady laminar flow. Reducing the force of flow, or turbulent conditions, caused a decrease in NKCC1 mRNA levels. These findings implicate the involvement of the cotransporter in vascular homeostasis as well as inflammation. In addition to these findings, other groups have implicated NKCC1 in specific inflammatory disorders.

Eight-fold increases in NKCC1 expression have been found in bronchial biopsies from asthmatic patients (Dolganov *et al*, 2001). Increased expression was confined to goblet cells, as shown by immunohistochemistry. This, and the observation that inhaled furosemide has beneficial effects in asthmatic patients (Niven and Argyros, 2003; Pendino *et al*, 1998), strongly suggest the involvement of the cotransporter in this inflammatory condition. The expression of NKCC1 in spinal sensory neurons and dorsal root ganglion (DRG) was found to be altered in mice with either chronic or acute arthritis (Morales-Aza *et al*, 2004). NKCC1 expression was reduced in DRG and increased in spinal sensory neurons in both chronic and acute arthritis. The authors suggest that this may result in neuronal excitability and that NKCC1 could be a potential therapeutic target for inflammatory pain treatment. Bacterial pneumonia in mice (by introduction of *Klebsiella pneumoniae*) can lead to sepsis and hypothermia, effects which are not observed in NKCC1-null mice (Nguyen *et al*, 2007). It was observed that although the total neutrophils present in the lung were not different from wild-type more of these cells were present in the alveolar spaces of mutant mice. Through evidence from further experiments, the authors propose that loss of NKCC1 results in altered trafficking of neutrophils to the site of infection, reducing bacterial load and protection against the secondary effects of sepsis and hypothermia. Interestingly, *K. pneumonia*-induced peritonitis showed the same severity and progression as found in wild-type mice, suggesting that the effects of blocking NKCC1 activity are only protective against lung infection.

1.6.5 - Ischaemia

NKCC1 has been implicated in cerebral ischaemic injury. NKCC1-null mice showed less infarct volume and neuronal cell death after induced focal ischaemia

(Chen *et al*, 2005). These neuroprotective effects were mimicked in wild-type mice that were treated with bumetanide (O'Donnell *et al*, 2004). Pond *et al* (2006) showed that oxygen-glucose deprivation, which is an *in vitro* model of ischemia, induced Cl^- uptake into neurons in mouse hippocampal slices. Rises in $[Cl^-]_i$ were observed during reoxygenation, along with increased phosphorylation on NKCC1. Increased neuronal $[Cl^-]_i$ was shown to be necessary and sufficient for cell damage after oxygen-glucose deprivation, an effect which was reduced by treatment with bumetanide or furosemide. This is of clinical interest, where treatment of stroke patients with a loop diuretic (or an as yet undiscovered NKCC1 inhibitor) could help reduce the pathology associated with oedema.

1.7 - Experimental Approaches

1.7.1 - The red cell as a model

There are several reasons to use the red blood cell to study Na-K-Cl cotransport. Apart from variability in age, cell populations are fairly homogeneous and have a single compartment, making measurements of cotransporter activity simpler to understand. Radioactive rubidium (^{86}Rb) is transported by NKCC in place of potassium and is used to trace the movement of ions. They are easy to manipulate pharmacologically in the test tube and are also easy to acquire and separate from other cell types. Much of the early work into the features of cotransport was conducted in avian red cells (Muzyamba *et al*, 1999; Lytle, 1997; Pewitt *et al*, 1990). Ferret red blood cells offer the opportunity to examine NKCC from the mammalian viewpoint. They show a thirty-fold higher rate of cotransport compared with those from human, rat, and guinea pig (Lytle, 2003) and possess little, if any, Na^+ pump activity (Flatman, 1983). This allows study of cotransporter without the need for

ouabain, and makes interpretation of flux results less complicated. Ferret red blood cells are used in this work as the major source of NKCC. As red blood cells are anuclear and do not possess the machinery capable of producing new protein, the genetic component of NKCC activity cannot be measured. In some ways this is a disadvantage, but in others it is advantageous. We cannot decipher the components involved with gene up-regulation and protein-trafficking that are features of cotransporter regulation in other cell types. However, because these features are not present in the red blood cell we are able to examine the effects that protein-protein interactions and post-translational modifications may have on cotransport with less complication.

As mentioned previously, it may be possible to use the red cell as an aid to diagnose diseases, where cotransport in these cells may reflect cotransport in the kidney (Righetti *et al*, 1995). If this is the case, then the red blood cell may offer a simpler and more patient-friendly biopsy sample compared with the kidney.

1.7.2 – Rationale for Methods Used

The standard approach to investigating phosphorylation on a protein is to measure the incorporation of radioactive ^{32}P. This approach, coupled to phospho-labelled peptide isolation and sequencing have identified residues that are phosphorylated on the cotransporter. Another method is by the separation of proteins in two-dimensions, based on their isoelectric point (pI) and molecular size, which should allow resolution of proteins with different post-translational modifications such as phosphorylation. The addition of a phosphate group to a protein adds only 80 Daltons, a change which is not likely to be detectable on standard SDS-PAGE (the second dimension) (Mann *et al*, 2001). However, the change that addition of a

phosphate brings to the pI of a protein is theoretically detectable in the first dimension (isoelectric focussing). Along with the use of phospho-specific antibodies, this thesis presents evidence that NKCC with different numbers of phosphate groups is detectable with this method. Phosphorylation of immunoprecipitated cotransporter is also investigated by the use of the same phospho-specific antibodies, as well as those to total phosphothreonine. This allows measurement of global changes in NKCC phosphorylation in response to a number of different stimuli. To look for proteins that interact with NKCCs, perhaps in a regulatory capacity, co-immunoprecipitation experiments were performed. In conjunction with mass spectrometry and western blotting certain NKCC interacting proteins identified in other cell types have been confirmed in the ferret erythrocyte. Finally, molecular biological techniques were employed to verify the isoform present in the red blood cell.

Chapter 2

Materials and Methods

Chapter 2 - Materials and Methods

The majority of reagents commonly used throughout this project were sourced from either Sigma-Aldrich (St. Louis, MO) or BDH Laboratory Supplies (from Merck, Germany), choosing analytical grade options where available. A list of these reagents and supplier information is given at the end of this chapter. Other reagents and kits are given within the method descriptions. Unless otherwise stated, aqueous solutions were made up with double glass-distilled water or Elix10 grade Millipore water.

2.1 – General Methods

2.1.1 - Centrifugation

Several centrifuge instruments were used to provide all of the conditions required. An Eppendorf MiniSpin Plus bench-top microfuge was used for most purposes. To spin samples of larger volume, and those that required to be kept cool, a Sorvall RC 26 Plus with an SS34 fixed-angle rotor or Biofuge Stratos (Heraeus Instruments) with fixed-angle (#3335) or swing-out (#8172) rotors were used. Both instruments are refrigerated. High speed centrifugation was achieved using a Beckman TL-100, which is capable of speeds up to 300,000 x *g*. The relative centrifugal field (RCF) or *g* value is calculated using the following equation:

$$g = \mathbf{RCF} = 1.18 \times 10^{-5} \times r \times \mathbf{rpm}^2$$

where ***r*** = the radius in centimetres from the centre of the rotor to the sample and **rpm** = the speed of the rotor in revolutions per minute (Dawson *et al*, 1986).

2.1.2 - Spectrophotometry

An UltroSpec 2000 from Pharmacia Biotech was used for determining both protein and nucleic acid content of samples. This is a UV/visible spectrophotometer, allowing measurement of wavelengths from 190-1100nm. For protein assays, absorbance at a specified wavelength was measured. Nucleic acid quantification is measured using absorbance at 260nm. Absorbance (A) is defined by Beer's Law:

$$\mathbf{A} = \varepsilon l c$$

where ε = molar absorption coefficient with units of L mol^{-1} cm^{-1}, l = pathlength in centimetres and c = the concentration of the solution in mol L^{-1} (Dawson *et al*, 1986). In a 1cm pathlength, a solution of DNA or RNA with an absorbance of 1.0 has a concentration of 50 or 40μg/ml, respectively (Maniatis *et al*, 1982). These rules can be applied to calculate a nucleic acid concentration from a measured absorbance. Sample purity is assessed by the ratio of absorbance at 260nm (nucleic acid) to absorbance at 280nm (protein). For pure DNA, the absorbance ratio is 1.8. For pure RNA, this ratio is 2.0. In all cases, quartz cuvettes with a 1cm pathlength were used.

2.1.3 – Analysis of 1- and 2-Dimensional Gel Images

TotalLab and 2DEvolution software packages were used to analyse 1- and 2-dimensional gel images and western blots. Both of these programs were developed by Non-linear Dynamics, UK. For 1-D images, TotalLab software allowed molecular weight estimation by log-linear interpolation from markers of known mass. Optical density values were also obtained from this program. Molecular weights were estimated on 2-D images using 2DEvolution software, which has since been renamed Progenesis, in the same method as for 1-D images. Estimation of isoelectric point for proteins on 2-D gel and western blot images was achieved by

interpolation from the pH range of the first dimension gel strip, taking into account those sections that are lost on the strip when cutting to fit the second dimension sample well. Although the strip manufacturer states that separation occurs from pH 4-7, the actual measured range is pH 4.3-6.3 as calculated from data provided by the strip manufacturer.

2.1.4 – Statistical Analysis

The GraphPad QuickCalcs online calculator (which is available from www.graphpad.com/quickcalcs/ttest1.cfm) was used to conduct two-tailed unpaired *t* tests. This program calculates the mean ($\bar{x}$), standard deviation (σ) and standard error of the mean (*SEM*) from two sets of data. It reports a p-value allowing decisions to be made about any significant differences between the means of the two sets of data. Where average molecular weights are shown in the results sections, they are given as mass ± standard deviation. Unless otherwise stated in the text, mean phosphorylation level (± standard deviation) refers to the mean phosphorylation from (*n*) different animals where the phosphorylation level from any one animal has been averaged from replicate determinations.

2.2 - Tissue and Membrane Preparation

2.2.1 - Blood

Human blood was drawn from the median cubital vein in the forearm. Rat blood was obtained from animals after being Schedule 1 sacrificed. Ferret blood was obtained by cardiac puncture after animals were given a lethal dose of Sagatal (pentobarbitone sodium B.P. 130 mg kg^{-1}, Rhône Mérieux). Blood was immediately mixed with 4

mM EDTA, to chelate divalent cations required for enzymes of the blood coagulation cascade. All animal work was in accordance with Home Office guidelines.

2.2.2 - Preparation of Membranes from Ferret, Rat and Human Erythrocytes

Packed cells were diluted with ferret basic medium (FBM; 145 mM NaCl, 5 mM KCl, 0.05 mM EGTA, 10 mM HEPES, pH 7.5 (neutralised with NaOH)) containing 11 mM D-glucose to give a cell suspension at approximately 10% haematocrit. The suspensions were incubated at 38°C (ferret) or 37°C (rat and human) for 10 minutes, with continuous gentle stirring. Pharmacological stimuli were applied after this time. The different conditions used are described in Table 2.1. Cell suspensions were transferred to test tubes and spun at 2,500 x *g* (4°C) for 5 minutes to separate the

	Concentration	Incubation period
Calyculin A	50 nM	15 minutes
Na Arsenite	1 mM	60 minutes
Untreated	-	10-30 minutes
PP1	20 or 50 μM	30 minutes
Mg^{2+} free	2 mM Tris-EDTA (TE), 10 μM A23187	TE 15 minutes, then A23187 15 minutes
Genistein	50 μM	20 minutes
Staurosporine	2 μM	20 minutes

Table 2.1 - Pharmacological Stimuli
Calyculin A is an inhibitor of protein phosphatases 1 and 2A. General kinase inhibition is mediated by removal of Mg^{2+} by Tris-EDTA and the mobile ion-carrier A23187 (Flatman and Lew, 1980). PP1, genistein and staurosporine are potent kinase inhibitors. Staurosporine inhibits a wide number of kinases. Genistein is a tyrosine kinase inhibitor and PP1 inhibits Src-family tyrosine kinases. In all cases, the solvents used to dissolve the various compounds were found not to cause cell lysis or interfere with NKCC activity and are described in papers by Flatman and Creanor (1999a and 1999b).

cells from sample medium. Cells were cooled on ice before being passed through a 19 gauge needle into 20 volumes of ice-cold red blood cell lysis buffer (1 mM β-glycerophosphate, 10 mM HEPES, 2 mM EDTA, 2 mM Na pyrophosphate, 1 mM Na vanadate, 2 mM NaF, pH 7.6) , with 1% protease inhibitor cocktail III (Calbiochem) and stirred continuously for 10 minutes. Sodium fluoride, β-glycerophosphate, sodium pyrophosphate and sodium vanadate are all included as protein phosphatase inhibitors (Jaumot and Hancock, 2001; Gordon, 1991). Lysates were spun at 25,000 x *g* (4˚C) for 10 minutes and supernatant discarded. Recovered membranes were washed twice more by resuspension in ice-cold lysis buffer (without protease inhibitors) and centrifugation (25,000 x *g*, 4˚C). All of the solutions during lysis and membrane recovery were kept ice-cold to ensure that the membranes did not reseal (Wood, 1987). The final membrane pellet volume was measured and protease inhibitor cocktail added to give 2% final concentration. All samples were stored in liquid nitrogen until use. This protocol was adapted from Flatman and Creanor (1999) and Matskevich *et al* (2005).

2.2.2.1 – Preparation of Sodium Vanadate

Stock solutions of 200 mM sodium vanadate (Na_3VO_4) were prepared in the following way. Na_3VO_4 powder was dissolved in boiling water and allowed to cool. The pH of the solution was measured and adjusted to pH 10 with HCl. This step produces a colour change (to orange), which indicates the presence of decavanadate. The solution was boiled again until colourless, and then allowed to cool. The pH was measured and adjusted as before if necessary. The boiling, cooling and pH adjustment steps were repeated until the solution was stable at pH 10 to ensure the

presence of monovanadate (Gordon, 1991). Aliquots were stored frozen until required for use.

2.2.3 – Deoxygenation of Erythrocytes

Ferret erythrocyte cells were deoxygenated according to Flatman (2005). Cells in FBM/glucose (at 10% haematocrit) were incubated for 30 minutes at 38˚C in a tonometer (Eschweiler, Kiel, Germany) that had been gassed with water-saturated argon. The final PO_2, measured with a Clark polargraphic oxygen electrode with a polypropylene membrane in thermostatic flow through cell and meter (Strathkelvin Instruments, Scotland), was less than 3mm Hg. After this period, cells were taken for membrane preparation as described in section 2.2.2. However, all solutions and centrifuge tubes were purged of oxygen with argon gas prior to addition of any cells or membranes. Cells were passed into cell lysis medium with a gas-tight syringe (Hamilton, USA).

2.2.4 - Salivary Gland and Kidney Membrane Isolation

Salivary glands and kidneys were carefully removed and stored cold in phosphate buffered saline (PBS; 137 mM NaCl, 10 mM Na_2HPO_4, 1.7 mM KH_2PO_4, 2.7 mM KCl, pH 7.4) until ready for dissection. Kidneys were dissected to isolate as much medulla as possible, an area which is indicated in Figure 2.1. Following a protocol adapted from Nielsen *et al* (1998), the separated tissues were homogenised with a Powergen 125 homogenizer (Fisher Scientific, UK) in membrane isolation solution (250 mM sucrose, 10 mM triethanolamine, 2% protease inhibitor cocktail). Homogenates were spun at 1,000 x *g* for 10 minutes (4°C) and the supernatants separated from the pellets. The pellet material was resuspended in membrane isolation solution, and then spun again at 1,000 x *g*. The supernatants were pooled

and spun at 17,000 x *g* for 20 minutes (4°C) to pellet the crude membrane fraction. These were mixed with protease inhibitors (at 2% final concentration) and stored in liquid nitrogen until required. This protocol was also used to recover cell membranes from bone marrow cells.

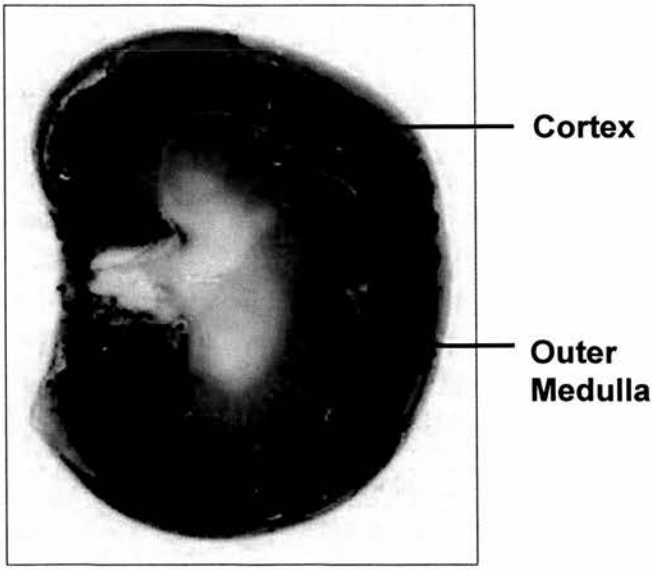

Figure 2.1 – Kidney dissection
This indicates the area dissected from all kidney samples for protein and nucleic acid isolation. As far as possible, only tissue from the medulla was used.

2.2.5 - Bone Marrow Preparation

Rat femurs were dissected from surrounding tissues and the knee and hip joints removed. A needle was inserted into the bone and PBS was flushed through with a needle (gauge varied depending on size of bone) and marrow collected. Any pieces of bone were carefully removed and then the bone marrow-PBS mix was triturated through a pipette tip several times to create a more uniform cell suspension.

2.2.6 – Separation of Erythrocytes using a Percoll® Gradient

Whole blood was centrifuged at 2,500 x *g* for 5 minutes and the plasma removed. The first few millilitres of cells which contain the most buoyant red cells and white blood cell layer were recovered and set aside. The remaining blood was mixed and spun again and the top few millilitres added to those cells recovered earlier. Percoll® was prepared with NaCl to give a density of 1.090 g/ml in 0.15 M NaCl, following

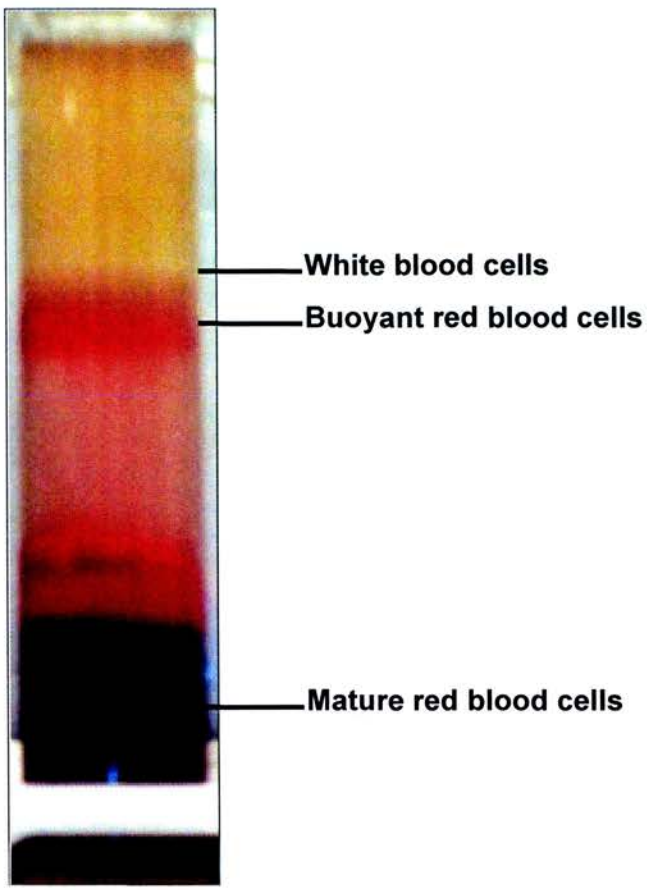

Figure 2.2 – Percoll® Separation of Human Blood Cells
After centrifugation, cells separate into discrete bands. The uppermost liquid and white cell layers were removed before careful pipette removal of the buoyant red blood cell layer. Cells can be separated from the Percoll® by washing in PBS and collected by centrifugation for further study. Both white and buoyant red blood cells were collected.

instructions in the Pharmacia publication, Percoll®, Methodology and Application. A gradient was prepared by spinning a tube of diluted Percoll® at 20,000 x *g* for 20 minutes in a fixed angle rotor. After this time, the pooled cells were carefully layered on top using a pipette, and spun in a swing-out rotor for 25 minutes at 1,000 x *g*. Figure 2.2 shows the separation of these cells. The most buoyant red cells and white cells were carefully removed and washed by resuspension in 0.9% NaCl and centrifugation at 200 x *g* for 10 minutes. The recovered cells were kept for RNA extraction, which is described in section 2.9.2.

2.3 - Protein Estimation

Two different assays were used to estimate the protein content of samples. For most situations, the Pierce BCA (bicinchoninic acid) assay was used. This is a colorimetric assay where Cu^{+2} is reduced to Cu^{+1}, with which the BCA forms a complex. This complex is purple in colour and is detectable at 562 nm, using a spectrophotometer. For samples containing substances that interfere with the BCA assay (such as urea, detergents and reducing agents), the 2-D Quant Kit from GE Healthcare Life Sciences (formerly Amersham Biosciences) was used. This assay precipitates proteins, leaving interfering substances in solution for easy removal. The protein is then resuspended in a copper-containing solution. As copper ions bind to the peptide backbone of protein, any unbound ions are reacted with a colorimetric agent, and measured at 480 nm. Protein concentrations were estimated by interpolation of standard curves drawn from known protein standards, using GraphPad Prism 4.00 software. Examples of these curves are given in figure 2.3.

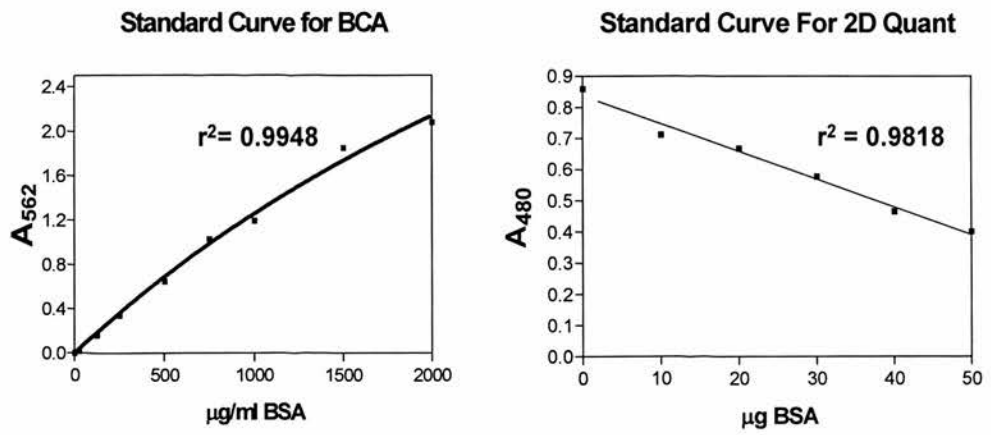

Figure 2.3 – Standard curves obtained from known protein standards for BCA and 2D Quant protein assays

From these curves, the absorbance of test samples can be related to an amount of protein or a protein concentration (usually bovine serum albumin, BSA). This is calculated automatically by the GraphPad Prism software using linear regression for 2D Quant standard curves and non-linear regression for BCA standard curves. The r^2 values show the correlation between the regression line the real data points (where $r^2 = 1.0$ is a perfect fit).

2.4 – One-Dimensional Electrophoresis and Protein Detection

Electrophoresis is the term used to describe the movement of charged particles in an electric field. In this project, various different electrophoretic techniques were used for the separation of proteins and are described here.

2.4.1 - Sodium Dodecyl Sulphate-Polyacrylamide Gel Electrophoresis (SDS-PAGE)

This process involves heat-denaturing proteins and coating them with SDS (or LDS; lithium dodecyl sulphate) molecules. This overrides any inherent charge that a protein may have. When an electric field is applied, the negatively charged molecules move towards the anode through a gel matrix. This allows separation of proteins based on their molecular mass. In most circumstances, pre-cast NuPAGE™ gels (8cm x 8cm, 1mm thick) were used with the XCell *SureLock*™ Mini-cell

electrophoresis module from Invitrogen. NuPAGE™ 4-12% Bis-Tris or, for better separation of larger proteins, 3-8% Tris-Acetate gels were used. Samples were prepared for electrophoresis by heating at 70°C for 10 minutes with LDS sample buffer (Invitrogen) and 100 mM DTT. LDS is preferred, as it protects proteins from peptide bond cleavage that may occur when samples are boiled with SDS (Kubo, 1995). The different gel types required different running conditions and these are listed in Table 2.2. Large home-cast gels were prepared, and run, using the SE 600 Ruby standard dual cooled gel electrophoresis unit (Amersham Biosciences) and the

Gel type	Buffer	Running parameters
3-8% Tris-acetate	Tris acetate SDS running buffer	150V constant for 1 hour
4-12% Bis-tris	MES SDS running buffer	200V constant for 35 minutes
4-12% Bis-tris	MOPS SDS running buffer	200V constant for 50 minutes

Table 2.2 – Denaturing SDS-PAGE running conditions using NuPAGE gels

Hoefer SG 100 gradient maker. The composition of these gels was 4-12% acrylamide (using a 40% acrylamide/N,N'-methylenbisacrylamide solution from Bio-rad), 0.1% SDS, 375 mM Tris-HCl (pH 8.8) and polymerised with 0.1% ammonium persulphate (APS) and 0.04% TEMED. Stacking gels (4% acrylamide) were prepared in the same way, but with Tris-HCl at pH 6.8.

2.4.2 - Staining

To visualise protein on gels, several stains were used. For low abundance protein detection either the PlusOne Silver Staining Kit (Amersham) or the fluorescent SYPRO® Ruby stain (Bio-rad) were used. In most other cases, the colloidal Coomassie stain GelCode Blue (Pierce) was used. A home-prepared Coomassie

stain was also used. For this, gels were fixed (35% isopropanol, 10% acetic acid for 1 hour) and then stained with 0.15% Coomassie blue R-250 in fixative (Sigma-Aldrich) for 15 minutes. To visualise the proteins, the gels were incubated for 15 minutes in 50% ethanol, 7.5% acetic acid, 5% glycerol. To give the best image, three further 20 minute washes were conducted using 5% ethanol, 7.5% acetic acid, 5% glycerol (protocol adapted from Hartinger *et al*, 1996). Images were captured on an Epson Perfection 3200 Photo scanner in transmission mode, except for SYPRO® Ruby stained gels, in which case the Typhoon™ variable mode imager (GE Healthcare) or with the Gene Genius Bio Imaging System (Syngene, Ltd.) using the transilluminator mode were used.

2.4.3 - Protein Molecular Weight Estimation

To assist in molecular weight estimation, protein standard markers were run alongside samples during electrophoresis. The HiMark™ protein standard was used for Tris-acetate SDS-PAGE only, and allows more reliable calculation of higher molecular weight proteins. Mark12™ and SeeBlue® Plus2 were used on Bis-tris gels, using either MES or MOPS buffers. Figure 2.4 demonstrates how these markers look after staining. TotalLab software (Nonlinear Dynamics, UK) was used to calculate molecular mass of sample proteins, by interpolation of Rf values compared with standards. Log-linear interpolation was used for each, except when HiMark was used to estimate molecular weight. In these cases the Invitrogen HiMark MW calculator was used (Excel file downloadable from www.invitrogen.com).

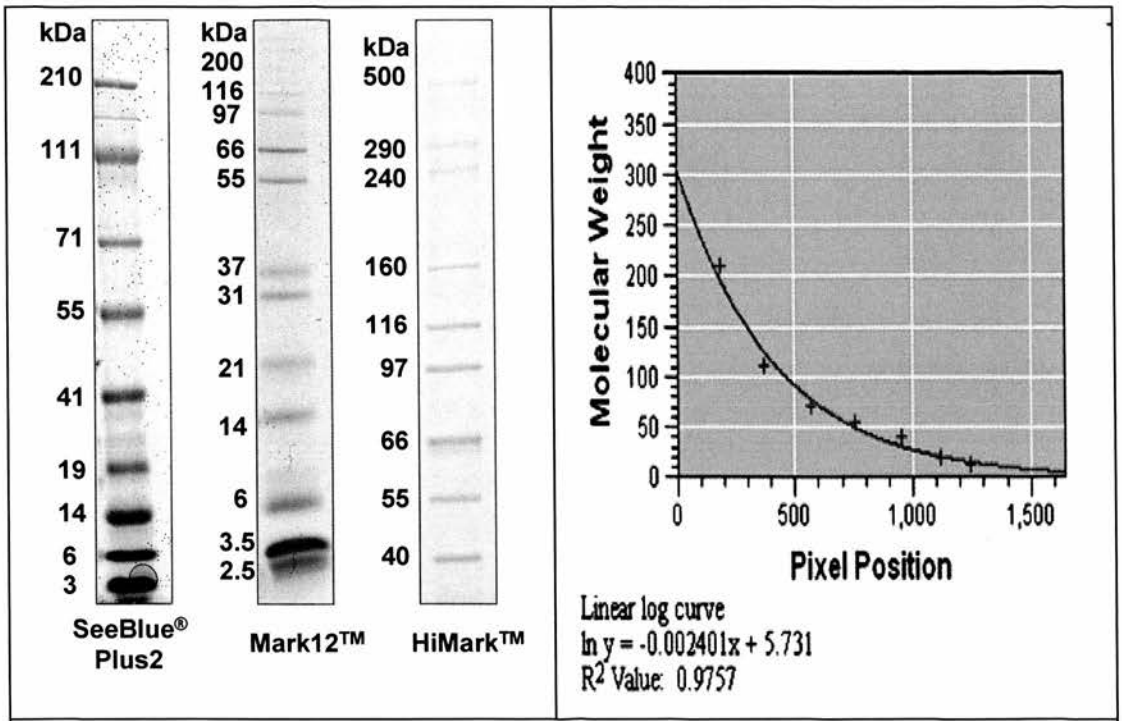

Figure 2.4 –Molecular Weight Standards for SDS-PAGE Gels

The left panel demonstrates the separation of molecular weight markers using 4-12% Bis-tris gels (SeeBlue® Plus2 and Mark12™) or 3-8% Tris-acetate NuPAGE™ gels (HiMark™) and are shown after staining with GelCode Blue (Pierce). The right panel shows an example of a log-linear curve fit to the SeeBlue® Plus2 protein ladder obtained using TotalLab software.

2.4.4 - Western Blotting

Western blotting (or immunoblotting) involves transferring proteins from a gel matrix onto an inert platform such as nitrocellulose or polyvinylidene fluoride (PVDF). After this, antibodies are used to detect proteins of interest. With the use of chemiluminescent reagents, specific proteins can be detected by exposure of photographic film to these light producing chemicals. The general protocol for blotting is described, with a list of antibodies used given in Table 2.3. Proteins separated by SDS-PAGE were transferred onto 0.45μm pore size Invitrogen nitrocellulose or PVDF, using the XCell II™ Blot Module in the XCell *SureLock*™ electrophoresis module from Invitrogen. Transfer was conducted at 30V (constant)

for 1.5 hours with Invitrogen transfer buffer, containing a proprietary antioxidant and 0.05% SDS. After transfer, membranes were blocked for 1 hour with 5% non-specific protein in Tris-buffered saline (40 mM Tris base, 270 mM NaCl, pH 7.6) with 0.1% Tween 20 (TBS-T). In most cases, the protein used was milk (Marvel). However, some antibodies will not bind their targets in this mix and so bovine serum albumin (BSA, fraction V, Merck) would be used in these instances. Primary antibody was added and the blots were incubated at room temperature for 1 hour or overnight at 4°C, with gentle rocking. These were washed three times in TBS-T, before an hour-long incubation with horseradish peroxidase-conjugated secondary antibody (in 5% protein, TBS-T). After final washes, the blots were treated with Enhanced Chemiluminescence (ECL) or ECLplus reagents (GE Healthcare Life Sciences). Amersham Hyperfilm™ ECL™ (GE Healthcare Life Sciences) was placed onto the membranes in a light-proof cassette and then developed in the Konica SRX-101A X-ray processor. In order to estimate molecular mass of proteins on western blots, special protein standards are required. The Biotinylated Protein Ladder from Cell Signalling Technology and MagicMark™ XP Western Protein Standard from Invitrogen were used. Figure 2.5 shows how these markers look on a photographic film after chemiluminescent detection.

2.4.5 - Western blot analysis

Photographic images were scanned on transparency mode using the Epson Perfection 3200 Photo scanner and analysed using TotalLab image analysis software (Nonlinear Dynamics, UK). This software allows calculation of molecular mass (by

extrapolation from protein standards) as well as background subtraction and quantitation of detected bands.

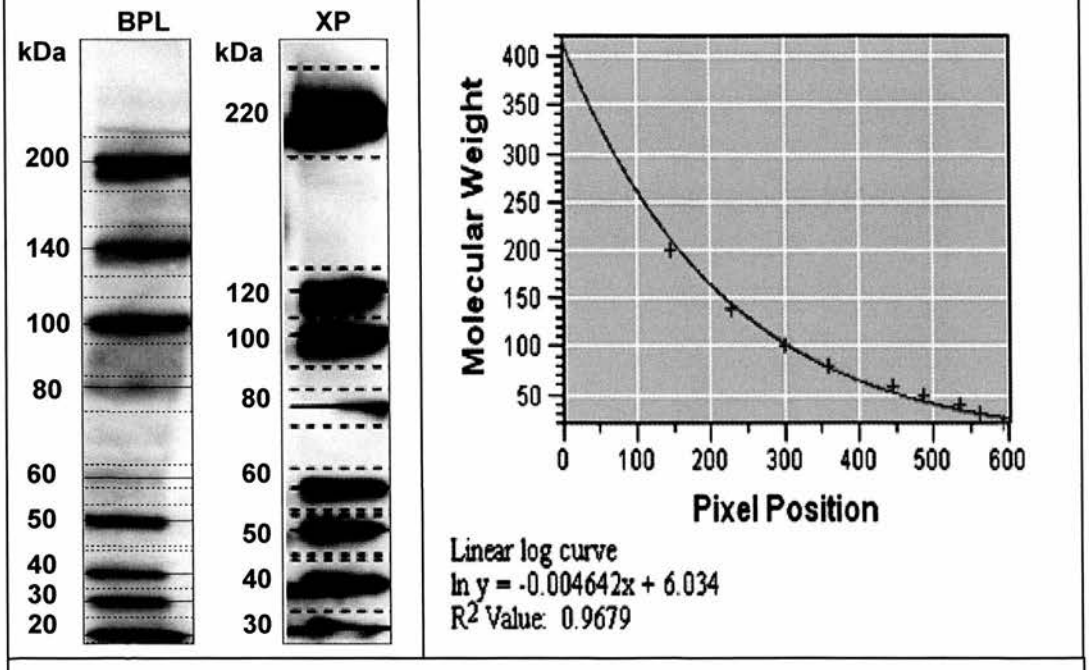

Figure 2.5 – Molecular weight standards used for western blotting

The left panel shows chemiluminescent detection of a biotinylated protein ladder (BPL) from Cell Signaling Technology and the MagicMark™ XP ladder from Invitrogen (XP) separated on 3-8% Tris-acetate gels. The right panel shows an example of curve fitting using TotalLab software to the BPL molecular weight standards after separation on a 3-8% Tris-acetate gel.

Antibody Name	Target	Source	Block	Immunoblot Dilution
T4	NKCC1 and NKCC2 C-terminus	Hybridoma Bank	5% milk	1 in 4000
N1	NKCC1 N-terminus	CovalAb	5% milk	1 in 4000
Anti-NKCC2	NKCC2 C-terminus	Alpha Diagnostic	5% BSA	1 in 1000
Anti-NKCC2	NKCC2-N-terminus	Gifted from Knepper, USA	5% milk	1 in 4000
IVF12	Band 3 erythrocyte anion exchanger	Hybridoma Bank	5% milk	1 in 4000
SPAK	SPAK	Gifted from Alessi, Dundee	10% milk	1 in 48
SPAK-P	Phosphorylated SPAK	Gifted from Alessi, Dundee	10% milk	1 in 100
Anti-PP1	Protein phosphatase 1	Upstate Biotechnology	5% milk	1 in 1000
Mouse monoclonal anti-phosphothreonine	Phosphorylated threonine	Cell Signalling Technology	5% BSA	1 in 2000
Rabbit polyclonal anti-phosphothreonine	Phosphorylated threonine	Cell Signalling Technology	5% BSA	1 in 2000
Monoclonal Mouse anti-phosphotyrosine (cocktail)	Phosphorylated tyrosine monoclonal PY-7E1 and PY20 antibodies	Zymed Laboratories	5% BSA	1 in 500
NKCC-P	NKCC phosphorylated on T^{203}, T^{207} and T^{212}	Gifted from Alessi, Dundee	10% milk	1 in 300
R5	NKCC phosphorylated on T^{212} and T^{217}	Gifted from Forbush, USA	5% milk	1 in 5000
Goat anti-rabbit	Rabbit IgG	Jackson ImmunoResearch Laboratories, Inc.	5% milk	1 in 10000
Goat anti-mouse	Mouse IgG	Jackson ImmunoResearch Laboratories, Inc.	5% milk	1 in 10000
Goat anti-sheep	Sheep IgG	Upstate Biotechnology	5% milk	1 in 1500

Table 2.3 – Antibodies used in western blot

Primary and secondary antibodies are shown here, with their western blot dilutions. Block refers to the solution the antibody and blot membrane are incubated in during the procedure. Threonine phosphorylated residues are numbered from human NKCC1.

2.5 - Two-Dimensional Electrophoresis (2-DE)

Two-dimensional electrophoresis involves separation of proteins by one method, then a second separation using another. The most common approach is to first separate proteins based on their isoelectric point (pI) by isoelectric focusing (IEF), and then to separate these by size, using SDS-PAGE. Often, sample fractionation procedures can greatly improve the final picture, by reducing sample complexity. Liquid-phase IEF can be performed using the Invitrogen ZOOM® IEF Fractionator, and allows collection of proteins within a given pH range. Another approach is to separate protein complexes by native PAGE. Followed by SDS-PAGE, the individual proteins within these complexes can be resolved. These different methods are described individually.

2.5.1 - IEF and SDS-PAGE

An IEF/SDS-PAGE 2-DE protocol was already developed in our laboratory derived from "2-D Electrophoresis using immobilized pH gradients: Principles and Methods", which is an Amersham Biosciences publication. The starting protocol is given, with adaptations listed in Table 2.4. The adaptations made to this protocol are described in chapter 3.

2.5.1.1 - Sample Preparation

Erythrocyte membrane samples were spun at 100,000 x *g* for 15 minutes (at 4°C) in order to pellet membranes from any solution. After removal of supernatant, the pellet was resuspended in 140µl rehydration solution (7 M urea, 2 M thiourea, 1%

IPG buffer (Immobilised pH Gradient; Amersham), 0.5% ASB 16, 4% CHAPS, 1% NP 40, 1 mM EDTA, and trace bromophenol blue) containing 5 mM iodoacetamide and 2% protease inhibitor cocktail III in order to block the actions of proteases. Proteins were solubilised by 30 minute incubation at room temperature. DTT was

Change to Protocol	Rationale
Reduced IEF sample volume from 140µl to 125µl	Protocol exceeded maximum volume capacity of IPG strip
Reduced protein content of IEF sample to maximum of 100µg	Maximum protein recommended for 7cm IPG strip Protein overload can cause precipitation in IPG strip
Altered detergent composition of solubilisation/rehydration solution	To improve solubilisation of membrane proteins
Addition of Tris base to IEF sample solution	For full range protein solubilisation
ZOOM® fractionation (liquid phase IEF) of sample prior to 2-DE	To concentrate and simplify protein sample to allow better chance of finding Na-K-2Cl cotransporter

Table 2.4 – Adaptations to Isoelectric Focusing Protocol
These changes were made to the standard IEF protocol given and then the resultant 2D picture compared to the original.

added to give a final concentration of 160 mM and incubated at room temperature for

a further 60 minutes. Remaining insoluble material was removed by centrifugation at 14,000 x *g* for 10 minutes and the supernatant taken for isoelectric focusing.

2.5.1.2 - First Dimension Isoelectric Focusing

Samples were loaded onto ceramic strip holders (Amersham) and any bubbles removed. Amersham pH 4-7 Immobiline DryStrips were gently placed on top of the protein samples and then covered with Immobiline DryStrip cover fluid (Amersham). IEF was performed with the IPGphor unit (Pharmacia Biotech) using the following parameters: 30 minutes with no voltage (rehydration), 50V step for 12 hours (active rehydration), the voltage was then increased to 2000V over 4 hours, and then stepped up to 4000V step for 6 hours. The first 12.5 hours are to allow sample entry to the strip, and are conducted at low voltage to prevent aggregation. The first gradient allows a more gentle start to the focusing process, which is followed by the step-and-hold high voltage. This allows the proteins to reach their isoelectric point and prevents diffusion from this.

2.5.1.3 - Equilibration

At the end of the isoelectric focussing period, strips were carefully removed from their holders and immersed in equilibration buffer (6 M urea, 4% SDS, 30% glycerol, 50 mM Tris-HCl pH 6.8) to remove the DryStrip cover fluid, and gently rocked at room temperature in equilibration buffer containing 50 mM DTT for 45 minutes (to reduce cysteine residues). This step was repeated with fresh buffer and DTT for 30 minutes. The strips were then washed in equilibration buffer with 150 mM iodoacetamide by gentle rocking for 15 minutes (to alkylate reduced cysteine residues). The equilibration buffer was pre-warmed (60˚C) before adding the strips

and then allowed to cool to room temperature during the various incubations. Strips were cut to fit the second dimension gel loading well.

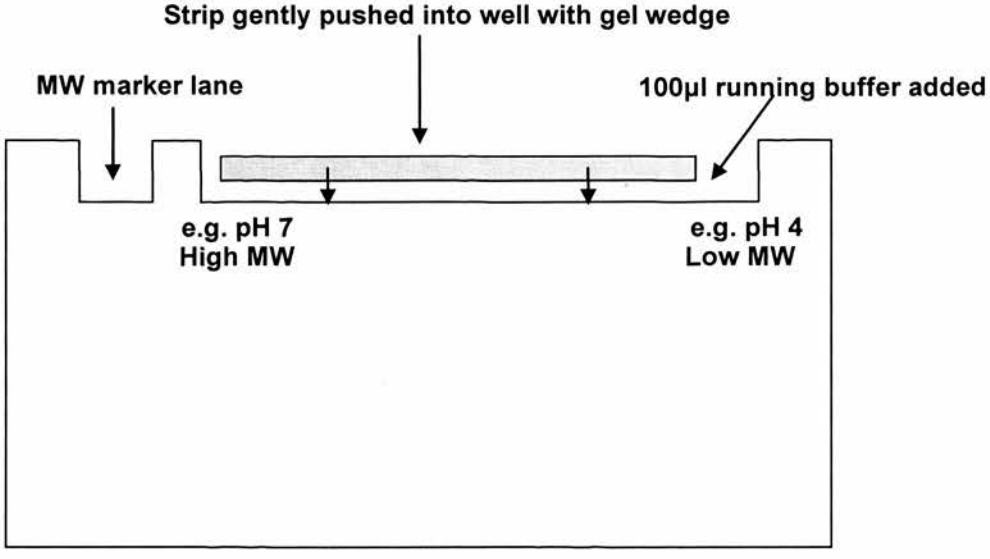

Figure 2.6 – Diagram representing the layout of the second dimension SDS gel The IEF gel (or native gel) is placed into the sample well and gently pushed down to make contact with the SDS gel at all points. The presence of the running buffer allows easier movement of the gel strip. Gentle pushing onto the top of the gel helps to remove bubbles. This ensures the current flows through properly and gives a greater chance that the proteins in the strip enter the SDS gel. Strips were always loaded with the high MW or high pH end next to the marker lane to allow easier comparison of gels.

2.5.1.4 - Second Dimension SDS-PAGE

Equilibrated IEF strips were loaded onto NuPAGE™ mini-gels or home-cast 14 x 14cm gels, as depicted in Figure 2.6. Running buffer appropriate to the NuPAGE™ gel used (see Table 2.2) was then added to the anode tank and molecular weight markers were loaded. Only then was the cathode tank filled. Regardless of the gel type, electrophoresis was conducted at 20mA for 20 minutes, then at 40mA until the dye front had reached the bottom of the gel. The lower voltage at the start of the run

was to assist in the transition of proteins from the IEF strip to the separating gel. After electrophoresis, the gels would be stained or processed for western blot.

2.5.2 - ZOOM® IEF

This involves fractionation of protein samples using liquid-phase isoelectric focusing, which allows separation of proteins into a discrete pH range and maximises the amount of total protein that can be applied to narrow range IPG strips (Zuo and Speicher, 2000). Membrane protein samples were prepared by solubilisation (30 minutes, RT) in IEF denaturant (7 M urea, 2 M thiourea, 3% CHAPS, 1% NP-40, 1% ASB-16, 1 mM EDTA), 2% protease inhibitor cocktail, 20 mM DTT and 10 mM Tris (all concentrations are for the final mix). The detergent concentrations for this protocol were adapted from information supplied with the kit and as such differ slightly from the IEF solubilisation buffer presented in section 2.5.1.1. N,N-Dimethylacrylamide (DMA) was added (to give approximately 50% final concentration) and incubated at room temperature for 30 minutes. To quench, DTT (20 mM final concentration) was added and the sample incubated for 5 minutes (RT). The reduced and alkylated lysate was centrifuged at 14,000 x *g* for 20 minutes (RT) and an aliquot of the supernatant removed for protein concentration determination. The remaining supernatant could then be prepared for ZOOM fractionation, by addition of DTT (10 mM), ZOOM® Carrier Ampholytes, pH 3-10 (Invitrogen) and dH_2O. A trace amount of bromophenol blue was also added. Five samples were prepared, giving one for each sample chamber. Figure 2.7 shows a representation of the ZOOM® IEF Fractionator kit. Fractionation was at 100V for 20 minutes, 200V for 80 minutes and then 600V for 80 minutes, as recommended by the manufacturer (Invitrogen). Samples were easily collected from the chambers for further study. By

addition of the appropriate IPG buffer (Amersham) these can be used directly for gel based IEF, which was conducted using 7cm Immobiline DryStrips of single pH units (e.g. pH 5.3-6.3). For one-dimensional SDS-PAGE and immunoblot applications, the proteins were first precipitated from the mix (using the SDS-PAGE Clean-Up Kit from Amersham) and then prepared for 1-D SDS-PAGE as previously described in section 2.4.1.

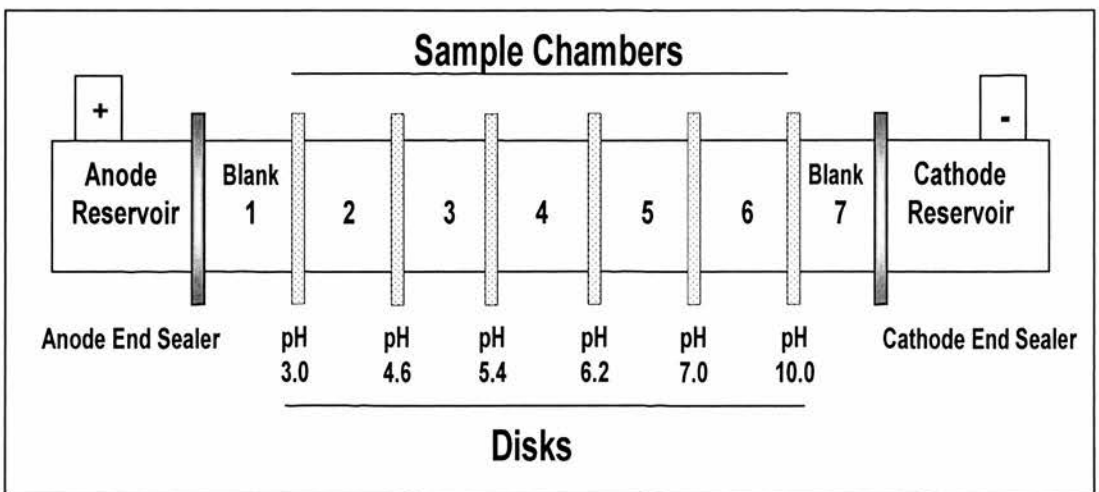

Figure 2.7 – Representation of the ZOOM IEF Fractionator
Solubilised protein samples are added to the sample chambers, which are separated by pH disks. When the current is applied the proteins migrate through the chambers until they reach their isoelectric point. They then will not pass beyond a particular pH cut-off. After electrophoresis, the samples can be recovered and used in downstream applications.

2.5.3 - Blue-Native Polyacrylamide Gel Electrophoresis (BN-PAGE)

This form of electrophoresis maintains the native state of proteins allowing separation of non-denatured proteins and the complexes they may be in with other proteins. Coomassie G-250 is used to bind and charge the proteins for electrophoresis. The Invitrogen NativePAGE™ system was used which was adapted from work by Schägger and von Jagow (1991). There are several advantages to

using this system. Firstly, gels are bought pre-cast which reduces user error. Secondly, the gels are Bis-tris rather than Tris-glycine. This allows the experiment to be conducted at near neutral pH, which increases protein complex stability and resolution (Invitrogen, 2006). Erythroctye cell membranes (200μg) were gently mixed with NativePAGE™ sample buffer (Invitrogen) and 2% dodecylmaltoside (Fluka) and incubated on ice for 15 minutes. After centrifugation at 20,000 x *g* for 30 minutes (4°C), the soluble protein supernatant was mixed with NativePAGE™ G-250 sample additive (Invitrogen) to give a final G-250 concentration of 0.5%. Pre-cast 3-12% NativePAGE™ Bis-tris gels were loaded with sample, alongside High MW Calibration Kit for Native Electrophoresis (Amersham) standards. The cathode chamber was filled with NativePAGE™ running buffer that was mixed NativePAGE™ Cathode additive. This gives a buffer with 0.02% G-250 included. The anode chamber was filled with NativePAGE™ running buffer with no G-250 added. Electrophoresis was at 150V constant. Once the dye front had run into the first third of the gel, the cathode buffer was exchanged for buffer that contained only 0.002% G-250. Electrophoresis then continued until the free dye had run off the bottom of the gel. Bands were excised and digested with Promega sequencing grade trypsin (for HPLC-MS as described in section 2.7.2), western blotting was conducted (described in section 2.4.1) or entire lanes were excised and prepared for second dimension SDS-PAGE. This was achieved by several incubations at room temperature. Sample reduction was by 20 minute incubation in Invitrogen LDS sample buffer plus 50 mM DTT. Alkylation was as above but with LDS sample buffer plus 50 mM DMA. Finally, this reaction was quenched by 15 minute incubation in LDS buffer, 20% ethanol and 5 mM DTT. Sample lanes were layered

onto the sample well of an SDS gel (see figure 2.6) and electrophoresis was conducted as relevant to the composition of the gel and buffer type (e.g. Tris-acetate or Bis-tris; see Table 2.2).

2.6 - Immunoprecipitation

To isolate the cotransporter for further study, protein was immunoprecipitated using T4 and N1 antibodies. Two variations of the same protocol were used, which was followed from Matskevich *et al* (2005). SDS-denaturation of samples was required when using T4 monoclonal antibody (Hybridoma Bank, Iowa) as the antibody was raised to denatured antigen (Lytle *et al*, 1995). N1 does not require this step. This antibody was raised in rabbits for us by CovalAb (France) and the testing of the efficacy of this antibody in western blot and immunoprecipitation experiments is described in Chapter 3. Membrane samples (150μg) were incubated at 60°C for 20 minutes in the presence of 1% SDS (only when T4 antibody used). Samples were diluted 5-fold with IP buffer (150 mM NaCl, 20 mM HEPES, 1 mM EDTA, 2 mM Na pyrophosphate) with 0.5% ASB-16, 1% Triton X-100, 1 mM Na vanadate, 1 μM Microcystin-LR and 2% protease inhibitor cocktail and incubated at 4°C for 1 hour, with end-over-end mixing. Insoluble material was removed by centrifugation (14,000 x *g*, 10 min) and the supernatant pre-cleared with 20μl 50% Protein G-sepharose 4 Fast Flow (Amersham) for 1 hour at 4°C. The protein G-sepharose was prepared by 1:1 dilution with IP buffer, plus 0.5% ASB-16 and 1% Triton X-100. Pre-cleared supernatants were incubated with antibody for 1 hour at 4°C, then incubated (1 hour, 4°C) with 10μl 50% Protein G-sepharose in a fresh sample tube. Beads were spun out and washed three times with IP wash buffer. Proteins were

eluted by incubating beads at 70°C with LDS sample buffer (Invitrogen) and 100 mM DTT. The supernatants were removed for SDS-PAGE (as in section 2.4.1).

2.7 - Mass Spectrometry

After electrophoretic separation and protein detection, by staining or western blotting, mass spectrometric methods were used for identification and/or verification of protein species. This involves proteolytic digestion, mass spectrometry to generate a peptide spectrum and database searching to match these peptides against theoretical digests of known proteins. This process is called peptide mass fingerprinting. Alternatively, sequence data may be obtained by tandem mass spectrometry which can be used to match known proteins to the sample. Two different mass spectrometric methods were used during this project and are described separately.

2.7.1 - Matrix-Assisted Laser Desorption Ionisation Time-of-Flight (MALDI-TOF) Mass Spectrometry

MALDI involves the ionisation of peptides from a matrix platform after bombardment with a laser. These are accelerated by high voltage, and then allowed to travel along a flight tube. Smaller peptides travel faster than larger ones, and the time taken to fly is measured by a high speed detector. The steps involved in this method are described separately.

2.7.1.1 - Trypsin Digestion

Following a protocol provided by the Edinburgh Protein Interaction Centre (EPIC, www.epic.ed.ac.uk), bands (from 1-D gels) or spots (from 2-D gels) were excised from gels using a sterile scalpel and transferred to autoclaved 1.5ml microfuge tubes.

Gel pieces were incubated at 30˚C with 200 mM ammonium bicarbonate (ABC)/50% acetonitrile (ACN; Rathburn) for 30 minutes. This step was repeated twice more with fresh solutions, with the liquid being drawn off by pipette between steps. Reduction, by 60 minutes at 30˚C in 20 mM DTT/200 mM ABC/50% ACN, was followed by three wash steps in 200 mM ABC/50% ACN. Alkylation of cysteine residues was achieved by incubation for 20 minutes (RT) in 50 mM iodoacetamide/200 mM ABC/50% ACN. The samples were wrapped in foil at this stage to ensure the reaction occurred in the dark. Gel chips were washed three times with 20 mM ABC/50% ACN and then cut into smaller pieces using a sterile scalpel. Any remaining liquid was removed by pipette after 2 minutes centrifugation at 13,000 x *g*. Gel pieces were covered with ACN, left for a few minutes to turn white in colour, after which time the ACN was removed and the samples air dried for 5 minutes under a light source. The gel chips were rehydrated with 50 mM ABC containing sequencing grade modified trypsin (Promega; 1U per gel piece) for 30 minutes at 4˚C, after which time more enzyme solution was added if required (enough to cover gel). All tubes were wrapped in Parafilm (Pechiney Plastic Packaging) and incubated for 16-24 hours at 32˚C, to allow digestion of proteins to occur. Gel spots from 2-dimensional gels were prepared in the same way, with the alkylation and reduction steps omitted, as this is conducted during IEF strip equilibration prior to SDS-PAGE. Spots from silver stained gels were first covered with a solution of 30 mM potassium ferricyanide and 100 mM sodium thiosulphate until the gel pieces were clear (according to Gharahdaghi *et al*, 1999). These were washed in 200 mM ABC and then treated like other samples. Before spotting onto the MALDI target, samples were desalted and concentrated using C_{18} ZipTip®

pipette tips (Millipore). The specifications of these are: resin - silica, 15 μm, 200 Å pore size, and volume - 10μl pipette tip with 0.6μl resin bed volume. ZipTips act like chromatography columns, allowing trapping of peptides, washing to desalt, and then elution in a solvent that is compatible with MALDI-TOF.

2.7.1.2 - Matrix Preparation

Approximately 1mg of α-cyano-4-hydroxy-cinnaminic acid was added to a microfuge tube and mixed with the following: 400μl 0.1% TFA in H_2O, 100μl 3% TFA in H_2O, and finally 500μl 0.1% TFA in ACN. After each addition, the sample was vortexed for 1 minute and finally centrifuged for 2 minutes at 14,000 x *g*. A visible yellow matrix pellet was always seen and indicated a desirable saturated solution.

2.7.1.3 - Preparation of MALDI Plate

A 96 well x2 MALDI target plate (PerSeptive Biosystems) was used. A small amount of trypsin digest sample (0.5μl) was spotted onto the plate and then 0.5μl of saturated matrix solution was gently spotted on top of this. All samples on the plate were left to dry before analysis.

2.7.1.4 - MALDI-TOF

The Voyager™-DE STR Biospectrometry™ Workstation (PerSeptive Biosystems, Inc, Framingham, MA, USA) was controlled via computer using the Voyager Instrument Control Panel. The instrument settings were as follows: reflective mode, manual instrument mode, acceleration voltage 20,000V, and spectrum acquisition delay of 150-225nsec. The laser intensity was around 2100V (but was varied to

improve spectra when necessary) and was set to fire 300 (also variable) laser shots. Data was collected within the 800-3500Da mass range.

2.7.1.5 – Spectrum Processing and Database Interrogation

Applied Biosystem's Data Explorer software was used to prepare the mass spectra for database interrogation. This involves advanced baseline correction, noise filtering, de-isotoping and mass calibration to an internal standard. Mass calibration was achieved by using the auto-digested peptide masses of trypsin. Mass lists generated from this program were used to search both MASCOT and MS-FIT peptide mass fingerprinting search engines (www.matrixscience.com and prospector.ucsf.edu respectively).

2.7.2 - High Performance Liquid Chromatography (HPLC) on-line with Electrospray Ionisation (ESI) Ion Trap Mass Spectrometry

HPLC collects peptides, desalts and concentrates them, before eluting them directly to a mass spectrometer. In this case, an electrospray-ion trap mass spectrometer was used. The HPLC passes the eluted peptides to the mass spectrometer via the electrospray needle, which has a charge applied to it. A fine spray of highly charged droplets (at the same polarity as the needle) is forced from the needle to the mass spectrometer inlet. Dry gas (N_2) and heat cause the solvent droplets to evaporate and as they lose size, the surface tension can no longer withstand the charge. The droplets then "explode" to form smaller droplets and multiply charged analyte molecules. The analytes enter the mass spectrometer and are trapped by a 3-D electric field. The voltages across these are variable creating a field within that traps the ions in a stable oscillating trajectory. Changing these fields causes the ions to eject in order of increasing mass/charge ratio, which are detected to produce a mass

spectrum (Mann *et al*, 2001). The ion trap MS allows multiple stages of mass spectrometry, giving sequence detail about the analytes. The HPLC system consists of a FAMOS™ well plate autosampler, Switchos™ II advanced microcolumn switching unit for automated sample preparation, and the UltiMate™ integrated micro-, capillary-, and nano-HPLC. This is coupled to a Finnigan LCQ Deca ion trap mass spectrometer (Thermo Electron Corporation). Figure 2.8 shows the experimental set-up used in this project. Peptide samples (prepared as for MALDI-TOF) were spun (16,000 x *g*) through a Microcon centrifugal filter unit (0.22µm) (Millipore, USA) to ensure no particulate matter remained in the sample, and the resulting liquid added to a loading vial on the autosampler. The HPLC is controlled by Chromeleon software (Dionex) and is fully automated. Briefly, the enzymatic peptides are drawn up by a needle in the Famos unit, desalted and concentrated on a trapping column in the Switchos module (flow rate of 0.030ml/min), and then eluted onto a PepMAP C18 reverse phase column (3µm particle size; 75µm internal diameter x 15cm length; LC Packings), at a flow rate of 0.200µl/min. The peptides are loaded in the high aqueous phase (solution A - 0.1% formic acid in H_2O) and eluted with a linear gradient of 0-90% solvent B (0.09% formic acid in 100% acetonitrile) over 45 minutes. Peptide elution from the column is monitored by absorbance at 214nm by the UltiMate UV detector. Ionisation and mass measurement is performed by the ESI-MS and the RAW data files managed by Xcalibur software (Thermo Electron Corporation). These are converted to DTA mass list files (using Sequest, distributed by Thermo Finnigan) and compiled before submission to MASCOT (www.matrixscience.com) or Phenyx MS/MS (www.phenyx-ms.com) search engines.

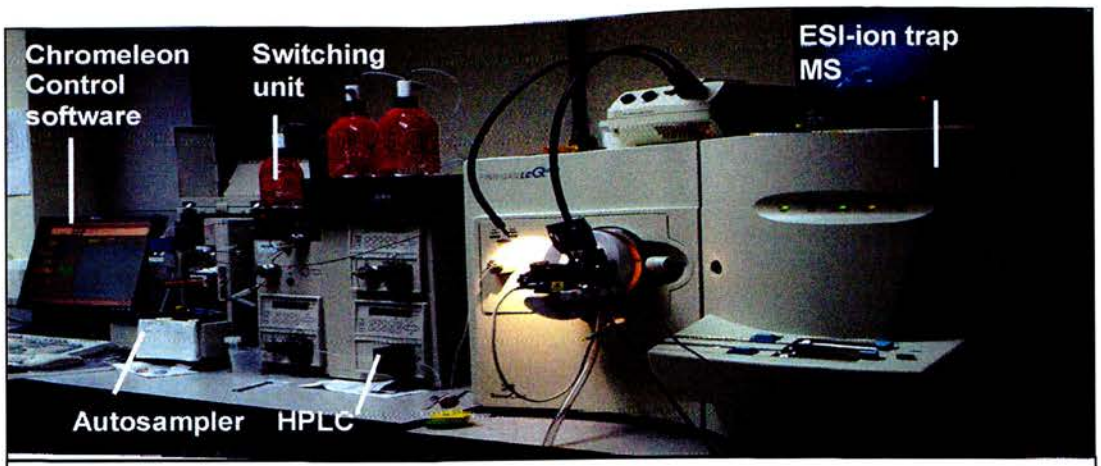

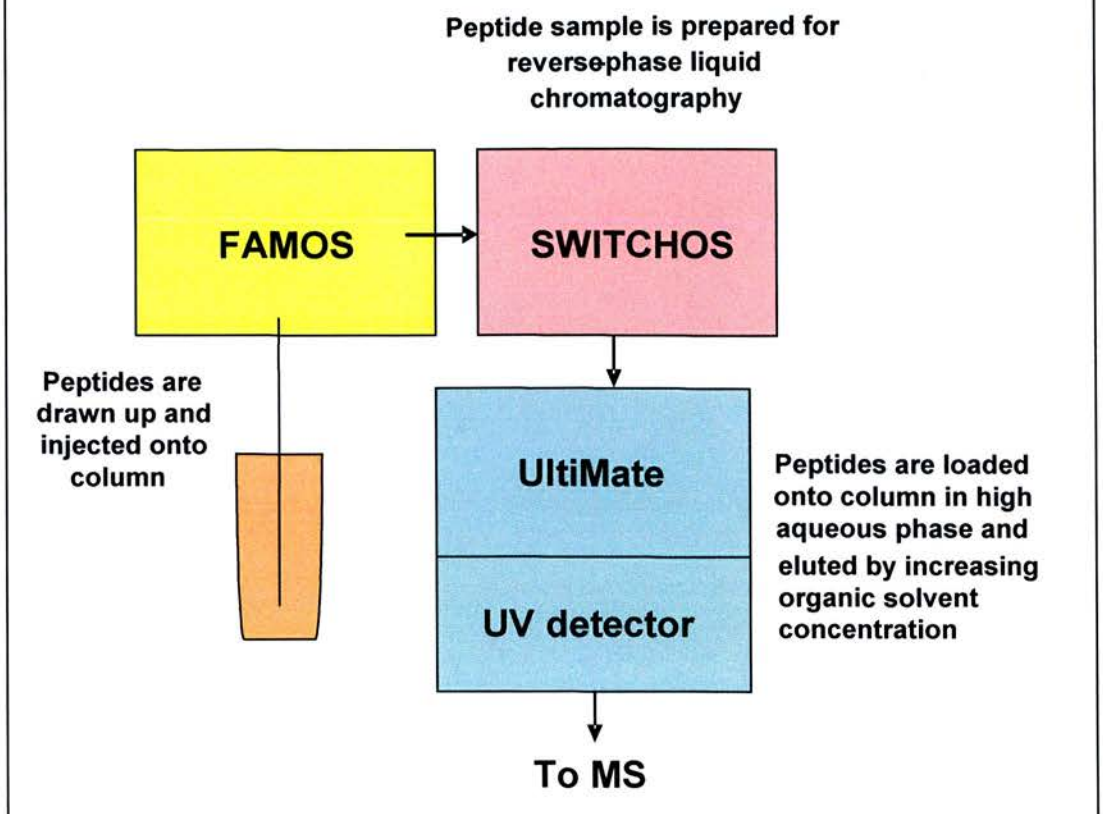

Figure 2.8 -The HPLC-MS Station and Depiction of Sample Flow During High Performance Liquid Chromatography

The upper panel shows the equipment used and the lower panel describes the flow of samples through the LC unit, comprising of the autosampler, the switching unit and the chromatography column.

2.8 – Deglycosylation of Proteins

The cotransporter band appears as a fairly broad smear on a western blot. NKCC proteins are potentially glycosylated, which may be the cause of this phenomenon. To test this, red blood cell membranes were heated at 60°C for 20 minutes with SDS at 1%, then diluted to give 0.2% SDS with the following mix: deglycosylation buffer (150 mM NaCl, 20 mM HEPES, 1 mM EDTA, pH 7.44), 1% CHAPS, 1% Triton X-100, 10 mM EDTA and 2% protease inhibitor cocktail, with 1% β-mercaptoethanol. An hour-long incubation at 4°C, with end-over-end mixing, prepared the samples for deglycosylation. Recombinant N-glycosidase F (Roche) was added and the samples incubated at 37°C overnight. SDS-denaturation was required to expose the sites for the enzyme to act upon. It did need to be diluted, however, so as not to denature the enzyme itself. Aliquots were removed and prepared for SDS-PAGE using the NuPAGE™ system, then transferred to nitrocellulose for western blotting.

2.9 – Reverse-Transcription Polymerase Chain Reaction (RT-PCR)

This technique allows amplification of messenger ribonucleic acid (mRNA) by use of a reverse transcription reaction followed by polymerase chain reaction. First, complementary deoxyribonucleic acid (cDNA) is generated from mRNA using deoxynucleotide triphosphates (dNTPs) and a reverse transcriptase enzyme. This cDNA is used as a template in the PCR, where specific DNA fragments are amplified using the appropriate DNA primers and the thermostable enzyme, Taq polymerase.

2.9.1 - Primer Design

Rat, human and mouse NKCC1 and NKCC2 cDNA (from mRNA) sequences were obtained from the Entrez nucleotide database from the National Center for

Biotechnology (NCBI) website (www.ncbi.nlm.nih.gov). Accession numbers are shown in the table 2.5. The cDNA sequences were aligned using ClustalW, a multiple sequence alignment tool, obtained from the European Bioinformatics Institute (EBI) website (www.ebi.ac.uk). A list of non-identical regions (exclusion list) was generated. Primer 3, a tool that picks primers from a given DNA sequence (http://frodo.wi.mit.edu/cgi-bin/primer3/primer3_www.cgi), was used to generate primer sets. The exclusion list was included to ensure that the chosen primers would only detect regions common to the three species (human, rat and mouse in this case).

Species	NKCC1	NKCC2
Rat (*Rattus norvegicus*)	NM_031798	NM_019134
Human (*Homo sapiens*)	U30246	NM_000338
Mouse (*Mus musculus*)	NM_009194	U20973

Table 2.5 – Accession numbers from NCBI database used for PCR primer design

Primer sets were chosen (see Table 2.6) for both NKCC1 and 2 and produced by Invitrogen on request. Nucleotide-nucleotide BLAST searches (using tool from www.ncbi.nlm.nih.gov/BLAST) revealed that the primers chosen matched sequence in cDNA from a number of mammalian species, suggesting that these would be good candidates for detection of NKCC isoforms in different animal species. The sequences that are amplified by these primers are shown in Appendix I, with details of exon-exon boundaries. Primers were also generated for human and rat β-actin using the Invitrogen OligoPerfect™ Designer application available from www.invitrogen.com and shown alongside the NKCC1 and 2 primers in table 2.6.

2.9.2 - RNA Isolation

Two different kits were used to isolate RNA, with similar results. The Qiagen RNeasy® kit and Invitrogen's PureLink™ Micro-to-Midi Total RNA Purification

System were used following the protocols supplied. Both kits use spin-cup columns, containing silica membranes that bind RNA. Cell or tissue lysates were added to these, washed and the RNA eluted with nuclease-free water (supplied with kits). The absorbance ratio (A_{260}/A_{280}) was determined to assess sample purity and yield as described in section 2.1.2.

Primer Name	Sequence 5' to 3'	Product Size
NKCC1 forward	GAAGAAAGTACTCCAACCAGAGATG	237
NKCC1 reverse	TATTGCTGAAGTAGACAATCCTGTG	
NKCC2 forward	CTCTTCATTCGCCTCTCCTG	455
NKCC2 reverse	ATGACAGTTCCAATGAAGAAGTTTG	
β-actin human forward	GGACTTCGAGCAGCAAGAGATGG	234
β-actin human reverse	AGCACTGTGTTGGCGTACAG	
β-actin rat forward	GTCGTACCACTGGCATTGTG	181
β-actin rat reverse	CTCTCAGCTGTGGTGAA	

Table 2.6 – NKCC 1, NKCC2 and β-actin primer sequences

2.9.3 - Reverse Transcription

ImProm^{TM}-II reverse transcriptase was used to generate cDNA from RNA, following the instructions given by the manufacturer (Promega). Up to 1μg of total RNA was present in each first-strand reaction. Oligo dTs (15 thymine bases; Promega) were used to act as primers for the poly-adenine tails found on mRNA molecules.

2.9.4 - PCR

Promega Master Mix was chosen for PCR, as it contains all the necessary components at optimal conditions for production of DNA products up to 2kb in size (Taq polymerase, dNTPs, buffer, and $MgCl_2$) except primers and DNA template. This allows easier sample preparation and reduces the risk of sample contamination,

due to reduced pipetting steps. The GeneAmp® PCR System 9700 (Applied Biosystems) thermal cycler was used in all cases. The conditions for the different primer sets are shown in table 2.7.

NKCC1 and NKCC2	β-actin
Start 94°C 3 minutes	**Start 94°C 3 minutes**
Denaturation 94°C 30s **Annealing 53°C 30s** **Extension 72°C 45s** } **35 cycles**	**Denaturation 94°C 30s** **Annealing 60°C 30s** **Extension 72°C 45s** } **35 cycles**
Final extension 72°C 10min	**Final extension 72°C 10min**

Table 2.7 – Polymerase Chain Reaction Conditions to Amplify NKCC and Actin Products

The cDNA templates are denatured to separate the strands, the temperature lowered to allow the primers to anneal to the templates and then increased again to allow DNA polymerisation (extension).

2.9.5 - DNA Gel Electrophoresis

PCR products were run on 1% agarose (in TBE; 89 mM Tris, 89 mM Boric acid, 1 mM EDTA in Milli-Q water) gels containing SYBR® Safe DNA gel stain (Invitrogen). DNA was mixed with loading dye (Fermentas) and electrophoresis was for 30 minutes at 180V. Base pair markers were run alongside (GeneRuler™ 100bp DNA ladder, Fermentas). Gels were visualised with the Gene Genius Bio Imaging System (Syngene, Ltd.). TotalLab software was used to interpolate PCR product size, by comparison to the base pair markers.

2.10 – Materials

The following comprises supplier details for all materials not already stated in the previous methods sections.

Sigma-Aldrich

Common name or abbreviation	Alternative Name
ABC	Ammonium bicarbonate
Arsenite	Sodium arsenite
Brilliant Blue G-250	Acid blue 90
Brilliant Blue R-250	Acid Blue 83
Cinnaminic acid	α-cyano-4-hydroxy-cinnaminic acid
EDTA	Ethylenediaminetetraacetic acid
Genistein	4,5,7-Trihydroxyisoflavone
HEPES	4-(2-hydroxyethyl)-1-piperazineethanesulfonic acid
Glycine	Aminoacetic acid
B-glycerophosphate	Glycerol 2-phosphate
Tris base/Trizma base	2-Amino-2-(hydroxymethyl)-1,3-propanediol
triethanolamine	2,2′,2″-Nitrilotriethanol
Triton X-100	t-Octylphenoxypolyethoxyethanol
Tween 20	Polyoxyethylene sorbitan monolaurate
Urea	Carbamide
Vanadate	Sodium orthovanadate

Fluka (Sigma-Aldrich)

Common name or abbreviation	Alternative Name
Boric acid	
DDM	dodecylmaltoside
DMA	N,N-Dimethylacrylamide
Iodoacetamide	
TEMED	N,N,N,N -Tetramethyl-Ethylenediamine
TFA	Trifluoroacetic acid
NaF	Sodium fluoride
$Na_4P_2O_7$	Sodium pyrophosphate
Thiourea	Sulfourea

BDH Laboratory Supplies

Common name/abbreviation	Alternative Name
β-Mercaptoethanol	2-mercaptoethanol
APS	Ammonium persulphate
D-glucose	dextrose
ethanol	Ethyl alcohol
Glacial acetic acid	Ethanoic acid
glycerol	

HCl	Hydrochloric acid
K_2HPO_4	Di-potassium hydrogen orthophosphate
KH_2PO_4	Potassium dihydrogen orthophosphate
NaCl	Sodium chloride
isopropanol	propan-2-ol
SDS	Sodium dodecyl sulphate
Sucrose	

Alexis Biochemicals

Common name/abbreviation	Alternative Name
Calyculin A	
PP1/PP1i	4-amino-5-(4-methylphenyl)-7-(t-butyl) pyrazolo[3,4-d] pyrimidine
Staurosporine	Antibiotic AM-2282
Microcystin-LR	
NP-40	Polyethyleneglycol-p-isooctylphenyl ether

Calbiochem

Common name/abbreviation	Alternative Name
A23187	Calcimycin
ASB - 16	Amidosulfobetaine 16
$C_{12}E_8$	Octaethyleneglycol mono-*n*-dodecyl ether
CHAPS	3-[(3-Cholamidopropyl)dimethylammonio]-1-propanesulfonate
ASB - C6Φ	4-*n*-Hexylbenzoylamido-propyl-dimethylammoniosulfobetaine
ASB - C8Φ	4-*n*-Octylbenzoylamido-propyl-dimethylammoniosulfobetaine
ASB - C7BzO	3-(4-Heptyl)phenyl-3-hydroxy-propyl-dimethylammonio- sulfobetaine
Protease Inhibitor Cocktail Set III	AEBSF, hydrochloride (100 mM), Aprotinin (80 µM), Bestatin (5 mM), E-64 (1.5 mM), Leupeptin, hemisulfate (2 mM), Pepstatin A (1 mM)

GE Healthcare/Amersham

Common name/abbreviation	Alternative Name
Bromophenol blue	3′,3″,5′,5″-Tetrabromophenolsulfonephthalein
DTT	dithiothreitol

Chapter 3

Using Proteomic Tools to Study the Na-K-2Cl Cotransporter

Chapter 3: Using Proteomic Tools to Study the Na-K-2Cl Cotransporter

In order to obtain more information about phosphorylation on the cotransporter, 2-dimensional electrophoresis (2-DE) techniques were employed. Standardly, 2-DE is used to look at proteomes, but using isoelectric focussing (IEF) as a first dimension separation, differently phosphorylated cotransporter species should focus at distinct isoelectric points (pI); so-called "phosphorylation trains" (Carter *et al*, 2004). IEF followed by denaturing SDS-PAGE, allows visualisation of these different species. Coupled with mass spectrometry, this approach allows identification of the specific parts of the protein that are phosphorylated. There are difficulties in obtaining good separation and representation of membrane proteins on 2-DE gels, mainly due to issues with solubility in the media used for isoelectric focussing (Santoni *et al*, 2000). Improvements in the representation of membrane proteins on 2-D gels have been made, particularly with the inclusion of thiourea (Rabilloud, 1998) and using a variety of zwitterionic detergents (Chevallet *et al*, 1998), but there is still room for improvement. Alternative methods for protein separation include native-PAGE coupled with SDS-PAGE. Native-PAGE allows separation of protein complexes and following this with SDS-PAGE could help identify proteins that NKCC interacts with. Both methods are described in this chapter.

3.1 - 2D – IEF/SDS-PAGE

A protocol was devised, in the Flatman laboratory, to maximise cotransporter signal in western blot using the T4 antibody. Large sample loads were required in order to achieve this and as figure 3.1 shows this results in obscured visualisation of spots in the

upper ranges of the 2-D gel. Using this method as a start point, several features of this protocol were adapted and tested, with the aim of improving the representation and

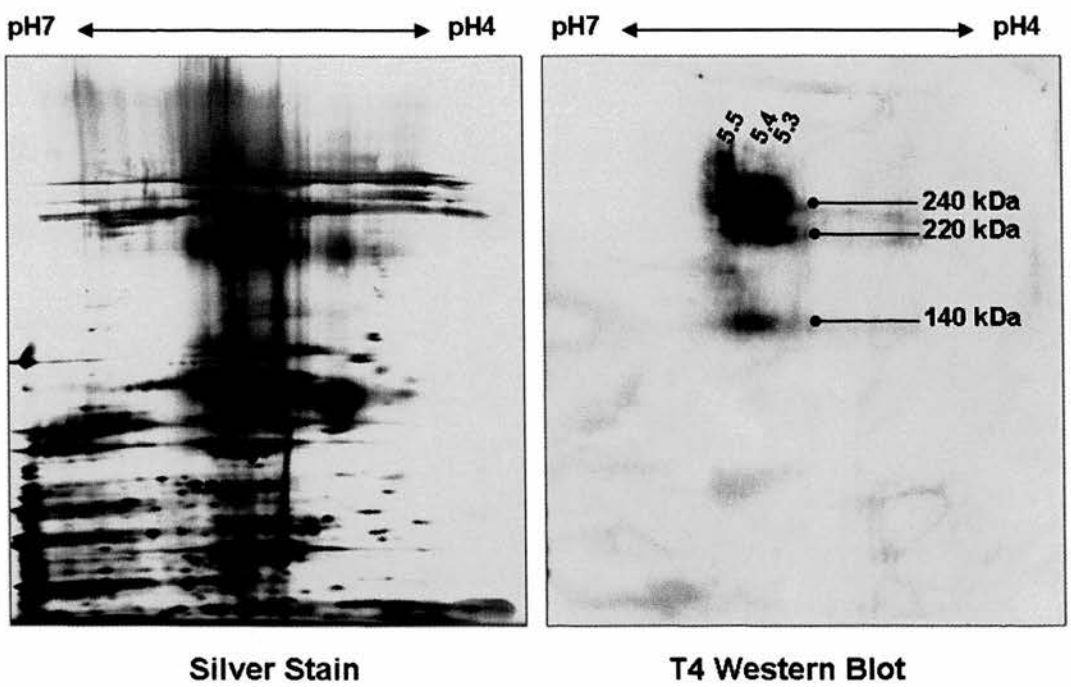

Figure 3.1 – Two-Dimensional Electrophoresis of Ferret Erythrocyte Membrane Proteins Ferret red blood cell membrane proteins were first separated by IEF (pH 4-7, 7cm strip) and then SDS-PAGE using 3-8% Tris-acetate NuPAGE™ gels. Some molecular weights are shown for reference and were interpolated from a biotinylated protein ladder (Cell Signaling Technology). Some estimated pI values are also shown.

separation of membrane proteins on 2D gels and to finally identify the cotransporter by mass spectrometry. Following the protocol, silver stained 3-8% tris-acetate mini NuPAGE gels showed fairly good separation of moderate to low molecular weight proteins (Fig 3.1). However, streaking of poorly focussed proteins masks areas of the gel where higher molecular weight species would separate. Western blotting of 2-DE separated proteins with T4 antibody showed cotransporter protein in several areas. The isoelectric points of human NKCC1 and rat NKCC1 are 5.98 (131 kDa) and 6.08 (130 kDa) respectively (based on the amino acid sequence using the Compute pI/Mw tool

from Expasy.org). Post-translational modifications such as phosphorylation make the isoelectric point of a protein more acidic and may explain why the T4 detected spots are at more acidic isoelectric points than we may predict for the cotransporter. Using the Scansite molecular weight and isoelectric point calculator (available from scansite.mit.edu/calc_mw_pi.html) changes to protein pI can be estimated after theoretical addition of any number of phosphate groups. Based on the human NKCC1 sequence, at least 10 phosphates would need to be added to achieve a pI of 5.5. This suggests that there are other modifications present that are responsible for the shifts in pI found, such as glycosylation. Spots are present at higher molecular weights than predicted, based on the amino acid sequence. This could be explained to some extent by variable glycosylation, but may also represent the cotransporter bound to another protein(s). None of the spots detected by the T4 antibody corresponded clearly with visible spots on the stained gel. Much of this was due to problems distinguishing individual spots within these regions. 2DEvolution software finds it difficult to distinguish spots from areas of high background and streaking. An example of the capabilities of the spot detection is shown in figure 3.2. Panel A shows the area where T4 detects NKCC protein. The software indicates that there are many spots in this area, but closer examination shows that these are streaks and not defined spots. Hence, in order to use two-dimensional electrophoretic techniques for NKCC detection, improvements would be necessary to allow detection of higher molecular weight proteins. Several different adaptations and investigations into the original protocol were made and are described.

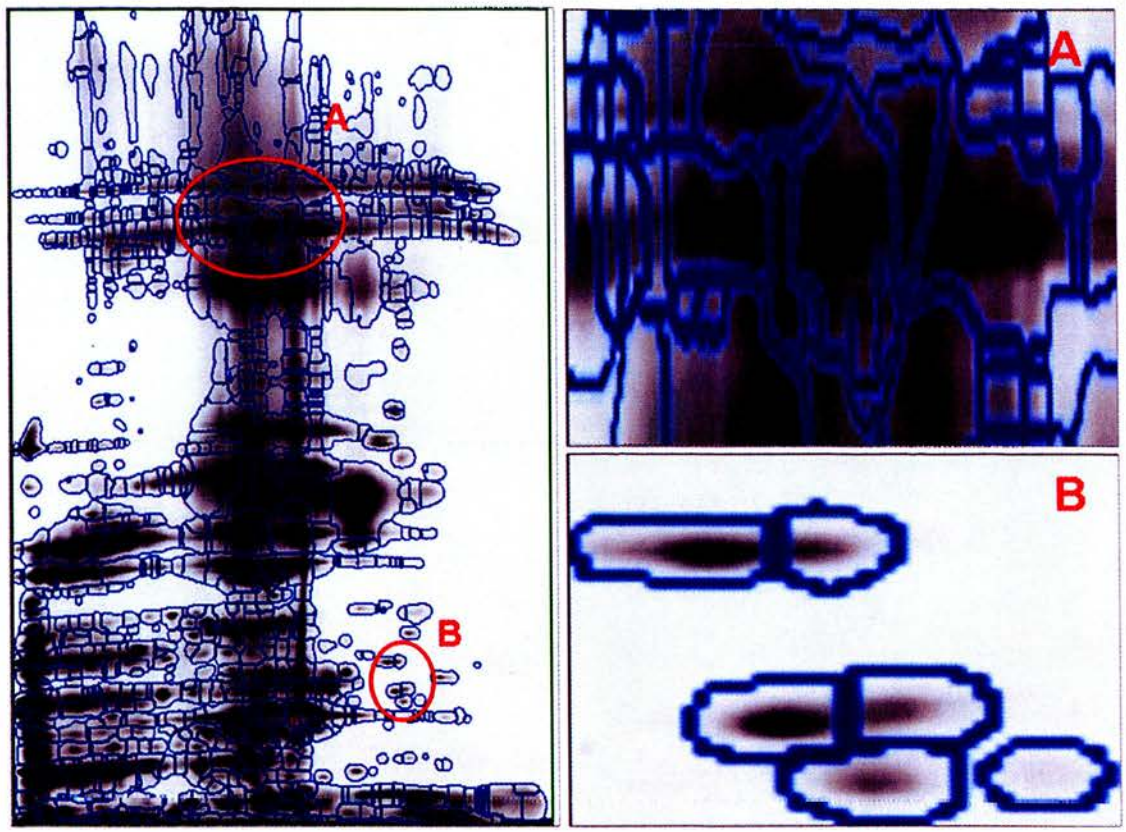

Figure 3.2 – 2DEvolution Spot Detection of 2-D Separated Ferret Membrane Proteins
2DEvolution software (Nonlinear Dynamics, UK) was used to detect the spots from the silver stained image shown in figure 4.1. Panel A shows an area of streaking where protein spot detection is difficult. Panel B shows an area where protein density is lower and spot detection is more successful.

3.1.1 - Sample preparation

To ensure that the method of sample preparation was not selectively reducing the amount of NKCC present, western blot of the different sample fractions was carried out. Prior to IEF, erythrocyte cell membranes were separated by ultracentrifugation and then the resultant pellet material resuspended in a solubilisation buffer compatible with IEF. Figure 3.3 demonstrates that the majority of T4 immunoreactivity resides in the membrane pellet and that no T4 immunoreactivity is found in the supernatant material that is discarded. Although reduced from the starting sample, it is clear that

cotransporter is present in the solubilised IEF sample. In order that a western blot could be performed an SDS-PAGE Clean-Up Kit was used (GE Healthcare) to precipitate the proteins from the IEF sample buffer. These were then resuspended in buffer more compatible with SDS-PAGE. This step may well account for the reduction of NKCC as

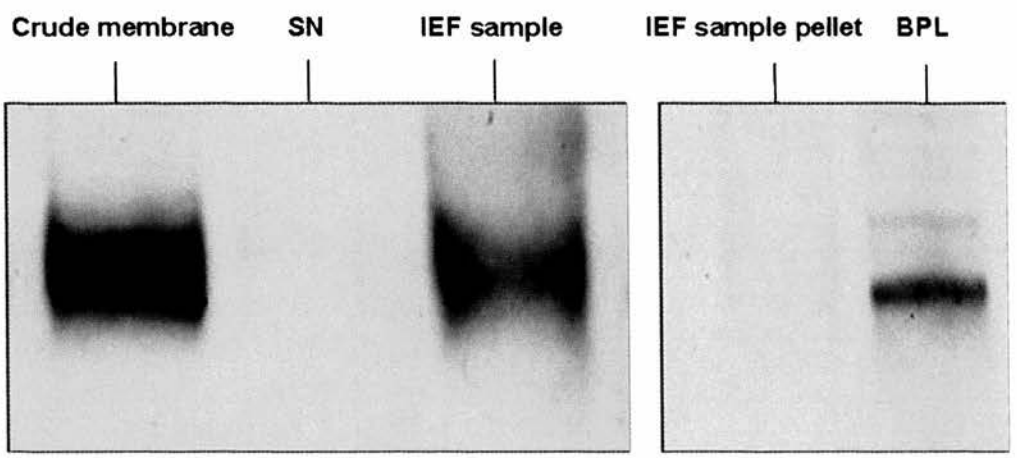

Figure 3.3 – T4 Western Blot Analysis of NKCC in 2DE Sample Preparations
The various stages of membrane sample preparation for isoelectric focussing are tested for the presence of NKCC. Crude membrane samples are prepared in the ultracentrifuge at 100,000 x *g* (4°C) and the supernatant (SN) separated from the membrane pellet. These membranes are resuspended for IEF before a final spin (14,000 x *g*) and the supernatant loaded for the first dimension. Any remaining pellet material (IEF sample pellet) is discarded. To obtain equal loading of total protein in each sample lane, protein from SN and IEF samples was precipitated using SDS-PAGE Clean-Up Kit (Amersham) before preparation of the samples for SDS-PAGE. The 140 kDa biotinylated protein ladder (BPL) marker is shown for molecular weight reference.

precipitated membrane proteins are often difficult to resuspend. There is no visible evidence for the presence of NKCC in the residual pellet material that is not soluble after incubation with the IEF buffer. This demonstrates that the use of ultracentrifugation to concentrate the membranes (and resultant protein) provides a simple enrichment step with minimal NKCC loss.

3.1.2 - Reduced Sample Volume and Protein Load

Revisiting the recommendations made by the immobilised pH gradient (IPG) strip manufacturer revealed that the starting protocol exceeded strip volume and protein capacity during the first dimension (Berkelman and Stendstedt, 1998). Reduction of sample volume and protein in the IEF step results in improved second dimension resolution. Silver staining of the SDS-PAGE gel shows that the issue of smearing is

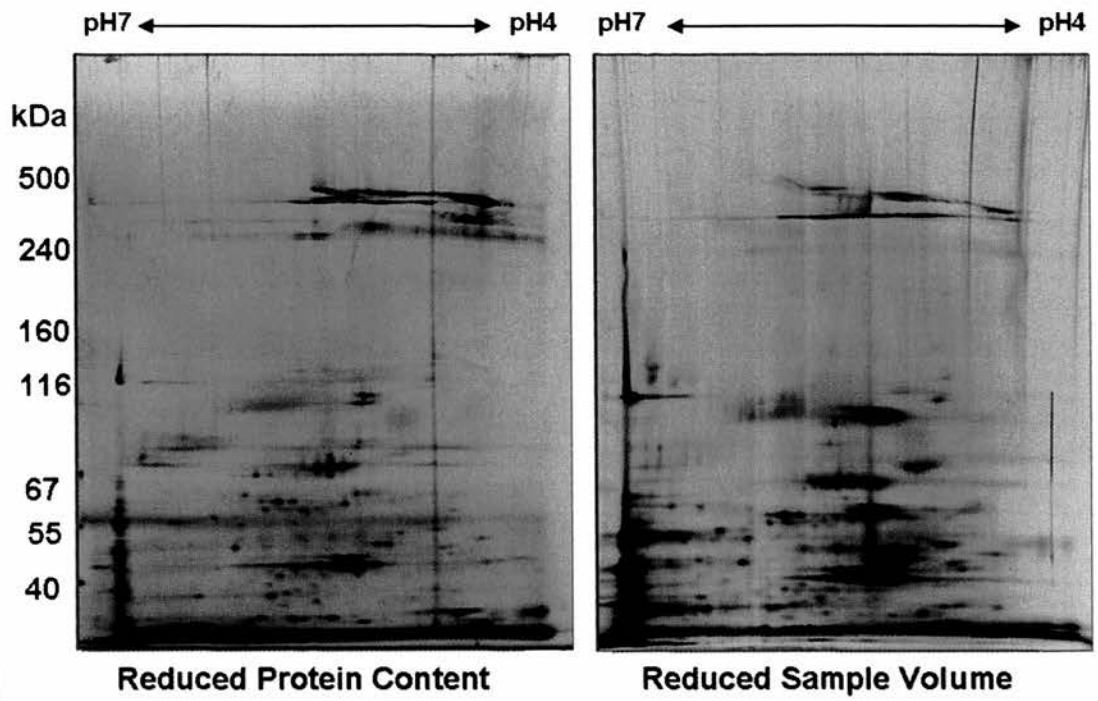

Figure 3.4 – Reduced Protein and Sample Volume Improves Gel Appearance
According to 2-D Electrophoresis using immobilized pH gradients: Principles and Methods (Amersham Biosciences) there is a maximal protein and volume set for each strip size. Starting sample protein content in the left panel was 30µg and sample volume of 140µl. The right panel had a start sample protein content of 50µg and sample volume not exceeding 125µl. Silver stained 3-8% Tris-acetate NuPAGE™ gels are shown. Guide molecular masses were interpolated from the Invitrogen HiMark™ marker set.

largely resolved (Fig 3.4). This improves the spot detection by 2DE analysis software (Fig 3.5). However, larger molecular weight proteins are mostly absent from these gels. This may be as a result of protein precipitation in the IPG strip. This is a particular

problem with integral membrane proteins, which often possess many hydrophobic transmembrane spanning regions. Their solubility is reduced as they become concentrated at their pI, causing aggregation. It is possible that altering the detergent and ionic strength composition of rehydration/solubilisation buffer could reduce this problem. A number of experiments were conducted to address this issue.

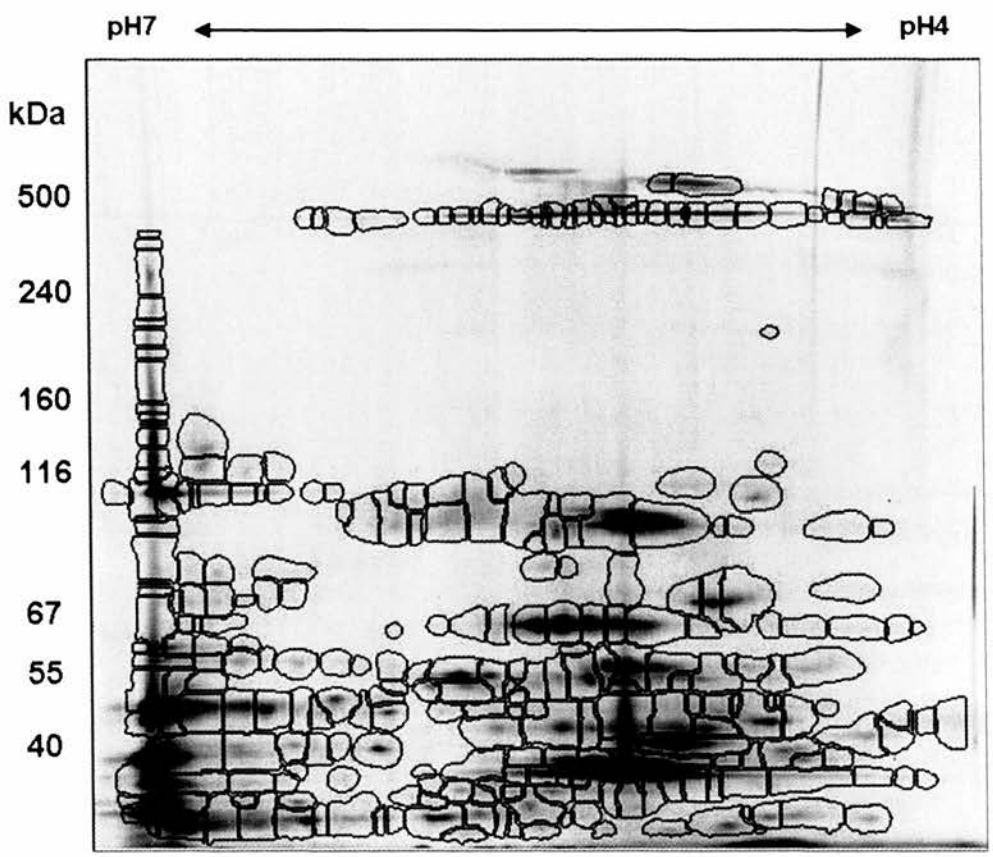

Figure 3.5 – Improved 2DEvolution Spot Detection by Reducing IEF Sample Volume
This figure shows the result of spot detection on a 2D gel where IEF sample volume was reduced. A silver stained 3-8% Tris-acetate NuPAGE™ gel is shown. Guide molecular masses were obtained from the Invitrogen HiMark™ marker set.

3.1.3 - Tris Base Inclusion

Pasquali *et al* (1997) suggest that tris base improves the solubilisation of hydrophobic membrane proteins, many of which are optimally soluble at a higher pH. The addition of 20mM tris base to the sample buffer increases the amount of material seen at the mid to high molecular weight range (figure 3.6). There is a drawback in that much of this protein is poorly focussed as may be expected by the addition of a charged chemical to the first dimension. However, it does greatly increase the amount of protein on gels and is a useful addition to the protocol.

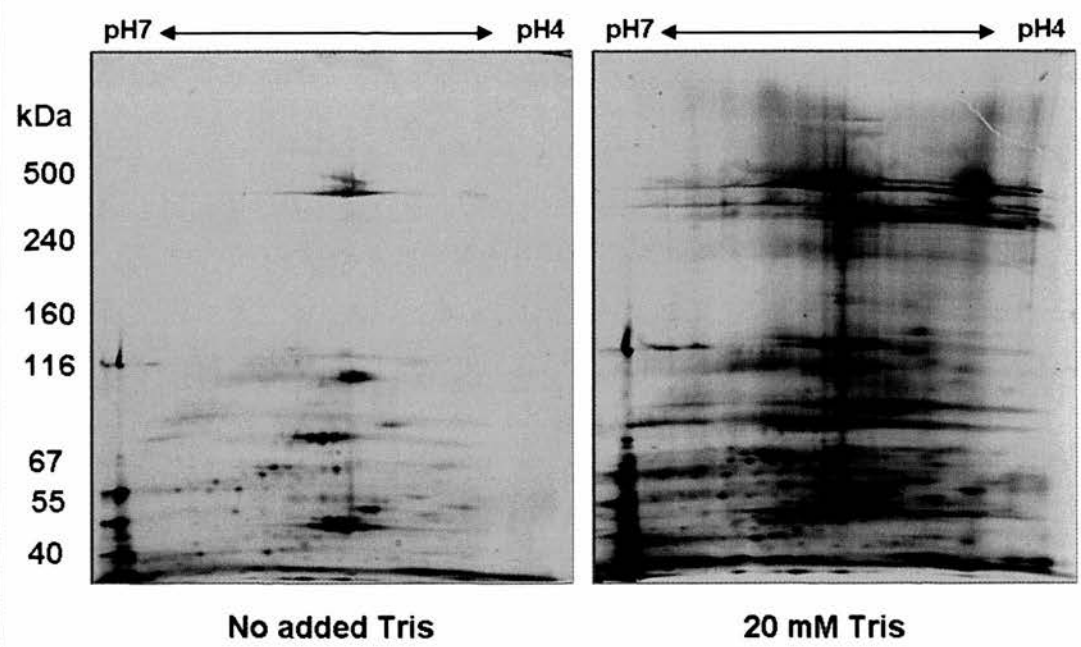

Figure 3.6 – Inclusion of Tris in IEF Sample Buffer Increases Protein Content on 2D Gels
Samples of (30µg) protein were prepared for IEF/SDS-PAGE with or without Tris added to the solubilisation buffer during sample preparation. Silver stained 3-8% Tris-acetate NuPAGE™ gels are shown. Guide molecular masses were taken from the Invitrogen HiMark™ marker set.

3.1.4 - Increased Ampholyte Concentration

Increased concentration of IPG buffer can help to increase protein solubility (Shaw and Riederer, 2003). The starting protocol already had IPG buffer at 1%, with 0.5% being the standard, according to the strip manufacturer's instructions. Figure 3.7 shows the results of increasing IPG buffer concentration from 1% to 2%. Although there is little visible difference between the gels there was difficulty in achieving the appropriate voltage during IEF. In conclusion, this does not greatly improve the outcome of the experiment and as such was not used again.

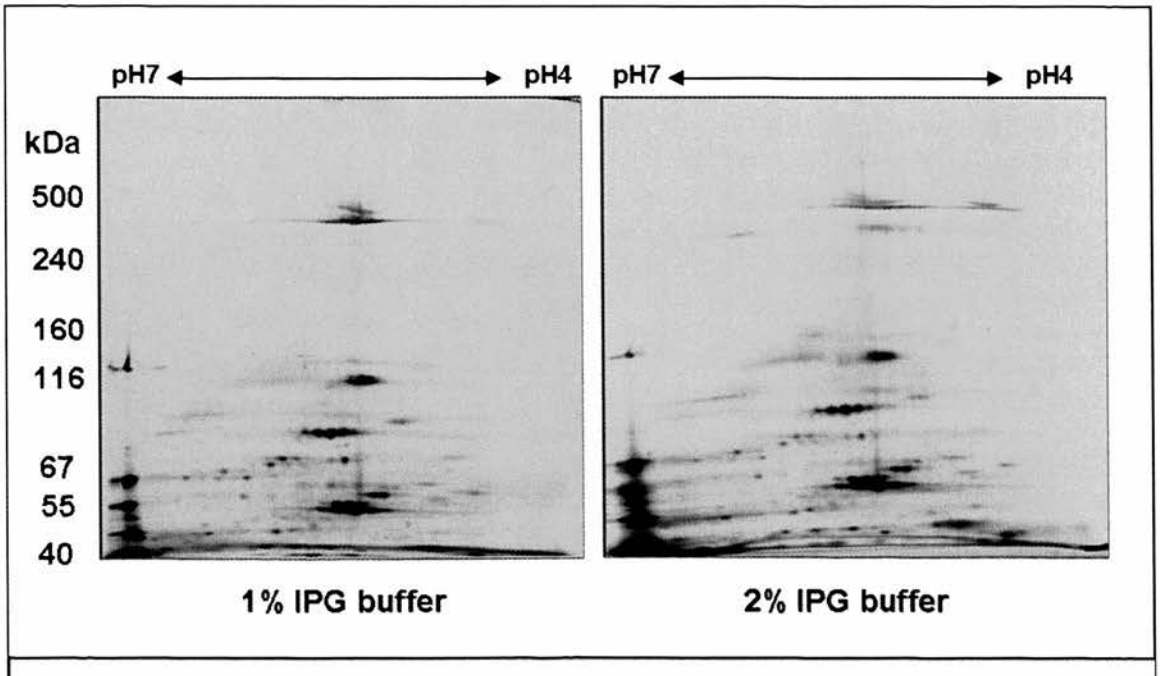

Figure 3.7 – Increased Ampholyte Concentration During IEF
IPG buffer (pH4-7) was added to the solubilisation solution at either 1 or 2% concentration. Amersham pH 4-7 IPG strips were used. Silver stained 3-8% Tris-acetate NuPAGE™ gels are shown. Guide molecular masses were taken from the Invitrogen HiMark™ marker set.

3.1.5 – Use of Different Detergents for Membrane Protein Solubilisation

The best detergents for the solubilisation of membrane proteins are generally charged (i.e. SDS) and therefore not suitable for use during IEF. A panel of newer zwitterionic

detergents have shown to be efficient at solubilisation of membrane proteins, allowing

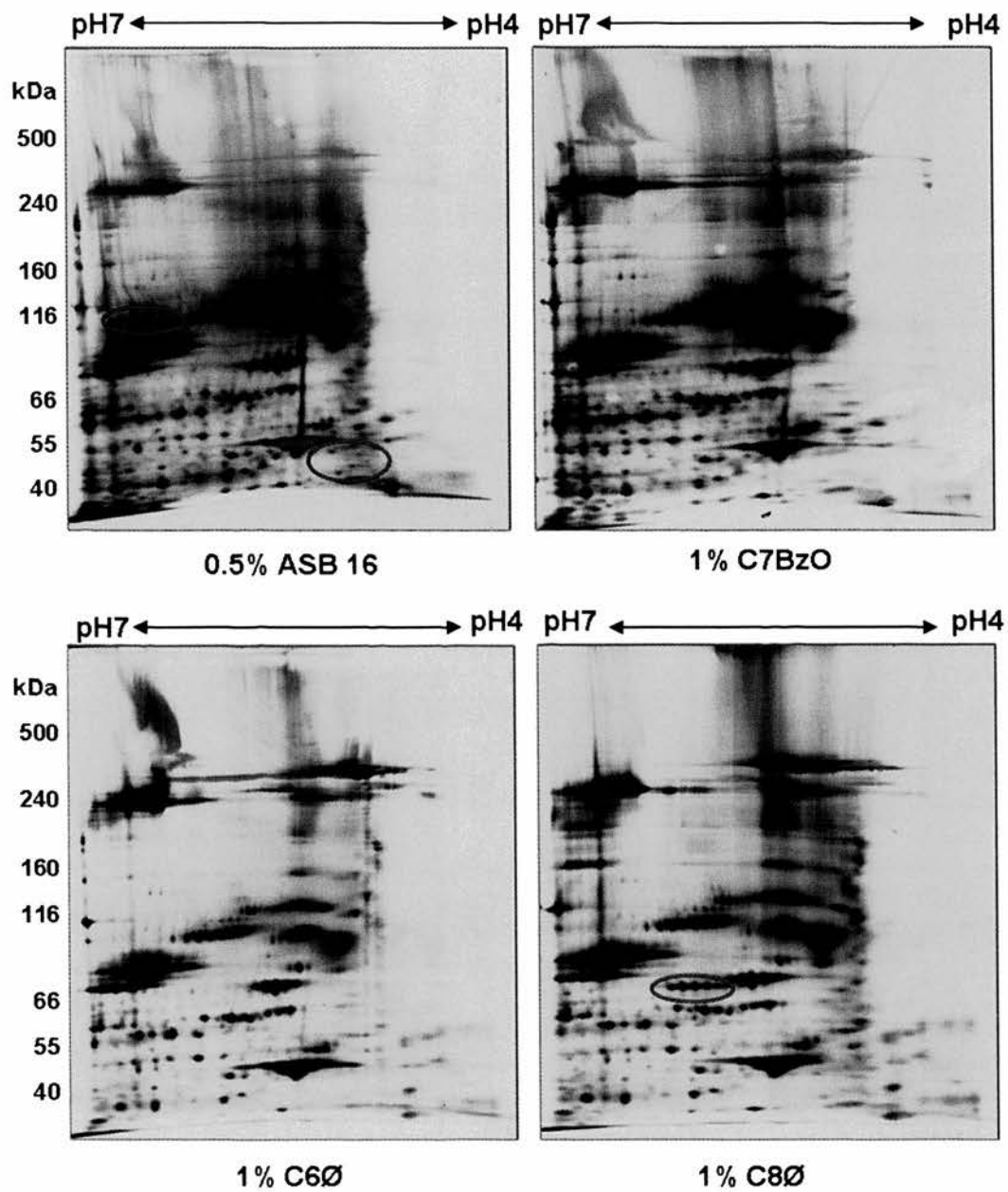

Figure 3.8 – 2DE Separation of Membrane Proteins Solubilised with Zwitterionic Detergents
Ferret erythrocyte membrane proteins (100µg) were solubilised in IEF buffer with 4% CHAPS, 1% Triton X-100, 1% NP40 and each of the detergents named above (see chapter 2 for full details of solubilisation buffer). Silver stained NuPAGE™ 3-8% Tris-acetate gels are shown, with proteins separated on pH 4-7, 7cm IPG strips. Molecular masses were obtained from the Invitrogen HiMark™ marker set. Red circles surround spots that are not well represented on each of the other gels.

identification of a greater number of membrane proteins on 2D gels (Chevallet *et al*, 1998). The amidosulfobetaines have been shown to be effective at solubilisation and are compatible with high concentrations of urea and thiourea (Shaw and Riederer, 2003). One of these, ASB-16, is the detergent used in the original protocol, along with CHAPS, Triton X-100 and NP-40. A variety of other detergents were tested and their effects on the 2D map observed (figure 3.8). Structures of these detergents are shown in figure 3.23. With spot detection software, and the naked eye, you can clearly observe extra spots on the gel using the C8Ø detergent, which are marked with a red circle in figure 3.8. Other changes are not clear due to the streaking on the gels. Both the C8Ø and the C6Ø detergents give cleaner looking gels with less overall streaking. However, the ASB-16 gels do have areas where spots are present that are not well represented on other gels (red circles on figure 3.8). Though not investigated further, the use of different detergents could be a useful area to explore in improving the 2-D separation of erythrocyte membrane samples.

3.1.6 - ZOOM® Fractionation

This method involves liquid-phase isoelectric focussing of protein samples, which can then be separated by gel-based isoelectric focussing and SDS-PAGE. Figure 3.9 shows that it is possible to separate the cotransporter into a particular fraction, which ranges from pH 5.4-6.2. However, as figure 3.10 demonstrates, attempts to separate these proteins using 2-DE were disappointing. T4 western blots of these gels showed no evidence of NKCC present (data not shown). This method should provide the best separation of any modified forms of the cotransporter by reducing sample complexity and allowing separation of proteins within a single pH unit. However, several

modifications and attempts to improve this protocol were made but the proteins were never well resolved and there was generally very little protein where the cotransporter would separate on a gel. As such, this protocol was not further investigated.

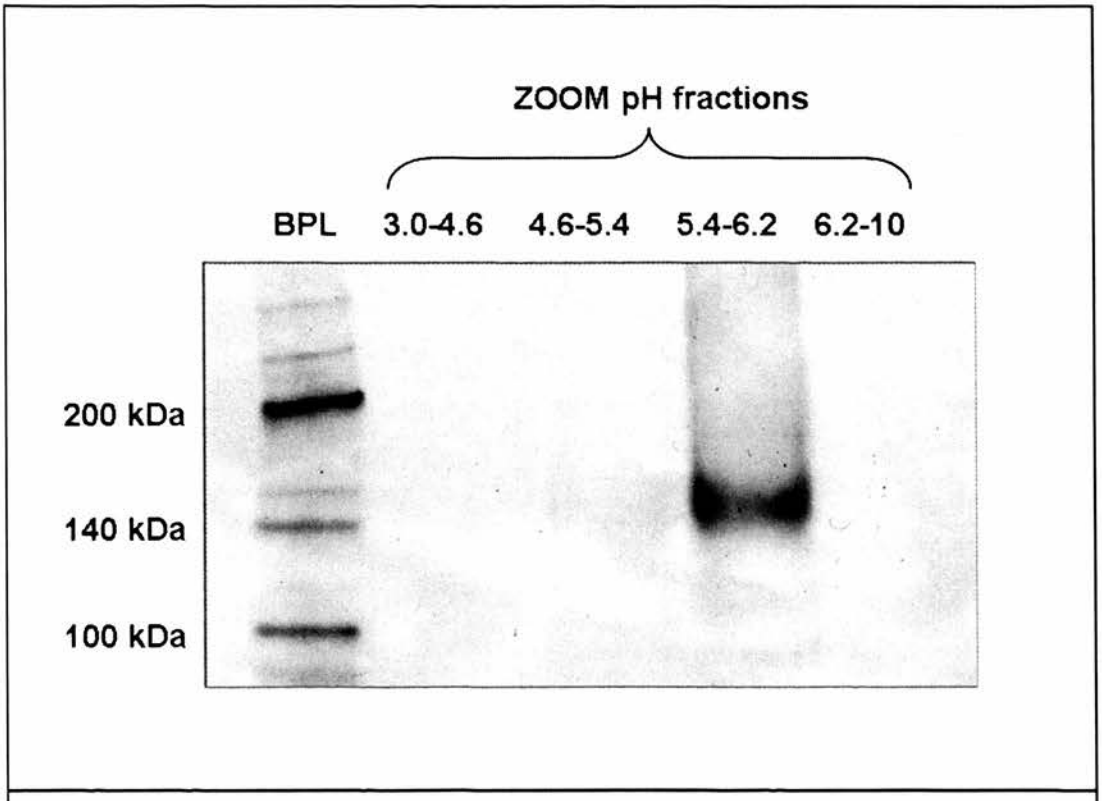

Figure 3.9 –T4 Detection of Ferret Erythrocyte NKCC after ZOOM® Fractionation
Equal amounts of protein were loaded per lane (2.5µg) and separated on 3-8% Tris-acetate gels. After transfer to nitrocellulose, the membrane was probed with T4 antibody to detect NKCC. The masses shown are from a biotinylated protein ladder (BPL).

3.1.7 – Studying NKCC

All investigative work to this protocol was performed using 3-8% tris-acetate NuPAGE gels for the second dimension separation. The rationale for this was that they give greater separation of mid to large molecular weight proteins which are generally underrepresented on 2-D gels. However, using 4-12% bis-tris NuPAGE gels gives

greater separation of proteins within the range we are looking for the cotransporter, as well as improving separation of smaller proteins. Figure 3.11 shows a 2-D separation of ferret erythrocyte membranes using a pH 4-7 IPG strip and a 4-12% bis-tris NuPAGE gel with Coomassie stained proteins. This stain shows far fewer proteins but is

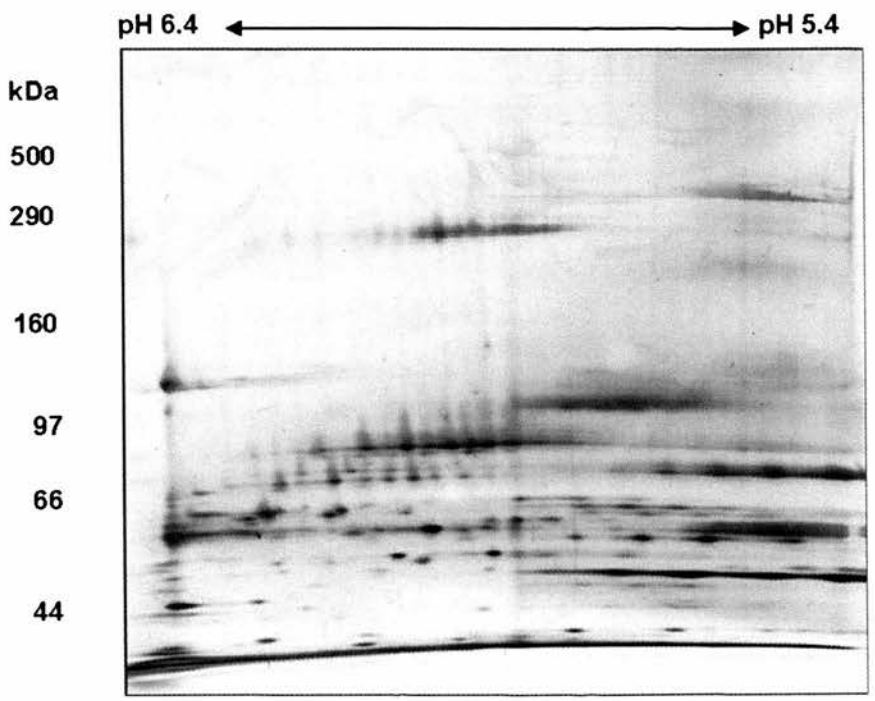

Figure 3.10 – ZOOM Fractionation and 2-D Separation of Erythrocyte Proteins
This shows a representative image of a 2-D separated pH 5.2-6.4 fraction on a single pH unit IPG strip and an 3-8% Tris-acetate SDS-PAGE gel. Proteins were silver stained and the guide masses shown were taken from Invitrogen HiMark™ markers.

compatible with mass spectrometry. A few protein identifications were made and mostly represent cytoskeletal proteins, with the only certain red blood cell membrane protein being band 4.1. Although the samples used should contain predominantly membrane proteins, there will be residual haemoglobin and cytoskeletal proteins present due to the gentle method of membrane preparation. Band 3, the most abundant red

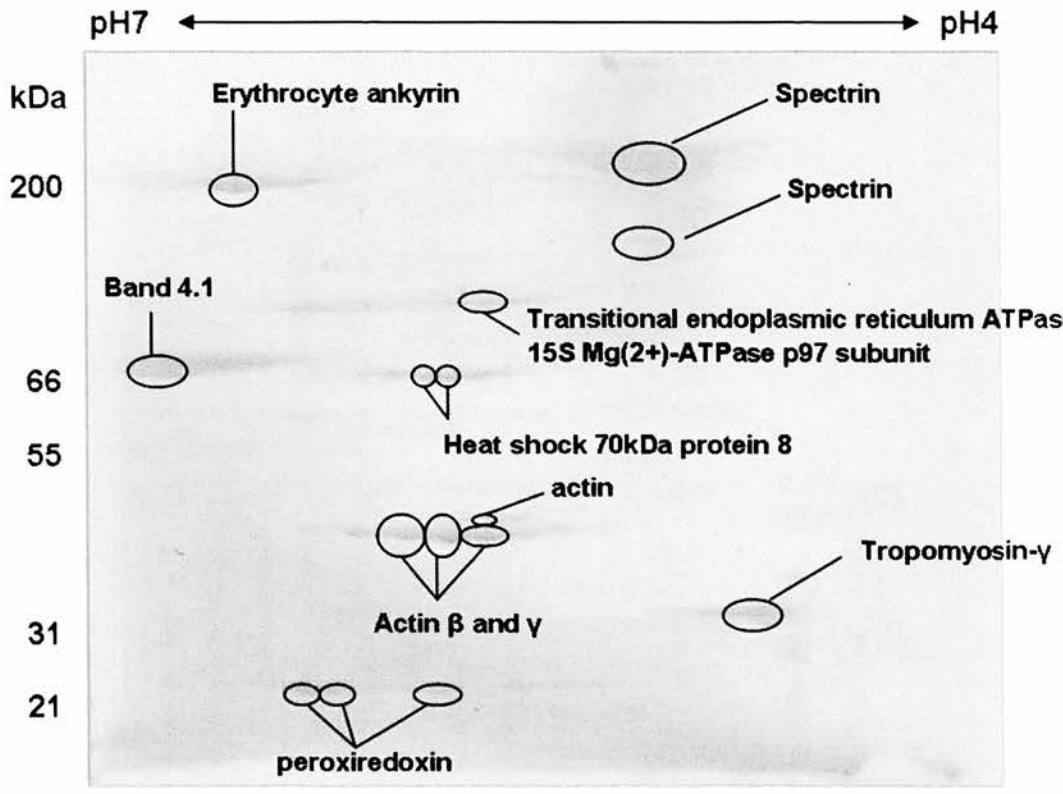

Figure 3.11 – Identification of Proteins from Ferret Erythrocyte Samples by MALDI-TOF Proteins were separated by IEF on pH 4-7 IPG strips, followed by SDS-PAGE on 4-12% Bis-tris gels. Guide molecular masses are shown and were taken from the Invitrogen Mark12™ marker set. The gel was stained with GelCode Blue (Pierce) and visible spots excised, digested and subjected to MALDI-TOF mass spectrometry. Proteins were identified using the MASCOT peptide mass fingerprinting utility.

blood cell membrane protein, is conspicuously absent. The isoelectric point for this protein (approximately pH 5, based on the amino acid sequence) means that it should be detectable using pH 4-7 IPG strips. Figure 3.12a shows a 2-D separation of ferret erythrocyte membranes under the same conditions as for figure 3.11, but with silver staining of the proteins. 2DEvolution software detected 334 spots (figure 3.12b). However, only 9 proteins were identified. This may be due to incomplete removal of silver ions, which can result in poor quality mass spectra (Gharahdaghi *et al*, 1999). It

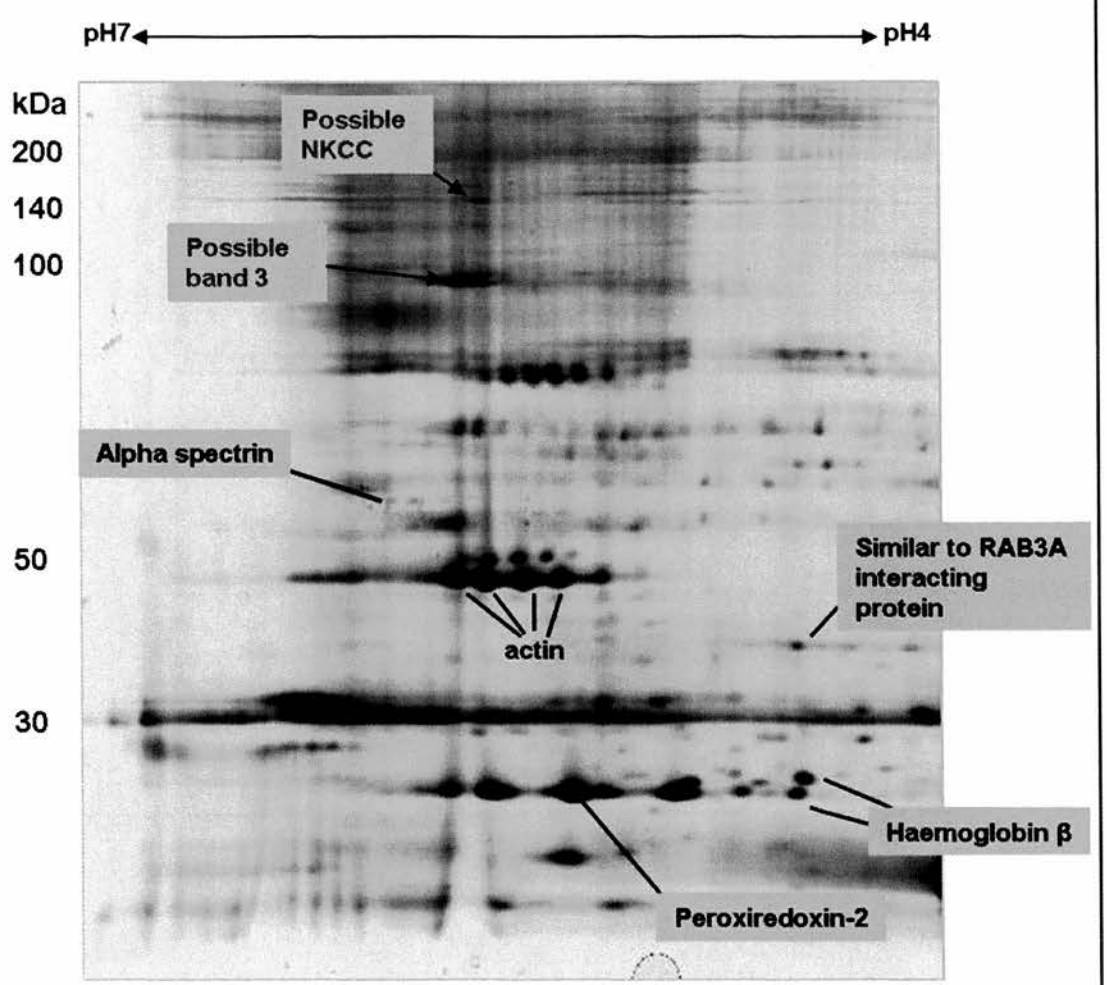

Figure 3.12a – Identification of Proteins from Ferret Erythrocyte Samples by MALDI-TOF
The gel was stained with PlusOne Silver Stain (Amersham) and spots excised, digested and subjected to MALDI-TOF mass spectrometry. Proteins were identified using the MASCOT peptide mass fingerprinting utility. The areas indicated in red are where cotransporter and band 3 are likely to separate. Identified proteins are labelled. The mass markers were taken from a biotinylated protein ladder.

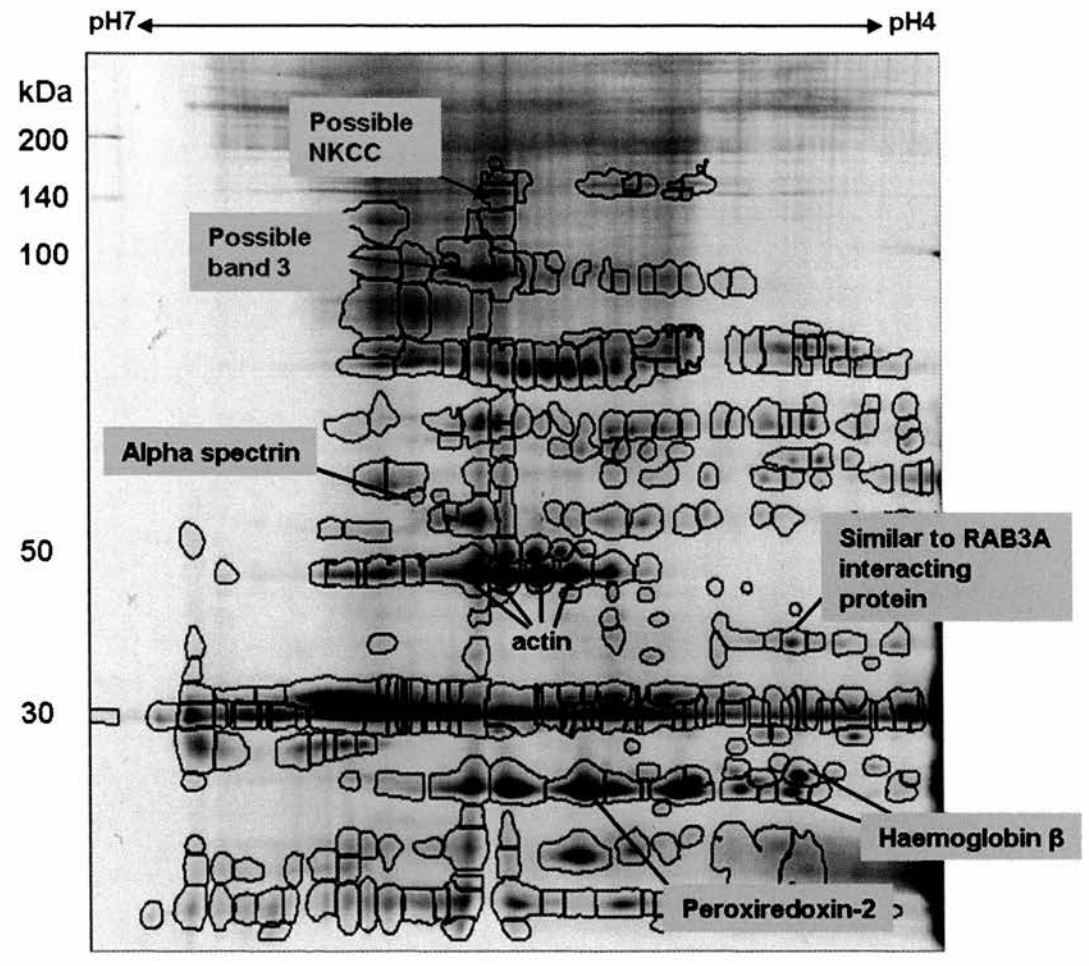

Figure 3.12b – Identification of Proteins from Ferret Erythrocyte Samples by MALDI-TOF
The gel was stained with PlusOne Silver Stain (Amersham) and spots excised, digested and subjected to MALDI-TOF mass spectrometry. Proteins were identified using the MASCOT peptide mass fingerprinting utility. The areas indicated in red are where cotransporter and band 3 are likely to separate. From over 300 proteins on this gel (marked in blue; detected by 2DEvolution software) only 9 identifications were made. The mass markers were taken from a biotinylated protein ladder.

may also be due to the small amounts of protein present in each spot which are detectable with silver stain but perhaps not by the MALDI-TOF. Figure 3.13 shows the separation of proteins using pH 3-10 IPG strips and the proteins here are stained with SYPRO Ruby stain. This stain has similar sensitivity to silver stain, but is compatible

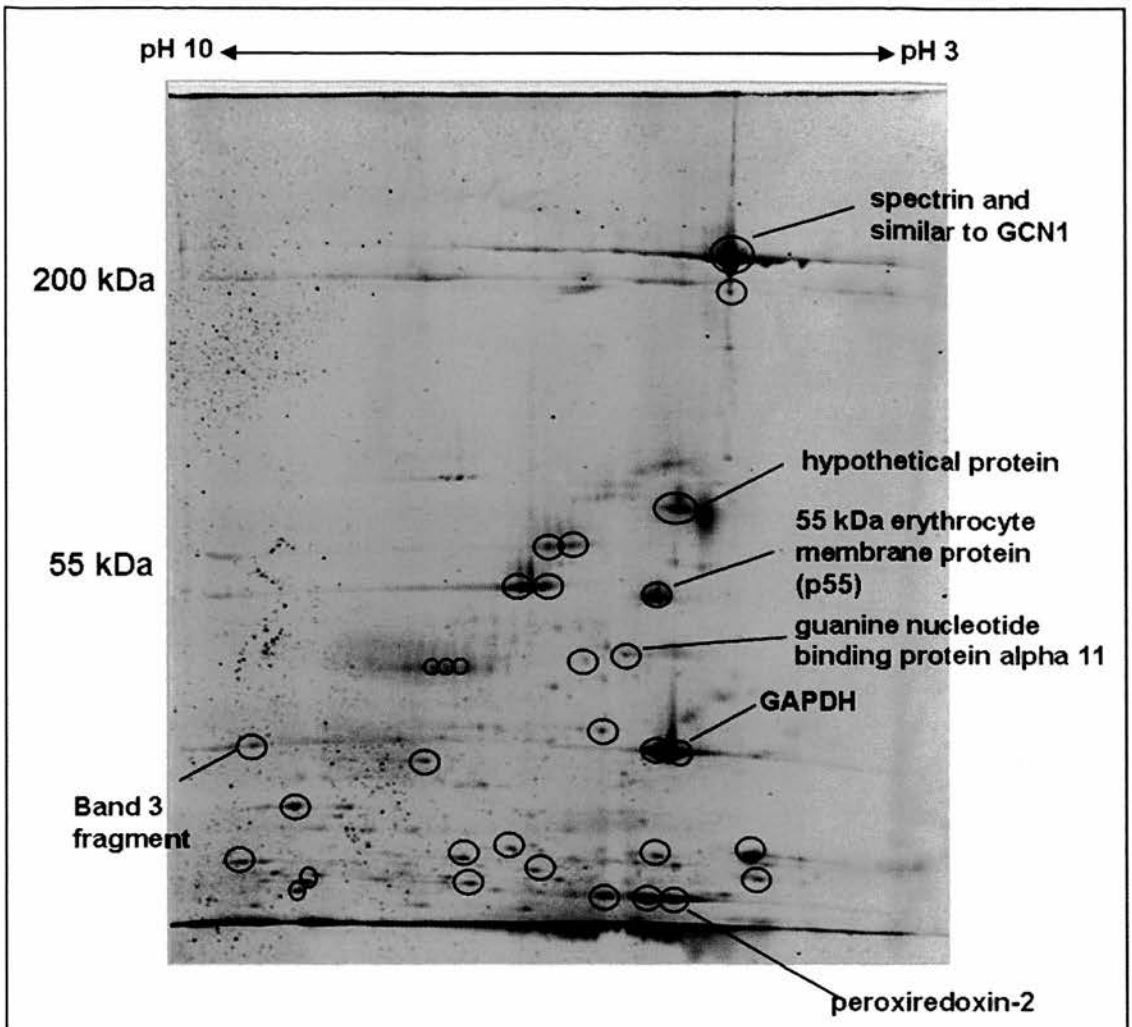

Figure 3.13 – MALDI-TOF ID of Erythrocyte Proteins Separated on pH 3-10 IPG Strip
Proteins were separated on a 13cm pH 3-10 IPG strip and 4-12% Tris-glycine home-cast gel. The proteins were stained SYPRO Ruby (BioRad) and the circled spots excised and digested with trypsin and subjected to MALDI-TOF mass spectrometry. Proteins were identified using the MASCOT peptide mass fingerprinting utility. Only those proteins that were identified are labelled. The other circled spots were not identified. Molecular mass markers were taken from the SeeBlue® Plus2 marker set from Invitrogen.

with mass spectrometry. Again, we see poor coverage of membrane proteins. However, band 3 is detected with this method, but it is at the wrong molecular weight approximately 45 kDa and not 90-100 kDa) and isoelectric point (pH 9 and not pH 6). This may represent a proteolytic cleavage product of band 3 which is not normally seen

when using pH 4-7 IPG strips. Using the method that gave the most clearly resolved gel images, western blots were obtained and probed with T4, R5 and NKCC-P antibodies. Figure 3.14 shows NKCC spots from control ferret erythrocyte membrane samples using the T4 antibody and unlike the blot shown in figure 3.1, there is significantly more cotransporter found at the monomer weight. The estimated pI values are very

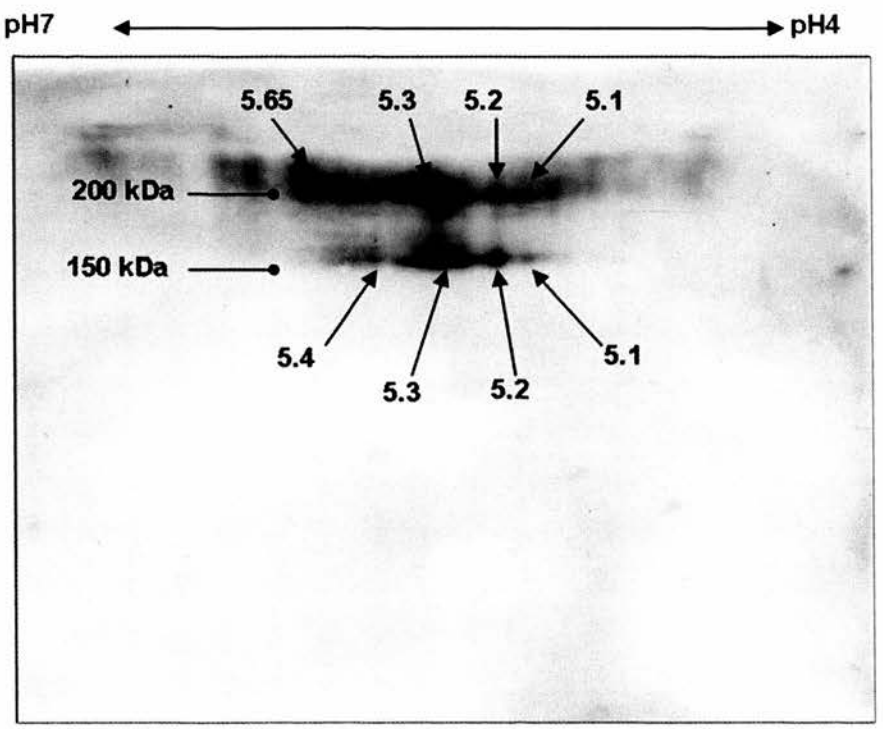

Figure 3.14 – T4 Detection of NKCC after 2-DE Separation of RBC Membranes
Gels were prepared on 7cm pH 4-7 IPG strips and 4-12% Bis-tris NuPAGE gels and transferred to nitrocellulose and probed with T4 antibody. Isoelectric points (marked with arrows) and molecular masses (shown with circles) were estimated using 2DEvolution software.

similar, with each differing by 0.1 of a pH unit. Figure 3.15 shows spots detected by phospho-specific NKCC antibodies. The spots identified by T4 are also identified by R5 and NKCC-P antibodies. Three R5 spots are seen and correspond to the major spots

seen on T4 blots at the molecular weight of approximately 150kDa. The NKCC-P antibody detects spots only at a pI of 5.3, but at several molecular weights. These sizes correspond well with what is observed using the T4 antibody, from figures 3.14 and 3.1.

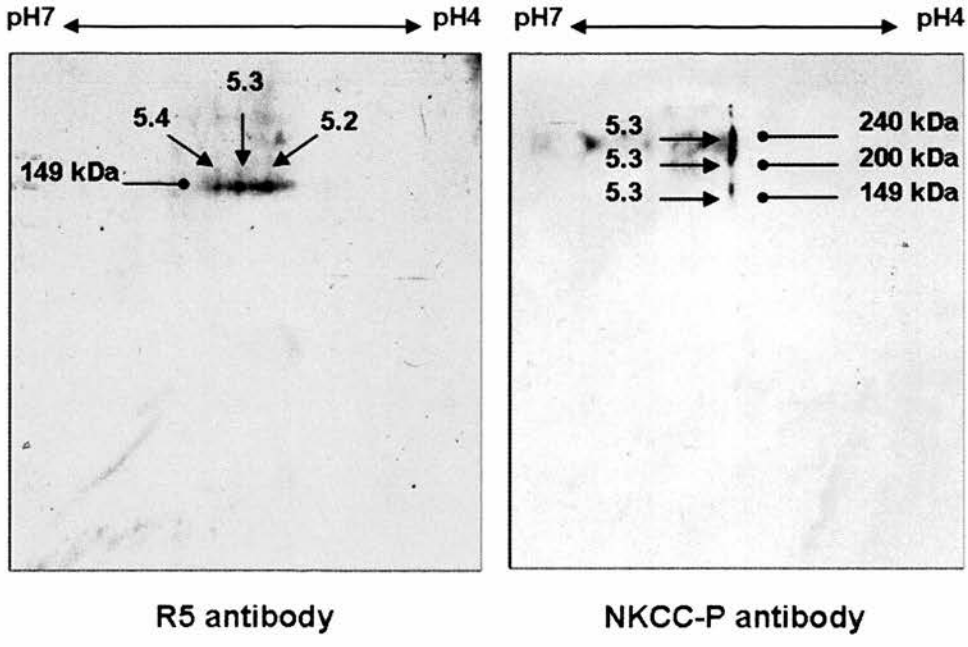

Figure 3.15 – Detection of Phosphorylated NKCC after 2-DE Separation
Gels were prepared on 7cm pH 4-7 IPG strips and 4-12% Bis-tris NuPAGE gels, then transferred to nitrocellulose. Blots were probed with either the R5 antibody or NKCC-P antibody and the spots detected with ECLplus. Isolectric points (marked with arrows) were estimated using 2DEvolution software and the molecular masses (marked with circles) were interpolated from a biotinylated protein ladder.

As far as improving the overall picture of 2-DE separated erythrocyte membrane samples this has been best achieved by reduction of sample volume, sample protein content, inclusion of tris base in the IEF solubilisation buffer and by separating proteins on 4-12% Bis-tris gels. Overall, this method has improved but as the mass spectrometry

data shows still operates at the limits of the technology as far as membrane protein identification is concerned.

3.2 - Blue-Native/SDS-PAGE

Blue-native polyacrylamide gel electrophoresis (BN-PAGE) allows the separation of very high molecular weight species, including native proteins in complex with others.

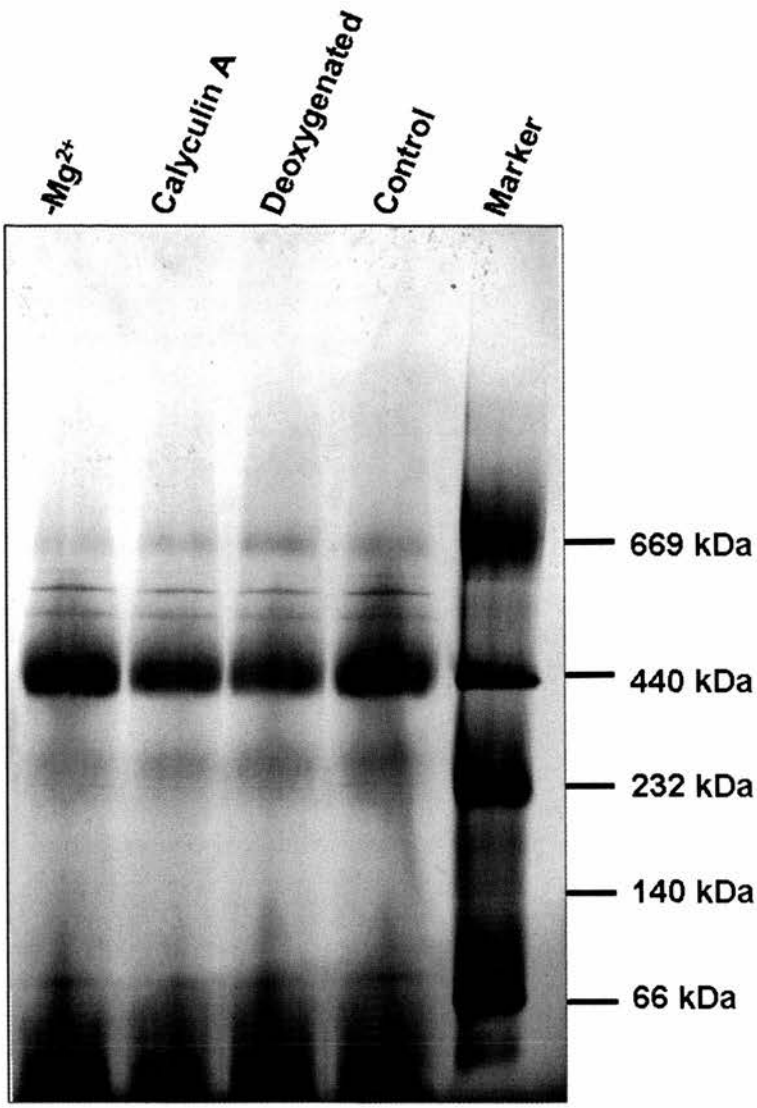

Figure 3.16 – Native-PAGE of Ferret Erythrocyte Membrane Proteins
Ferret red blood cell membranes were separated by native-PAGE and stained with Coomassie R-250. High Molecular Weight native markers (Amersham Biosciences) are shown with the molecular masses marked.

Coomassie blue is used to "label" protein with a non-denaturing negative charge allowing native proteins to run towards the positive electrode during electrophoresis.

Comparing samples that have been given treatments to increase or decrease cotransport may identify proteins that are involved in the regulation of this activity. Home-cast and pre-cast gels were used to separate erythrocyte membrane protein complexes for either LC-MS/MS or for a second dimension separation of SDS-PAGE, followed by MALDI-TOF MS or transfer to nitrocellulose for western blotting. BN-PAGE on mini-gels separated proteins into five major complexes (Fig 3.16). There were no detectable differences in the number or pattern of complex separation between the different samples tested. Figure 3.17 shows identification of proteins from these complexes using liquid chromatography and tandem mass spectrometry (see Appendix for supplementary data). This method allows identification of proteins from more complex samples such as these. Unfortunately, no cotransporter was identified in these samples. Figure 3.18 shows western blot detection of NKCC on BN-PAGE gels using the T4 antibody. Again there are no obvious differences between the samples in terms of T4 immunoreactivity. The cotransporter appears as two major bands with some material at higher positions, but the masses of these were not able to be estimated due to lack of suitable markers for both BN-PAGE and western blotting. Based on the size and position of these bands it does appear that they correspond to the complexes at around 250 kDa and 440 kDa (see figure 3.16). Two-dimensional separation followed by T4 western blotting, as in figure 3.19, shows cotransporter at several positions in the gels. T4 immunoreactivity is still present in the native gel after 2-D separation showing that not all of the cotransporter manages to exit the first dimension gel. The protein that

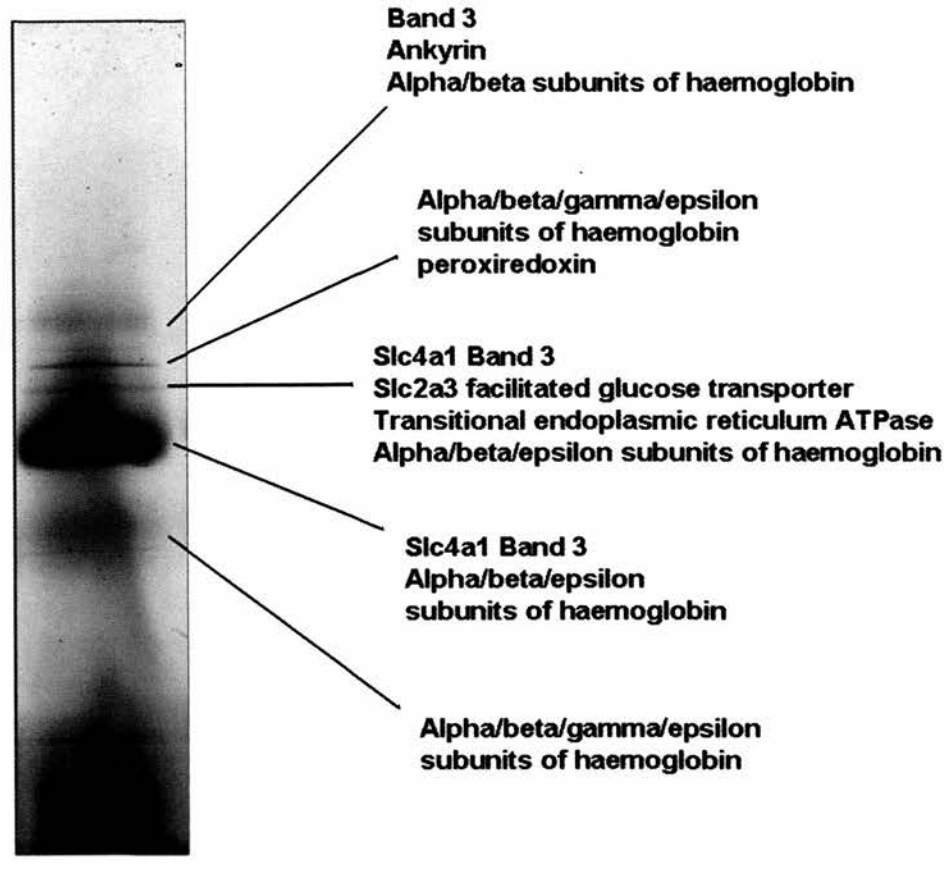

Figure 3.17 – LC-MSMS Identification of Proteins from Native-PAGE Gels
Identification of proteins was based on raw MS/MS data from one or more peptides using the MASCOT MSMS Ion search tool and confirmed with the Phenyx search tool.

does leave this gel into the second dimension separates at approximately 150 kDa and at around 250-300 kDa. From the two original protein complexes, only one has the higher molecular mass form of 250-300 kDa. Figure 3.20 shows identification of proteins by MALDI-TOF after 2-DE separation. The first dimension is shown at the top of the gel to aid understanding of which complexes the proteins come from. As with LC-MSMS of the complexes themselves, MALDI-TOF of the separated proteins provides complementary evidence for the presence of band 3 in the largest protein complex.

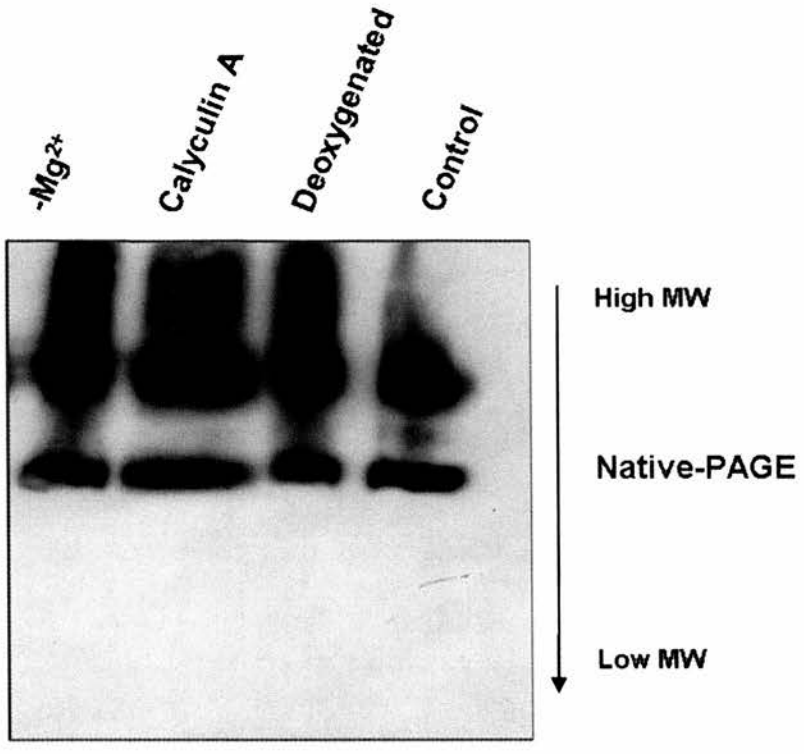

Figure 3.18 – T4 Detection of NKCC after Native-PAGE Separation of Ferret Erythrocyte Proteins

Native gels were equilibrated in western blotting transfer buffer and then proteins were transferred to nitrocellulose and proteins detected with ECL reagents. Molecular weight estimation was not performed as suitable mass markers were not available for western blotting from native-PAGE gels.

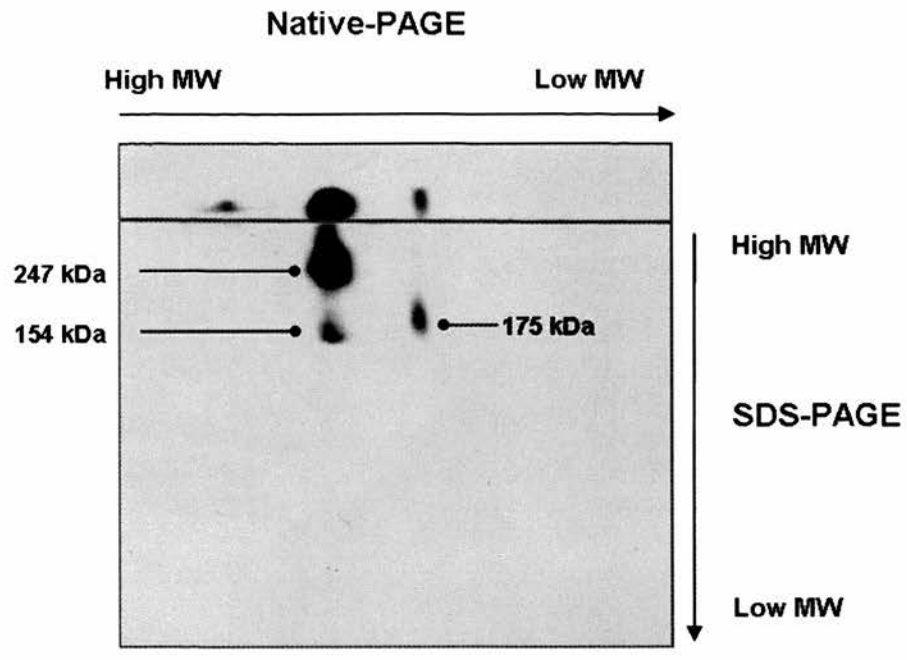

Figure 3.19 – Western Blot of Ferret Erythrocyte Proteins Separated by Two-Dimensional Native-PAGE and Denaturing SDS-PAGE

The two gels were transferred together onto nitrocellulose after 4-12% Bis-tris SDS-PAGE. T4 antibody was used to detect NKCC proteins. The masses shown were estimated using TotalLab software and were interpolated from a biotinylated protein ladder.

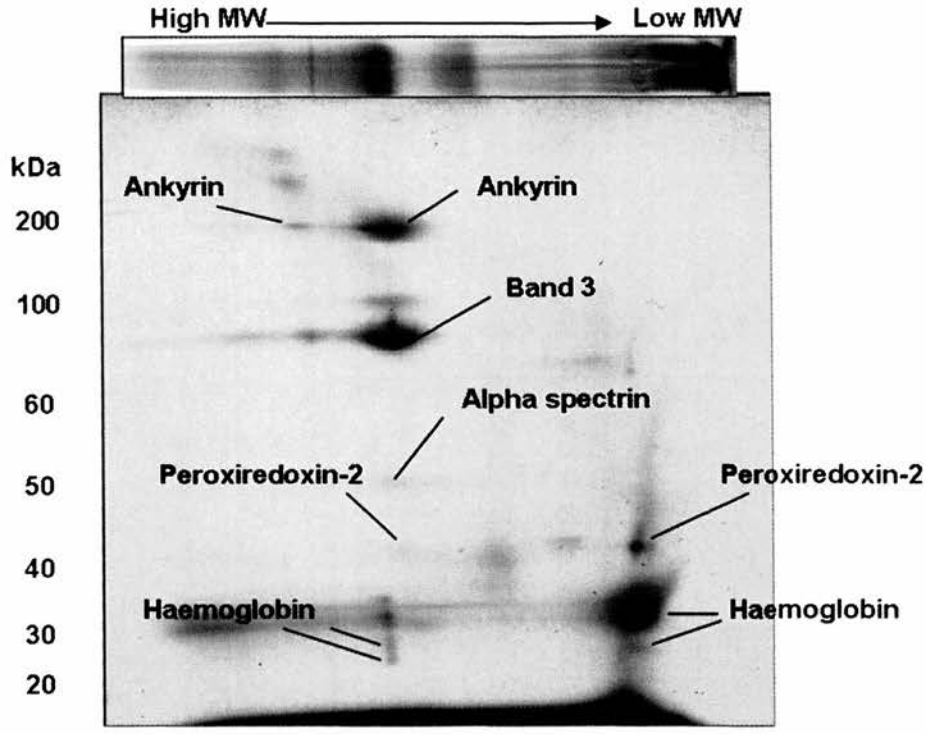

Figure 3.20 – 2D Native-PAGE and SDS-PAGE of Ferret Erythrocyte Membranes Protein identifications were made from MALDI-TOF generated mass spectra and the MASCOT peptide mass fingerprint utility. The first dimension is shown at the top of the image. The molecular weights shown were interpolated from the SeeBlue® Plus2 marker set from Invitrogen.

Based on these separations, it would appear that the cotransporter is in complex with haemoglobin, peroxiredoxin-2, band 3, spectrin and ankyrin in red blood cell membranes. To substantiate this, mass spectrometric identification of the cotransporter from the native complexes or from a spot on a 2-DE gel would be of benefit. Figure 3.21 shows the output from Mascot for a significant hit and figure 3.22 shows the mass spectrum for this hit, which is typical of data from 2-DE separated samples. This example was for a BN-PAGE/SDS-PAGE spot and shows a hit for peroxiredoxin-2.

3.3 – Discussion of Results

As the results in this chapter demonstrate, it is extremely difficult to achieve good separation and representation of membrane proteins using a 2-DE protocol featuring IEF and SDS-PAGE. Although improvements were made to the overall appearance of the protein map, no identification of the cotransporter or other large membrane proteins was made by mass spectrometric methods. It would be of use to repeat these experiments with parallel western blotting of more abundant erythrocyte membrane proteins such as band 3, to track any improvements in the representation of membrane proteins on 2D gels. Rabilloud *et al* (1999) first tested many of the detergents used in this thesis on erythrocyte membrane preparations and were able to identify band 3 on 2-DE gels but only using the more sensitive LC-MSMS method. Olivieri *et al* (2001) identified many of the same proteins that are presented in this thesis, but were also able to identify band 3 by MALDI-TOF. However, in both of these studies large first dimension gels were used (18 cm or more), which allows both better separation of proteins and larger protein loads. In this thesis, due to reduced sample availability, only 7 cm and occasionally 13 cm IPG strips were used. Churchward *et al* (2005) claim that inclusion of detergent-like phospholipids in IEF samples increased the amount of band 3 on 2-DE gels, but show no western blot or mass spectrometric evidence for this. As with the other proteomic studies cited here the SDS-PAGE separation that these authors used was for resolution of proteins not much larger than band 3. As such, it is not clear if this method is useful for resolution of larger proteins, including the cotransporter. Similar attempts to those made in this thesis to improve the representation of membrane proteins using the standard 2-DE protocol were investigated by Klein *et al* (2005) when studying the membrane proteome of *Halobacterium salinarum*. The authors of this

paper also performed a number of fractionation steps to improve their chances of obtaining membrane protein identification. They showed that by fluorescent labelling of membrane protein preparations that most were precipitating within the strip and were unable to leave this into the second dimension. They concluded that a gel-based IEF step along with SDS-PAGE is not a suitable method for identification of integral membrane proteins. This paper also suggests that digestion of integral membrane proteins with trypsin creates difficulties for their identification due to the size of peptides. Theoretical digest of human NKCC1 with trypsin using the Expasy PeptideCutter tool generates 98 peptides from a protein sequence 1212 amino acids long. A large number of these are smaller than the cut-off for mass spectral identification (around 800 Daltons) and others are larger (above 4000 Daltons). This means that peptide coverage may be poor and significant scores and identifications not be obtained from peptide mass fingerprinting. Overexpression of ferret NKCC1 in HEK-293 cells, gel separation, trypsin digestion and MALDI-TOF mass spectrometry did reveal the cotransporter using a peptide mass fingerprint tool (unpublished, Hannemann). In a natural situation, such as the ferret erythrocyte, it is unlikely that the amount of protein present is sufficient to generate enough peptide in the measured mass range to obtain protein identification. However, as lower levels of protein are required for detection on western blots 2-DE separation can provide some information about differently phosphorylated version of the cotransporter, although it is unlikely that enough protein will be present on 2-D gels to identify specific phosphorylated residues by mass spectrometry. The Scansite molecular weight and isoelectric point calculator suggests that changes of approximately 0.05 pH units will occur with the addition of each phosphate to human NKCC1. However, other modifications such as glycosylation

could affect the shift. This could explain why changes of 0.1 pH units are observed. Using phospho-specific antibodies we see a difference in the spot pattern. Western blots of control membrane samples with the R5 antibody show three distinct spots. This antibody detects a portion of the N-terminus of NKCC1 that has phosphate on Thr^{206}, Thr^{211} or both (numbering from mouse sequence). As three spots are detected, it suggests that in addition to detecting NKCC singly phosphorylated on Thr^{206} or Thr^{211} and doubly phosphorylated on both, a third moiety exists that is phosphorylated on these residues but also at another position on the cotransporter. This results in a shift in pI, making it more acidic but still allows detection by the R5 antibody. The NKCC-P antibody was raised against a section of NKCC1 that was phosphorylated on three threonine residues (Thr^{197}, Thr^{201} and Thr^{206}). Spots detected with this antibody all have a pI of 5.3, but show different molecular weights. It is not known if this antibody detects only the triply phosphorylated section of the cotransporter or could bind NKCC with one or more of the residues phosphorylated. Based on this evidence, it would seem that under control conditions only one species exists but is in complex with other molecules. Comparison of these spots in erythrocyte samples that have been exposed to different cotransport stimuli may yield extra information about differences in phosphorylation on the cotransporter.

ZOOM fractionation could be used as a method for pre-fractionation of samples prior to SDS-PAGE on large format gels. This would give greater concentration of NKCC within a sample and reduce the number of total proteins present. Separating the fraction on large SDS-PAGE gels may give enough separation to allow visualisation of the cotransporter. This method would also avoid the need for a gel-based first dimension

separation which generally results in the loss of membrane proteins. This is an area that could be investigated in the future.

Blue-native SDS-PAGE is an alternative method for two-dimensional separation of proteins. Using this to look for proteins that may be in complex with cotransporter suggested an interaction with band 3, ankyrin, spectrin, peroxiredoxin-2 and haemoglobin. It should be noted that the levels of haemoglobin and cytoskeletal proteins may vary depending on the stringency of the membrane sample preparation. A link between the trout erythrocyte anion exchanger 1 and the endogenous NKCC in *Xenopus* oocytes was made by Guizouarn *et al* (2004). Expression of the anion exchanger resulted in increased Rb influx in oocytes. This was found not to be dependent on the ion transport capability of the exchanger, but on a possible C-terminal interaction with NKCC. Band 3 is known to interact with many other proteins including ankyrin, band 4.1 and 4.2, deoxyhaemoglobin and many glycolytic enzymes (Campanella *et al*, 2005; Zhang *et al*, 2000). The interaction between band 3 and ankyrin provides a direct link for the membrane and the underlying cytoskeleton including spectrin (Ding *et al*, 1996). The presence of ankyrin in these samples may simply be due to its interaction with band 3. However, Michaely and Bennett (1995) have reported that ankyrin is able to bind multiple types of membrane proteins and it is therefore possible that NKCC directly interacts with this molecule. Haemoglobin also interacts with the C-terminal domain of band 3, with deoxyhaemoglobin binding with greater affinity than oxyhaemoglobin (Chétrite and Cassoly, 1985). Band 3 and NKCC show different oxygen sensitivities. Band 3 is stimulated by oxygenation whereas NKCC is stimulated by deoxygenation (Flatman, 2005; Drew *et al*, 2004). It has been

suggested that there may be a common oxygen sensor which could coordinate the activity of these transporters (Drew *et al*, 2004). Perhaps the interactions of the cotransporter and band 3 are a part of the regulatory control of ion transport in response to oxygen tension. Peroxiredoxin-2 was also present, a protein involved in antioxidant defence in cells including erythrocytes (Low *et al*, 2007). This protein has been shown to prevent the formation of methaemoglobin and is found to interact with haemoglobin via the haem group (Stuhlmeier *et al*, 2003). This may be in the complex purely due to its association with haemoglobin, but its function could be required to protect the cotransporter and other proteins in the cell from damage by reactive oxygen species. Figure 3.19 shows the 2-D separation of cotransporter. Assuming that these proteins come from the larger complexes of 440 and 250 kDa (on figure 3.16), it would seem that there is some difference to the cotransporter that is within these. T4 immunoreactivity from the 440 kDa complex separates at approximately 154 and 247 kDa, whereas the protein from the 250 kDa complex is found at 175 kDa. The proteins found at 175 and 247 kDa may be bound to other protein(s) that shift the molecular weight on the gel. The 154 kDa protein is likely to represent monomeric cotransporter. These differences may reflect variability of cotransporter and its binding partners in the erythrocyte membrane.

The BN-PAGE method has room for alteration of sample preparation, particularly with respect to detergents used. It can tolerate different detergents, including non-ionic and zwitterionic detergents (Krause, 2006). The non-ionic detergent dodecylmaltoside was used in the experiments shown here but others could be used, such as those used in the IEF/SDS-PAGE approach (CHAPS or ASB-16). This may improve the resolution of

the complexes and result in clearer data. Pre-labelling of samples with fluorescent dyes may allow analysis of different samples (e.g. control *versus* deoxygenated) within the same 2-DE separation (Granvogl *et al*, 2006). This would provide direct comparison for any differences in sample protein complex content and is of interest for future work.

Other methods of 2-DE could be used in the future to study the erythrocyte proteome. Two SDS-PAGE steps, such as a 10% acrylamide/6 M urea tricine-SDS step followed by a 16% acrylamide tricine-SDS step, can also resolve more proteins than either one alone (Rais *et al*, 2004). This method was able to separate highly hydrophobic proteins but was limited to those proteins smaller than 100 kDa. The cotransporter is larger than this, meaning that it is unlikely that we would achieve good resolution of NKCC using this approach. 16-BAC/SDS-PAGE uses the cationic detergent benzyl-*n*-hexadecylammonium chloride in the first dimension separation, followed by standard denaturing SDS-PAGE for the second dimension. The BAC-PAGE separates proteins, like SDS-PAGE, according to their molecular weight (Hartinger *et al*, 1996). This method has been shown to resolve hydrophobic and integral membrane proteins, including proteins with 12 transmembrane domains (Zahedi *et al*, 2005). This method is one worth investigating as it gives better resolution of either 1-D method alone, with the benefit of not having the same protein losses as standard 2-DE does. This could be used to compare global changes to proteins present in or at the erythrocyte membrane. Comparison of samples with different levels of cotransport could perhaps implicate proteins in NKCC regulation.

{MATRIX SCIENCE} Mascot Search Results

```
User            : Karen Hegney
Email           : karen.hegney@ed.ac.uk
Search title    : BNPAGE band d1
Database        : NCBInr 20071130 (5678482 sequences; 1961803296 residues)
Taxonomy        : Mammalia (mammals) (672434 sequences)
Timestamp       : 10 Dec 2007 at 15:11:55 GMT
Top Score       : 78 for gi|119604714, peroxiredoxin 2, isoform CRA_a [Homo sapiens]
```

Probability Based Mowse Score

Protein score is -10*Log(P), where P is the probability that the observed match is a random event.
Protein scores greater than 71 are significant (p<0.05).

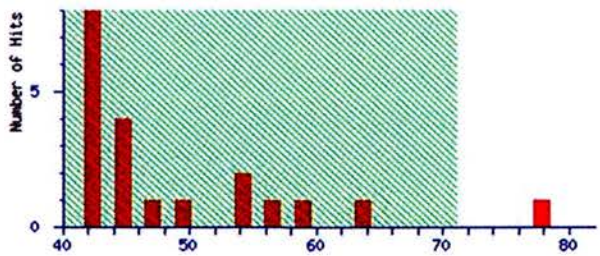

Figure 3.21 – Example of Mascot Identification of Protein from a 2-DE Gel Separation
The example shown here is for the peroxiredoxin-2 spot shown in figure 3.20 from a two-dimensional BN-PAGE and SDS-PAGE experiment. Scores over the threshold are indicated in red outside the green shaded area and are considered to be significant.

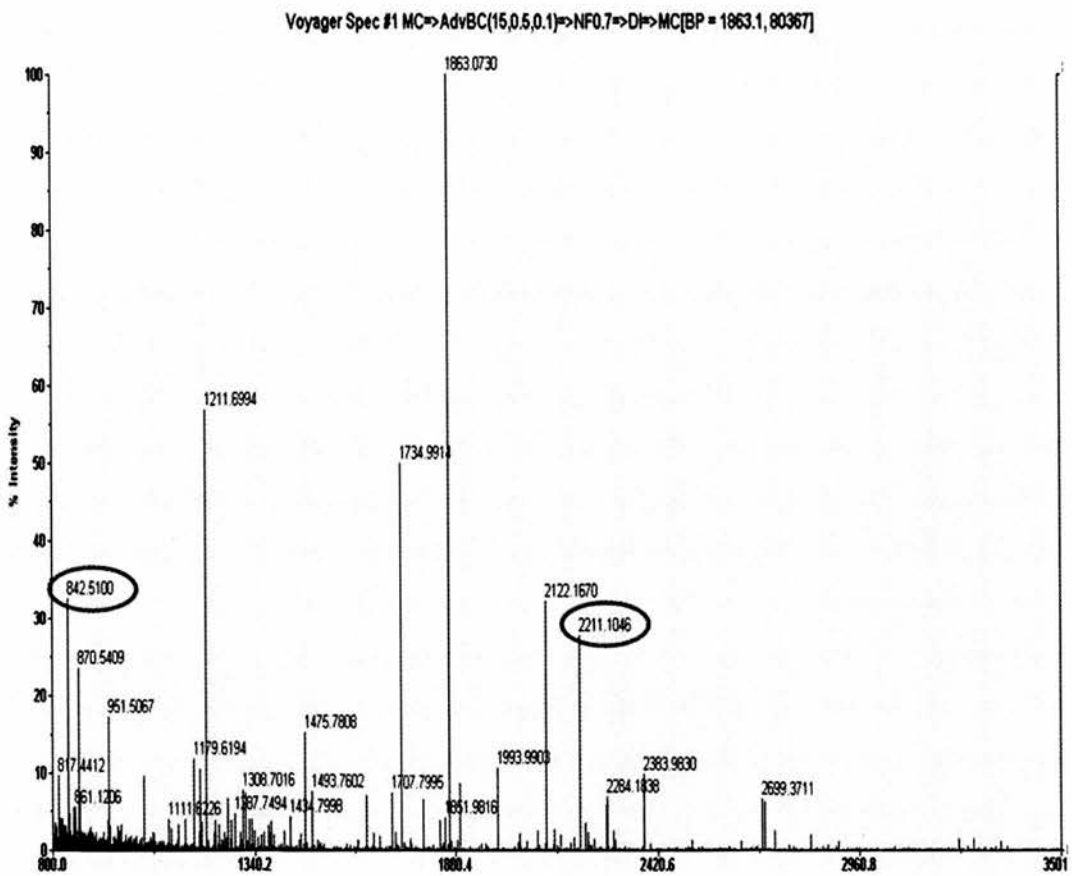

Figure 3.22 – Example of MALDI-TOF Mass Spectrum

This spectrum shown was that generated by digestion of the spot labelled peroxiredoxin-2 on figure 3.20. The spectrum was processed using Data Explorer software. The red circled peaks are the trypsin peaks that all other masses were calibrated to. All masses over a certain percentage intensity are submitted to a search engine for peptide mass fingerprinting. This spectrum generated the result shown in figure 3.21.

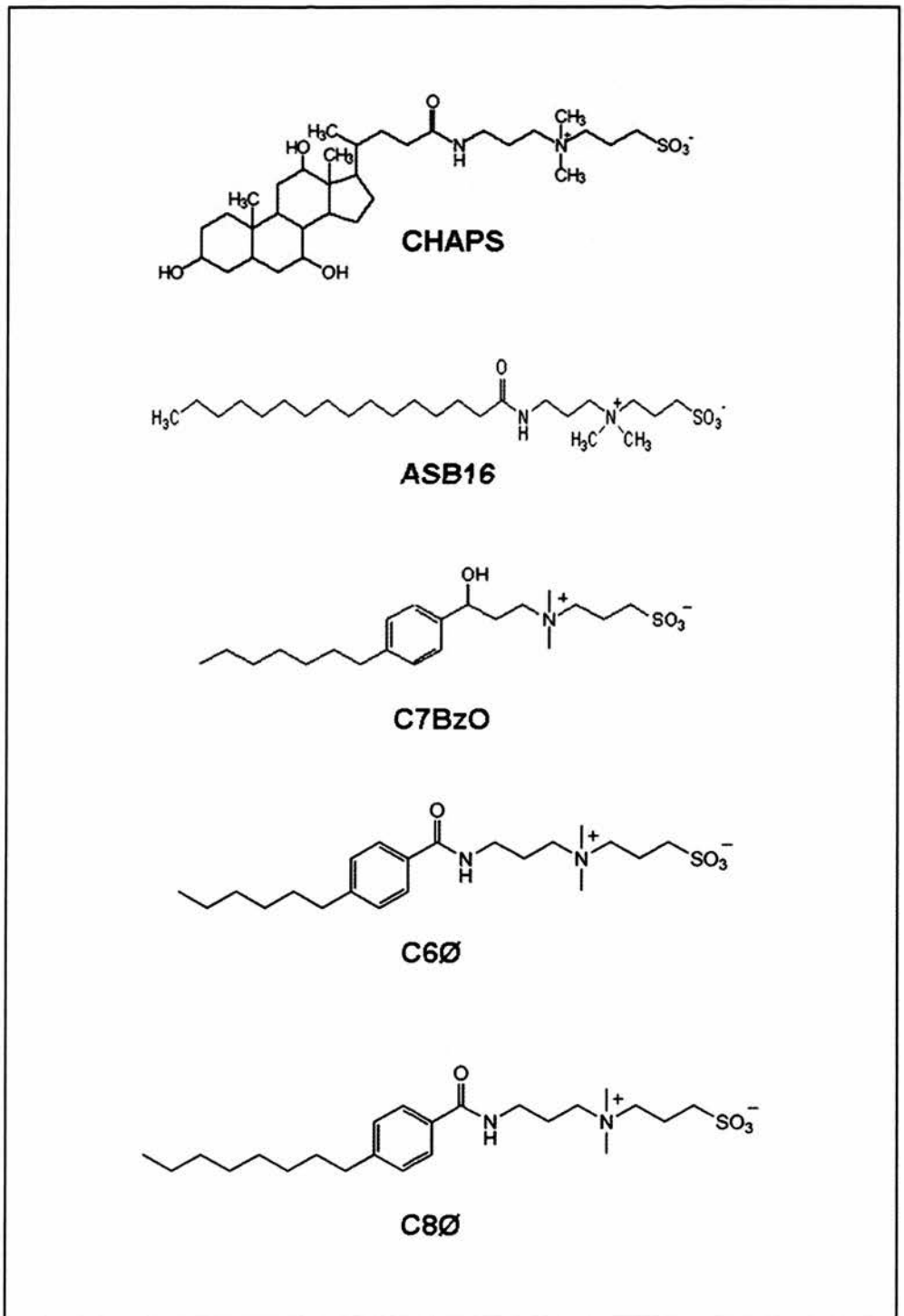

Figure 3.23 – Structures of Detergents Tested in 2-D Electrophoresis

All images were obtained from www.merckbiosciences.co.uk

Chapter 4

Characterisation and Use of a New N-Terminal NKCC1 Antibody for Western Blot and Immunoprecipitation

Chapter 4 – Characterisation and use of new N-terminal NKCC1 antibody for western blot and immunoprecipitation

T4 monoclonal antibody (Lytle *et al*, 1995) has been used successfully in western blot, immunoprecipitation and immunohistochemical applications (Matskevich *et al*, 2005; Marty *et al,* 2002; Alvarez-Leefmans *et al*, 2001; Bildin *et al,* 2001; Maglova *et al,* 1998; Crouch *et al*, 1997). This antibody is specific for regions in the C-terminal portion of both NKCC isoforms. Although raised against human cotransporter, due to the homology that exists in these regions, it also recognises NKCC from many other animal species. However, T4 antibody is specific only for SDS-denatured cotransporter and therefore limits its use. In order to gain more specific information about the basolateral or housekeeping isoform, NKCC1, it would be advantageous to have an effective antibody to this isoform only. An antibody raised against two sequences in the N-terminal portion of human NKCC1 was custom-made (dubbed N1) and tested in western blot and IP applications.

4.1 – N1 Antibody Information

Rabbits were immunised with peptide sequences from the N-terminus of human NKCC1. These regions are P71- F84 (PLGPTPSQSRFQVD) and R240 – F255 (RPSLAELHDELEKEPF). These peptides were synthesised with a terminal cysteine residue to allow coupling to a carrier protein and/or sepharose beads via sulfhydryl linkage. Covalab, France, (www.covalab.fr) prepared the peptides, immunised the animals and supplied us with pre-immune and immune sera. They also supplied immobilised peptides on a gel matrix to allow peptide-purification of the N1 polyclonal antibodies.

4.2 - Western Blotting Using N1 Antibody

Ferret erythrocyte membrane proteins (approximately 5μg total membrane protein) were separated by SDS-PAGE. After transfer onto nitrocellulose or PVDF, NKCC protein was probed for with T4 monoclonal antibody (1 in 4000 dilution; 18.5μg total Ig in 20ml total volume), N1 peptide-purified antibody (1 in 2500 dilution; 7.2μg peptide-pure antibody in 20ml total volume) and N1 immune-serum. Figure 4.1 shows a comparison of a western blot using T4 as primary antibody, with that of N1 peptide-purified antibody. These both show strong bands of immunoreactivity with a molecular weight of around 146kDa, as calculated using TotalLab software. Measurements from experiments on five different samples gave a mean value of 146 ± 4 kDa ($\bar{x} \pm \sigma$) for N1 and 146 ± 2 kDa for T4. An unpaired *t* test reports that these means are not significantly different (p = 0.9550). Commonly, bands of apparent molecular masses above 200 kDa are seen using both antibodies. The presence of these varies, but the band of "monomer" mass is always present and strong. The larger bands will be discussed in later chapters of this thesis. The use of immune serum was also tested for immunoblotting. Sera from two rabbits, bled 81 days after immunisation, were tested. Several dilutions were used to assess the optimal usage of the serum. Figure 4.2 shows that NKCC could be detected on blots of ferret erythrocytes using sera diluted 200 or 1000 fold. By visual comparison of figures 4.1 and 4.2, it is clear that using peptide-purified antibody results in stronger western blot immunoreactivity from the same amount of starting protein. Also, with the use of serum, there is always the possibility of cross-reactivity of the secondary antibody to other rabbit proteins present and as such, the peptide-pure antibody gives a cleaner result. The predicted mass for human NKCC1 is calculated at 132 kDa (protein

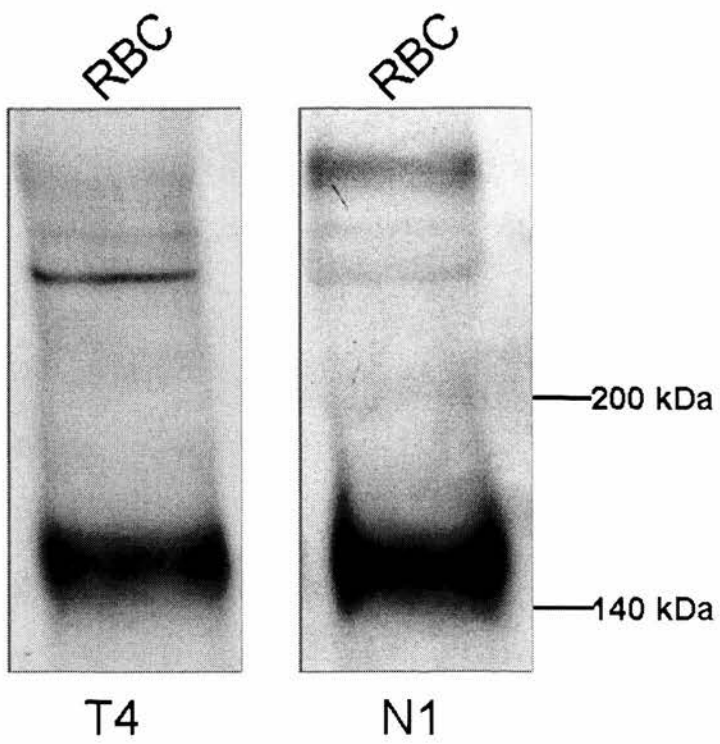

Figure 4.1 – Western blot detection of NKCC using T4 and N1 antibodies
Ferret red blood cell (RBC) membranes (5µg per lane) were separated by SDS-PAGE and transferred to nitrocellulose. T4 monoclonal antibody and peptide-purified N1 antibody were used to detect NKCC protein. Some guide molecular masses are shown and were taken from a biotinylated protein ladder.

sequence NP_001037 from NCBI protein database) using the Compute pI/MW tool from the Expasy tools website (www.expasy.ch/cgi-bin/pi_tool). The apparent molecular mass on SDS-PAGE gels may vary from the predicted mass due to glycosylation. Figure 4.3 shows an example of three experiments, where ferret red blood cell membranes were treated with N-glycosidase F and the molecular masses then calculated. Treatment reduced the apparent molecular mass of the cotransporter from 147 ± 3 kDa to 135 ± 4 kDa ($\bar{x} \pm \sigma$), which correlates with the predicted mass for human NKCC1. A two-tailed unpaired *t* test implies that these means are

significantly different ($p = 0.0129$). This gives further weight to the conclusion that the protein detected by N1 antibody in ferret samples is indeed NKCC1.

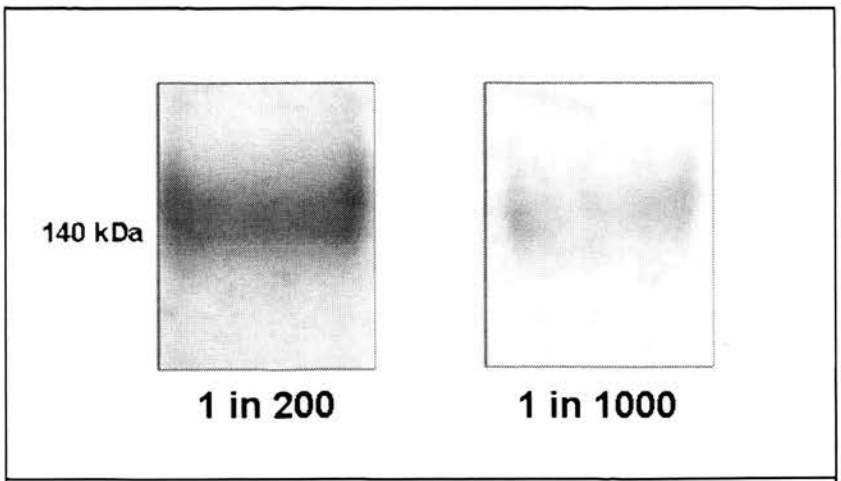

Figure 4.2 – Western blot detection of NKCC using N1 immune serum

SDS-PAGE separated ferret RBC membrane proteins (5µg per lane) were transferred to nitrocellulose and the blots probed with immune serum at dilutions of 1 in 200 and 1 in 1000. A guide molecular mass is shown which was taken from a biotinylated protein ladder.

4.3 - N1 Westerns on Various Tissues from Different Animal Species

Although the antibody was raised to sequences from human NKCC1, figures 4.1 and 4.2 clearly show detection of NKCC1 from ferret red blood cells. BLAST of the peptide sequences shows their presence in a variety of animal species with 100% sequence identity (shown in table 4.1). Recent work from our laboratory indicates that both peptides are present in the ferret cotransporter sequence (Hannemann, unpublished). For comparison, western blot experiments were carried out on various tissues from ferret and on rat erythrocytes (figure 4.4). Although kidney expresses high levels of the NKCC2 isoform, there is also expression of NKCC1 (Delpire *et al*, 1996). Salivary glands and testes are known to express NKCC1 (Flemmer *et al*,

2002; Delpire *et al*, 1994; Xu *et al*, 1994), and although there are no published immunohistochemical or western blot data for rat erythrocytes, there is strong evidence from cotransport studies to suggest that NKCC is present (Hannaert *et al*, 2002; Mairbaurl *et* al, 2000; Alvarez-Guerra *et al*, 1998). All samples show a band of immunoreactivity at positions between 130-176 kDa, except for the bacterial cell lysate (donated by Heather McLafferty) which was included as a negative control. The variability of these apparent molecular masses may be due to the cotransporter being differently glycosylated from the various tissues. Also, there may be species variability between ferret and rat.

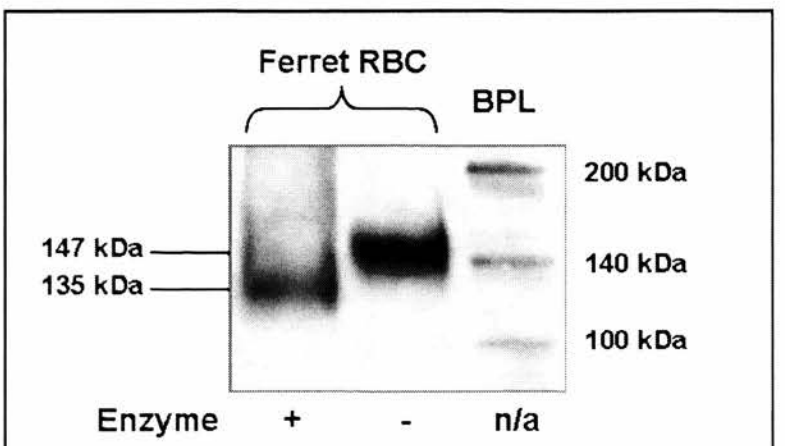

Figure 4.3 – Deglycosylation of ferret erythrocyte NKCC
Recombinant N-glycosidase F was used to deglycosylate ferret erythrocyte membranes. T4 antibody was used to detect NKCC protein. Apparent molecular mass was measured using TotalLab software by comparison to a biotinylated protein ladder (BPL).

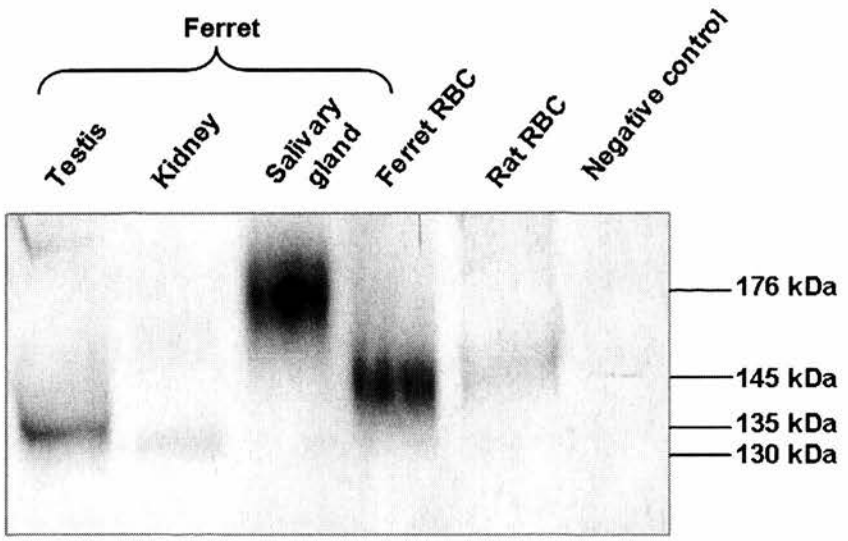

Figure 4.4 – Detection of NKCC1 from different tissues and species using N1 peptide-purified antibody
Isolated cell membrane (or bacterial cell lysate in the case of the negative control) proteins were separated by SDS-PAGE and transferred to nitrocellulose. Peptide-purified N1 antibody was used at 1 in 1000 dilution to detect NKCC protein.

RPSLAELHDELEKEPF	
Species	*Protein*
Mouse	NKCC1
Chimpanzee	NKCC1
Rhesus macaque	NKCC1
Rat	NKCC1
Cow	NKCC1
Dog	NKCC1

PLGPTPSQSRFQVD	
Species	*Protein*
Mouse	NKCC1
Chimpanzee	NKCC1
Rhesus macaque	NKCC1
Rat	NKCC1
Cow	NKCC1

Table 4.1 – Proteins with N1 antibody sequence determinants present
A non-redundant database search using Blastp (protein-protein) reveals the presence of the sequences used to create the N1 antibody in NKCC1 of all mammalian species recorded. Blastp can be found at www.ncbi.nlm.nih.gov/BLAST.

4.4 – N1 Immunodetection of Phosphorylated NKCC1

The Na-K-2Cl cotransporter has previously been shown to be phosphorylated on threonine and serine residues when actively transporting ions (Lytle, 1997). Both

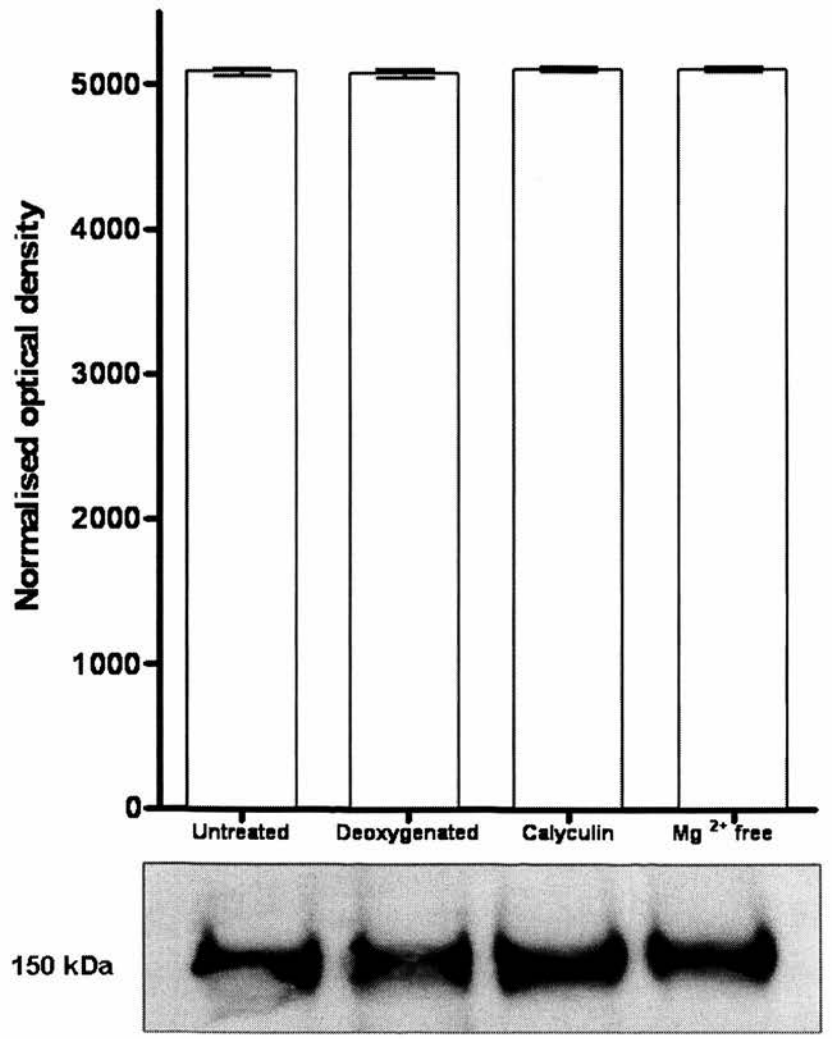

Figure 4.5 – N1 antibody binding is not affected by the phosphorylation state of the cotransporter

Ferret erythrocyte membrane samples (n=3) of differing NKCC phosphorylation state were prepared for SDS-PAGE according to total protein content (10µg). Optical densities for each band were obtained using TotalLab software. These values were normalised to the density of a sample of known protein content (from a molecular weight marker reference). This allowed the optical densities to be corrected for slight variations in sample protein content. Error bars show ± standard deviation.

peptide sequences used to create the N1 antibody contain serine residues and peptide P71- F84 contains one threonine. Although it is not known whether or not these residues could be phosphorylated on the cotransporter, it is important to test whether or not NKCC phosphorylation could cause altered N1 antibody binding. Ferret erythrocyte membranes, isolated from cells that had first been exposed to conditions that increase or reduce phosphorylation on the cotransporter, were prepared for SDS-PAGE and transferred to nitrocellulose. Deoxygenation or treatment of cells with calyculin A results in increased cotransporter activity (Matskevich *et al*, 2005; Flatman, 2005) and as shown in chapter 5, increased cotransporter phosphorylation. The removal of cell magnesium results in the inhibition of kinases and reduces phosphorylation and cotransporter activity (Matskevich *et al*, 2005). N1 peptide-purified antibody was then used to detect NKCC1 and the blots were analysed using TotalLab software. Figure 4.5 demonstrates that, regardless of cotransporter phosphorylation, N1 antibody binds to NKCC1.

4.5 - Immunoprecipitation Using N1 Antibody

This set of experiments was to determine whether the N1 antibody could effectively immunoprecipitate NKCC protein. Ferret membrane samples were prepared for immunoprecipitation. A number of different control and test conditions were examined and are described in table 4.2 and demonstrated in figure 4.6. A major band is detected at ~150kDa after IP with either T4 or N1 antibody, which is not present in the negative control samples (lanes 4 and 5). Using pre-immune serum (denoted N1Pi in figure 4.6) does not result in the presence of the major band. The band was not present in the absence of erythrocyte membrane protein. These tests

			Western Blot		
Membrane Protein	**SDS Denaturation**	**IP Antibody (μg)**	**Primary Antibody**	**Secondary Antibody**	**Reason for Test**
Y	Y	T4 (18.5)	T4	GAM	Standard T4 IP protocol
Y	Y	N1peptide purified (0.9)	T4	GAM	To compare with standard T4 IP
Y	N	N1peptide purified (0.9)	T4	GAM	To test necessity of SDS in protocol
Y	N	Pre-immune serum	T4	GAM	Negative control
None (ddH_2O)	N	N1 peptide purified (0.9)	T4	GAM	Negative control
Y	Y	T4 (18.5)	N1 immune serum	GAR	Secondary antibody not specific to IP antibody species
Y	N	T4 (18.5)	N1 immune serum	GAR	To test necessity of SDS in protocol

Table 4.2 – N1 Immunoprecipitation Test Samples
The upper section of the table describes the samples shown in figure 4.6 (left panel) and the lower section represents figure 4.6 (right panel). Y = yes N = no GAM = goat anti-mouse antibody GAR = goat anti-rabbit antibody ddH_2O = double glass distilled water

confirm several important features. Firstly, inoculation with NKCC1 specific peptides is responsible for the immunoreactive antibodies found in the rabbit serum. Also, when sample was not included bands were not found at NKCC1 monomer molecular weight. This shows that those detected in lanes 1-3 are likely to be

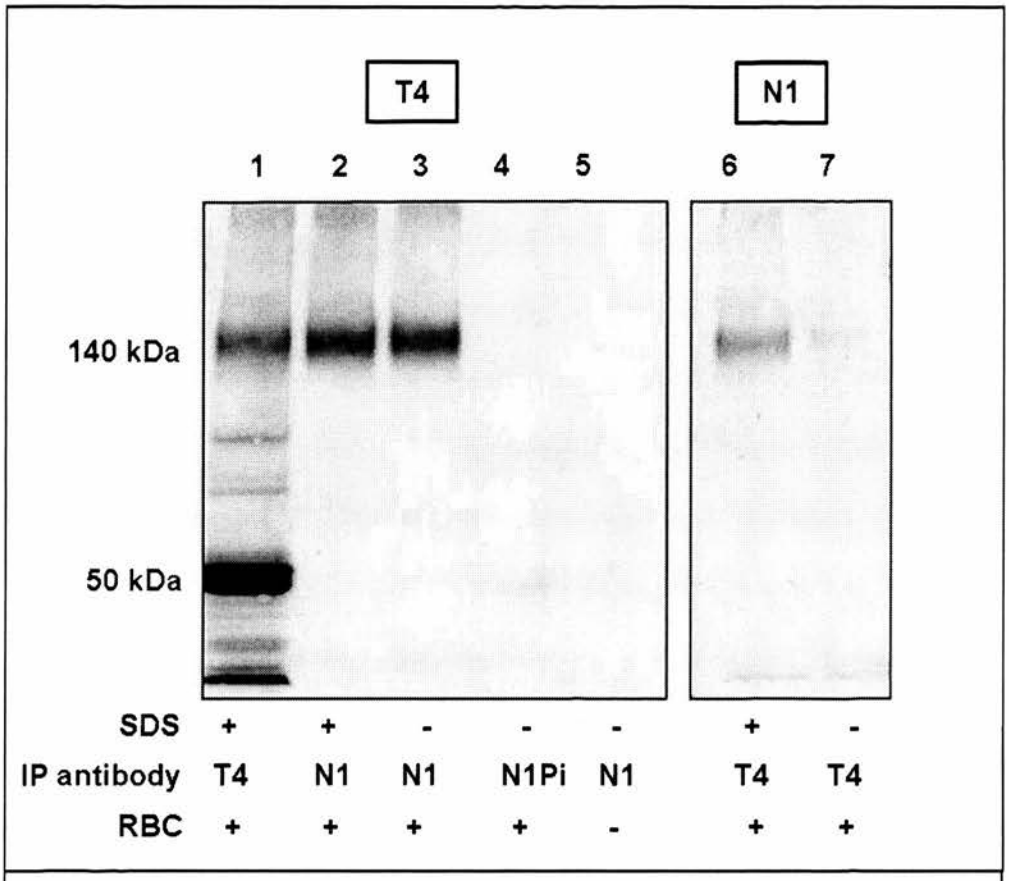

Figure 4.6 – Immunodetection of NKCC after immunoprecipitation of ferret erythrocyte membrane proteins using T4 and N1 antibodies

T4 (left panel) and N1 (right panel) immune serum antibodies were used to detect NKCC protein. Some guide molecular weights are shown and were calculated from a biotinylated protein ladder that was run on the gels alongside the samples.

specific to the ferret sample and not any cross-reactivity with proteins in the immune serum or to the T4 ascites. Lane 1 shows a number of additional bands. The IP antibody here was T4 monoclonal mouse IgG. The western blot detection antibody was also T4 and as such the secondary antibody (goat anti-mouse) will detect the IP antibody. Results of further investigations of this are shown in figures 4.7 and 4.8. This experiment also demonstrates that there is no requirement for SDS-denaturation of the membrane sample prior to immunoprecipitation with N1 antibody, as demonstrated in lanes 2 and 3 in fig 4.6. On the other hand, lanes 6 and 7 highlight

how necessary it is for NKCC to be SDS-denatured before immunoprecipitation with T4 antibody. Where no SDS was included in the sample preparation, very little

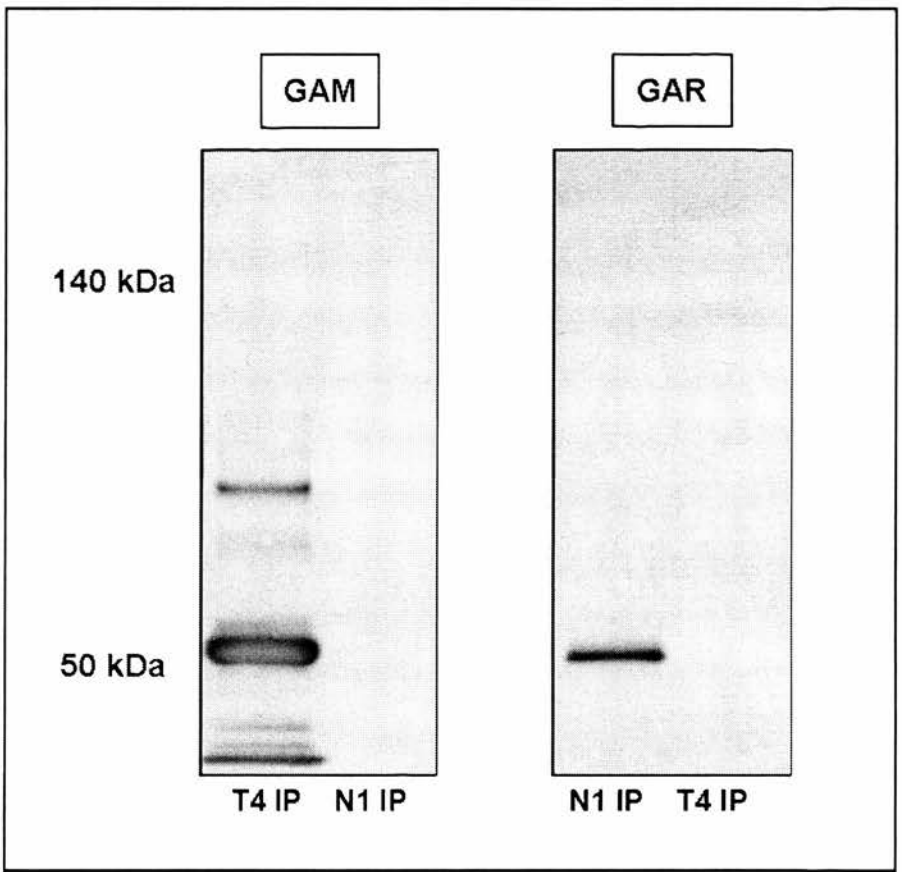

Figure 4.7 – Secondary antibody probe of IP samples
After IP of ferret membrane proteins, SDS-PAGE and transfer to nitrocellulose, proteins were detected using only secondary antibodies as probes. The left panel shows the results of a western blot using goat anti-mouse (GAM) antibody. The right panel shows the results of a western blot using goat anti-rabbit (GAR) antibody. Some guide molecular masses are shown and were taken from a biotinylated protein ladder run alongside the samples.

immunoreactivity is present in comparison to the sample where our standard protocol is used (see chapter 2 for details of protocol). As mentioned, experiments were conducted to assess any cross-reactivity of western blot secondary antibodies to those used in immunoprecipitation and the results are shown in figures 4.7 and 4.8. In both

figures, no bands are visible at the expected cotransporter monomer molecular weight position of 140-160kDa, showing that the secondary antibodies used throughout do not cross-react with NKCC. The left panel of figure 4.7 shows several bands of GAM reactivity to T4 antibody. This is not surprising as T4 was raised in mouse. However, there are bands other than the expected heavy and light chains (approximately 55kDa and 25kDa respectively) and show the same pattern as those in figure 4.6 lane 1. Although T4 is a monoclonal antibody, it comes as ascites fluid and there may be other antibodies/proteins from the mouse that GAM reacts with. Importantly, there is no reactivity of GAM to N1 antibody. The right panel shows that GAR does not react with T4 antibody. GAR only appears to detect the heavy chain of the N1 antibody.

Figure 4.8 shows that when these antibodies are run as the protein sample and probed with secondary antibody on a western blot several bands are visible. Again, most are likely to correspond to antibody heavy and light chains. Several different amounts of T4 antibody were prepared to determine if the extra bands found were present in the ascites fluid, or pulled out from the ferret sample during immunoprecipitation. More bands appear with increasing antibody amount and are marked with asterisks on the figure and appear correspond to those found on figure 4.6 lane 1. This confirms that this reactivity is inherent to the T4 antibody ascites fluid /GAM interaction and not to GAM showing cross-species immunoreactivity to ferret proteins. This experiment also confirms that shown in figure 4.7, namely, that GAM does not detect ferret or rabbit protein and that GAR does not detect ferret or mouse protein.

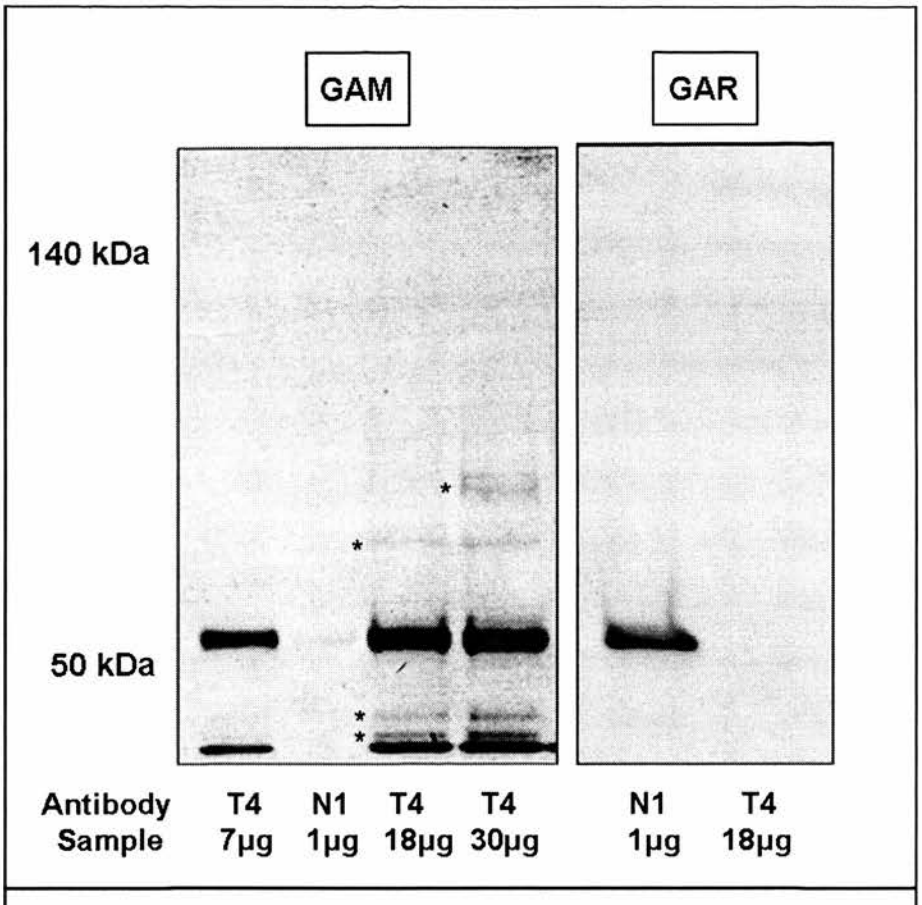

Figure 4.8 – Immunoreactivity of secondary antibodies to T4 and N1 The left panel shows a western blot using only goat anti-mouse (GAM) secondary antibody as the probe. Different amounts of T4 antibody were used to highlight the increase in number of bands present that are detected by GAM. The right panel shows a western blot using only goat anti-rabbit (GAR) secondary antibody as the probe.

4.6 – Using the N1 Antibody in Co-Immunoprecipitation Experiments

4.6.1 – Western Blotting

Other studies have shown that the SPAK and OSR1 kinases directly interact with the cotransporter (Gagnon *et al*, 2007a; Piechotta *et al*, 2002). Using antibodies gifted by the Alessi group (Dundee), the interaction of these kinases with the cotransporter from ferret erythrocytes was examined by western blots of N1-immunoprecipitates. Figure 4.9 shows bands at expected molecular masses for SPAK (approximately 66

kDa) based on the migration of this on SDS-PAGE gels in other animal species (Ushiro *et al*, 1998). Phosphorylated SPAK is also present in immunoprecipitates.

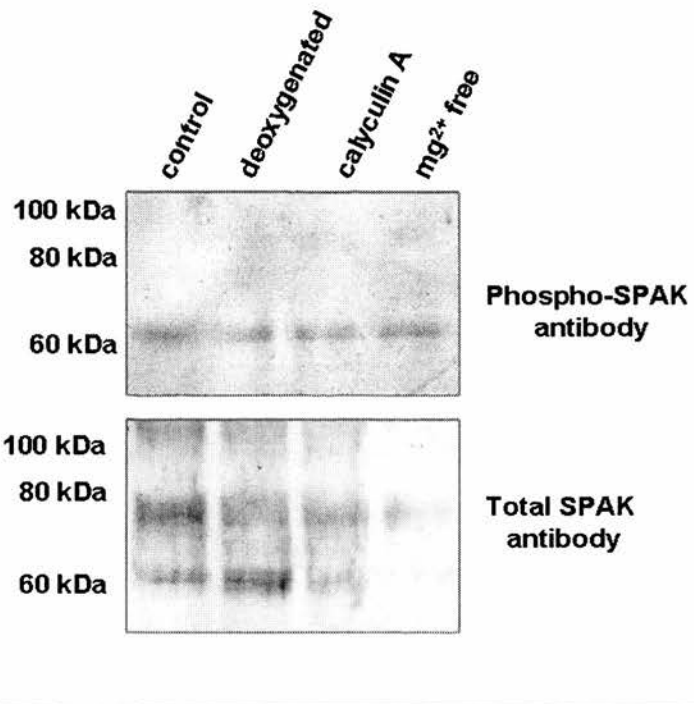

Figure 4.9 – N1 Immunoprecipitation of SPAK with NKCC
Ferret erythrocyte membranes (150 µg total protein) were immunoprecipitated with N1 peptide-purified antibody and protein G-sepharose. Western blots were performed using total and phospho-SPAK antibodies. Molecular weights were taken from a biotinylated protein ladder.

Other bands are visible at an estimated molecular mass of 75 kDa when using the total SPAK antibody. This antibody was raised to peptide that is present in both SPAK and OSR1. However, OSR1 has been shown to migrate at around 58 kDa on SDS-PAGE gels (Chen *et al*, 2004) and it unlikely that this is what is present at this higher position on the western blot. Unfortunately, as figure 4.10 shows, SPAK is also present in negative control samples and so we cannot make any assumptions about the relative amounts found in the N1 immunoprecipitates shown in figure 4.9.

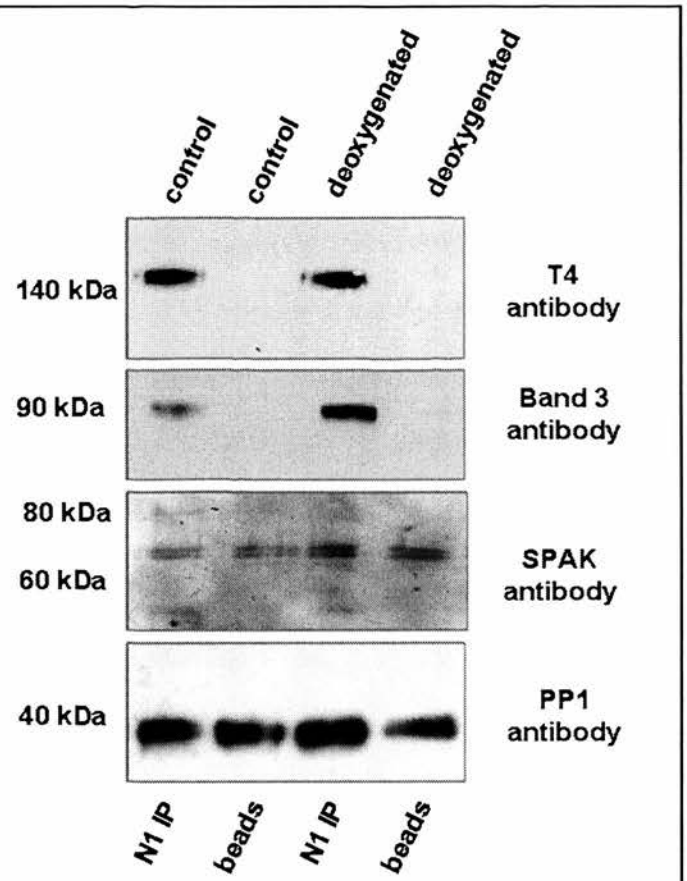

Figure 4.10 – Co-Immunoprecipitation with NKCC1
Control and deoxygenated ferret erythrocyte membrane samples (150µg total protein) were mixed N1 peptide-purified antibody and protein G-sepharose beads. Immunoprecipitates were run on SDS-PAGE gels and western blots probed with various antibodies. Samples mixed with beads and no antibody are included as negative controls. Molecular weights were interpolated from a biotinylated protein ladder.

Figure 4.10 also shows that protein phosphatase 1 (PP1) is present in N1 and bead negative control samples. Even though PP1 has been shown to co-precipitate with the cotransporter in previous studies (Darman *et al*, 2001) and that cotransporter also is pulled down with PP1 using microcystin-sepharose (Matskevich *et al*, 2005), we

cannot infer anything from these experiments due to the presence of PP1 in the negative controls. However, these experiments do demonstrate the presence of these regulatory proteins in the ferret erythrocyte and they may therefore be involved in cotransport regulation. Using an antibody to the erythrocyte anion exchanger, band 3, we see the presence of this in N1 immunoprecipitates, but not in negative controls. This is suggestive of NKCC1 interaction with band 3 in the ferret erythrocyte membrane.

4.6.2 – N1 Immunoprecipitation, SDS-PAGE and Mass Spectrometry

Attempts were made to isolate proteins interacting with NKCC1 by larger scale immunoprecipitation and separation of resulting proteins by SDS-PAGE. Figure 4.11 shows an example of a gel with ferret erythrocyte membrane proteins after N1 or bead only IP experiments. The only different bands between test and control samples were the IP antibody heavy and light chains, which were identified as rabbit IgG by MALDI-TOF mass spectrometry. Pre-clearance of the samples with protein G-sepharose results in the loss of most bands on the gel, as shown in figure 4.12. Again, apart from the heavy and light chains of the N1 antibody itself, there is little that is distinct between the test and control samples. However, a very faint band of approximately 150 kDa is present in the test samples and not in the negative control. This band was excised and digested with trypsin and a mass spectrum generated using MALDI-TOF. Peptide mass fingerprinting revealed no positive significant identification for this protein. Using a shotgun approach, N1 antibody immunoprecipitates were subjected to LC-MS/MS and subsequent Mascot MSMS ions search revealed the presence of malate dehydrogenase and heat shock 70 kDa protein 8 as well as antibody fragments, which are to be expected. Peptides for band

3 were also present but not enough peptides were present to make the score for this significant. This may be due to the large amount of contamination from keratin.

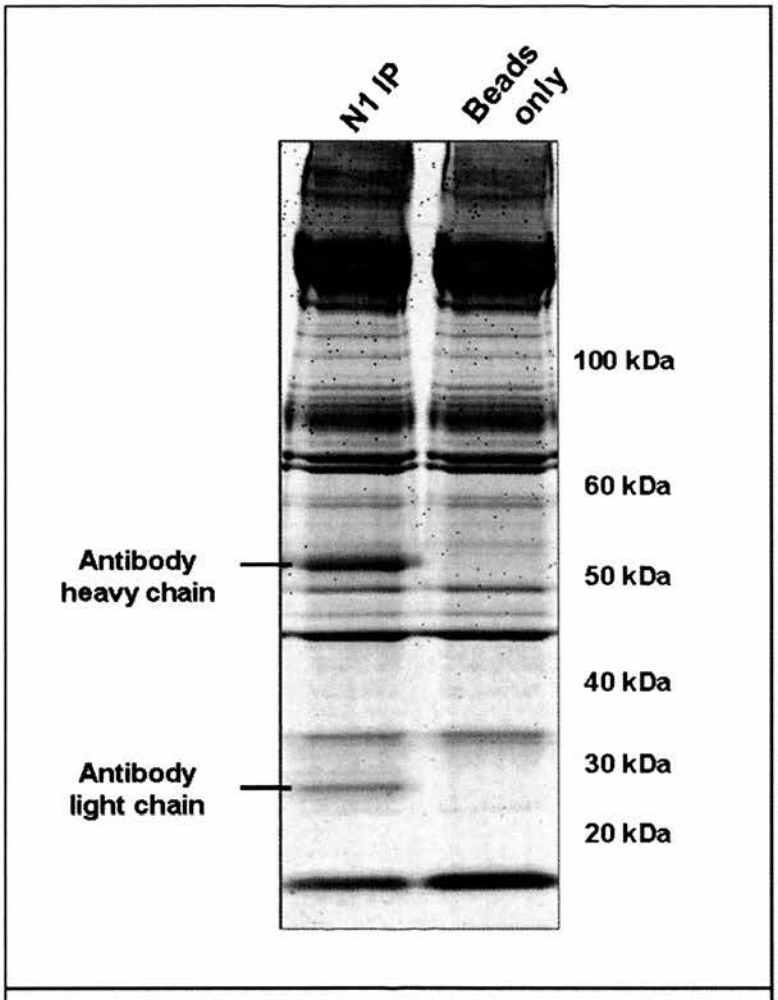

Figure 4.11 – Large Scale N1 Immunoprecipitation
Ferret erythrocyte membranes (500 µg total protein) were prepared for immunoprecipitation with N1 antibody. Samples were pre-cleared with protein G-sepharose and this was also used as a control for comparison with the sample including antibody. The molecular masses were interpolated from the SeeBlue® Plus2 marker set from Invitrogen.

This is a common problem when conducting work of this type and is often difficult to avoid. Due to their abundance they can mask less common peptides during the liquid chromatography and mass spectrometry steps and could account for the non-

significant score for band 3. These peptide matches were also observed using the Phenyx search tool (see Appendix for supplementary data). However, at no point were peptides for the cotransporter observed and thus any proteins identified from these experiments cannot truly be suggestive of protein interactions with NKCC.

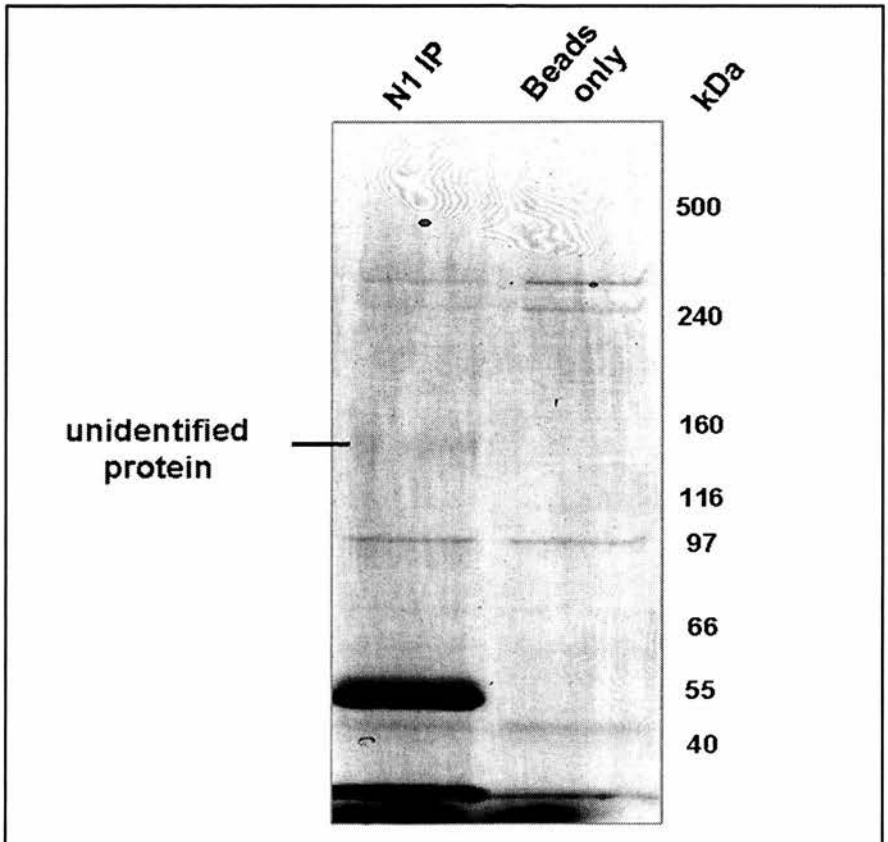

Figure 4.12 – N1 IP of a 150 kDa Protein from Ferret Erythrocytes
Pre-cleared samples (500 µg total starting protein) were mixed with N1 and protein G-sepharose beads or beads alone and the resultant precipitated proteins separated by SDS-PAGE. Molecular weights shown are from the HiMark™ marker set made by Invitrogen.

4.7 – Discussion of results

Overall, these experiments indicate that the custom-made N1 antibody is effective at western blot detection and immunoprecipitation of a protein that is consistent with the Na-K-2Cl cotransporter. The previously characterised T4 monoclonal antibody

is commonly used as the 'gold standard' in NKCC antibodies. N1 immuno-detects protein that migrates on SDS-PAGE gels at the same position as T4 detects. Deglycosylation of the cotransporter reduces the apparent molecular mass to that similar to the predicted molecular mass for human NKCC1, to which the N1 antibody was raised. This, along with the evidence from known NKCC1 expressing tissues, is suggestive that N1 does indeed detect NKCC1. Also, this interaction is not inhibited by the phosphorylation state of the cotransporter. This antibody does not detect protein from a bacterial cell lysate, which serves as a useful negative control. Although an uncharacterised homologue is found in cyanobacterium Synechococcus species (Park and Saier, 1996), NKCCs are generally not found in bacteria. What is not tested is whether or not the N1 antibody detects NKCC2. As mentioned, kidney is cited as the only source of NKCC2, but it also expresses NKCC1. Without a pure source of NKCC2 protein this aspect of the N1 antibody must go uncharacterised. N1 is also effective for use as an immunoprecipitation antibody. Most importantly, SDS-denaturation is not required for this interaction to occur. Unlike T4 antibody, this allows the use of the N1 antibody for co-immunoprecipitation experiments. Using the antibody for larger scale co-IP experiments had disappointing results. The only protein observed on SDS-PAGE gels in test samples not found in control samples was not able to be identified by MALDI-TOF mass spectrometry. This may have been due to an issue with protein abundance as the bands were always very faint. Due to the migration of this protein on SDS-PAGE gels at approximately 150 kDa it may even have been the cotransporter itself, but without positive mass spectrometry identification this is only a speculation. Although ferret erythrocytes possess greater amounts of cotransporter compared to red cells from other animal

species it is still present at fairly low levels. This is reflected by the LC-MSMS data of N1 immunoprecipitates, where no NKCC was detected. This issue could be further affected by the nature of the sample itself, where the fairly gentle method of erythrocyte membrane preparation results in there being large amounts of remaining haemoglobin and cytoskeletal proteins present. Perhaps this technique would be put to better use in samples with higher levels of cotransporter expression, but still represents a sensitive and useful technique for the detection of cotransporter interacting proteins.

SPAK has been shown to interact with NKCC in yeast-2-hybrid assays and co-IP experiments from brain lysates (Piechotta *et al*, 2002) and is known to be a cotransporter kinase (Vitari *et al*, 2006). SPAK and OSR1 have been shown to phosphorylate the cotransporter in response to hyperosmotic stress (Zagórska *et al*, 2007; Villa *et al*, 2007). Exposure of ferret erythrocytes to conditions that increase or decrease cotransport activity, followed by membrane preparation and immunoprecipitation with the N1 antibody allows investigation of any differences in binding of proteins to the cotransporter. Western blotting of N1 immunoprecipitates showed the presence of SPAK and/or OSR1, as detected by an antibody that is specific for regions present in both of these cotransporter kinases. However, the presence of SPAK immunoreactivity in sepharose-bead (no IP antibody) negative control samples prevents any comparison being made about the binding of SPAK and phosphorylated SPAK (and therefore activated) to the cotransporter under any of the conditions shown. The total SPAK antibody shows the presence of a band at an unusual molecular weight of approximately 75 kDa. This does not correspond to any published masses for either SPAK or OSR1. BLAST (Basic Local Alignment Search

Tool) of the human SPAK amino acid sequence brings up a sequence for a putative SPAK in dog, which is approximately 75 kDa in size. As dog and ferret are both within the order of Carnivora and it is possible that ferret may have a kinase of similar size which could account for the bands detected at this position on the western blots. PP1 was also detected in the ferret red blood cell, but as with the findings for SPAK, the phosphatase is also precipitated with protein G-sepharose. As calyculin A stimulates increased cotransport and increased threonine phosphorylation (as shown in chapter 5) it is strongly suggestive of a role for PP1 in NKCC regulation. Unfortunately, the data presented in this chapter are unable to provide further insight into the role of PP1 in cotransport regulation.

Band 3 is detected by antibody and mass spectrometry from N1 immunoprecipitates. Other studies have looked at the interaction of this protein with the cotransporter. As already mentioned in section 3.3, the trout erythrocyte anion exchanger has been shown to change the activity of endogenous NKCC in *Xenopus* oocytes when expressed in these cells (Guizouarn *et al*, 2004). The evidence from this paper, the presence of band 3 in complex with the cotransporter (suggested in chapter 3 of this thesis) and the co-IP of the protein with NKCC1 shown in this chapter do imply an interaction of these two proteins. The presence of malate dehydrogenase may be due to an interaction with band 3, as it is known to bind a number of glycolytic enzymes under oxygenated conditions (Campanella *et al*, 2005). It would be of interest to see if this protein is still detectable from N1 immunoprecitates from deoxygenated red blood cell samples. The presence of a heat shock protein may present a direct interaction with the cotransporter. Heat shock protein 90 has been shown to interact with NKCC1 (Simard *et al*, 2004b), and so it may be feasible that HSP70 directly

interacts with the cotransporter itself, rather than indirectly via Band 3 as is likely to be the case with malate dehydrogenase. These proteins may represent the NKCC environment under basal cotransport conditions. It will be of interest to study interactions in stimulated cells, to identify further NKCC regulatory proteins. This method and others could be used to achieve this. Using, for example, GST-NKCC fusion proteins we could fish for interactions by using the affinity of GST for glutathione (on beads). Cell lysates would be mixed with the NKCC fusion protein and beads and any interacting proteins could be pulled-down and identified by mass spectrometric methods (Monti *et al*, 2005). This method will only reflect the *in vitro* situation and may not help when assigning functional significance to interactions. Cross-linking of proteins, and then capture of these with the N1 antibody, could allow more meaningful identification of proteins interacting with NKCC. A method described by Vasilescu *et al* (2004) involves treating samples with cell permeant formaldehyde and immunocapture of desired protein complexes. Boiling of the samples in SDS reverses the cross-links and allows separation of the individual proteins again by SDS-PAGE. Mass spectrometry was used to identify individual proteins. This method is useful in that it allows for more stable isolation of protein complexes, which may otherwise dissociate during sample preparation. This could uncover novel interacting partners for NKCC.

A method that shows far fewer non-specific protein interactions in complexes is known as tandem affinity purification (TAP). This involves the expression of a desired protein containing two affinity tags, protein A and calmodulin-binding peptide, which are separated by a tobacco etch virus (TEV) protease cleavage site (Puig *et al*, 2001). This allows affinity purification first by an IgG column and then

cleavage of the complex with the TEV protease. This is then further purified using a calmodulin column and elution is achieved by alteration of calcium concentration. The eluents are analysed by mass spectrometric methods. This approach was originally developed in a yeast expression system, but has now been developed for examination of mammalian proteins (Knuesel *et al*, 2003). This allows more appropriate expression of mammalian proteins of interest and importantly, they can be expressed at near physiological levels meaning that any information obtained from these experiments has more physiological relevance than systems where proteins are over-expressed.

Changes to the LC-MSMS method itself could result in greater numbers of peptides being found. The protocol used here was fairly short and it may be that many peptides remained on the column after the run was complete. These simple modifications could improve the method described in this thesis. Also, multi-dimensional liquid chromatography could be used. For example, strong cation exchange chromatography could be used for the first dimension separation with reverse-phase HPLC (performed in this thesis) as the second (Tomer, 2001). This would allow improved resolution of these complex sample mixes and may help to identify more proteins. This could also be used for the study of the blue-native PAGE complexes described in chapter 3.

Chapter 5

Phosphorylation of the Na-K-2Cl Cotransporter

Chapter 5: Phosphorylation of the Na-K-2Cl Cotransporter

Phosphorylation of the Na-K-2Cl cotransporter is linked to its transport activity. Lytle (1997) showed a proportionate increase in duck erythrocyte NKCC phosphorylation in response to a variety of cotransport activating stimuli. Studies of NKCC recovered from shark rectal gland have identified three key threonine residues, in the cytoplasmic N-terminal region, that are phosphorylated when the cotransporter is active (Darman & Forbush, 2002) and more recently, another two residues have been mapped to this region (Vitari *et al*, 2006). However, there may be other threonine or serine residues whose phosphorylation could modulate cotransporter function. Indeed, activation of NKCC in duck erythrocytes shows the cotransporter to be phosphorylated at both threonine and serine sites, but not phosphotyrosine, within the N- and C-termini (Lytle, 1997). This chapter includes analysis of general threonine phosphorylation on the ferret erythrocyte cotransporter and investigates threonine phosphorylation of the residues that are thought to be key in NKCC regulation.

5.1 – NKCC Phosphorylation Using General Phospho-Antibodies

5.1.1 - Tyrosine phosphorylation

Phosphorylation of tyrosine residues on the cotransporter is not considered to occur (Lytle, 1997). Western blot analysis of total phosphotyrosine was examined in T4 immunoprecipitates from ferret RBCs, after SDS-PAGE separation as shown in figure 5.1. A number of sample conditions are shown. The left hand panel of figure 5.1 represents samples where cotransport rate was reduced by the effects of inhibiting kinase activity, whereas the right hand panel shows those samples where

cotransport activity was increased (as determined by Rb^{86} flux; Flatman and Creanor, 1999a and 1999b). No phosphotyrosine was observed on the cotransporter and this did not change under any of the conditions used to modulate cotransport. This provides further evidence that the activity of NKCC is not modulated by addition of phosphate to tyrosine residues.

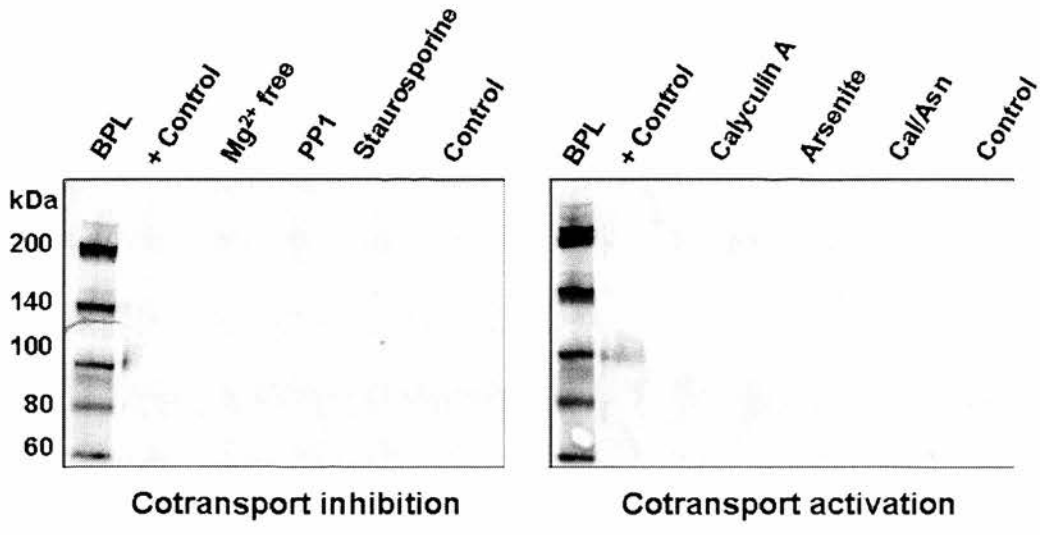

Figure 5.1 – Phosphotyrosine on T4 Immunoprecipitated NKCC from Ferret RBCs
All cells were incubated with 11 mM glucose in FBM for 10 minutes at 38°C to allow cells to equilibrate, before treatment to inhibit or activate NKCC cotransport. The following additions were made: none (control), 50 µM PP1 for 30 minutes, 2 µM staurosporine for 20 minutes, 2 mM Tris-EDTA plus 10 µM A23187 for 15 minutes (Mg^{2+} free), 50 nM Calyculin A for 15 minutes, 1 mM Na+ arsenite for 60 minutes, 50 nM Calyculin A and 1 mM Na+ arsenite for 60 minutes (Cal/Asn). In each immunoprecipitation, 150 µg of total membrane protein was included. The + control sample is a phosphotyrosine positive cell lysate (Zymed) and anti-phosphotyrosine antibody was used as the primary antibody. A biotinylated protein ladder (BPL) is shown alongside.

5.1.2 – Threonine phosphorylation

To show threonine phosphorylation of the cotransporter, T4 monoclonal antibody was first used to precipitate protein from ferret erythrocyte cell membranes. The immunoprecipitates were separated by denaturing SDS-PAGE and transferred to

nitrocellulose for immunodetection with anti-phosphothreonine antibodies. This method allows visualisation of total threonine phosphorylation (detectable by the antibody), and also gives an easy method of comparison. As such, cell membranes from ferret erythrocytes, treated with various compounds that affect cotransport rate, are directly comparable on a single blot. Figure 5.2 shows a representative western blot of anti-phosphothreonine on NKCC under unstimulated control conditions and treatments where cotransporter activity is increased with pharmacological agents and figure 5.4 shows the same, but with deoxygenated samples, a strong physiological stimulus of cotransport (Flatman, 2005). An increase in threonine phosphorylation is seen when cells are under stimulating conditions and lower levels of phosphorylation are present on cells under normal conditions. The optical densities of each sample were calculated using TotalLab software and normalised to the control within each experiment. This allows comparison of phosphorylation between each sample. Treating erythrocytes with a number of different compounds that inhibit protein kinase activity reduces NKCC threonine phosphorylation, but does not abolish it completely. Figure 5.3 shows this with phosphorylation levels relative to control cells. In all cases, phosphorylation is reduced, but never completely lost. These experiments show (see also Matskevich *et al*, 2005) that the overall trend in ferret erythrocytes fits with that observed in other animal species, where inhibition of phosphatases increases NKCC phosphorylation and inhibition of kinases reduces NKCC phosphorylation. Arsenite, particularly in combination with Calyculin A, produces the greatest increases in threonine phosphorylation. General kinase inhibition by removal of cell magnesium and inhibition of serine/threonine kinases with staurosporine results in an expected reduction of cotransporter phosphorylation.

Although we do not observe tyrosine phosphorylation on the cotransporter, treatment of cells with genistein and PP1i (considered to be tyrosine kinase inhibitors) results in reduced threonine phosphorylation. Table 5.1 summarises the changes in phosphorylation on the cotransporter compared with control samples.

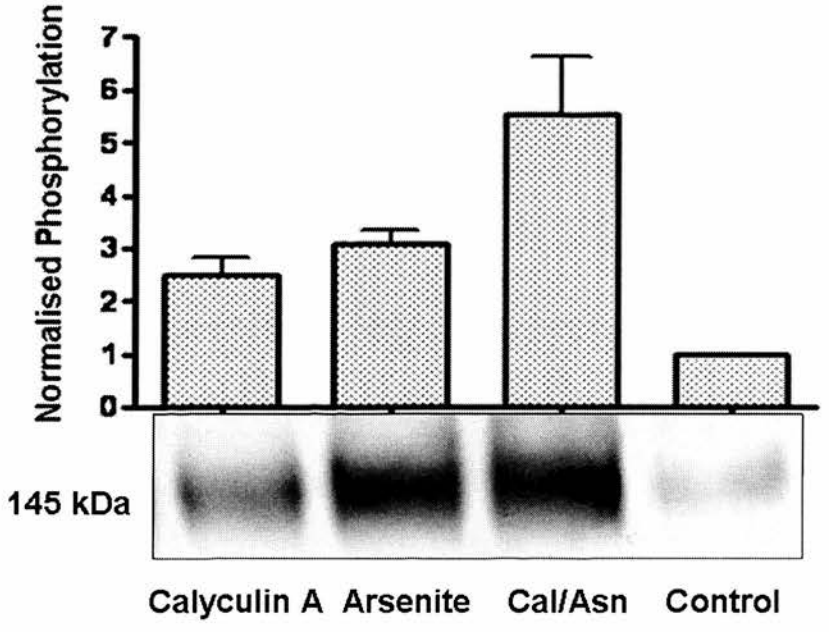

Figure 5.2 – Phosphothreonine on T4 immunoprecipitated NKCC
All cells were incubated with 11 mM glucose in FBM for 10 minutes at 38°C to equilibrate. The following additions were then made: none (control), 50 nM Calyculin A for 15 minutes (Calyculin A), 1 mM Na^+ arsenite for 60 minutes (Arsenite), 50 nM Calyculin A and 1 mM Na^+ arsenite for 60 minutes (Cal/Asn). A guide molecular mass is shown and was interpolated from a biotinylated protein ladder using TotalLab software. Error bars show ± standard deviation. These data were compiled from replicate experiments on samples from three different ferrets using a total phosphothreonine antibody.

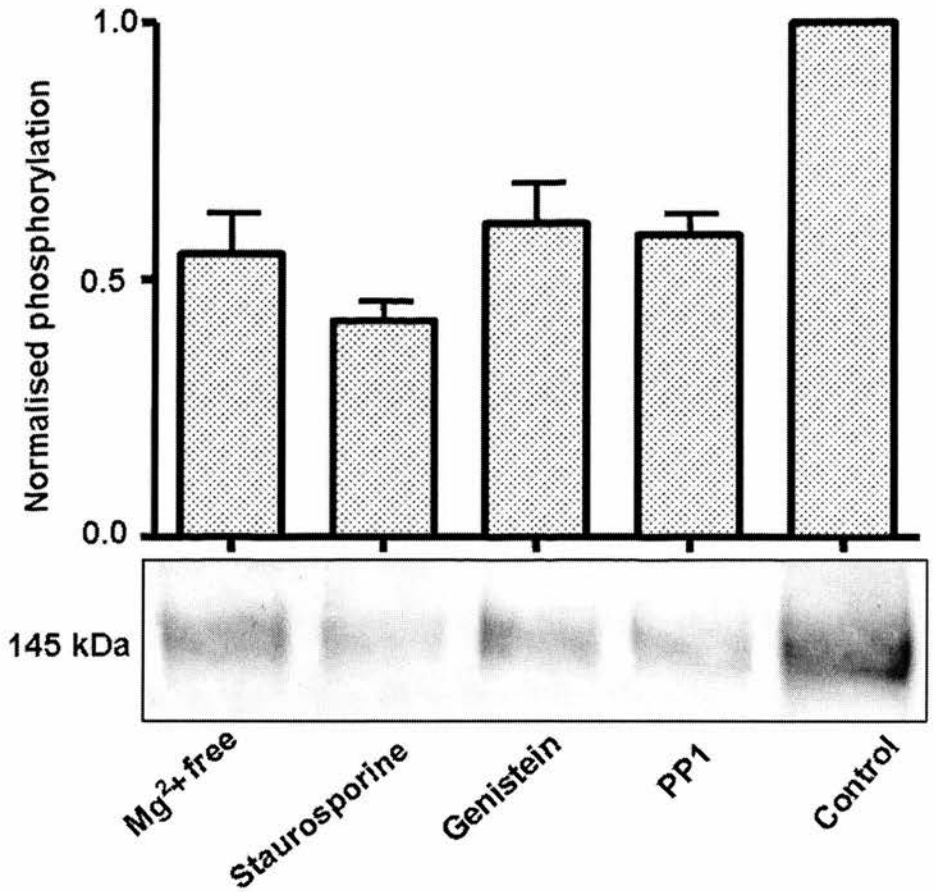

Figure 5.3 -Kinase Inhibition Reduces NKCC Threonine Phosphorylation
All cells were incubated with 11 mM glucose in FBM for 10 minutes at 38°C to allow cells to equilibrate, before treatment to inhibit or activate NKCC cotransport. The following additions were made: none (control), 50 µM PP1 for 30 minutes, 2 µM staurosporine for 20 minutes, 2 mM Tris-EDTA plus 10 µM A23187 for 15 minutes (Mg2+ free), 50 µM genistein for 20 minutes. A guide molecular mass is shown and was interpolated from a biotinylated protein ladder using TotalLab software. Error bars show ± standard deviation. These data were compiled from replicate experiments on samples from three different ferrets using a total phosphothreonine antibody.

Increased Phosphorylation	***Calyculin A***	***Arsenite***	***Calyculin A/Arsenite***	***Deoxygenated***
	2.5	3.0	5.5	2.0
Decreased Phosphorylation	***PP1***	***Genistein***	***Staurosporine***	***Mg^{2+} free***
	0.55	0.5	0.45	0.55

Table 5.1 – Threonine Phosphorylation of NKCC as a Proportion of Control Levels
These data were compiled from replicate experiments from at least three different ferrets and shows average levels of phosphorylation in comparison to control samples, apart from deoxygenated samples where data from only two ferrets were available.

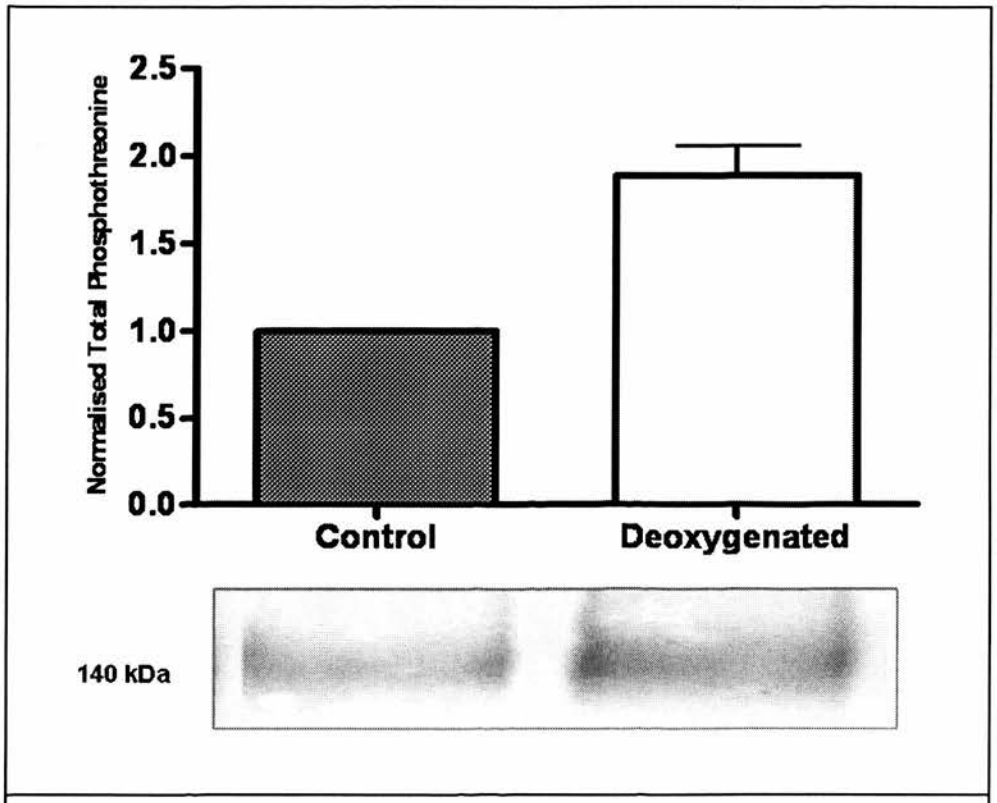

Figure 5.4 – Deoxygenation Increases NKCC Threonine Phosphorylation This shows a representative western blot using a total phosphothreonine antibody from replicate experiments from two ferrets. Deoxygenation was achieved according to Flatman (2005). A guide molecular mass is shown which was taken from a biotinylated protein ladder.

5.2 – NKCC Phosphorylation Using NKCC-Specific Antibodies

5.2.1 – Membranes

Ferret red blood cell membranes were run on SDS-PAGE gels and probed with antibodies that were raised against certain threonine phosphorylated residues of the cotransporter itself. Figure 5.12 (and figure 1.8) shows which threonine residues each of these antibodies detect. R5 was raised against a doubly phosphorylated peptide (Thr^{206} and Thr^{211} in mouse) and NKCC-P was raised against a triply phosphorylated peptide (Thr^{197}, Thr^{201} and Thr^{206} in mouse). These antibodies overlap by one of these phosphorylated threonine residues, all of which reside in the

so-called "regulatory locus" within the N-terminus of the cotransporter. Figure 5.5

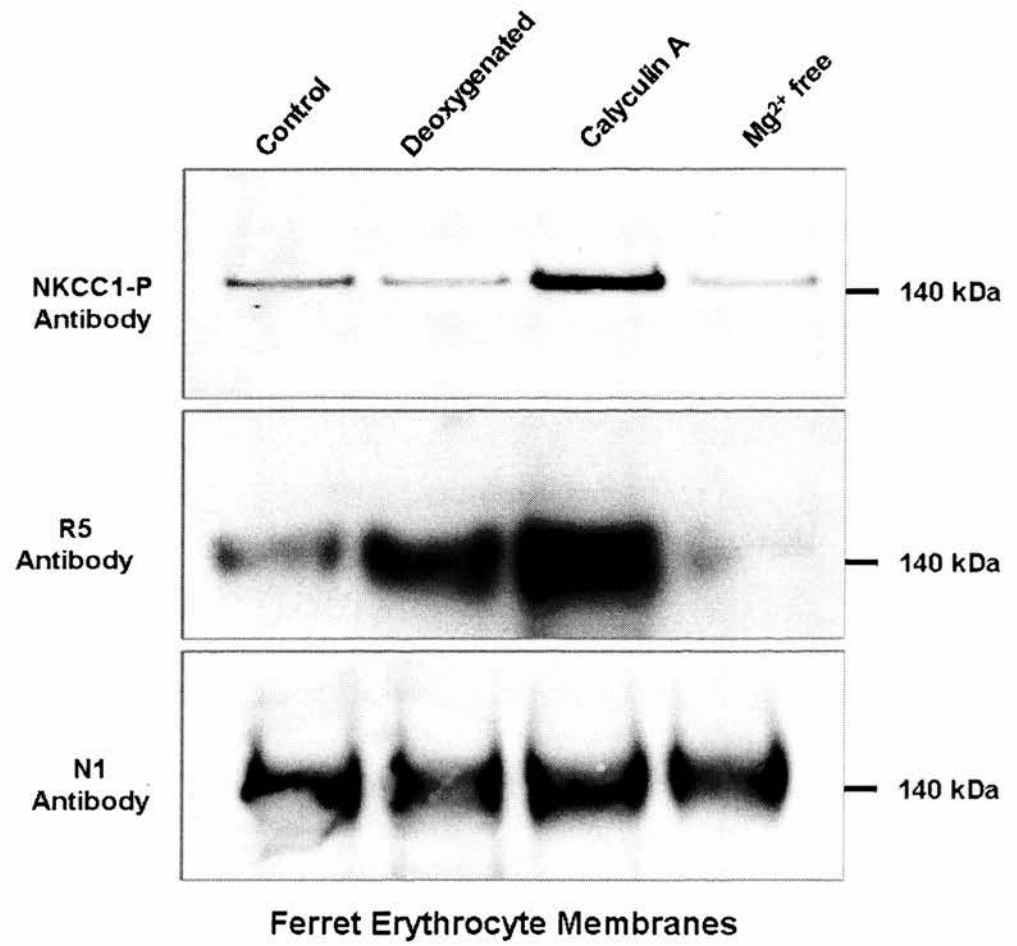

Figure 5.5 – Threonine Phosphorylation Using NKCC Specific Antibodies
Each lane of an SDS-PAGE gel was loaded with 10 µg of total protein. A western blot using the N1 antibody is shown to demonstrate that changes in threonine phosphorylation are not due to differences in the amount of NKCC present in the sample. A guide molecular mass is shown, which was taken from a biotinylated protein ladder. These images are representative of replicate experiments from one ferret only.

shows western blots of membranes from cells that were inhibited or activated for cotransport. A blot using the N1 antibody shows that each sample has similar amounts of cotransporter. Phosphorylation of residues 206 and 211, as detected by the R5 antibody, is increased upon stimulation of cotransport with deoxygenation

and calyculin A and reduced when cotransport is inhibited by removal of cell

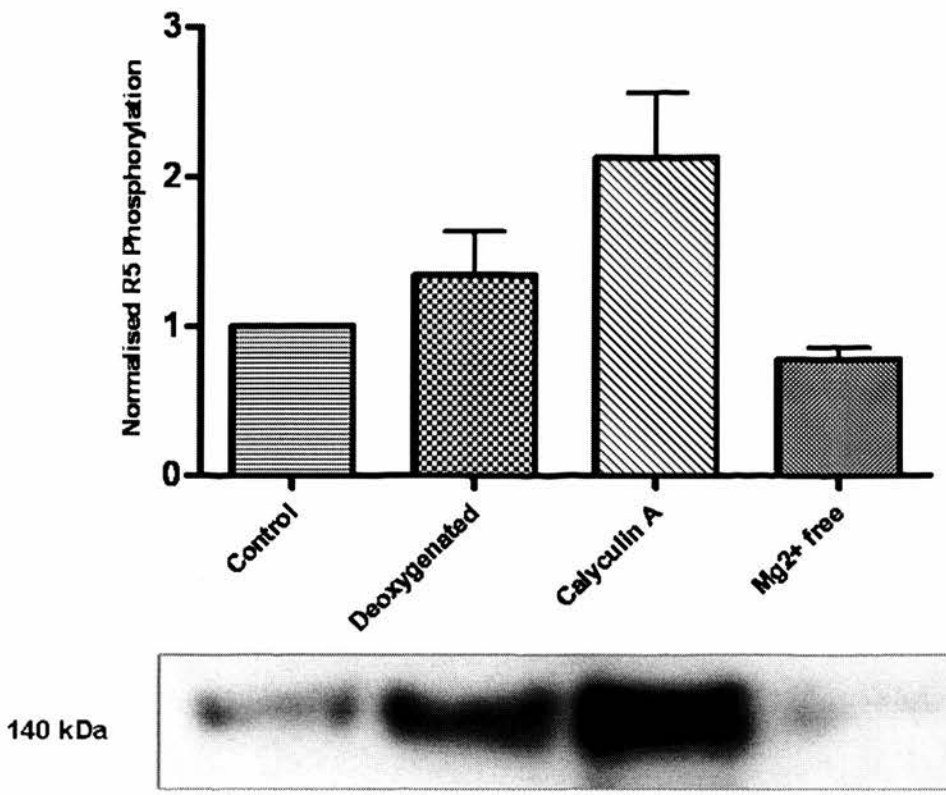

Figure 5.6 – R5 Phosphorylation of Ferret Erythrocyte Membranes
Ferret erythrocytes were incubated with 11 mM glucose in FBM for 10 minutes at 38°C to allow cells to equilibrate, before treatment to inhibit or activate NKCC cotransport. Deoxygenation was achieved according to Flatman (2005) and all other treatments were as previously described. Normalised phosphorylation is given as optical density relative to control. R5 antibody was used as primary antibody and a guide molecular mass is shown from a biotinylated protein ladder. These images are representative of replicate experiments from one ferret only.

magnesium, as shown in figure 5.6. The relative levels of phosphorylation largely follow those presented in table 5.1. However, the pattern of phosphorylation observed when the NKCC-P antibody is used as a western probe shows some differences (figure 5.7). Most obvious is the reduction of phosphorylation seen in the

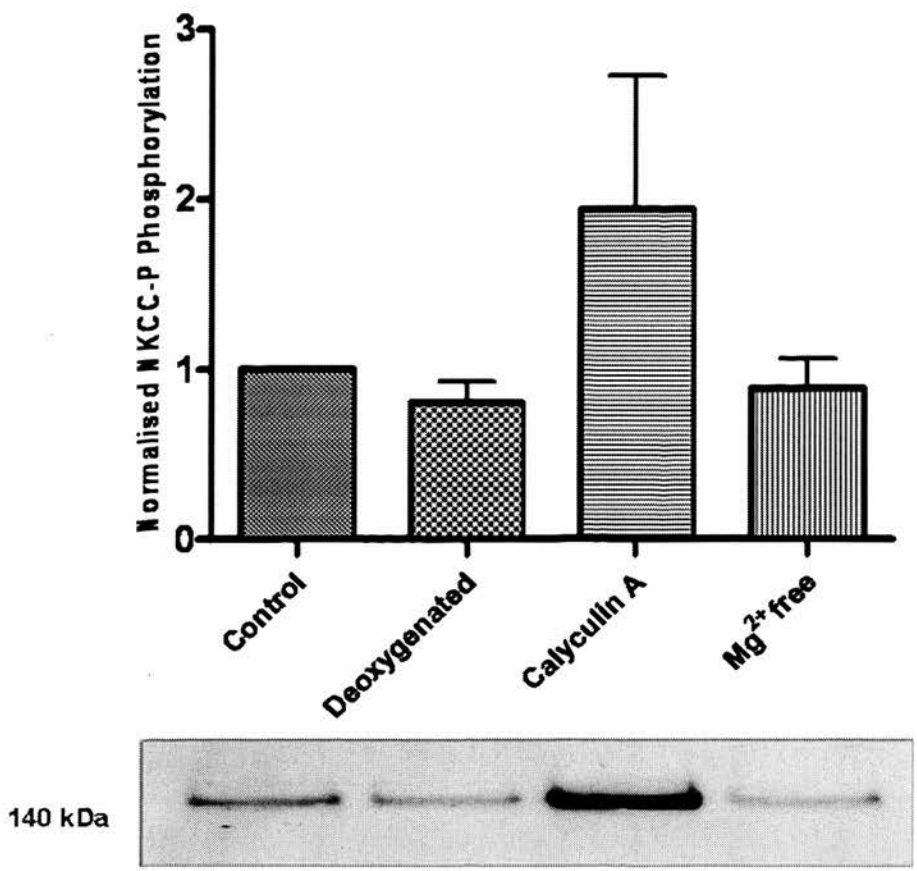

Figure 5.7 – NKCC-P Phosphorylation of Ferret Erythrocyte Membranes
Ferret erythrocytes were incubated with 11 mM glucose in FBM for 10 minutes at 38°C to allow cells to equilibrate, before treatment to inhibit or activate NKCC cotransport. Treatments were as previously described. Normalised phosphorylation is given as optical density relative to control. NKCC-P antibody was used as primary antibody and a guide molecular mass is shown from a biotinylated protein ladder. These images are representative of replicate experiments from one ferret only.

deoxygenated samples. Although the overall trend is for an increase in threonine phosphorylation on the cotransporter when red cells are deoxygenated (figure 5.4), this antibody detects a visually obvious but not quite statistically significant reduction ($p = 0.0903$). However, figures 5.6 and 5.7 were constructed from replicate determinations of phosphorylation level, for each condition, from one

animal only. The experiment must be repeated with blood from other animals to test the significance of the findings. The other conditions follow the same trend as the R5 and total threonine phosphorylation antibodies.

5.2.2 – Immunoprecipitated NKCC

In order to be able to compare phosphorylation using the R5 and NKCC-P antibodies with total threonine phosphorylation on the cotransporter, immunoprecipitation experiments were performed using both the N1 antibody described in chapter 4 and

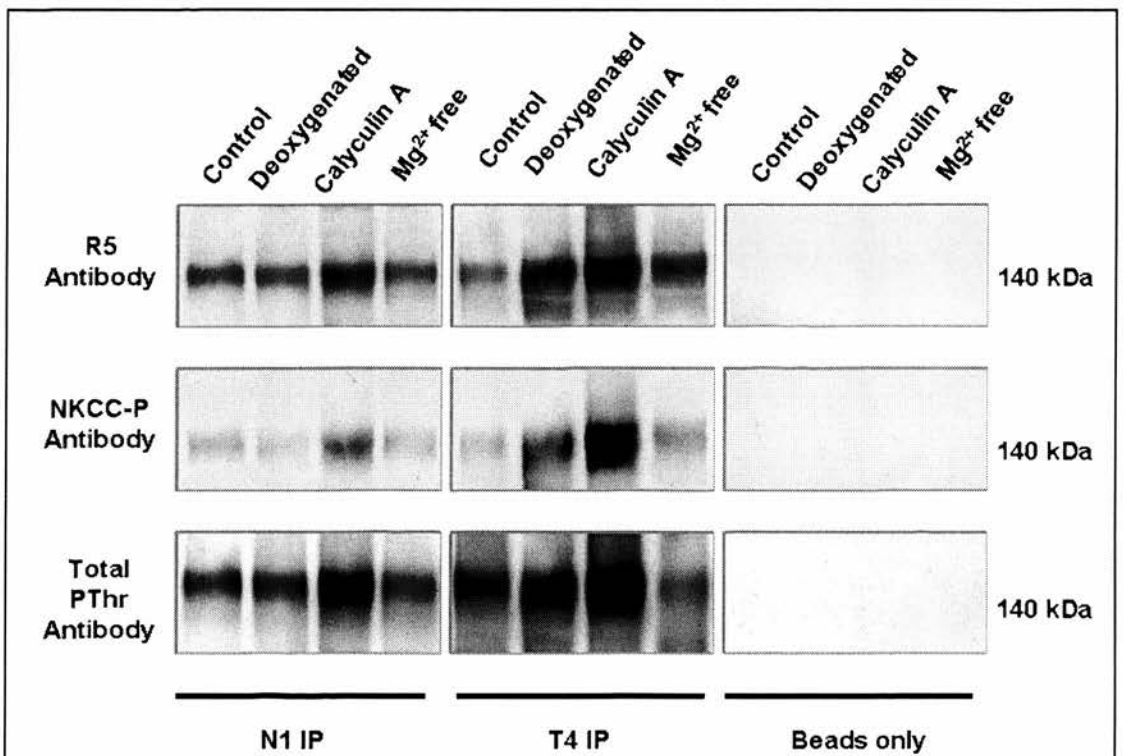

Figure 5.8 – Threonine Phosphorylation on Immunoprecipitated NKCC
N1 and T4 antibodies were used to immunoprecipitate NKCC from ferret erythrocyte membranes that had been exposed to treatments that activate or inhibit cotransport. Each sample contained 150 µg total ferret protein. Total phosphothreonine (PThr), R5 and NKCC-P antibodies were used in western blots of immunoprecipitated protein. A guide molecular mass is shown from a biotinylated protein ladder. Representative blots are shown from replicate experiments from at least one ferret.

the well characterised T4 antibody. Figure 5.8 shows western blots using the various antibodies to detect phosphothreonine. Here we see that R5 antibody follows the same pattern as total phosphothreonine, but that the NKCC-P antibody again differs. When the N1 antibody, which is specific for the NKCC1 isoform, is used to immunoprecipitate the cotransporter we see a reduction of phosphorylation when cells are deoxygenated. When the T4 antibody is used, there is an increase in phosphorylation observed that mimics the trend for total phosphothreonine. Figures 5.9-5.11 show the levels of phosphorylation compared with control samples for each of the three antibodies used. Total phosphothreonine (figure 5.9) is comparable between N1 and T4 immunoprecipitates. This is not the case for the NKCC-P antibody, where a significant rise in phosphorylation was not detected in deoxygenated samples (figure 5.10). In some cases a reduction of phosphorylation was observed when using the N1 antibody to immunoprecipitate NKCC. However, as the error bars show, there is overlap between this and the samples where T4 was the immunoprecipitation antibody. There is an increase in phosphorylation detected by the NKCC-P antibody, when cells are treated with calyculin A. There is only a small decrease observed when cell magnesium is removed. Figure 5.11 shows a comparison of phosphorylation on NKCC, detected by the R5 antibody. Although the errors are greater, this antibody follows the same trend as that observed when using the total phosphothreonine antibody. There is a doubling of phosphorylation when cells are deoxygenated and a tripling of phosphorylation when cells are treated with calyculin A. Like total phosphothreonine, reduction of cell magnesium results in phosphorylation levels on the cotransporter being roughly half that of control. Table 5.2 pools all of the normalised phosphorylation data which was used to

construct figures 5.9-5.11 and compares this with levels of Na-K-2Cl cotransport, the data for which was obtained from Matskevich *et al* (2005) and Flatman (2005). The table reflects the general trend for increased phosphorylation with cotransport.

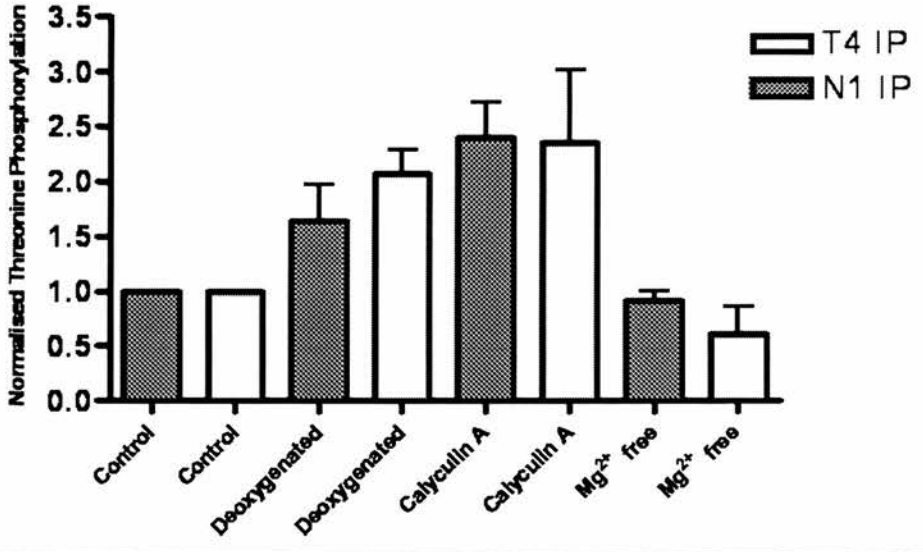

Figure 5.9 – Comparison of Total Phosphothreonine on Ferret NKCC
Normalised phosphorylation is given as optical density relative to control. This data was compiled from replicate experiments from at least three ferrets. Error bars show ± standard deviation.

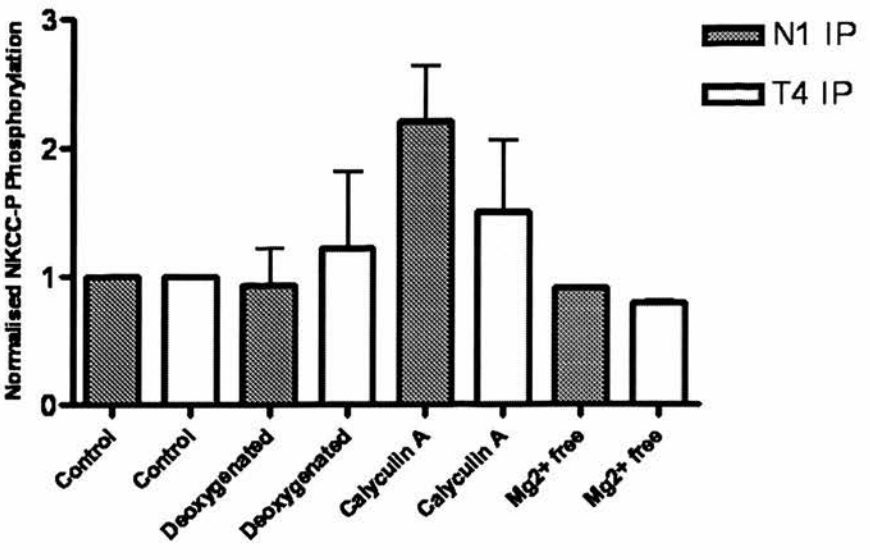

Figure 5.10 – Comparison of NKCC-P Phosphorylation on Ferret NKCC
Normalised phosphorylation is given as optical density relative to control. This data was compiled from replicate experiments from at least three ferrets. Error bars show ± standard deviation.

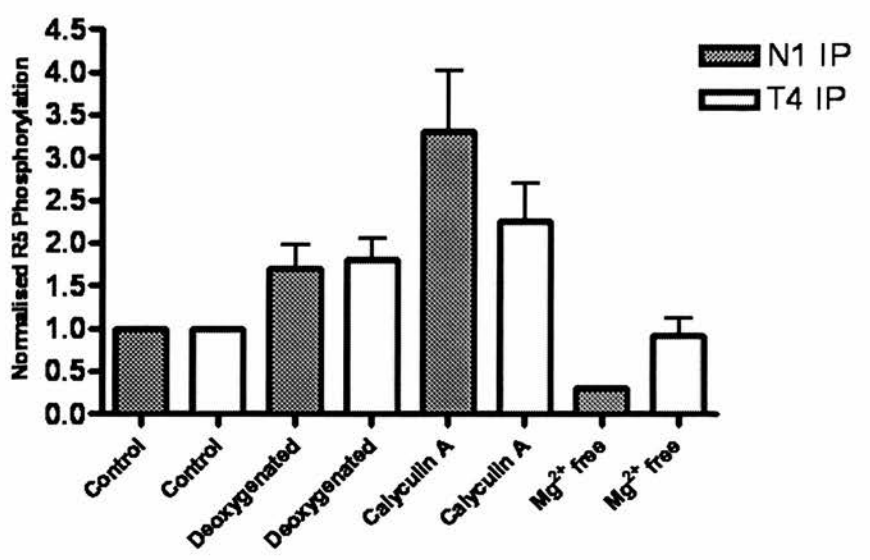

Figure 5.11 – Comparison of R5 Phosphorylation on Ferret NKCC
Normalised phosphorylation is given as optical density relative to control. This data was compiled from replicate experiments from at least three ferrets. Error bars show ± standard deviation.

		Immunoprecipitation		
Condition	**Transport***	**PThr**	**R5**	**NKCCP**
Control	1.0	1	1	1
Deoxy	2.1 ± 0.4	1.8 ± 0.7	2.1 ± 0.9	1.7 ± 0.5
Calyculin A	2.5 ± 0.4	2.4 ± 0.9	3.8 ± 1.9	2.7 ± 1.1
Mg^{2+} free	0.7 ± 0.1	0.8 ± 0.3	0.8 ± 0.5	0.7 ± 0.4

Table 5.2 – Comparison of Phosphorylation and Cotransport in Ferret RBCs

Cotransport and phosphorylation levels are normalised to control samples to allow comparison. Relative levels of phosphorylation detected by the different antibodies are shown as normalised phosphorylation ± standard deviation (n = 3 - 6 animals; the phosphorylation on NKCC from each animal is averaged from replicate experiments). PThr = total phosphothreonine antibody. R5 = antibody detecting phosphorylated Thr^{206} and Thr^{211}. NKCCP = antibody detecting phosphorylated Thr^{198}, Thr^{201} and Thr^{206}. N1 and T4 antibodies were used to immunoprecipitate NKCC from ferret erythrocytes treated with calyculin A, the ionophore A23187 and Tris-EDTA or deoxygenated as described in sections 2.2.2 and 2.2.3. *Transport values were obtained from ^{86}Rb flux experiments performed by Matskevich *et al* (2005) and Flatman (2005) and are presented as cotransport rate normalised to control ± standard deviation (n = 3 - 12 animals).

5.3 – Discussion of Results

The data presented in this chapter shows that ferret erythrocytes behave similarly to other cell types in that phosphorylation is increased under conditions that produce greater cotransport activity and reduced when cotransport activity is less. Using antibodies to specific threonine residues that have been previously shown to be phosphorylated on the cotransporter and a total phosphothreonine antibody have highlighted some interesting features. Firstly, there appears to be phosphorylation on the cotransporter under resting conditions, which may correspond to the significant transport seen in ferret erythrocytes under these conditions (Matskevich *et al*, 2005).

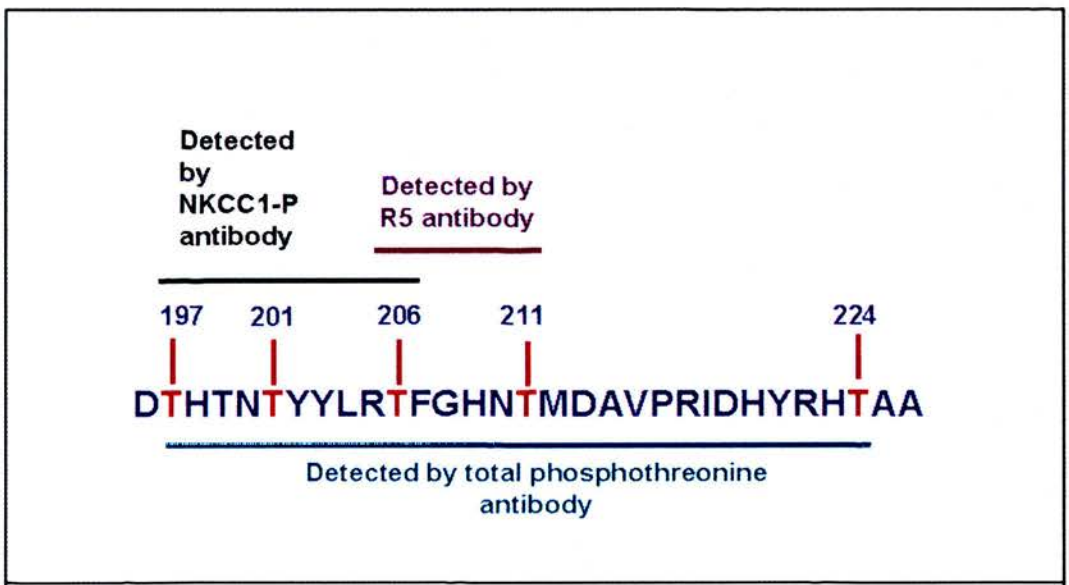

Figure 5.12 – Detection of NKCC Threonine Phosphorylation
The sites that should be detected by the various anti-phospho antibodies used in this thesis are shown above in relation to a section of mouse NKCC1.

This is detectable with all three of the antibodies used. This could suggest phosphorylation of threonine residue 206 (using mouse numbering; see figure 5.12) under basal conditions and account for the levels of cotransport that are seen in unstimulated ferret erythrocytes. However, there is still detectable phosphorylation

on the cotransporter when kinases are inhibited and cotransporter activity is reduced, which is about 60% of control cotransport and phosphorylation (Matskevich *et al*, 2005). The relative levels of phosphorylation are also similar between detection with R5 and total phosphothreonine antibodies, even though the R5 antibody is only able to detect phosphorylation on two threonines. These features highlight that although using the total phosphothreonine antibody is a useful method for measuring relative changes in phosphorylation on the cotransporter in response to various conditions the same cannot be said for the NKCC phospho-specific antibodies. They can tell us that certain residues are phosphorylated under different conditions, but the fact that the antibodies are not specific for a single phosphothreonine makes interpretation of these results difficult. In the case of the R5 antibody, at least, it also detects phosphorylated NKCC2 (Giménez and Forbush, 2003). The R5 antibody has been shown to detect both mono- and di-phosphorylated forms of the cotransporter, although it has the greatest affinity for cotransporter that is phosphorylated on both threonines (Flemmer *et al*, 2002). However, there is no such information available about the NKCC-P antibody other than it detects threonine residues that have been found to be phosphorylated by SPAK and OSR1 (Vitari *et al*, 2006). This antibody was raised to a triply phosphorylated peptide, but could potentially bind singly and doubly phosphorylated protein. As such, there is a potential for the antibody to detect seven different permutations. These would not be distinguishable under the given experimental conditions. Like the R5 antibody, it may be the case that the antibody can bind when phosphate is present on one or more of the three threonine residues, but at a lower affinity. This could account for any reductions seen in relative phosphorylation. If one or more of the three residues is not phosphorylated,

then the antibody does not bind so strongly and gives a weaker signal. Despite this, the use of this antibody does tell us that the ferret erythrocyte cotransporter is phosphorylated by SPAK or OSR1. Based on these data, one could speculate that these kinases are not responsible for the increase in cotransporter activity seen when cells are deoxygenated. We could assume then that the rise in total threonine phosphorylation, which is paralleled by the increase in R5 antibody signal, is as a result of the actions of another kinase(s). We can also speculate from the experiments in this thesis that there may be involvement of a tyrosine kinase in the activation pathway for Na-K-2Cl cotransport. As mentioned in section 1.5.3.6 and depicted in figure 1.7, Gagnon *et al* (2007b) have found that the apoptosis-associated tyrosine kinase1, AATYK1, is responsible for an inhibitory action on cotransport. Although this protein is a tyrosine kinase and one might imagine that inhibition of its catalytic activity could result in an increase in cotransporter activation (and phosphorylation), it has been shown that a catalytically inactive version of this tyrosine kinase is still able to exert its inhibitory effects on cotransport. As such, the use of tyrosine kinase inhibitors would be unlikely to affect this part of the pathway. However, there may be as yet unidentified tyrosine kinases whose catalytic activity is required for cotransport activation. Although, as figure 5.1 shows, direct tyrosine phosphorylation of the cotransporter is not present, the actions of these kinases could be involved at stages of the activation pathway that are yet to be elucidated.

The data shown here suggests that the ferret red blood cell offers an interesting source for study of cotransporter phosphorylation. The cotransporter follows some of the trends that have already been observed in other cell types in response to various stimuli. The response to deoxygenation is not clear and as it is a

physiological stimulus that an erythrocyte is likely to encounter is one of great interest. Although cotransporter activity is raised under deoxygenated conditions to similar levels when cells are treated with calyculin A or arsenite, the threonine phosphorylation is generally lower (Flatman, 2005). This offers an opportunity to investigate modifications that affect cotransport that are not necessarily reliant on threonine phosphorylation, but perhaps serine phosphorylation. As these modifications will occur on the cytoplasmic N- and C-termini it would be of interest to be able to isolate these for further analysis.

Chapter 6

NKCC Isoforms in the Erythrocyte

Chapter 6 – NKCC Isoforms in the Erythrocyte

The erythrocyte has been used in many studies of ion cotransport (Lytle, 1997; Flatman, 1991; Pewitt *et al*, 1990) and it has always been assumed that in the case of Na-K-2Cl cotransport, NKCC1 is the isoform responsible for this activity (Lytle, 2003). However, this has never been properly investigated and thus far western blot analysis of red blood cells has used the T4 antibody which detects both NKCC1 and 2 (Matskevich *et al*, 2005; Lytle *et al*, 1995). The isoform(s) present in the red cell may have consequences for how cotransport data is interpreted and could have implications when studying cotransport regulation in this cell type. As such, several experiments were undertaken to try to clearly identify which isoform(s) are present in erythrocytes.

6.1 - Western Blot Analysis of NKCC Isoforms in the Erythrocyte

6.1.1 – Ferret Erythrocytes

Ferret erythrocyte cell membranes were prepared for SDS-PAGE, and then probed with NKCC1 and NKCC2 (C-terminal) specific antibodies. The monoclonal antibody, T4, which detects both forms, was also used. Figure 6.1 shows the presence of NKCC isoforms in kidney, salivary gland tissue and red blood cell membranes. Kidney tissue provides a source of NKCC2 and to a lesser extent NKCC1, whereas salivary gland is a source of NKCC1 only. There are several observations to be made from this experiment. Immunoreactivity is present at the expected "monomer" position, but also as several higher molecular weights. T4 antibody shows several bands in the red blood cell, which are also detected by the NKCC1 specific N1 antibody. Interestingly, NKCC2 immunoreactivity is present in

ferret red blood cell membranes, but at an apparent molecular weight of 240 kDa and not at the monomer position observed in the kidney (~134 kDa). However, the kidney sample does display NKCC2 immunoreactivity at a higher molecular weight which is similar to that found in the ferret red blood cell. Importantly, the NKCC2 antibody does not detect anything in the salivary gland tissue sample, which is considered to only express the NKCC1 isoform (Kurihara *et al*, 2002 and 1999).

6.1.2 – Rat Erythrocytes

As with the ferret erythrocyte, rat cells show NKCC2 immunoreactivity but at a mass of 240 kDa and not at an expected monomer mass (figure 6.2). Also, T4 detects bands of higher molecular weight in rat samples, as does the N1 antibody. The detection of larger bands using N1 antibody was however more variable than is the case in the ferret. Figure 6.2 demonstrates the detection of phosphorylated NKCC isoforms using the R5 antibody. This detects NKCC at a monomer mass of 150 kDa and a higher molecular weight of 220 kDa. Another negative control was included in these experiments. Bacteria do not widely express NKCC and as such make a good control for the possibility of non-specific antibody interactions. As was also shown in figure 6.1, no NKCC2 is observed in salivary gland tissue. In comparison to the ferret erythrocyte, NKCCs are present at lower levels. The same amount of total erythrocyte membrane protein was loaded, including the ferret kidney and salivary gland samples, in the rat experiments as the ferret experiments. Greater exposure times were required to detect NKCCs in the rat erythrocytes. This results in over-exposure of the control tissue samples as is shown in figure 6.2. However, they still allow overall comparison of tissues that are known to express the different isoforms, with the rat red blood cells.

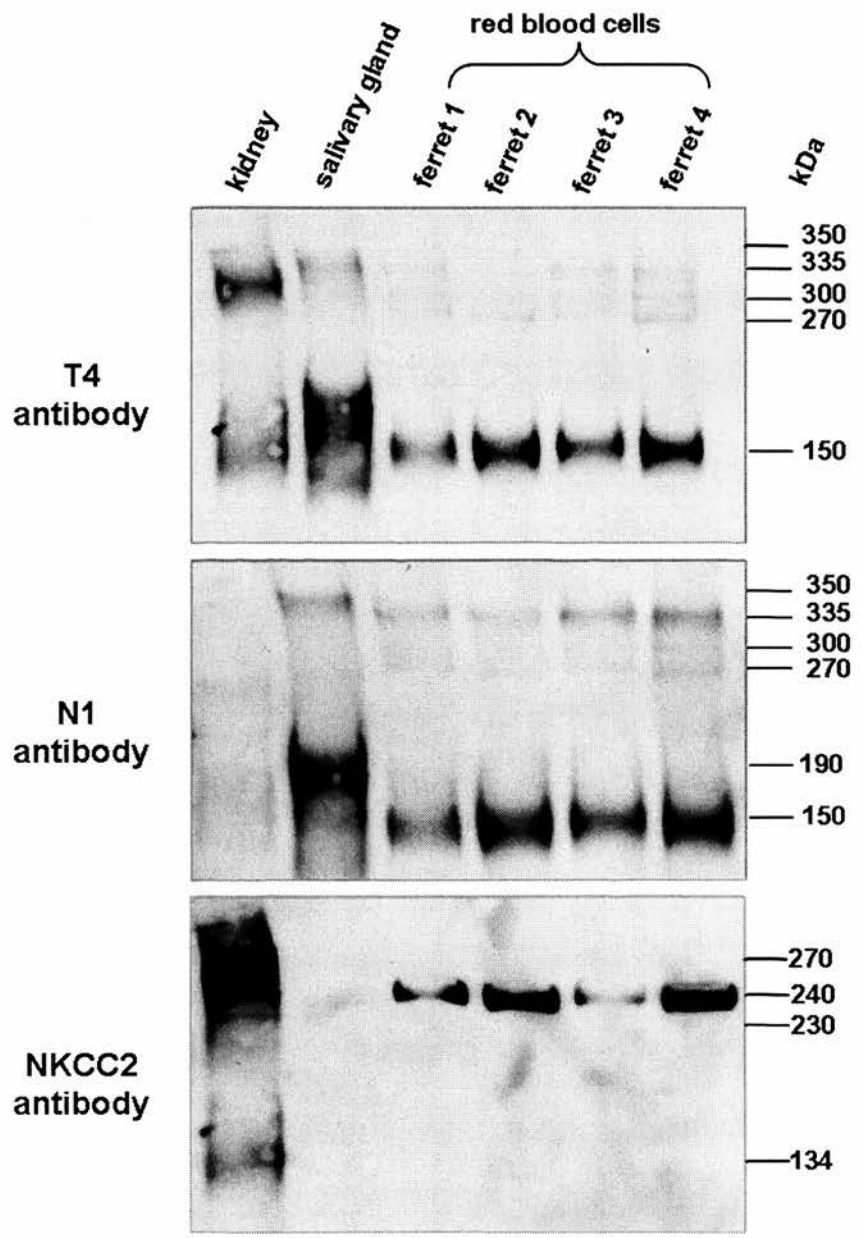

Figure 6.1 – Immunodetection of NKCC Isoforms in Ferret Erythrocytes
Estimated molecular weights (in kDa) are shown for the bands present and were interpolated from a biotinylated protein ladder using TotalLab software. The images shown are representative of replicate experiments performed on red blood cell samples from four different ferrets. Kidney and salivary gland membrane samples are included as control tissues.

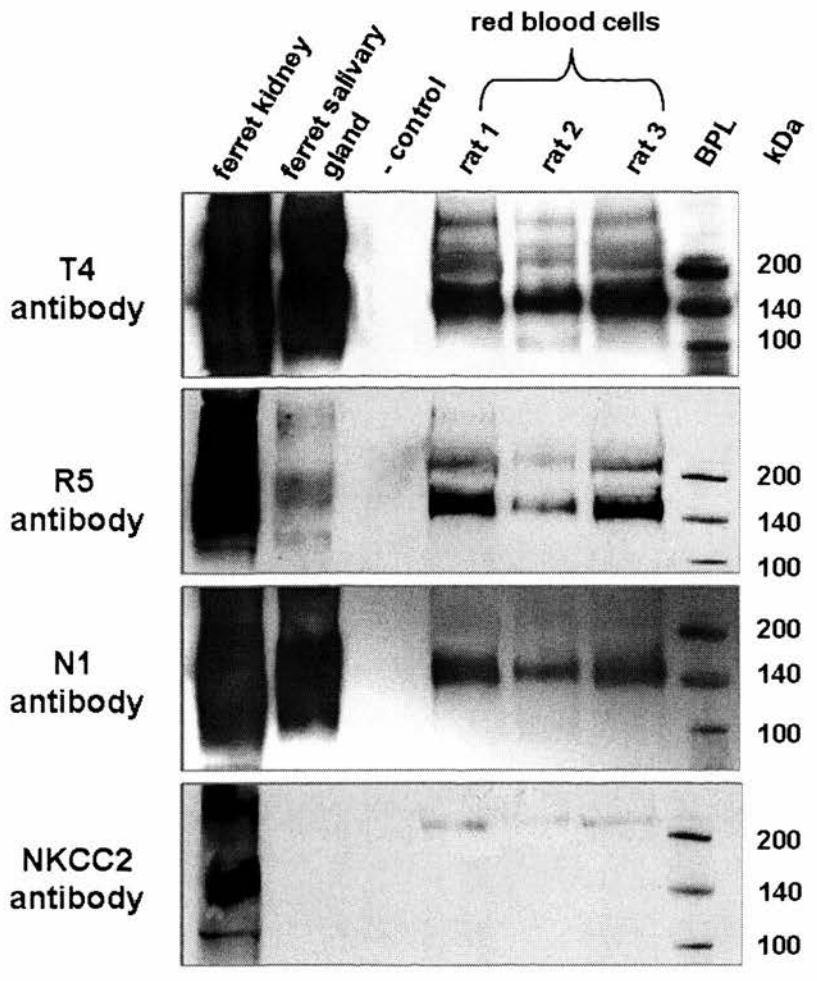

Figure 6.2 – Immunodetection of NKCC Isoforms in Rat Erythrocytes
This figure shows representative images of replicate experiments performed on red blood cell samples from three different rats. Ferret kidney and salivary gland membrane samples are shown as control tissues. The negative control shown in this experiment is a bacterial cell lysate pre-cleared with goat anti-rabbit and goat anti-mouse antibodies. Some markers from a biotinylated protein ladder (BPL) are shown as a guide to protein molecular mass (in kDa).

6.1.3- Human Erythrocytes

Human red blood cells have low levels of Na-K-2Cl cotransport and this is likely to be reflected in the number of cotransporter molecules present in cell membranes

(Lytle, 2003). In order to improve the chance of protein detection higher levels of total protein were loaded onto gels. This was achieved by ultracentrifugation of larger volumes of human red blood cell crude membrane preparations and resuspension of the resultant pellet in SDS-PAGE sample buffer. As figure 6.3 shows, there is immunoreactivity present for all antibodies used, but that the detected protein is poorly separated and resolved. This is often the case when loading large amounts of protein, which then exceeds the capacity of the gel lane. HEK-293 cells were used in these experiments as a human control tissue. These cell preparations show clear bands present at monomer molecular weight (~150 kDa) when antibodies that detect NKCC1 are used. No immunoreactivity is observed when an anti-NKCC2 antibody is used. HEK cells have been previously shown to express only NKCC1 (Isenring *et al*, 1998c). Like rat and ferret, immunoreactivity in red blood cells is present for both NKCC isoforms. This, however, was so poorly resolved that precise molecular weight estimations were not obtainable.

6.1.4 – NKCC2 Immunodetection Using an Alternative Antibody

A second NKCC2 antibody was gifted from M. Knepper and was used in western blots on ferret and rat erythrocyte samples, as shown in figure 6.4. This antibody was raised against a different epitope from the commercially available anti-NKCC2 antibody used in figures 6.1-6.3. The Alpha Diagnostics antibody is raised to a 15 amino acid section of the C-terminal cytoplasmic domain of NKCC2 (residues 859-873), whereas the Knepper antibody is to 22 amino acids from the N-terminal cytoplasmic domain (residues 109-129; Ecelbarger *et al*, 1996). This N-terminal antibody only detects protein from kidney samples.

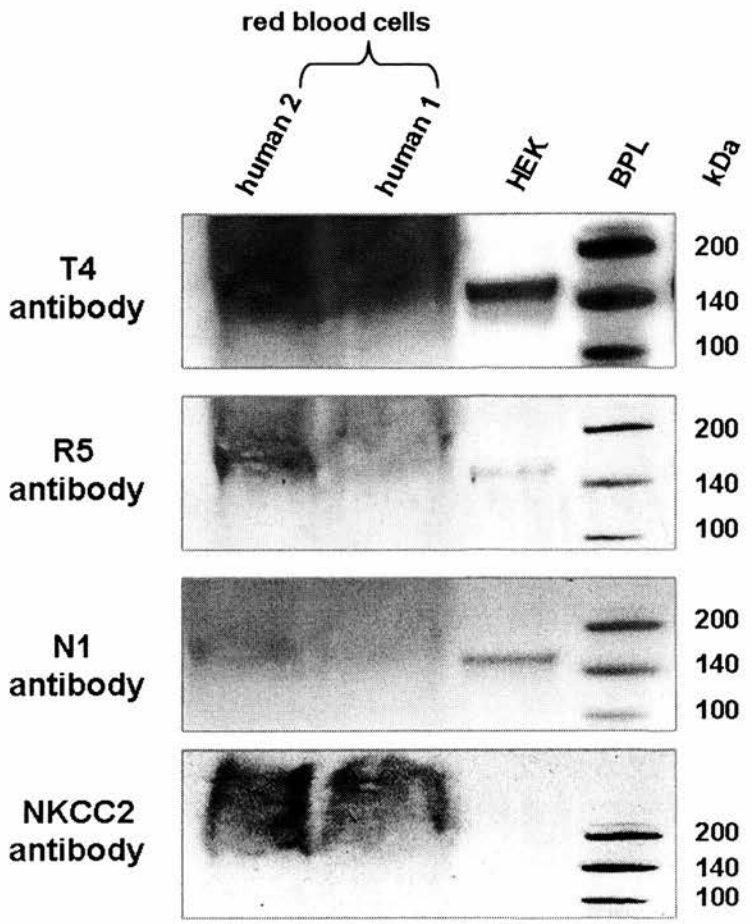

Figure 6.3 – Immunodetection of NKCC Isoforms in Human Erythrocytes
Erythrocyte membranes were collected by ultracentrifugation (100,000 x *g*) and resuspended in LDS sample buffer and 100 mM DTT and prepared for SDS-PAGE. HEK cells are shown as a positive control for NKCC1 and a negative control for NKCC2. The images shown are representative of replicate experiments on samples from two human donors. Some markers from a biotinylated protein ladder (BPL) are shown as a guide to protein molecular mass (in kDa).

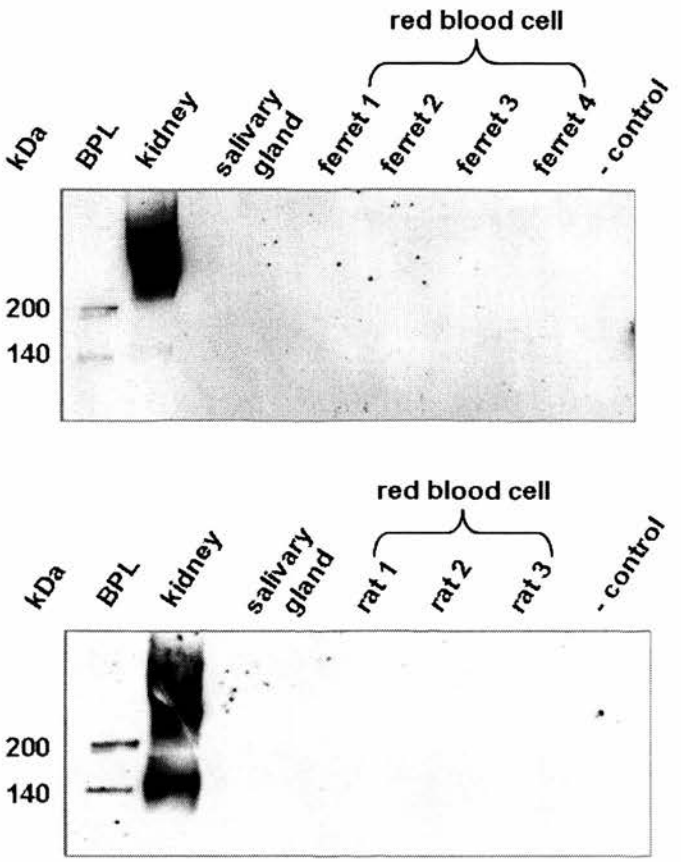

Figure 6.4 – NKCC2 Detection with an N-terminal Antibody
Representative images are shown of rat and ferret western blots using an N-terminal anti-NKCC2 (gifted by M. Knepper). Rat kidney is shown alongside rat erythrocytes and ferret kidney is shown alongside ferret erythrocytes. In both cases, ferret salivary gland tissue was used as a negative control tissue. Another negative control is a bacterial cell lysate pre-cleared with goat anti-rabbit and goat anti-mouse antibodies. Some molecular masses are shown (in kDa) and are from a biotinylated protein ladder (BPL).

6.2 – Detection of NKCC1 and NKCC2 mRNA from Erythroid Cells

Another method for the examination of protein expression is reverse-transcription polymerase chain reaction (RT-PCR). This process involves the generation of complementary DNA from messenger RNA strands and then PCR using oligonucleotide primers that are specific for regions within certain sections of a gene

of a specific protein. Using sequences common to mouse, rat and human NKCC1 and NKCC2, primers were designed and used in PCR. In order to determine the isoforms present in red blood cells, reticulocytes were isolated from whole blood using a density gradient method (see section 2.2.8), which allows separation based on

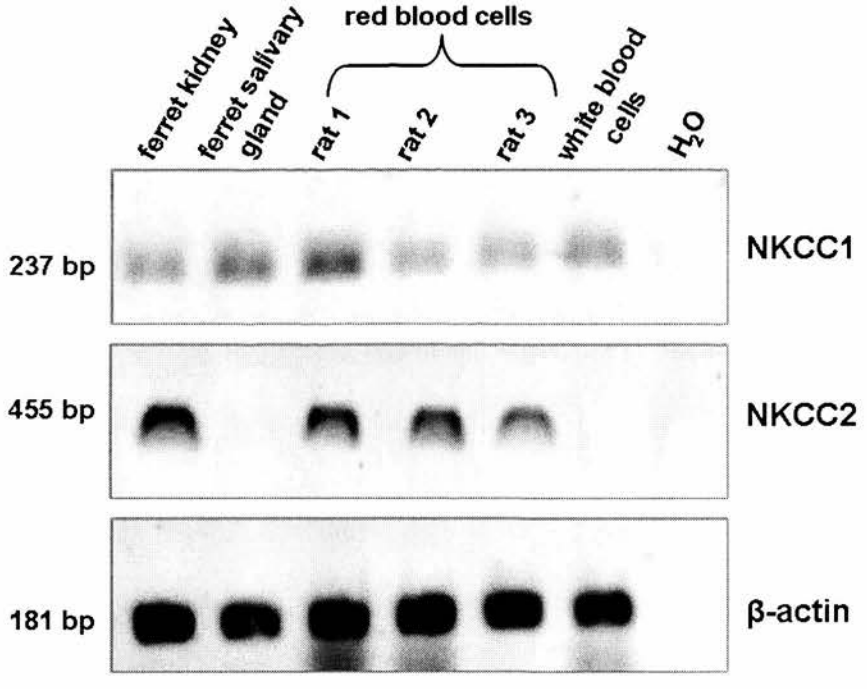

Figure 6.5 – RT-PCR of Rat Erythrocytes and Leukocytes
Ferret kidney is included as a positive control for both isoforms. Ferret salivary gland is included as a positive control for NKCC1 and a negative control for NKCC2. White blood cells are included as a control for expression of NKCC isoforms in the blood. β-actin is included as a positive control for the PCR reaction, whereas the water sample acts as a negative control. Base pair (bp) numbers are shown for each PCR product.

the observation that these cells possess around 10% less haemoglobin than mature red blood cells and are therefore more buoyant (Rapoport, 2000). Figure 6.5 shows PCR products for NKCC1 and NKCC2 in kidney and red blood cells from rats. As expected, no NKCC2 product is present in salivary gland samples. Also, no NKCC2

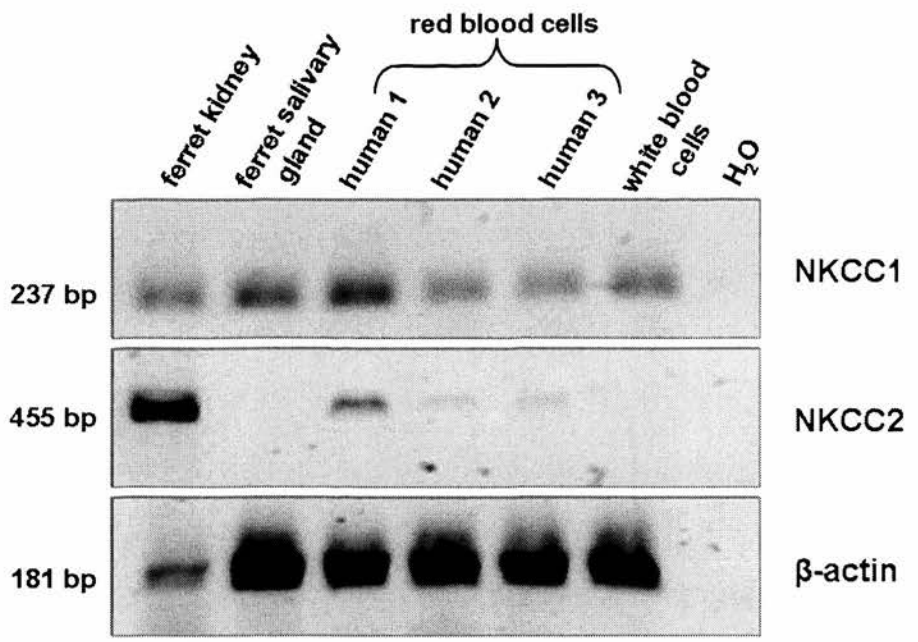

Figure 6.6 – RT-PCR of Human Erythrocytes and Leukocytes
Ferret kidney acts as positive control for NKCC1 and NKCC2 expression, whereas ferret salivary gland acts as a positive control for NKCC1 only. This tissue does not express NKCC2 and provides a negative control for NKCC2 expression. White blood cells are included as a control for expression of NKCC isoforms in the blood. β-actin is included as a positive control for the PCR reaction, whereas the water sample acts as a negative control. Base pair (bp) numbers are shown for each PCR product.

PCR product is present in white blood cell samples indicating that the product present from red cell samples is not likely to be from contaminating leukocytes. The same pattern of NKCC expression is observed in human red and white blood cells, as shown in figure 6.6. Bone marrow was isolated from rat femurs and RNA was

extracted and reverse-transcribed. Figure 6.7 demonstrates that NKCC1 and NKCC2 are expressed in cells from this tissue. This is an important control as bone marrow

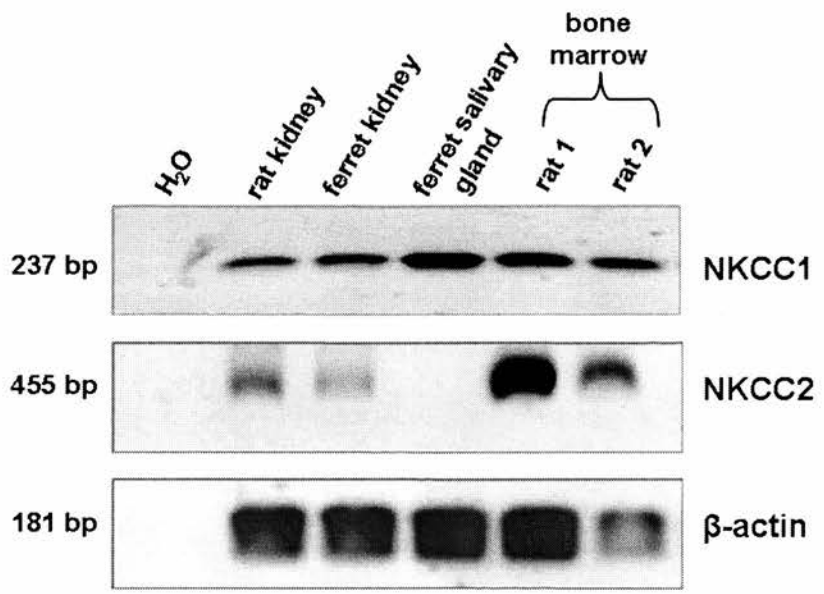

Figure 6.7 - RT-PCR of Rat Bone Marrow Cells
Rat and ferret kidney act as positive controls for NKCC1 and NKCC2 expression, whereas ferret salivary gland acts as a positive control for NKCC1 only. This tissue does not express NKCC2 and provides a negative control for NKCC2 expression. β-actin is included as a positive control for the PCR reaction, whereas the water sample acts as a negative control. Base pair (bp) numbers are shown for each PCR product.

is the site of blood cell generation. Ferret kidney and salivary gland cDNA was prepared for use as control tissue samples. In all cases, the PCR products were of the expected size based on the sections of DNA that are covered by the primer sets.

6.3 – Discussion of Results

These findings indicate that NKCC1 is the major isoform present in the red blood cell. However, it would appear that there is some expression of NKCC2. Western

blotting showed the presence of a protein detected by a C-terminal anti-peptide NKCC2 antibody but at an unusual molecular mass. The N-terminal NKCC2 antibody was not able to detect this, or any other protein from red blood cell samples. It is interesting that the C-terminal antibody detects cotransporter and the N-terminal antibody does not. Perhaps the C-terminal antibody is binding to something in a non-specific manner. However, the same pattern is observed from three different animal species. Also, it does not detect any protein in the salivary gland negative control tissue. Perhaps, the form of NKCC2 present in the red cell is such that the N-terminal antibody is unable to bind it. Or it may be the case that it is bound to another protein at its N-terminus, making it both appear at a higher apparent molecular weight and unable to be recognised by the Knepper antibody. Although confirmation with the N-terminal antibody is lacking, nonetheless these findings are interesting as NKCC2 is considered to be a kidney-specific isoform. To investigate this further, the RT-PCR technique was employed. Although mature erythrocytes are anuclear, younger red cells can still possess nucleic acid. Hoffman *et al* (2002) and Stengelin and Hoffmann (1997) successfully performed experiments looking for different isoforms of Na^+ pump in reticulocytes and earlier erythroid progenitor cells and these studies inspired the experiments presented in this thesis. NKCC1 and NKCC2 PCR products were observed from rat and human red blood cells. As there is a difference between these and the expression of cotransporter from isolated white blood cells, it is assumed that the presence of NKCC2 is purely erythroid in nature. The presence of NKCC2 mRNA was also detected in rat bone marrow where erythroid precursor cells reside. The RT-PCR and western blot data do indeed strongly suggest the presence of NKCC1 in the red cell, but also that NKCC2 is

present. The significance of this is unclear, but it may have consequences for the interpretation of cotransport data. As mentioned in sections 1.2.2 and 1.4.2, NKCC2 has a number of splice isoforms that display different transport and ion binding capacities. Also, the splice isoforms have been shown to have modulatory effects on cotransport in the kidney (Gagnon *et al*, 2002; Plata *et al*, 2002; Plata *et al*, 1999). Also, NKCC1 and NKCC2 may be able to interact with each other, as demonstrated in yeast-two-hybrid experiments by Brunet *et al* (2005). If this is the case, then NKCC2 could potentially influence the activity of NKCC1 in the red cell, and vice versa. The splice isoforms differ at regions within the second transmembrane domain (residues 204-237 in mouse) of NKCC2. The primers used to amplify NKCC2 in this project are for a region of the gene which is outwith the splice cassette exon and as such do not differentiate between any of these splice variants. As mentioned in section 1.5.3.7, NKCC2 can be phosphorylated on Ser^{126} by AMP-activated protein kinase (Fraser *et al*, 2007). The authors observed that this residue was phosphorylated under non-stimulated conditions and suggested that it was responsible for maintaining the basal activity of NKCC2 in mouse macula densa-derived cells. Ferret erythrocytes show high levels of basal cotransport activity and perhaps a proportion of this is due to the presence of NKCC2. However, in the absence of data showing the presence and activity of AMP kinase in erythrocytes and the absolute quantities of NKCC2 in the erythrocyte, this is purely speculative. The literature has always quoted NKCC2 as being "kidney specific" and this data contradicts this. As such, it would be prudent to further investigate the presence of NKCC2 in erythrocytes. Several modifications could be made to the experiments performed here that could provide more conclusive data. First of all, it would be

prudent to formally identify the cells that the RNA is extracted from. As suggested, the NKCC2 mRNA is not likely to come from white blood cells. The method of cell separation used here, although cheap and easy to perform, does not ensure that there will be no contamination of the samples with other cell types. Magnetic cell sorting (MACS) or fluorescence-activated cell sorting (FACS) techniques could be employed to obtain purer erythroid cell samples. Both of these techniques depend on the expression of cell type-specific markers to isolate cells. CD34 has been used as a marker for erythroid cell isolation (Hoffman *et al*, 2002) and could be used with either cell sorting technique. However, these cells require culture with agents that induce erythropoiesis in order to obtain pure samples of erythroid cells and their progenitors, which is both an expense and time consuming. Another possibility would be to inject animals with erythropoietin, to increase the numbers of circulating erythroid progenitor cells found, making isolation via density gradients more fruitful. These methods would provide purer cell samples or greater cell numbers in order to obtain protein and RNA from. The generation of a new NKCC2 specific antibody would also be of great use. A highly specific antibody, that was useful in not only western blot but immunoprecipitation applications, would help to clear up the disparity between the two antibodies used in the experiments presented here. Finally, identification of the protein by mass spectrometry would lend further support. As demonstrated in chapter 3, this is not easy to achieve. More sophisticated separation methods, such as two-dimensional liquid chromatography, and tandem mass spectrometry would be best employed if this was to be achieved. Lu *et al* (2004), using visible isotope-coded affinity tags (VICAT), showed the presence and relative abundance of human group V phospholipase A_2 from lung

macrophages, whereas their western blot data were inconclusive. This method uses a biotinylated tag (the VICAT tag) which is able to attach to peptides via thiol linkage of cysteine residues and a radioactively-labelled VICAT-tagged pure peptide from the protein of interest. This pure peptide is mixed with the test sample and separated on an IPG strip. The radioactive peptide will separate to the same position as peptide from the test sample (if it is present in the mix) and as such provides a marker for this in the strip. This can be isolated, the peptides eluted and then those bearing the VICAT tag captured by streptavidin-agarose. The peptides can then be analysed by mass spectrometry. The quantity of sample-derived peptide can be inferred from an internal standard.

There is still a great deal to explore regarding the presence of NKCC2 in the red blood cell and represents an interesting area for future research.

Chapter 7

Discussion

Chapter 7 – Discussion

7.1 – NKCC Interacting Proteins

Chapters 3 and 4 of this thesis suggest that several proteins may interact with the Na-K-2Cl cotransporter in the ferret erythrocyte membrane. These are band 3, haemoglobin, ankyrin, peroxiredoxin-2, alpha spectrin, heat shock protein 70 and malate dehydrogenase. Some proteins were identified by only one method, whereas others were identified using several (table 7.1). Band 3, the erythrocyte anion exchanger, emerges as a strong candidate for an NKCC binding partner. As mentioned, expression of a trout erythrocyte anion exchanger in *Xenopus* oocytes

Protein	Methods of Separation	Identified By
Band 3	N1 co-IP	LC-MSMS
	N1 co-IP	Western blot
	Blue-native PAGE and BN/SDS-PAGE	MALDI-TOF and LC-MSMS
Haemoglobin	Blue-native PAGE and BN/SDS-PAGE	MALDI-TOF and LC-MSMS
Peroxiredoxin-2	BN/SDS-PAGE	MALDI-TOF MS
Ankyrin	Blue-native PAGE and BN/SDS-PAGE	MALDI-TOF and LC-MSMS
HSP70	N1 co-IP	LC-MSMS
Malate dehydrogenase	N1 co-IP	LC-MSMS
Alpha spectrin	BN/SDS-PAGE	MALDI-TOF MS

Table 7.1 - Potential Binding Partners of NKCC

produced increased endogenous Na-K-2Cl cotransport and was thought to involve an interaction between these two proteins (Guizouarn *et al*, 2004). The evidence presented here further implicates an interaction between NKCC and band 3, this time in the mammalian erythrocyte. T4 western blotting places NKCC within one of the native-PAGE complexes that contain band 3. Further experimentation should be performed to validate these findings. As the cotransporter was not identified with

mass spectrometry other methods would need to be employed. Multiplex western blotting of native-PAGE gels, using antibodies for band 3, NKCC and fluorescently labelled secondary antibodies, would allow us to identify if both proteins really are present within the same complex on a gel. For example, secondary antibodies labelled with Cy3 (green) and Cy 5 (red) dyes could be used and the western blots scanned using a laser scanner. If the two proteins were at the same position on a blot then the band would appear as yellow in overlaid images. The two bands observed in the native-PAGE experiments that contain NKCC (as detected by western blotting) are fairly broad and range from 225-290 kDa and 396-500 kDa. It is possible that more than one protein complex exists within these bands. As such, it may be that the proteins identified by mass spectrometry in this thesis may not all be from the same complex. In the future, it would be prudent to perform cross-linking of proteins and separate these by SDS-PAGE. Again, multiplex western blotting could be performed with NKCC and band 3 antibodies. LC-MSMS could also be used to analyse the proteins present in separated cross-linked complexes. Band 3 was found to co-immunoprecipitate with NKCC1 from ferret erythrocytes. An important experiment to perform in the future would be to identify proteins that co-immunoprecipitate with band 3 using the band 3 specific antibody. Western blot detection of NKCC using T4 or N1 antibodies from band 3 immunoprecipitates would provide important complementary evidence.

What is the significance of an interaction between these two proteins?

Band 3 interacts with many proteins, including haemoglobin and ankyrin. Ankyrin links band 3 to the cytoskeleton and haemoglobin has been shown to interact with peroxiredoxin-2. These proteins were also identified by mass spectrometry from

native-PAGE experiments. The interactions of band 3 with the cytoskeleton are important for maintaining the shape of erythrocytes (Wang, 1994). Perhaps this interaction with the cytoskeleton via band 3 provides NKCC the means to physically sense changes in cell volume, which also vary under different oxygen tensions. However, changes in cell volume cannot explain the extent of activation by deoxygenation, as volume changes under these conditions are minor in red cells (Flatman, 2005). Band 3 has increased tyrosine phosphorylation and increased interactions with the cytoskeleton under deoxygenating conditions (Barvitenko *et al*, 2005). Band 3 has been shown to bind to haemoglobin and this interaction strengthens on deoxygenation (Chétrite and Cassoly, 1985). Deoxygenation is a strong activator of Na-K-2Cl cotransport in erythrocytes (Flatman, 2005; Muzyamba *et al*, 1999). Perhaps under conditions of deoxygenation, the binding of deoxyhaemoglobin to band 3 has a functional consequence for NKCC activity. Indeed, haemoglobin may act as the oxygen sensor for NKCC activity within the red blood cell. This may be directly through an interaction with the cotransporter itself, or indirectly via band 3 (figure 7.1). If the interaction between band 3 and deoxyhaemoglobin could be interrupted under deoxygenating conditions and the activity of NKCC measured we may be able to infer some relationship between these proteins. Likewise, if we could interfere with the interaction between NKCC and band 3 we could measure cotransport activity in response to a number of stimuli and determine if their interaction is required for cotransport activation in all cases. It would also be of interest to determine if NKCC interacts with different anion exchanger isoforms in other cell types, as their interaction may represent a part of cotransport regulation that is not purely confined to the erythrocyte.

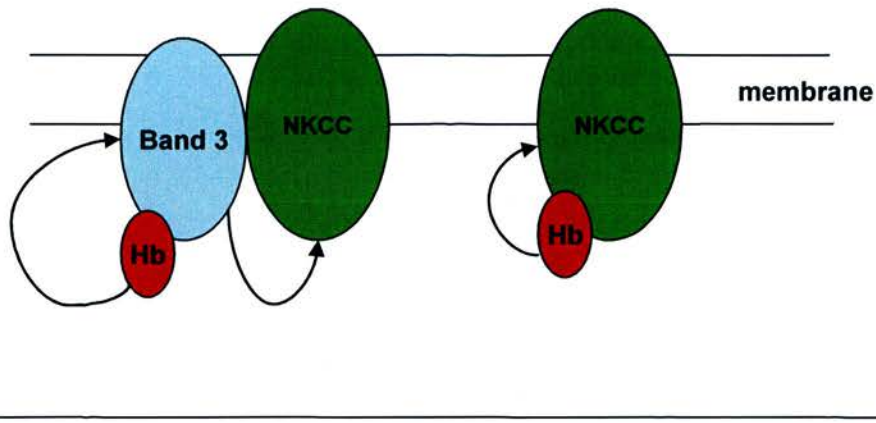

Figure 7.1 – Possible Activation of Erythrocyte NKCC by Deoxygenation
The left hand section of this diagram involves indirect activiation of NKCC via the increased binding of deoxyhaemoglobin (Hb) to band 3 when cells are deoxygenated. The right hand section suggests that Hb may directly interact with the cotransporter and activates it when oxygen levels are low.

The presence of peroxiredoxin-2 (PrxII) in native-PAGE complex with band 3 may be simply due to its interaction with haemoglobin. As mentioned in chapter 3, this protein is important in protection against oxidative stress by preventing the formation of methaemoblobin (Stuhlmeier *et al*, 2003). The importance of this protein in the red blood cell is demonstrated with a knockout mouse. These animals have haemolytic anaemia, splenomegaly and increased haematopoiesis (Lee *et al*, 2003). Peroxiredoxin proteins, of which there are six in mammals, have also been shown to interact with membrane proteins (Rhee *et al*, 2005). Peroxiredoxin-1 interacts with and increases androgen receptor activation in response to hypoxia/reoxygenation in prostate cancer cell lines (Park *et al*, 2007b) and the thromboxane receptor is regulated by an interaction with peroxiredoxin-4 (Giguère *et al*, 2007). It is therefore possible that peroxiredoxin-2 interacts directly with band 3 and/or NKCC. PrxII has

been found to modulate the activity of JNK and p38, two kinases that have been suggested to regulate cotransporter activity. In this case PrxII prevented TNF-α induced H_2O_2 activation of JNK and p38 in HeLa cells (Kang *et al*, 2004). Not only are the peroxiredoxins able to interact with integral membrane proteins and modulate their activity, they are able to influence kinase activity due to their ability to remove reactive oxygen species (ROS). Thus, PrxII present in the red cell may not only function to protect proteins from ROS, but as a modulator of protein function. It would be of interest to measure erythrocyte Na-K-2Cl cotransport in response to different stimuli from the $PrxII^{-/-}$ knockout mouse produced by Lee *et al* (2003). LC-MSMS identified heat shock protein 70 from N1 immunoprecipitated control ferret erythrocyte material. This protein was also identified by MALDI-TOF mass spectrometry from 2-DE separated control ferret erythrocyte membrane samples. Malate dehydrogenase may also help to protect the cotransporter from damage within the cell due to its reductive properties. However, this protein may also function as a molecular chaperone. The expression of malate dehydrogenase was increased in *E. coli* under conditions of heat shock and when, used as an expression partner for heterologous protein expression in these bacteria, improved the solubility of proteins which often aggregate (Park *et al*, 2007a). Interestingly, expression of malate dehydrogenase is increased in TAL cells from the loop of Henle in response to hyperosmotic stress (Dihazi *et al*, 2005). In this work, increased expression of hsp70 and hsp90 were also observed. Simard *et al* (2004b) have shown that hsp90 interacts with NKCC from HEK-293 cells. The authors indicate that this interaction is not only relevant for the proper folding of NKCC, but in regulating the activity of the mature cotransporter. Geldanamycin (an inhibitor of hsp90) was found to inhibit Rb^+

influx in low chloride medium, a stimulus that normally increases activity of NKCC. A slight increase in NKCC activity was observed under normal conditions when geldanamycin was present. Due to these findings, the authors speculate that hsp90 is able to inhibit NKCC activity when $[Cl^-]_i$ is normal, but activates cotransport when $[Cl^-]_i$ is low, perhaps by chaperoning a conformational change in the cotransporter that allows optimal ion translocation. Hsp70 may be involved in NKCC regulation in a similar manner, particularly as it is upregulated in response to hypertonicity (Dihazi *et al*, 2005). However, low $[Cl^-]_i$ is unlikely to be a stimulus in the red blood cell as the levels of chloride are much higher than other cell types due to the actions of band 3. Gagnon *et al* (1999) found that hyperosmotic stress increased hsp70 mRNA 8-fold in Madin-Derby canine kidney epithelial cells which translated to a near doubling of protein expression (this mode of stimulation of hsp70 is not possible in the RBC as they do not synthesise new protein). Hsp70 has been shown to be involved in erythroid cell maturation, ensuring that a necessary transcription factor, GATA-1, is protected from caspase cleavage (Ribeil *et al*, 2007). This protein may help to protect NKCC in the mature erythrocyte from proteolysis or chaperone a conformational change that allows cotransport activation. It will be of interest to examine if hsp70 is present in N1 immunoprecipitates from ferret erythrocyte membranes pre-treated with different cotransport activating stimuli as its interaction with the cotransporter may represent a level of cotransport regulation.

7.2 – Phosphorylation of NKCC

Study of threonine phosphorylation of the ferret erythrocyte cotransporter under different activation states has highlighted some interesting features and indicates

areas of research that will be of interest in the future. Using total phosphothreonine antibody it was observed that increased NKCC phosphorylation closely followed increased Na-K-2Cl cotransport (Matskevich *et al*, 2005). It is shown in this thesis, by experiments using antibodies that detect changes in phosphorylation on specific NKCC threonine residues, that the SPAK/OSR1 kinases are not likely to be responsible for the increased activity of the cotransporter in response to deoxygenation even though their presence in the ferret red blood cell was shown by western blot. A direct interaction of SPAK or phosphorylated SPAK with NKCC was not able to be confirmed due to the presence of SPAK immunoreactivity in sepharose-bead negative control samples in co-IP experiments. As such, the models, proposed by Gagnon *et al* (2006a and 2006b) and Villa *et al* (2007) and summarised in figure 1.6, regarding the activity and interactions of SPAK/OSR 1 with NKCC cannot be confirmed in the ferret erythrocyte. This is also true for the involvement of PP1 but as already discussed in chapter 4 there is strong evidence for it being a regulatory phosphatase of the cotransporter. It may be possible in the future to apply more thorough pre-clearance of samples with beads, or to use beads of a different type that will reduce non-specific interactions of proteins. However, the fact that increased phosphorylation is observed using the NKCC-P antibody when cells are treated with calyculin A does implicate SPAK/OSR1 as kinases (and PP1 as a phosphatase) of the cotransporter in ferret erythrocytes. *In vitro* kinase assays using SPAK/OSR1 isolated from deoxygenated red blood cells similar to those described by Vitari *et al* (2006) may help define if this cotransport stimulus does result in activation of these kinases. If a viable SPAK/OSR1 knockout animal could be

produced, the activity of erythrocyte NKCC could be measured in response to deoxygenation and the impact of the absence of these kinases observed.

The R5 antibody detects threonine phosphorylation on another NKCC threonine that is not covered by the NKCC-P antibody (Thr^{211} as numbered in mouse NKCC1; see figure 5.12). R5 phosphorylation was increased in response to treatment with calyculin A and deoxygenation. It would appear that whatever kinase is responsible for phosphorylation of this residue is active in the deoxygenated red cell. It will be of importance now to map the different threonines, and perhaps serine residues, that are phosphorylated on erythrocyte NKCC under the various different conditions that inhibit or activate cotransport. It is important that both N- and C-termini are studied to obtain a full picture of phosphorylation of the cotransporter. This may not be easy to achieve, due to the low abundance of the protein, but is definitely worth investigating.

7.3 – NKCC Isoforms

Western blot and RT-PCR data presented in this thesis suggest that the red blood cell has both NKCC1 and NKCC2 isoforms present. This is the first time NKCC2 has been observed outside the context of the kidney. However, some of the data in chapter 3 of this thesis may appear to be contradictory. The theoretical pI for human NKCC1 is 5.98 and 7.18 for NKCC2, and these are similar for other mammalian NKCCs. Figure 3.9 shows an example of a T4 western blot of ZOOM fractions. T4 immunoreactivity was only present in fraction pH 5.4-6.2. This fits with the theoretical pI for NKCC1, but immunoreactivity would also be expected in fractions above pH 6.2 if NKCC2 were present. A single ZOOM fractionation of ferret kidney

membranes was conducted (data not shown) and T4 immunoreactivity was observed in fractions pH 5.4-6.2 and pH 6.2-7.0. Although it is possible that the quantities of NKCC2 present in red blood cells are lower than NKCC1 and therefore not visible in the ZOOM fractionations above pH 6.2, it may also be the case that the red cell isoform is sufficiently different as to have a more acidic pI placing it within the same fraction as NKCC1. We observe NKCC2 immunoreactivity from ferret and rat erythrocyte membranes at a molecular weight of approximately 240 kDa on western blots. This is around 100-120 kDa larger than expected based on the amino acid sequence of kidney NKCC2. Based on the size of the band, the most obvious assumption to make would be that this is a dimer formed from two NKCC monomers. It could also indicate heavy glycosylation of the protein. This would be easily tested by the deglycosylation experiment demonstrated in figure 4.3, followed by western blotting with the anti-NKCC2 antibody. It may also indicate that any NKCC2 present in the red blood cell is different to that found in the kidney, based on its estimated molecular mass and pI (if present in the same ZOOM fraction as NKCC1). In order to understand this we may wish to purify the proteins for further study. As shown in this thesis, 2-DE and IP yield disappointing results in red blood cells. Another approach would be to sequence the whole cDNA for the cotransporter isoforms present and infer protein sequence and molecular weight from this. This may be more easily achieved in avian erythrocytes, which are nucleated. This would allow isolation of better quality nucleic acid than was obtained using the methods described in chapter 6 of this thesis.

Why would the red blood cell possess NKCC2?

NKCC2 splice variants can interact with NKCC1 and may confer a level of cotransport regulation (Brunet *et al*, 2005; Gagnon *et al*, 2002; Plata *et al*, 2002; Plata *et al*, 1999). This may be particularly important in the red blood cell where cotransport activity cannot be upregulated by increased expression of the cotransport protein. The various isoforms and splice variants have different transport and ion binding capacities. This panel of slightly different NKCC proteins may be required for the cell to handle different needs for ion transport. In the absence of specific inhibitors to each isoform, this idea is not currently able to be tested. It is of interest though, to identify which of the various NKCC2 variants are present in the erythrocyte and this could be achieved with splice isoform-specific PCR primers.

7.4 – Conclusions

There are three main findings from the research conducted for this thesis. Firstly, band 3 and NKCC interact within the erythrocyte. Secondly, phosphorylation of the cotransporter is increased or reduced when transport is increased or reduced and that although the red blood cell expresses SPAK/OSR1 kinases these are not responsible for the increase of phosphorylation and cotransport observed in response to deoxygenation. Thirdly, for the first time evidence is provided that the RBC expresses NKCC2.

A model is presented in figure 7.2 that suggests increased activity of NKCC under deoxygenating conditions and when plasma potassium concentration is high. Physiologically, this situation is likely to occur in blood vessels associated with exercising muscle. Here oxygen is rapidly consumed and potassium is released into

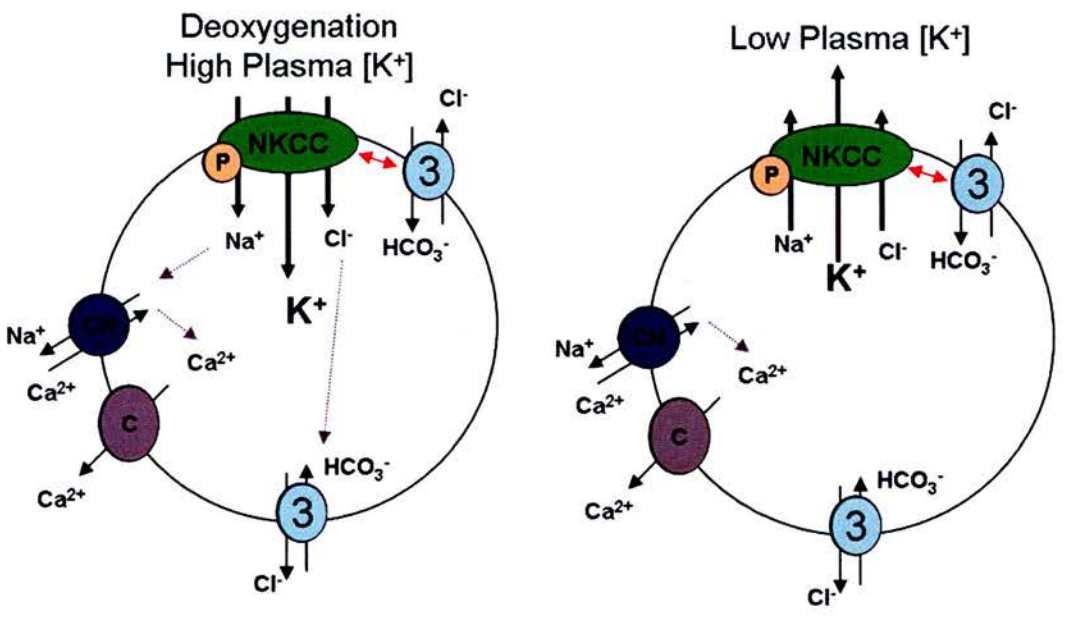

Figure 7.2 – Model for Function of NKCC in Ferret Red Blood Cells

Under deoxygenating conditions, or where plasma potassium is high, NKCC becomes active and drives net influx of ions and acts as a sink for potassium. As NKCC is capable of bi-directional cotransport, it can release stored potassium when necessary. At rest, NKCC cotransport is close to equilibrium. As shown in this thesis, this activity is regulated via protein phosphorylation but the mechanisms for how this occurs in response to deoxygenation is not yet understood. Other than via NKCC, the major route for chloride ion transport is via band 3 (3). An interaction between band 3 and NKCC may offer a further level of NKCC cotransport regulation. Ca-Na (CN) exchange driven by the Ca gradient created by the Ca pump (C) help to extrude sodium from ferret red blood cells (Milanick, 1989).

the plasma. Hyperkalemia is an undesirable state which can result in abnormal heart rhythms and in severe states can cause the heart to stop beating. The situation present in the ferret red blood cell (and perhaps other animals) appears poised to take up potassium from the blood. Flatman (1983) showed that by increasing the potassium concentration of the medium, ferret erythrocytes increased uptake via NKCC. Potassium content in ferret red blood cells is normally low at about 4 mM (Flatman and Andrews, 1983) and extracellular changes above this level would result in influx of ions via NKCC. The converse was true when medium initially containing no potassium was used, indicating that ion cotransport is bi-directional

and that potassium could be also released from the cell. As suggested in figure 7.2, the red cell could take up potassium from the plasma effectively removing it from the circulating blood and away from the heart. The cells could then release this potassium when necessary in different sites within the body.

7.5 - Future Directions

The objective now will be to further understand the significance of the findings presented in this thesis. This will again involve a multi-disciplinary approach.

7.5.1 - Protein-Protein Interactions

Other tissue types should be used to investigate the interactions of NKCC and the proteins identified by IP and native-PAGE experiments. The shotgun N1 IP LC-MSMS method described in chapter 4 of this thesis could be explored using other tissue samples, as well as the various 2-D electrophoresis techniques. We could then investigate if any novel interactions uncovered from other cell types are of relevance in the red blood cell using a standard co-IP and western blotting approach.

7.5.2 - Phosphorylation

It may be necessary to use other cell types for some of the research, due to the difficulties in obtaining sufficient protein from red blood cells. This will be useful for studying aspects of cotransport that are not red blood cell specific. For example, using salivary gland or kidney tissue we may be better able to separate out differently phosphorylated cotransporter molecules using the 2-DE approach used in this thesis, in particular, the spots identified by the R5 and NKCC-P antibodies. This would allow mass spectrometric identification of the phosphorylated residues of each

individual species. Further experiments could include isolation of smaller fragments of NKCC, by immunoprecipitation with N1 and T4 antibodies after chemical cleavage with formic acid, allowing a means to study phosphorylation on the N- and C-termini. Figure 7.3 shows the hypothetical NKCC products of formic acid hydrolysis and the epitopes that the N1 and T4 antibodies were raised against. Based on this it is theoretically possible to isolate different sections of the cotransporter, which may then be enzymatically digested and the peptides (and any phospho-modifications) analysed by LC-MSMS. This, and perhaps more standard ^{32}phosphorylation experiments in this cell type, could be used to look at the residues that are modified across the whole protein rather than just in the N-terminus as is currently the focus. This may help to further understand how the cotransporter is regulated and could help clear up which of the N-terminal residues are phosphorylated under the conditions used in this thesis.

7.5.2 - Molecular Biology

It is important now to ensure that the products amplified by the NKCC 1 and 2 primers from red blood cells used in this project are actually from NKCC 1 and 2 mRNA. Sequencing of the PCR products would confirm or deny this. If these are correct, then identification of which NKCC2 splice variants are present in the erythrocyte will be important. The use of nucleated avian erythrocytes for RNA interference experiments, or NKCC2 variant knockout animals, may be required in order to decipher the functional significance of these proteins in the red blood cell. Overall, the erythrocyte remains a powerful functional model for the study of Na-K-2Cl cotransport. As well as having unique features of regulation that are relevant to

its own function it may help us to understand general cotransport regulation as applicable to other systems.

Figure 7.3 – Hypothetical Cleavage Products of Human NKCC1 by Formic Acid

Formic acid cleavage between an aspartate and proline residue results in three segments based on the human NKCC1 sequence. N1 antibody was raised against two peptide sequences (labelled in green) and the T4 antibody was raised to a section of the C-terminus (whole terminus labelled in red as actual epitope is not known).

Chapter 8

References

Chapter 8 – References

Altamirano, A.A., Breitwieser, G.E., and Russell, J.M. (1988) Vanadate and fluoride effects on Na^+-K^+-Cl^- cotransport in squid giant axon. *American Journal of Physiology.* **254,** C582-C586.

Alvarez-Guerra, M., Nazaret, C. and Garay, R.P. (1998) The erythrocyte Na,K,Cl cotransporter and its circulating inhibitor in Dahl salt-sensitive rats. *Journal of Hypertension.* **16,** 1499-1504.

Alvarez-Leefmans, F.J., Gamino, S.M., Giraldez, F. and Nogueron, I. (1988) Intracellular chloride regulation in amphibian dorsal root ganglion neurones studied with ion-selective microelectrodes. *The Journal of Physiology.* **406,** 225-246.

Anselmo, A.N., Earnest, S., Chen, W., Juang, Y.C., Kim, S.C., Zhao, Y. and Cobb, M.H. (2006) WNK1 and OSR1 regulate the Na+, K+, 2Cl- cotransporter in HeLa cells.*Proceedings of the National Academy of Sciences of the United States of America.* **103,** 10883-10888.

Bain, J., Plater, L., Elliott, M., Shpiro, N., Hastie, J., McLauchlan, H., Klevernic, I., Arthur, S., Alessi, D. and Cohen, P. (2007) The selectivity of protein kinase inhibitors; a further update. *Biochemical Journal.* **408,** 297-315.

Bain, J., McLauchlan, H., Elliott, M. and Cohen, P. (2003) The specificities of protein kinase inhibitors: an update. *Biochemical Journal.* **371,** 199-204.

Bartter, F.C., Pronove, P., Gill, J.R. Jr. and MacCardle, R.C. (1998) Hyperplasia of the juxtaglomerular complex with hyperaldosteronism and hypokalemic alkalosis. A new syndrome. 1962. *Journal of the American Society of Nephrology.* **9,** 516-528.

Barvitenko, N.N., Adragna, N.C. and Weber, R.E. (2005) Erythrocyte signal transduction pathways, their oxygenation dependence and functional significance. *Cellular Physiology and Biochemistry.* **15,** 1-18.

Berkelman, T. and Stenstedt, T. (1998) 2-D Electrophoresis using immobilized pH gradients: Principles and methods. *Amersham Pharmacia Biotech Inc,* UK.

Bildin, V.N., Iserovich, P., Fischbarg, J. and Reinach, P.S. (2001) Differential expression of Na:K:2Cl cotransporter, glucose transporter 1, and aquaporin 1 in freshly isolated and cultured bovine corneal tissues. *Experimental Biology and Medicine.* **226,** 919-926.

Breitwieser, G.E., Altamirano, A.A. and Russell, J.M. (1990) Osmotic stimulation of Na(+)-K(+)-Cl- cotransport in squid giant axon is [Cl-]i dependent. *American Journal of Physiology.* **258**, C749-C753.

Brunet, G.M., Gagnon, E., Simard, C.F., Daigle, N.D., Caron, L., Noël, M., Lefoll, M-H., Bergeron, M.J. and Isenring, P. (2005) Novel insights regarding the operational characteristics and teleological purpose of the renal Na^+-K^+-Cl^- cotransporter (NKCC2s) splice variants. *The Journal of General Physiology.* **126,** 325-337.

Campanella, M.E., Chu, H. and Low, P.S. (2005) Assembly and regulation of a glycolytic enzyme complex on the human erythrocyte membrane. *Proceedings of the National Academy of Science of the United States of America.* **15,** 2402-2407.

Caron, L., Rousseau, F., Gagnon, E. and Isenring, P. (2000) Cloning and functional characterization of a cation-Cl- cotransporter-interacting protein. *The Journal of Biological Chemistry.* **275,** 32027-32036.

Carter, M.D., Southwick, K., Lukov, G., Willardson, B.M. and Thulin, C.D. (2004) Identification of phosphorylation sites on phosducin-like protein by QTOF mass spectrometry. *Journal of Biomolecular Techniques.* **15,** 257-264.

Castrop, H., Lorenz, J.N., Hansen, P.B., Friis, U., Mizel, D., Oppermann, M., Jensen, B.L., Briggs, J., Skøtt, O. and Schnermann, J. (2005) Contribution of the basolateral isoform of the Na-K-2Cl cotransporter (NKCC1/BSC2) to renin secretion. *American Journal of Physiology.* **289,** F1185-F1192.

Chen, H., Luo, J., Kintner, D.B., Shull, G.E. and Sun, D. (2005) Na^+-dependent chloride transporter (NKCC1)-null mice exhibit less gray and white matter damage after focal cerebral ischemia. *Journal of Cerebral Blood Flow & Metabolism.* **25,** 54–66.

Chen, W., Yazicioglu, M. and Cobb, M.H. (2004) Characterization of OSR1, a member of the mammalian Ste20p/germinal center kinase subfamily. *The Journal of Biological Chemistry.* **279,** 11129-11136.

Chétrite, G. and Cassoly, R. (1985) Affinity of haemoglobin for the cytoplasmic fragment of human erythrocyte membrane band 3. Equilibrium measurements at physiological pH using matrix-bound proteins: the effects of ionic strength, deoxygenation and 2,3-diphosphoglycerate. *The Journal of Molecular Biology.* **185,** 639-644.

Chevallet, M., Santoni, V., Poinas, A., Rouquié, D., Fuchs, A., Kieffer, S., Rossignol, M., Lunardi, J., Garin, J. and Rabilloud, T. (1998) New zwitterionic detergents improve the analysis of membrane proteins by two-dimensional electrophoresis. *Electrophoresis.* **19,** 1901-1909.

Churchward, M.A., Butt, R.H., Lang, J.C., Hsu, K.K. and Coorssen, J.R. (2005) Enhanced detergent extraction for analysis of membrane proteomes by two-dimensional electrophoresis. *Proteome Science.* **3,** 5.

Crouch, J.J., Sakaguchi, N., Lytle, C. and Schulte, B.A. (1997) Immunohistochemical localization of the Na-K-Cl co-transporter (NKCC1) in the gerbil inner ear. *The Journal of Histochemistry and Cytochemistry.* **45,** 773-778.

Darman, R.B., and Forbush, B. (2002) A regulatory locus of phosphorylation in the N terminus of the Na-K-Cl cotransporter, NKCC1. *The Journal of Biological* Chemistry. **277,** 37542-37550.

Darman, R.B., Flemmer, A. and Forbush, B. (2001) Modulation of ion transport by direct targeting of protein phosphatase 1 to the Na-K-Cl cotransporter. *The Journal of Biological Chemistry.* **276,** 34359-34362.

Dawson, R.M.C., Elliot, D.C., Elliot, W.H. and Jones, K.M. (1986) Data for Biochemical Research. 3rd Edition. Oxford Scientific Publications, Clarendon Press. Oxford, U.K.

Delpire, E., Kaplan, M.R., Plotkin, M.D. and Hebert, S.C. (1996) The Na-(K)-Cl cotransporter family in the mammalian kidney: molecular identification and function(s). *Nephrology, Dialysis, Transplantation.* **11,** 1967-1973.

Delpire, E., Rauchaman, M.I., Beier, D.R., Hebert, S.C. and Gullans, S.R. (1994) Molecular cloning and chromosome localization of a putative basolateral Na^+-K^+-$2Cl^-$ cotransporter from mouse inner medullary collecting duct (mIMCD-3) cells. *The Journal of Biological Chemistry.* **269,** 25677-25683.

Di Ciano-Oliveira, C., Lodyga, M., Fan, L., Szászi, K., Hosoya, H., Rotstein, O.D. and Kapus, A. (2005) Is myosin light-chain phosphorylation a regulatory signal for the osmotic activation of the Na^+-K^+-$2Cl^-$ cotransporter? *American Journal of Physiology.* **289,** C68-C81.

Di Ciano-Oliveira, C., Sirokmány, G., Szászi, K., Arthur, W.T., Masszi, A., Peterson, M., Rotstein, O.D., and Kapus, A. (2003) Hyperosmotic stress activates Rho: differential involvement in Rho kinase-dependent MLC phosphorylation and NKCC activation. *American Journal of Physiology.* **285,** C555-C566.

Dihazi, H., Asif, A.R., Agarwal, N.K., Doncheva, Y. and Müller, G.A. (2005) Proteomic analysis of cellular response to osmotic stress in thick ascending limb of Henle's loop (TALH) cells. *Molecular and Cellular Proteomics*. **4,** 1445-1458.

Ding, Y., Kobayashi, S. and Kopito, R. (1996) Mapping of ankyrin binding determinants on the erythroid anion exchanger, AE1. *The Journal of Biological Chemistry.* **37,** 22494-22498.

Dolganov, G.M., Woodruff, P.G., Novikov, A.A., Zhang, Y., Ferrando, R.E., Szubin, R. and Fahy, J.V. (2001) A novel method of gene transcript profiling in airway biopsy homogenates reveals increased expression of a Na^+-K^+-Cl^- cotransporter (NKCC1) in asthmatic subjects. *Genome Research.* **11,** 1473-1483.

Dowd, B.F. and Forbush, B. (2003) PASK (proline-alanine-rich STE20-related kinase), a regulatory kinase of the Na-K-Cl cotransporter (NKCC1). *The Journal of Biological Chemistry.* **278,** 27347-27353.

Drew, C., Ball, V., Robinson, H., Ellory, J.C. and Gibson, J.S. (2004) Oxygen sensitivity of red cell membrane transporters revisited. *Bioelectrochemistry.* **62,** 153-158.

Dunn, C.J., Fitton, A. and Brogden, R.N. (1995) Torasemide. An update of its pharmacological properties and therapeutic efficacy. *Drugs.* **49,** 121-142.

Ecelbarger, C.A., Terris, J., Hoyer, J.R., Nielsen, S., Wade, J.B. and Knepper, M.A. (1996) Localization and regulation of the rat renal Na(+)-K(+)-2Cl- cotransporter, BSC-1. *American Journal of Physiology.* **271,** F619-F628.

Flagella, M., Clarke, L.L., Miller, M.L., Erway, L.C., Giannella, R.A., Andringa, A., Gawenis, L.R., Kramer, J., Duffy, J.J., Doetschman, T., Lorenz, J.N., Yamoah, E.N., Cardell, E.L. and Shull, G.E. (1999) Mice lacking the basolateral Na-K-2Cl cotransporter have impaired epithelial chloride secretion and are profoundly deaf. *The Journal of Biological Chemistry.* **274,** 26946-26955.

Flatman, P.W. (2005) Activation of ferret erythrocyte Na^+-K^+-$2Cl^-$ cotransport by deoxygenation. *The Journal of Physiology.* **563,** 421-431.

Flatman, P.W., and Creanor, J. (1999a) Regulation of Na^+-K^+-$2Cl^-$ cotransport by protein phosphorylation in ferret erythrocytes. *Journal of Physiology.* **517**, 699-708.

Flatman, P.W., and Creanor, J. (1999b) Stimulation of Na^+-K^+-$2Cl^-$ cotransport by arsenite in ferret erythrocytes. *Journal of Physiology.* **519**, 143-152.

Flatman, P.W. (1991) The effects of metabolism on Na^+-K^+-Cl^- co-transport in ferret red cells. *The Journal of Physiology.* **437,** 495-510.

Flatman, P.W. (1988) The effects of magnesium on potassium transport in ferret red cells. *The Journal of Physiology.* **397,** 471-487.

Flatman, P.W. (1983) Sodium and potassium transport in ferret red cells. *The Journal of Physiology.* **341,** 545-557.

Flatman, P.W. and Andrews, P.L. (1983) Cation and ATP content of ferret red cells. Comp Biochem Physiol A. **74,** 939-943.

Flemmer, A.W., Giménez, I., Dowd, B.F., Darman, R.B., and Forbush, B. (2002) Activation of the Na-K-Cl cotransporter NKCC1 detected with a phospho-specific antibody. *The Journal of Biological Chemistry.* **277,** 37551-37558.

Fraser, S.A., Giménez, I., Cook, N., Jennings, I., Katerelos, M., Katsis, F., Levidiotis, V., Kemp, B.E. and Power, D.A. (2007) Regulation of the renal-specific Na^+-K^+-$2Cl^-$ co-transporter NKCC2 by AMP-activated protein kinase (AMP). *Biochemical Journal.* **405,** 85-93.

Friedel, H.A. and Buckley, M.M. (1991) Torasemide. A review of its pharmacological properties and therapeutic potential. *Drugs.* **41,** 81-103.

Gagnon. E., Forbush, B., Flemmer, A.W., Gimenez, I., Caron, L. and Isenring, P. (2002) Functional and molecular characterization of the shark renal Na-K-Cl cotransporter: novel aspects. *American Journal of Physiology.* **283,** F1046-F1055.

Gagnon, F., Orlov, S.N., Champagne, M.J., Tremblay, J. and Hamet, P. (1999) Heat stress preconditioning does not protect renal epithelial Na(+),K(+),Cl(-) and Na(+),P(i) cotransporters from their modulation by severe heat stress. *Biochimica et Biophysica Acta.* **1421,** 163-174.

Gagnon, K.B., England, R. and Delpire, E. (2007a) A single binding motif is required for SPAK activation of the Na-K-2Cl cotransporter. *Cellular Physiology and Biochemistry.* **20,**131-142.

Gagnon, K.B., England, R., Diehl, L. and Delpire, E. (2007b) Apoptosis-associated tyrosine kinase scaffolding of protein phosphatase 1 and SPAK reveals a novel pathway for Na-K-2C1 cotransporter regulation. *American Journal of Physiology.* **292,** C1809-C1815.

Gagnon, K.B., England, R. and Delpire, E. (2006a) Characterization of SPAK and OSR1, regulatory kinases of the Na-K-2Cl cotransporter. *Molecular and Cellular Biology.* **26,** 689-698.

Gagnon, K.B., England, R. and Delpire, E. (2006b) Volume sensitivity of cation-Cl- cotransporters is modulated by the interaction of two kinases: Ste20-related proline-alanine-rich kinase and WNK4. *American Journal of Physiology.* **290,** C134-C142.

Gamba, G. (2005) Molecular physiology and pathophysiology of electroneutral cation-chloride cotransporters. *Physiological Reviews.* **85,** 423-493.

Gamba, G., Miyanoshita, A., Lombardi, M., Lytton, J., Lee, W-S., Hediger, M.A. and Hebert, S.C. (1994) Molecular cloning, primary structure, and characterization of two members of the mammalian electroneutral sodium-(potassium)-chloride cotransporter family expressed in kidney. *The Journal of Biological Chemistry.* **269,** 17713-17722.

Garg, P., Martin, C.F., Elms, S.C., Gordon, F.J., Wall, S.M., Garland, C.J., Sutliff, R.L. and O'Neill, W.C. (2007) Effect of the Na-K-2Cl cotransporter NKCC1 on systemic blood pressure and smooth muscle tone. *American Journal of Physiology.* **292,** H2100-H2105.

Geck, P., Pietrzyk, C., Burckhardt, B.C., Pfeiffer, B. and Heinz, E. (1980) Electrically silent cotransport of Na^+, K^+ and Cl^- in Ehrlich cells. *Biochimica et Biophysica Acta.* **600,** 432-447.

Gerelsaikhan, T., Nahid Parvin, M. and Turner, J.R. (2006) Biogenesis and topology of the secretory Na^+-K^+-$2Cl^-$ cotransporter (NKCC1) studied in intact mammalian cells. *Biochemistry.* **45,** 12060-12067.

Gerelsaikhan, T., and Turner, J.R. (2000) Transmembrane topology of the secretory Na^+ -K^+ -$2Cl^-$ cotransporter NKCC1 studied by *in vitro* translation. *The Journal of Biological Chemistry.* **275,** 40471-40477.

Gharahdaghi, F., Weinberg, C.R., Meagher, D.A., Imai, B.S. and Mische, S.M. (1999) Mass spectrometric identification of proteins from silver-stained polyacrylamide gel: A method for the removal of silver ions to enhance sensitivity. *Electrophoresis.* **20,** 601-605.

Giguère, P., Turcotte, M.E., Hamelin, E., Parent, A., Brisson, J., Laroche, G., Labrecque, P., Dupuis, G. and Parent, J.L. (2007) Peroxiredoxin-4 interacts with and regulates the thromboxane A(2) receptor. *FEBS Letters.* 581, 3863-3868.

Gill, J.R. and Bartter, F.C. (1978) Evidence for a prostaglandin-independent defect in chloride reabsorption in the loop of henle as a proximal cause of Bartter's syndrome. *The American Journal of Medicine*, **65,** 766-772.

Giménez, I. and Forbush, B. (2005) Regulatory phosphorylation sites in the NH2 terminus of the renal Na-K-Cl cotransporter (NKCC2). *American Journal of Physiology.* **289,** F1341–F1345.

Giménez, I. and Forbush, B. (2003) Short-term stimulation of the renal Na-K-Cl cotransporter (NKCC2) by vasopressin involves phosphorylation and membrane translocation of the protein. *The Journal of Biological Chemistry.* **278,** 26946-26951.

Giménez, I., Isenring, P. and Forbush, B. (2002) Spatially distributed alternative splice variants of the renal Na-K-Cl cotransporter exhibit dramatically different affinities for the transported ions. *The Journal of Biological Chemistry.* **277,** 8767-8770.

Glanville, M., Kingscote, S., Thwaites, D.T. and Simmons, N.L. (2001) Expression and role of sodium, potassium, chloride cotransport (NKCC1) in mouse inner medullary collecting duct (mIMCD-K2) epithelial cells. *Pflügers Archiv.* **443,** 123-131.

Gordon, J.A. (1991) Use of vanadate as protein-phosphotyrosine phosphatase inhibitor. *Methods in Enzymology.* **201,** 477-482.

Gordon RD (1986) Syndrome of hypertension and hyperkalemia with normal glomerular filtration rate. *Hypertension.* **8,** 93–102.

Gosmanov, A.R. and Thomason, D.B. (2003) Regulation of Na(+)-K(+)-2Cl-cotransporter activity in rat skeletal muscle and intestinal epithelial cells. *Tsitologiia.* **45,** 812-816.

Gosmanov, A.R., Nordtvedt, N.C., Brown, R., and Thomason, D.B. (2002) Exercise effects on muscle β-adrenergic signaling for MAPK-dependent NKCC activity are rapid and persistent. *Journal of Applied Physiology.* **93,** 1457-1465.

Granvogl, B., Reisinger, V. and Eichacker, L.A. (2006) Mapping the proteome of thylakoid membranes by *de novo* sequencing of intermembrane peptide domains. *Proteomics.* **6,** 3681-3695.

Greger, R., Lohrmann, E. and Bleich, M. (1994) Tubular actions of diuretics (overview). *The Clinical Investigator.* **72,** 690-691.

Guizouarn, H., Gabillat, N. and Borgese, F. (2004) Evidence for up-regulation of the endogenous Na-K-2Cl co-transporter by molecular interactions with the anion exchanger tAE1 expressed in Xenopus oocyte. *The Journal of Biological Chemistry.* **279,** 11513-11520.

Haas, M., McBrayer, D., and Lytle, C. (1995) [Cl^-]*i*-dependent phosphorylation of the Na-K-Cl cotransport protein of dog tracheal epithelial cells. *The Journal of Biological Chemistry.* **270,** 28955-28961.

Haas, M. (1994) The Na-K-Cl cotransporters. *American Journal of Physiology.* **267,** C869-C885.

Haas, M. and Forbush, B., 3rd. (2000) The Na-K-Cl cotransporter of secretory epithelia. *Annual Review of Physiology.* **62,** 515-534.

Haas, M. and Forbush, B., 3rd (1998) The Na-K-Cl cotransporters. Journal of *Bioenergetics and Biomembranes*. **30,** 161-172.

Haas, M. and McManus, T.J. (1983) Bumetanide inhibits (Na + K + 2Cl) co-transport at a chloride site. *American Journal of Physiology.* **243,** C235-C240.

Hall, A.C. and Ellory, J.C. (1985) Measurement and stoichiometry of bumetanide-sensitive (2Na:1K:3Cl) cotransport in ferret red cells. *The Journal of Membrane Biology.* **85,** 205-213.

Hannaert, P., Alvarez-Guerra, M., Pirot, D., Nazaret, C. and Garay, R.P. (2002) Rat NKCC2/NKCC1 cotransporter selectivity for loop diuretic drugs. *Naunyn-Schmiedeberg's Archives of Pharmacology.* **365,** 193-199.

Hartinger, J., Stenius, K., Högemann, D. and Jahn, R. (1996) 16-BAC/SDS-PAGE: A two-dimensional gel electrophoresis system suitable for the separation of integral membrane proteins. *Analytical Biochemistry.* **240,** 126-133.

Hebert, S.C., Mount, D.B., and Gamba, G. (2004) Molecular physiology of cation-chloride Cl^- cotransport: the SLC12 family. *Pflügers Archiv – European Journal of Physiology.* **447,** 580-593.

Hewett, D., Samuelsson, L., Polding, J., Enlund, F., Smart, D., Cantone, K., Gee See, C., Chadha, S., Inerot, A., Enerback, C., Montgomery, D., Christodolou, C., Robinson, P., Matthews, P., Plumpton, M., Dykes, C., Wahlstrom, J., Swanbeck, G., Martinsson, T., Roses, A., Riley, J., and Purvis, I. (2002) Identification of a psoriasis susceptibility candidate gene by linkage disequilibrium mapping with a localized single nucleotide polymorphism map. *Genomics.* **79,** 305-314.

Hoffmann, E.K. and Pedersen, S.F. (2007) Shrinkage insensitivity of NKCC1 in myosin II-depleted cytoplasts from Ehrlich ascites tumor cells. *American Journal of Physiology.* **292,** C1854-C1866.

Hoffman, J.F., Wickrema, A., Potapova, O., Milanick, M. and Yingst, D.R. (2002) Na pump isoforms in human erythroid progenitor cells and mature erythrocytes. *Proceedings of the National Academy of Sciences of the United States of America.* **99,** 14572-14577.

Invitrogen (2006) NativePAGE™ Novex® Bis-Tris Gel System User Manual: A system for native gel electrophoresis. Version A. California, U.S.A.

Isenring, P., Jacoby, S.C. and Forbush, B., III. (1998a) The role of transmembrane domain 2 in cation transport by the Na-K-Cl cotransporter. *Proceedings of the National Academy of Science of the United States of America.* **95,** 7179-7184.

Isenring, P., Jacoby, S.C., Chang, J. and Forbush, B., III. (1998b) Mutagenic mapping of the Na-K-Cl cotransporter for domains involved in ion transport and bumetanide binding. *Journal of General Physiology.* **112,** 549-558.

Isenring, P., Jacoby, S.C., Payne, J.A., and Forbush, B., III. (1998c) Comparison of Na-K-Cl cotransporters. NKCC1, NKCC2, and the HEK cell Na-L-Cl cotransporter. *The Journal of Biological Chemistry.* **273,** 11295-11301.

Isenring, P. and Forbush, B., III. (1997) Ion and bumetanide binding by the Na-K-Cl cotransporter – Importance of transmembrane domains. *The Journal of Biological Chemistry.* **272,** 24556-24562.

Ishihara, H., Martin, B.L., Brautigan, D.L., Karaki, H., Ozaki, H., Kato, Y., Fusetani, N., Watabe, S., Hashimoto, K., Uemura, D. and Hartshorne, D.J. (1989) Calyculin A and okadaic acid: inhibitors of protein phosphatase activity. *Biochemical and Biophysical Research Communications.* **159,** 871-877.

Jaumot, M. and Hancock, J.F. (2001) Protein phosphatases 1 and 2A promote Raf-1 activation by regulating 14-3-3 interactions. *Oncogene*. **20**, 3949-3958.

Jensen, B.S.and Hoffmann, E.K. (1997) Hypertonicity enhances expression of functional Na+/K+/2Cl- cotransporters in Ehrlich ascites tumour cells. *Biochimica et Biophysica Acta.* **1329,** 1-6.

Johnston, A.M., Naselli, G., Gonez, L.J., Martin, R.M., Harrison, L.C. and DeAizpurua, H.J. (2000) SPAK, a STE20/SPS1-related kinase that activates the p38 pathway. *Oncogene.* **19,** 4290-4297.

Kang, S.W., Chang, T.S., Lee, T.H., Kim, E.S., Yu, D.Y. and Rhee, S.G. (2004) Cytosolic peroxiredoxin attenuates the activation of Jnk and p38 but potentiates that of Erk in Hela cells stimulated with tumor necrosis factor-alpha. *The Journal of Biological Chemistry*. **279,** 2535-2543.

Keep, R.F., Xiang, J. and Betz, A.L. (1994) Potassium cotransport at the rat choroid plexus. *American Journal of Physiology.* **267,** C1616-C1622.

Klein, C., Garcia-Rizo, C., Bisle, B., Scheffer, B., Zischka, H., Pfeiffer, F., Siedler, F. and Oesterhelt, D. (2005) The membrane proteome of *Halobacterium salinarum*. *Proteomics.* **5,** 180-197.

Klein, J.D., Lamitina, S.T. and O'Neill, W.C. (1999) JNK is a volume-sensitive kinase that phosphorylates the Na-K-2Cl cotransporter in vitro. *The American Journal of Physiology.* **277,** C425-C431.

Klein, J.D. and O'Neill, W.C. (1995) Volume-sensitive myosin phosphorylation in vascular endothelial cells: correlation with Na-K-2Cl cotransport. *American Journal of Physiology.* **269,** C1524-C1531.

Knuesel, M., Wan, Y., Xiao, Z., Holinger, E., Lowe, N., Wang, W. and Liu, X. (2003) Identification of novel protein-protein interactions using a versatile mammalian tandem affinity purification expression system. *Molecular and Cellular Proteomics*. **2,** 1225-1233.

Köckerling, A., Reinalter S.C. and Seyberth, H.W. (1996) Impaired response to furosemide in hyperprostaglandin E syndrome: Evidence for a tubular defect in the loop of Henle. *The Journal of Pediatrics.* **129,** 519-528.

Krarup, T., Jakobsen, L.D., Jensen, B.S., and Hoffmann, E.K. (1998) Na^+-K^+-$2Cl^-$ cotransport in Ehrlich cells: regulation by protein phosphatases and kinases. *American Journal of Physiology.* **275,** C239-C250.

Krause, F. (2006) Detection and analysis of protein-protein interactions in organellar and prokaryotic proteomes by native gel electrophoresis: (Membrane) protein complexes and supercomplexes. *Electrophoresis.* **27,** 2759-2781.

Kubo, K. (1995) Effect of incubation of solutions of proteins containing dodecyl sulfate on the cleavage of peptide bonds by boiling. *Analytical Biochemistry.* **225,** 351-353.

Kurihara, K., Nakanishi, N., Moore-Hoon, M. and Turner, J.R. (2002) Phosphorylation of the salivary Na^+-K^+-$2Cl^-$ cotransporter. *American Journal of Physiology.* **282,** C817-C823.

Kurihara, K., Moore-Hoon, M., Saitoh, M. and Turner, J.R. (1999) Characterization of a phosphorylation event resulting in upregulation of the salivary Na^+-K^+-$2Cl^-$ cotransporter. *American Journal of Physiology.* **277,** C1184-C1193.

Layne, J., Yip, S. and Crook, R.B. (2001) Down-regulation of Na-K-Cl cotransport by protein kinase C is mediated by protein phosphatase 1 in pigmented ciliary epithelial cells. *Experimental Eye Research.* **72,** 371-379.

Lee, T.H., Kim, S.U., Yu, S.L., Kim, S.H., Park, D.S., Moon, H.B., Dho, S.H., Kwon, K.S., Kwon, H.J., Han, Y.H., Jeong, S., Kang, S.W., Shin, H.S., Lee, K.K., Rhee, S.G. and Yu, D.Y. (2003) Peroxiredoxin II is essential for sustaining life span of erythrocytes in mice. *Blood.* **101,** 5033-5038.

Liedtke, C.M., Wang, X. and Smallwood, N. (2005) Role for protein phosphatase 2A in the regulation of Calu-3 epithelial Na^+-K^+-$2Cl^-$, type 1 co-transport function. *The Journal of Biological Chemistry.* **280,** 25491-25498.

Liedtke, C.M., Hubbard, M. and Wang, X. (2003) Stability of actin cytoskeleton and PKC-delta binding to actin regulate NKCC1 function in airway epithelial cells. *American Journal of Physiology.* **284,** C487-C496.

Liedtke, C.M. and Cole, T.S. (2002) Activation of NKCC1 by hyperosmotic stress in human tracheal epithelial cells involves PKC-delta and ERK. *Biochimica et Biophysica Acta.* **1589,** 77–88.

Low, F.M., Hampton, M.B., Peskin, A.V. and Winterbourn, C.C. (2007) Peroxiredoxin 2 functions as a noncatalytic scavenger of low-level hydrogen peroxide in the erythrocyte. *Blood.* **109,** 2611-2617.

Lu, Y., Bottari, P., Turecek, F., Aebersold, R. and Gelb, M.H. (2004) Absolute quantification of specific proteins in complex mixtures using visible isotope-coded affinity tags. *Analytical Chemistry.* **76,** 4104-4111.

Lytle, C. (2003) Chapter 8: Na^+-K^+-$2Cl^-$ cotransport. In *Red Cell Membrane Transport in Health and Disease,* eds. Bernhardt, I. and Ellory, J.C. pp. 173-189. Springer-Verlag, Berlin.

Lytle, C. (1997) Activation of the avian erythrocyte Na-K-Cl cotransport protein by cell shrinkage, cAMP, fluoride, and calyculin-A involves phosphorylation at common sites. *The Journal of Biological Chemistry.* **272,** 15069-15077.

Lytle, C. and Forbush, B., III. (1996) Regulatory phosphorylation of the secretory Na-K-Cl cotransporter: modulation by cytoplasmic Cl. *American Journal of Physiology.* **270,** C437-C448.

Lytle, C., Xu, J-C., Biemesderfer, D. and Forbush, B., III. (1995) Distribution and diversity of Na-K-Cl cotransport proteins: a study with monoclonal antibodies. *American Journal of Physiology.* **269,** C1496-C1505.

Lytle, C. and Forbush, B., III. (1992) The Na-K-Cl cotransport protein of shark rectal gland. II. Regulation by direct phosphorylation. *The Journal of Biological Chemistry.* **267,** 25438-25443.

Maglova, L.M., Crowe, W.E., Smith, P.R., Altamirano, A.A. and Russell, J.M. (1998) Na+-K+-Cl- cotransport in human fibroblasts is inhibited by cytomegalovirus infection. *American Journal of Physiology.* **275,** C1330-C1341.

Mairbäurl, H., Schulz, S. and Hoffman, J.F. (2000) Cation transport and cell volume changes in maturing rat reticulocytes. *American Journal of Physiology.* **279,** C1621-C1630.

Maniatis, T., Fritsch, E.F. and Sambrook, J. (1982) Molecular Cloning: a laboratory manual. Cold Spring Harbor Laboratory: Cold Spring Harbor, N.Y.

Mann, M., Hendrickson, R.C., and Pandey, A. (2001) Analysis of proteins and proteomes by mass spectrometry. *Annual Review of Biochemistry.* **70,** 437-473.

Marty, M.C., Alliot, F., Rutin, J., Fritz, R., Trisler, D. and Pessac, B.(2002) The myelin basic protein gene is expressed in differentiated blood cell lineages and in hemopoietic progenitors. *Proceedings of the National Academy of Science of the United States of America.* **99,** 8856-8861.

Matskevich, I., Hegney, K.L. and Flatman, P.W. (2005) Regulation of erythrocyte Na-K-2Cl cotransport by threonine phosphorylation. *Biochimica et Biophysica Acta.* **1714,** 25-34.

Meade, P., Hoover, R.S., Plata, C., Vázquez, N., Bobadilla, N.A., Gamba, G. and Hebert, S.C. (2003) cAMP-dependent activation of the renal specific Na^+-K^+-$2Cl^-$ cotransporter is mediated by regulation of cotransporter trafficking. *American Journal of Physiology.* **284,** F1145-F1154.

Michaely, P. and Bennett, V. (1995) Mechanism for binding site diversity on ankyrin: comparison of binding sites on ankyrin for neurofascin and the Cl^-/HCO_3^- anion exchanger. *The Journal of Biological Chemistry.* **270,** 31298-31302.

Milanick, M. (1989) Na-Ca exchange in ferret red blood cells. *American Journal of Physiology.* **256**, C390-C398.

Monti, M., Orrù, S., Pagnozzi, D. and Pucci, P. (2005) Interaction proteomics. *Bioscience Reports.* **25,** 45-56.

Moore-Hoon, M.L. and Turner, R.J. (2000) The structural unit of the secretory Na^+-K^+-Cl^- cotransporter (NKCC1) is a homodimer. *Biochemistry.* **39,** 3718-3724.

Moore-Hoon, M.L. and Turner, R.J. (1998) Molecular and topological characterization of the rat parotid Na^+-K^+-2Cl^- cotransporter. *Biochimica et Biophysica Acta.* **1373,** 261-269.

Moorhead, G., MacKintosh, C., Morrice, N. and Cohen, P. (1995) Purification of the hepatic glycogen-associated for of protein phosphatase-1 by microcystin-Sepharose affinity chromatography. *FEBS Letters.* **362,** 101-105.

Morales-Aza, B.M., Chillingworth, N.L., Payne, J.A. and Donaldson, L.F. (2004) Inflammation alters cation chloride cotransporter expression in sensory neurons. *Neurobiology of Disease.* **17,** 62-69.

Moriguchi, T., Urushiyama, S., Hisamoto, N., Iemura, S., Uchida, S., Natsume, T., Matsumoto, K. and Shibuya, H. (2005) WNK1 regulates phosphorylation of cation-chloride-coupled cotransporters via the STE20-related kinases, SPAK and OSR1. *Journal of Biological Chemistry.* **280,** 42685-42693.

Mount, D.B., Baekgaard, A., Hall, A.E., Plata, C., Xu, J., Beier, D.R., Gamba, G. and Hebert, S.C. (1999) Isoforms of the Na-K-2Cl cotransporter in murine TAL I. Molecular characterization and intrarenal localization. *American Journal of Physiology.* **276,** F347-F358.

Mount, D.B., Delpire, E., Gamba, G., Hall, A.E., Poch, E., Hoover, R.S., Jr. and Hebert, S.C. (1998) The electroneutral cation-chloride cotransporters. *The Journal of Experimental Biology.* **201,** 2091-2102.

Muzyamba, M.C., Cossins, A.R. and Gibson, J.S. (1999) Regulation of Na^+-K^+-2Cl^- cotransport in turkey red cells: the role of oxygen tension and protein phosphorylation. *Journal of Physiology.* **517,** 421-429.

Nagy, A. and Turner, J.R. (2007) The membrane integration of a naturally occurring α-helical hairpin. *Biochemical and Biophysical Research Communications.* **356,** 392-397.

Nakajima, K., Miyazaki, H., Niisato, N. and Marunaka, Y. (2007) Essential role of NKCC1 in NGF-neurite outgrowth. *Biochemical and Biophysical Research Communications.* **359,** 604-610.

Nguyen, M., Pace, A.J. and Koller, B.H. (2007) Mice lacking NKCC1 are protected from development of bacteremia and hypothermic sepsis secondary to bacterial pneumonia. *The Journal of Experimental Medicine.* **204,** 1383-1393.

Nielsen, S., Maunsbach, A.B., Ecelbarger, C.A. and Knepper, M.A. (1998) Ultrastructural localization of Na-K-2Cl cotransporter in thick ascending limb and macula densa of rat kidney. *American Journal of Physiology.* **275,** F885-F893.

Niven, A.S. and Argyros, G. (2003) Alternate treatments in asthma. *Chest.* **123,** 1254-1265.

O'Brien, T.G., Prettyman, R., George, K.S. and Herschman, H.R. (1988) A phorbol ester-nonproliferative variant of Swiss 3T3 cells is deficient in Na+K+Cl-cotransport activity. *Journal of Cellular Physiology.* **134,** 302-6.

O'Donnell, M.E., Tran, L., Lam, T.I., Liu, X.B. and Anderson, S.E. (2004) Bumetanide Inhibition of the Blood-Brain Barrier Na-K-Cl Cotransporter Reduces Edema Formation in the Rat Middle Cerebral Artery Occlusion Model of Stroke. *Journal of Cerebral Blood Flow & Metabolism.* **24,**1046–1056.

O'Donnell ME, Martinez A, Sun D. (1995) Endothelial Na-K-Cl cotransport regulation by tonicity and hormones: phosphorylation of cotransport protein. *American Journal of Physiology.* **269,** C1513-23.

O'Neill, W.C. and Klein, J.D. (1992) Regulation of vascular endothelial cell volume by Na-K-2Cl cotransport. *American Journal of Physiology.* **262,** C436-C444.

Olivieri, E., Herbert, B. and Righetti, P.G. (2001) The effect of protease inhibitors on the two-dimensional electrophoresis pattern of red blood cell membranes. *Electrophoresis.* **22,** 560-565.

Orlov, S.N. (2007) NKCC1 as a regulator of vascular tone and a novel target for antihypertensive therapeutics. *American Journal of Physiology.* **292,** H2035-H2036.

Orlov, S.N., Adragna, N.C., Adarichev, V.A. and Hamet, P. (1999) Genetic and biochemical determinants of abnormal monovalent ion transport in primary hypertension. *American Journal of Physiology.* **276,** C511-C536.

Owen, N.E. and Prastein, M.L. (1985) Na/K/Cl cotransport in cultured human fibroblasts. *The Journal of Biological Chemistry.* **260,** 1445-1451.

Padilla, M.C., Armas-Hernández, M.J., Hernández, R.H., Israili, Z.H. and Valasco, M. (2007) Update of diuretics in the treatment of hypertension. *American Journal of Therapeutics.* **14,** 154-160.

Palfrey, H.C., and Pewitt, E.B. (1993) The ATP and Mg^{2+} dependence of Na-K-2Cl cotransport reflects a requirement for protein phosphorylation: studies using calyculin A. *Pflügers Archiv.* **425,** 321-328.

Palfrey, H.C., Silva, P. and Epstein, F.H. (1984) Sensitivity of cAMP-stimulated salt secretion in shark rectal gland to "loop" diuretics. *American Journal of Physiology.* **246,** C242-C246.

Palfrey, H.C. and Rao, M.C. (1983) Na/K/Cl Co-Transport and its Regulation. *The Journal of Experimental Biology.* **106,** 43-54.

Palfrey, H.C., Feit, P.W. and Greengard, P. (1980) cAMP-stimulated cation cotransport in avian erythrocytes: inhibition by "loop" diuretics. *American Journal of Physiology.* **238,** C139-C148.

Park, J.H. and Saier, M.H. Jr. (1996) Phylogenetic, structural and functional characteristics of the Na-K-Cl cotransporter family. *The Journal of Membrane Biology.* **149,** 161-168.

Park, J-S., Han, K-Y., Song, J-A., Ahn, K-Y., Seo, H-S. and Lee, J. (2007a) *Eschericia coli* malate dehydrogenase, a novel solubility enhancer for heterologous proteins synthesized in *Eschericia coli. Biotechnology Letters.* **29,** 1513-1518.

Park, S.Y., Yu, X., Ip, C., Mohler, J.L., Bogner, P.N. and Park, Y.M. (2007b) Peroxiredoxin 1 interacts with androgen receptor and enhances its transactivation. *Cancer Research.* **67,** 9294-303.

Parvin, M.N., Gerelsaikhan, T. and Turner, R.J. (2007) Regions in the cytosolic C-terminus of the secretory Na^+-K^+-$2Cl^-$ cotransporter NKCC1 are required for its homodimerization. *Biochemistry.* **46,** 9630-9637.

Pasquali, C., Fialka, I. and Huber, L.A. (1997) Preparative two-dimensional gel electrophoresis of membrane proteins. *Electrophoresis.* **18,** 2573-2581.

Payne, J.A., Rivera, C., Voipio, J. and Kaila, K. (2003) Cation-chloride co-transporters in neuronal communication, development and trauma. *Trends in Neurosciences.* **26,**199-206.

Payne, J.A., and Forbush, B., III. (1995) Molecular characterization of the epithelial Na-K-Cl cotransporter isoforms. *Current Opinion in Cell Biology.* **7,** 493-503.

Payne, J.A. and Forbush, B., III. (1994) Alternatively spliced isoforms of the putative renal Na-K-Cl cotransporter are differentially distributed within the rabbit kidney. *Proceedings of the National Academy of Science of the United States of America.* **91,** 4544-4548.

Pendino, J.C., Nannini, L.J., Chapman, K.R., Slutsky, A. and Molfino, N.A. (1998) Effect of inhaled furosemide in acute asthma. *The Journal of Asthma.* **35,** 89-93.

Percoll®: Methodology and Application. (1981) Pharmacia Fine Chemicals AB. Upsala, Sweden

Pewitt, E.B., Hedge, R.S., Haas, M. and Palfrey, H.C. (1990) The regulation of Na/K/2Cl cotransport and bumetanide binding in avian erythrocytes by protein phosphorylation and dephosphorylation. *The Journal of Biological Chemistry.* **265,** 20747-20756.

Pewitt, E.B., Hedge, R.S., Haas, M., and Palfrey, H.C. (1990) The regulation of Na/K/2Cl cotransport and bumetanide binding in avian erythrocytes by protein phosphorylation and dephosphorylation: effects of kinase inhibitors and okadaic acid. *The Journal of Biological Chemistry.* **265,** 20747-20756.

Piechotta, K., Garbarini, N., England, R. and Delpire, E. (2003) Characterization of the interaction of the stress kinase SPAK with the Na^+-K^+-$2Cl^-$ cotransporter in the nervous system. Evidence for a scaffolding role of the kinase. *The Journal of Biological Chemistry.* **278,** 52848-52856.

Piechotta, K., Lu, J. and Delpire, E. (2002) Cation chloride cotransporters interact with the stress-related kinases Ste20-related proline-alanine-rich kinase (SPAK) and oxidative stress response 1 (OSR1). *The Journal of Biological Chemistry.* **277,** 50812-50819.

Plata, C., Meade, P., Vázquez, N., Hebert, S.C. and Gamba, G. (2002) Functional properties of the apical Na^+-K^+-$2Cl^-$ cotransporter isoforms. *The Journal of Biological Chemistry.* **277,** 11004-11012.

Plata, C., Meade, P., Hall, A.E., Welch, R.C., Vázquez, N., Hebert, S.C. and Gamba, G. (2001) Alternatively spliced isoform of the apical Na-K-Cl cotransporter gene encodes a furosemide sensitive Na-Cl cotransporter. *American Journal of Physiology.* **280,** F574-F582.

Plata, C., Mount, D.B., Baekgaard, Rubio, V., Hebert, S.C. and Gamba, G. (1999) Isoforms of the Na-K-2Cl cotransporter in murine TAL II. Functional characterization and activation by cAMP. *American Journal of Physiology.* **276,** F359-F366.

Pond, B.B., Berglund, K., Kuner, T., Feng, G., Augustine, G.J., and Schwartz-Bloom, R.D. (2006) The Chloride Transporter Na_-K_-Cl_ Cotransporter Isoform-1 Contributes to Intracellular Chloride Increases after *In Vitro* Ischemia. *The Journal of Neuroscience.* **26,** 1396 –1406.

Praetorius, J. and Nielsen, S. (2006) Distribution of sodium transporters and aquaporin-1 in the human choroid plexus. *American Journal of Physiology.* **291,** C59-C67.

Puig, O., Caspary, F., Rigaut, G., Rutz, B., Bouveret, E., Bragado-Nilsson, E., Wilm, M. and Séraphin, B. (2001) The tandem affinity purification (TAP) method: a general procedure of protein complex purification. *Methods.* **24,** 218-229.

Rabilloud, T., Blisnick, T., Heller, M., Luche, S., Aebersold, R., Lunardi, J. and Braun-Breton. C. (1999) Analysis of membrane proteins by two-dimensional electrophoresis: comparison of the proteins extracted from normal or Plasmodium falciparum-infected erythrocyte ghosts. *Electrophoresis.* **20,** 3603-3610.

Rabilloud, T. (1998) Use of thiourea to increase the solubility of membrane proteins in two-dimensional electrophoresis. *Electrophoresis.* **19,** 758-760.

Rais, I., Karas, M. and Schägger, H. (2004) Two-dimensional electrophoresis for the isolation of integral membrane proteins and mass spectrometric identification. *Proteomics.* **4,** 2567-2571.

Randall, J., Thorne, T. and Delpire, E. (1997) Partial cloning and characterization of *Slc12a2*: the gene encoding the secretory Na^+-K^+-$2Cl^-$ cotransporter. *American Journal of Physiology.* **273,** C1267-C1277.

Rapoport, S.M. (2000) The Reticulocyte. CRC Press, Inc. Florida.

Resjö, S., Oknianska, A., Zolnierowicz, S., Manganiello, V. and Degerman E. (1999) Phosphorylation and activation of phosphodiesterase type 3B (PDE3B) in adipocytes in response to serine/threonine phosphatase inhibitors: deactivation of PDE3B in vitro by protein phosphatase type 2A. *Biochemical Journal.* **341,** 839-845.

Rhee, S.G., Chae, H.Z. and Kim, K. (2005) Peroxiredoxins: a historical overview and speculative preview of novel mechanisms and emerging concepts in cell signaling. *Free Radical Biology and Medicine.* **38,** 1543-1452.

Ribeil, J-A., Zermati, Y., Vandekerckhove, J., Cathelin, S., Kersual, J., Dussiot, M., Coulon, S., Moura, I.C., Zeuner, A., Kirkegaard-Sørensen, T., Varet, B., Solary, E., Garrido, C. and Hermine, O. (2007) Hsp70 regulates erythropoiesis by preventing caspase-3-mediated cleavage of GATA-1. *Nature.* 445, 102-105.

Righetti, M., Cusi, D., Stella, P., Rivera, R., Bernardi, L., del Vecchio, L. and Bianchi, G. (1995) Na+, K+, Cl- cotransport is a marker of distal tubular function in essential hypertension. *Journal of Hypertension.* **13,** 1775-1778.

Rindler, M.J., McRoberts, J.A. and Saier, M.H., Jr. (1982) (Na^+, K^+)-cotransport in the Madin-Darby Canine Kidney Cell Line. *The Journal of Biological Chemistry.* **257,** 2254-2259.

Rinehart, J., Kahle, K.T., de Los Heros, P., Vázquez, N., Meade, P., Wilson, F.H., Hebert, S.C., Giménez, I., Gamba, G. and Lifton, R.P. (2005) WNK3 kinase is a positive regulator of NKCC2 and NCC, renal cation-Cl- cotransporters required for normal blood pressure homeostasis. *Proceedings of the National Academy of Sciences of the United States of America.* **102,** 16777-16782.

Russell, J.M. (2000) Sodium-Potassium-Chloride Cotransport. *Physiological Reviews.* **80,** 211-276.

Russell, J.M. (1979) Chloride and Sodium Influx: a Coupled Uptake Mechanism in the Squid Giant Axon. *The Journal of General Physiology.* **73,** 801-818.

Russell, J.M. (1976) ATP-dependent chloride influx into internally dialyzed squid giant axons. *Journal of Membrane Biology.* **28,** 335-349.

Santoni, V., Molloy, M. and Rabilloud, T. (2000) Membrane proteins and proteomics: Un amour impossible? *Electrophoresis.* **21,** 1054-1070.

Schomberg, S.L., Bauer, J., Kintner, D.B., Su, G., Flemmer, A., Forbush, B. and Sun, D. (2003) Cross talk between the GABA(A) receptor and the Na-K-Cl cotransporter is mediated by intracellular Cl^-. *Journal of Neurophysiology.* **89,** 159-67.

Schägger, H. and von Jagow, G. (1991) Blue native electrophoresis for isolation of membrane protein complexes in enzymatically active form. *Analytical Biochemistry.* **199,** 223-31.

Schambelan, M., Sebastian, A. and Rector, F.C., Jr. (1981) Mineralocorticoid-resistant renal hyperkalemia without salt wasting (type II pseudohypoaldosteronism): role of increased renal chloride reabsorption. *Kidney International.* **19,** 716–727.

Shaw, M.M. and Riederer, B.M. (2003) Sample preparation for two-dimensional gel electrophoresis. *Proteomics.* **3,** 1408-1417.

Simard, C.F., Bergeron, M.J., Frenett-Cotton, R., Carpentier, G.A., Pelchat, M-E., Caron, L. and Isenring, P. (2007) Homooligomeric and heterooligomeric associations between K^+-Cl^- cotransporter isoforms and between K^+-Cl^- and Na^+-K^+-Cl^- cotransporters. *The Journal of Biological Chemistry.* **282,** 18083-18093.

Simard, C.F., Brunet, G.M., Daigle, N.D., Montminy, V., Caron, L. and Isenring, P. (2004a) Self-interacting domains in the C terminus o f a cation-Cl^- cotransporter described for the first time. *The Journal of Biological Chemistry.* **279,** 40769-40777.

Simard, C.F., Daigle, N.D., Bergeron, M.J., Brunet, G.M., Caron, L., Noël, M., Montminy, V. & Isenring, P. (2004b) Characterization of a novel interaction between the secretory Na^+-K^+-Cl^- cotransporter and the chaperone hsp90. *The Journal of Biological Chemistry.* **279,** 48449-48456

Simon, D.B., Karet, F.E., Hamdan, J.M., DiPietro, A., Sanjad, S.A. and Lifton, R.P. (1996) Bartter's syndrome, hypokalaemic alkalosis with hypercalciuria, is caused by mutations in the Na-K-2Cl cotransporter NKCC2. *Nature Genetics.* **13,** 183-188.

Smith, J.B. and Smith, L. (1987) Na+/K+/Cl- cotransport in cultured vascular smooth muscle cells: stimulation by angiotensin II and calcium ionophores, inhibition by cyclic AMP and calmodulin antagonists. *The Journal of Membrane Biology.* **99,** 51-63.

Stengelin, M.K. and Hoffman, J.F. (1997) Na,K-ATPase subunit isoforms in human reticulocytes: Evidence from reverse transcription-PCR for the presence of α1, α3, β2, β3, and γ. *Proceedings of the National Academy of Sciences of the United States of America.* **94,** 5943-5948.

Stiefel, P., García-Morillo, S., Miranda, M.L., García-Donas, M.A., Pamies, E., Villar, J. and Carneado, J. (2000) Gordon's syndrome: increased maximal rate of the Na-K-Cl cotransport and erythrocyte membrane replacement of sphingomyelin by phosphatidylethanolamine. *Journal of Hypertension.* **18,** 1327-1330.

Stuhlmeier, K.M., Kao, J.J., Wallbrandt, P., Lindberg, M., Hammarström, B., Broell, H. and Paigen, B. (2003) Antioxidant protein 2 prevents methemoglobin formation in erythrocyte hemolysates. *FEBS- European Journal of Biochemistry.* **270**, 334-341.

Sun, A., Grossman, E.B., Lombardi, M. and Hebert, S.C. (1991) Vasopressin alters the mechanism of apical Cl^- entry from Na^+:Cl^- to Na^+:K^+:$2Cl^-$ cotransport in mouse medullary thick ascending limb. *Journal of Membrane Biology.* **120,** 83-94.

Sung, K.W., Kirby, M., McDonald, M.P., Lovinger, D.M. and Delpire, E. (2000) Abnormal GABAa receptor-mediated currents in dorsal root ganglion neurons isolated from Na-K-2Cl cotransporter null mice. *Journal of Neuroscience.* **20,** 7531–7538.

Takahashi, N., Chernavvsky, D.R., Gomez, R.A., Igarashi, P., Gitelman, H.J. and Smithies, O. (2000) Uncompensated polyuria in a mouse model of Bartter's syndrome. *Proceedings of the National Academy of Sciences of the United States of America.* **97,** 5434-5439.

Tanimura, A., Kurihara, K., Reshkin, S.J. and Turner, R.J. (1995) Involvement of direct phosphorylation in the regulation of the rat parotid Na(+)-K(+)-2Cl-cotransporter. *The Journal of Biological Chemistry.* **270,** 25252-25258.

Tibbles, A. and Woodgett, J.R. (1999) The stress-activated protein kinase pathways. *Cellular and Molecular Life Sciences.* **55,** 1230-1254.

Tomer, K.B. (2001) Separations combined with mass spectrometry. *Chemical Reviews.* **101,** 297-328.

Topper, J.N., Wasserman, S.M., Anderson, K.R., Cai, J., Falb, D. and Gimbrone, M.A., Jr. (1997) Expression of the bumetanide-sensitive Na-K-Cl cotransporter BSC2 is differentially regulated by fluid mechanical and inflammatory cytokine stimuli in vascular endothelium.*The Journal of Clinical Investigation.* **99,** 2941-2949.

Torchia, J., Lytle, C., Pon, D.J., Forbush, B., III. And Sen, A.K. (1992) The Na-K-Cl cotransporter of avian salt gland. Phosphorylation in response to cAMP-dependent and calcium-dependent secretogogues. *The Journal of Biological Chemistry.* **267,** 25444-25450.

Turner, J.T., Franklin, C.C., Bollinger, D.W. and Kim, H.D. (1990) Vasoactive intestinal peptide stimulates active K+ transport and Na(+)-K(+)-Cl- cotransport in HT-29 cells. *American Journal of Physiology.* **258,** C266-C273.

Unwin, R.J. and Capasso, G. (2006) Bartter's and Gitelman's syndromes: their relationship to the actions of loop and thiazide diuretics. *Current Opinion in Pharmacology.* **6,** 208–213.

Ushiro, H., Tsutsumi, T., Suzuki, K., Kayahara, T. and Nakano, K. (1998) Molecular cloning and characterization of a novel Ste20-related protein kinase enriched in neurons and transporting epithelia. *Archives of Biochemistry and Biophysics.* **355,** 233-240.

Vasilescu, J., Guo, X. and Kast, J. (2004) Identification of protein-protein interactions using *in vivo* cross-linking and mass spectrometry. *Proteomics.* **4,** 3845-3854.

Veríssimo, F. and Jordan, P. (2001) WNK kinases, a novel protein kinase subfamily in multi-cellular organisms. *Oncogene*. **20,** 5562-5569.

Vibat, C.R.T., Holland, M.J., Kang, J.J., Putney, L.K. and O'Donnell, M.E. (2001) Quantitation of Na^+-K^+-$2Cl^-$ cotransport splice variants in human tissues using kinetic polymerase chain reaction. *Analytical Biochemistry.* **298,** 218-230.

Villa, F., Goebel, J., Rafiqi, F.H., Deak, M., Thastrup, J., Alessi, D.R. and van Aalten, D.M.F. (2007) Structural insights into the recognition of substrates and activators by the OSR1 kinase. *EMBO Reports.* **8,** 839-845.

Vitari, A.C., Thastrup, J., Rafiqi, F.H., Deak, M., Morrice, N.A., Karlsson, H.K. and Alessi, D.R. (2006) Functional interactions of the SPAK/OSR1 kinases with their upstream activator WNK1 and downstream substrate NKCC1. *Biochemical Journal.* **397,** 223-231.

Vitari, A.C., Deak, M., Morrice, N.A. and Alessi, D.R. (2005) The WNK1 and WNK4 protein kinases that are mutated in Gordon's hypertension syndrome

phosphorylate and activate SPAK and OSR1 protein kinases. *Biochemical Journal.* **391,** 17-24.

Wang, D.N. (1994) Band 3 protein: structure, flexibility and function. *FEBS Letters.* **346,** 26-31.

Wilson, F.H., Disse-Nicodème, S., Choate, K.A., Ishikawa, K., Nelson-Williams, C., Desitter, I., Gunel, M., Milford, D.V., Lipkin, G.W., Achard, J-M., Feely, M.P., Dussol, B., Berland, Y., Unwin, R.J., Mayan, H., Simon, D.B., Farfel, Z., Jeunemaitre, X. and Lifton, R.P. (2001) Human hypertension caused by mutations in WNK kinases. *Science.* **293,** 1107-1112.

Wong, J.A., Gosmanov, A.R., Schneider, E.G. and Thomason, D.B. (2001) Insulin-independent, MAPK-dependent stimulation of NKCC activity in skeletal muscle *American Journal of Physiology.* **281,** R561-R571.

Wood, P.G. (1987) Preparation of white resealable erythrocyte ghosts. *Methods in Enzymology.* **149**, 271-280.

Wu, Q., Delpire, E., Hebert, S.C. and Strange, K. (1998) Functional demonstration of Na^+-K^+-$2Cl^-$ cotransporter activity in isolated, polarized choroid plexus cells. *American Journal of Physiology.* **275,** C1565-C1572.

Xie, J., Craig, L., Cobb, M.H. and Huang, C.L. (2006) Role of with-no-lysine [K] kinases in the pathogenesis of Gordon's syndrome. *Pediatric Nephrology.* **21,** 1231-1236.

Xu, B-e., English, J.M., Wilsbacher, J.L., Stippee, S., Goldsmith, E.J. and Cobb, M.H. (2000) WNK1, a novel mammalian serine/threonine protein kinase lacking the catalytic lysine in subdomain II. *The Journal of Biological Chemistry.* **275,** 16795-16801.

Xu, J.-C., Lytle, C., Zhu, T.T., Payne, J.A., Benz, E., Jr., and Forbush, B., III. (1994) Molecular cloning and functional expression of the bumetanide-sensitive Na-K-Cl cotransporter. *Proceedings of the National Academy of Science of the United States of America.* **91,** 2201-2205.

Yang, S.S., Morimoto, T., Rai, T., Chiga, M., Sohara, E., Ohno, M., Uchida, K., Lin, S.H., Moriguchi, T., Shibuya, H., Kondo, Y., Sasaki, S. and Uchida, S. (2007) Molecular pathogenesis of pseudohypoaldosteronism type II: generation and analysis of a Wnk4(D561A/+) knockin mouse model. *Cell Metabolism.* **5,** 331-344.

Yang, T., Huang, Y.G., Singh, I., Schnermann, J. and Briggs, J.P. (1996) Localization of bumetanide- and thiazide-sensitive Na-K-Cl cotransporters along the rat nephron. *American Journal of Physiology.* **271,** F931-F939.

Zagórska, A., Pozo-Guisado, E., Boudeau, J., Vitari, A.C., Rafiqi, F.H., Thastrup, J., Deak, M., Campbell, D.G., Morrice, N.A., Prescott, A.R. and Alessi, D.R. (2007) Regulation of activity and localization of the WNK1 protein kinase by hyperosmotic stress. *Journal of Cell Biology.* **176,** 89-100.

Zahedi, R-P., Meisinger, C. and Sickmann, A. (2005) Two-dimensional benzyl-*n*-hexadecylammonium chloride/SDS-PAGE for membrane proteomics. *Proteomics.* **5,** 3581-3588.

Zhang, D., Kiyatkin, A., Bolin, J.T. and Low, P.S. (2000) Crystallographic structure and functional interpretation of the cytoplasmic domain of erythrocyte membrane band 3. *Blood.* **96,** 2925-2933.

Zhao, H., Hyde, R. and Hundal, H.S. (2004) Signalling mechanisms underlying the rapid and additive stimulation of NKCC activity by insulin and hypertonicity in rat L6 skeletal muscle cells. *The Journal of Physiology.* **560,** 123-136.

Appendices

Appendix I - Supplementary Data

Examples of Mascot Ion Searches

The following tables show data from the Mascot ion searches for LC-MSMS data from both Native-PAGE complexes and N1 immunoprecipitation experiments. The native-PAGE complexes (numbered 1-5) refer to those observed commonly on gels, as shown in figure 3.17.

Protein Identification	Mascot Score	Peptides Matched
Band 3	106	4
Ankyrin	47 but confirmed with Phenyx	2
Alpha haemoglobin	106	4
Beta haemoglobin	99	4
Gamma haemoglobin	70	3

Table A.1 - LC-MSMS Mascot Ion Search for Native-PAGE Complex 1
Scores greater than 52 indicate identity

Protein Identification	Mascot Score	Peptides Matched
Alpha haemoglobin	228	10
Beta haemoglobin	283	11
Gamma haemoglobin	101	4
Epsilon haemoglobin	89	6

Table A.2 - LC-MSMS Mascot Ion Search for Native-PAGE Complex 2
Scores greater than 52 indicate identity

Protein Identification	Mascot Score	Peptides Matched
Band 3	102	3
TER ATPase	269	10
Alpha haemoglobin	227	14
Beta haemoglobin	293	10
Gamma haemoglobin	113	4
Epsilon haemoglobin	77	3
Glucose transporter	54	2

Table A.3 - LC-MSMS Mascot Ion Search for Native-PAGE Complex 3
Scores greater than 52 indicate identity

Protein Identification	Mascot Score	Peptides Matched
Band 3	191	13
Alpha haemoglobin	278	17
Beta haemoglobin	309	14
Gamma haemoglobin	89	5
Epsilon haemoglobin	82	5

Table A.4 - LC-MSMS Mascot Ion Search for Native-PAGE Complex 4
Scores of 52 or more indicate identity.

Protein Identification	Mascot Score	Peptides Matched
Alpha haemoglobin	328	16
Beta haemoglobin	381	15
Gamma haemoglobin	122	5

Table A.5 - LC-MSMS Mascot Ion Search for Native-PAGE Complex 5
Scores of 52 or more indicate identity.

Protein Identification	Mascot Score	Peptides Matched
Malate dehydrogenase	88	4
Heat Shock Protein 70	46	3
Band 3	33	1

Table A.6 - LC-MSMS Mascot Ion Search for N1 Immunoprecipitated Proteins
Scores of 42 or more indicate identity. Where only one peptide is matched, scores are lower. Keratin contamination of these samples was evident with scores of 191.

Appendix II - NKCC1 and NKCC2 cDNA Sequences

NKCC1

951
>>>>>
GAAGAAAGTACTCCAACCAGAGATGCTGTGGTCACGTATACTGCAGAAAGTAAAGGA
GTCGTGAAGTTTGGCTGGATCAAGGGTGTATTA][GTACGTTGTATGTTAAACATTTGG
GGTGTGATGCTTTTCATTAGATTGTCATGGATTGTGGGTCAAGCTGGAATAG][GTCTA
TCAGTCCTTGTAATAATGATGGCCACTGTTGTGACAACTATCACAGGATTGTCTACTTC
AGCAATA
<<<<<
1187

NKCC2

605
>>>>>
CTCTTCATTCGCCTCTCCTGGATTGTAGGAGAAGCGGGAATTG][GTCTTGGAGTTCTT
ATAATTCTTCTTTCCACCATGGTAACCTCTATCACTGGGTTGTCAACTTCTGCAATAGC
AACAAACGGGTTTGTTCGTGGAGGTGGAGCCTACTACCTGATTTCCCGGAGCTTAGG
GCCTGAGTTCGGTGGGTCAATAGGCTTGATCTTTGCTTTTGCCAATGCAGTGGCTGTC
GCTATGTATGTGGTGGGATTCGCGGAGACTGTCGTGGATCTTCTTAAG][GAGAGCGA
TTCAATGATGGTGGATCCAACCAATGACATCCGCATCATCGGTTCCATCACCGTGGTG
ATTCTTCTAGGAATCTCAGTAGCTGGGATGGAGTGGGAAGCAAAG][GCTCAAGTCAT
TCTCCTGGTCATTCTTCTCATTGCCATTGCAAACTTCTTCATTGGAACTGTCAT
<<<<<
1059

][= exon-exon boundary

>>>>> = forward primer with base number where primer starts in cDNA sequence

<<<<< = reverse primer with base number where primer ends in cDNA sequence

The exon-exon boundaries were identified using the Human Blat Search Genome function (http://genome.ucsc.edu/cgi-bin/hgBlat) after input of the amplified region and examining where this is found within the genomic DNA sequence.

Appendix III - Publications

Available online at www.sciencedirect.com

SCIENCE DIRECT

Biochimica et Biophysica Acta 1714 (2005) 25 – 34

BIOCHIMICA ET BIOPHYSICA ACTA
BBA

http://www.elsevier.com/locate/bba

Regulation of erythrocyte Na–K–2Cl cotransport by threonine phosphorylation

Ioulia Matskevich, Karen L. Hegney, Peter W. Flatman*

Membrane Biology Group, College of Medicine and Veterinary Medicine, School of Biomedical and Clinical Laboratory Sciences, The University of Edinburgh, Hugh Robson Building, George Square, Edinburgh EH8 9XD, Scotland, UK

Received 15 November 2004; received in revised form 12 May 2005; accepted 6 June 2005
Available online 22 June 2005

Abstract

A method is described to measure threonine phosphorylation of the Na–K–2Cl cotransporter in ferret erythrocytes using readily available antibodies. We show that most, if not all, cotransporter in these cells is NKCC1, and this was immunoprecipitated with T4. Cotransport rate, measured as ^{86}Rb influx, correlates well with threonine phosphorylation of T4-immunoprecipitated protein. The cotransporter effects large fluxes and is significantly phosphorylated in cells under control conditions. Transport and phosphorylation increase 2.5- to 3-fold when cells are treated with calyculin A or Na^+ arsenite. Both fall to 60% control when cell [Mg^{2+}] is reduced below micromolar or when cells are treated with the kinase inhibitors, 4-amino-5-(4-methylphenyl)-7-(*t*-butyl)pyrazolo[3,4-d]pyrimidine or staurosporine. Importantly, these latter interventions do not abolish either phosphorylation or transport suggesting that a phosphorylated form of the cotransporter is responsible for residual fluxes. Our experiments suggest protein phosphatase 1 (PrP-1) is extremely active in these cells and dephosphorylates key regulatory threonine residues on the cotransporter. Examination of the effects of kinase inhibition after cells have been treated with high concentrations of calyculin indicates that residual PrP-1 activity is capable of rapidly dephosphorylating the cotransporter. Experiments on cotransporter precipitation with microcystin sepharose suggest that PrP-1 binds to a phosphorylated form of the cotransporter.

Keywords: Sodium-potassium-chloride symporters; Erythrocytes; Threonine phosphorylation; Protein phosphatase 1; Calyculin A; Arsenite; PP1

1. Introduction

Na–K–2Cl cotransporters play key roles in regulating cell K^+ and Cl^- content and cell volume. In epithelia they enable transepithelial fluxes by providing entry routes for Na^+ and Cl^-, whereas in erythrocytes they are mainly involved in regulating cell, and perhaps, plasma K^+ concentration [1–5]. Their activity is regulated by a variety of stimuli including cell volume, hypoxia, hormones, growth factors and cell Cl^- concentration [1,2]. The ability of the transporter to respond to these signals is prevented by treating cells with inhibitors of protein kinases or phosphatases suggesting that changes in protein phosphorylation are involved in the signal transduction pathway [6–8]. It is now clear that phosphorylation of the cotransporter itself is a major determinant of transport rate [9–14]. Initial studies using ^{32}P indicated that 5 or 6 threonine and serine (but not tyrosine) residues are phosphorylated when the transporter is maximally activated [9,15]. More recent work has focused on the phosphorylation of three threonine residues (^{184}Thr, ^{189}Thr and ^{202}Thr) in the N-terminus of the shark cotransporter that are particularly important in regulating transport in response to changes in cell volume and Cl^- [14]. These three residues are well conserved in the cotransporter from a wide variety of animal species so their phosphorylation is likely to be a common theme in cotransporter regulation, with phosphorylation of ^{189}Thr (or its equivalent) being the main determinant of activity, and phosphorylation of ^{184}Thr and ^{202}Thr modulating the response [14].

Studies using inhibitors of protein phosphatase 1 (PrP-1) suggest that this plays a major role in dephosphorylating and thus inactivating the cotransporter, and the recent demon-

* Corresponding author. Tel.: +44 131 650 3254; fax: +44 131 650 6527.
E-mail address: peter.flatman@ed.ac.uk (P.W. Flatman).

0005-2736/$ - see front matter © 2005 Elsevier B.V. All rights reserved.
doi:10.1016/j.bbamem.2005.06.001

stration that PrP-1 can bind to a motif on the cotransporter close to the key threonine residues in the N-terminus reinforces this idea [16]. However, the identity of the kinase, or kinases, that phosphorylate the cotransporter remains elusive [17–19].

Using ferret erythrocytes, a robust model for studying the properties of the mammalian cotransporter, we have explored the effects of inhibitors of kinases and phosphatases on transport [20,21]. Although the results indicate that transport is stimulated by phosphorylation, they are not consistent with the current view that cotransporter phosphorylation is regulated by a single kinase and phosphatase [15]. It seems more likely that the cotransporter is phosphorylated by several kinases and dephosphorylated by several phosphatases [3,5,22]. Transport is stimulated by calyculin A suggesting protein phosphatase 1 is one of the regulatory phosphatases [3,20]. It is also stimulated by Na^+ arsenite which is believed to activate a kinase [21]. However, treatment of cells in a variety of ways to inhibit protein kinases, including reduction of cell Mg^{2+} concentration to below 1 μM, inhibits only about 40% of the resting flux leaving a substantial residual flux [20]. This suggests that the cotransporter may exist in two forms, one that is constitutively active (it does not require to be phosphorylated) and one that is activated by phosphorylation in the conventional way, or, these procedures may trap the cotransporter in a partially phosphorylated, partially active state [3]. In order to resolve these issues and understand how cotransporter phosphorylation affects transport in ferret erythrocytes we describe a method that allows us to compare the extent to which the cotransporter is phosphorylated on threonine with transport rate under a variety of conditions. Some of these results have been published in abstract form [23,24].

2. Materials and methods

2.1. Solutions and chemicals

All solutions were prepared in double-glass distilled water with analytical grade reagents (BDH AnalaR, VWR International, Lutterworth, UK). Calyculin A, microcystin-LR and 4-amino-5-(4-methylphenyl)-7-(*t*-butyl)pyrazolo[3,4-d]pyrimidine (PP1) were obtained from Alexis Biochemicals (Carlsbad, CA). Protease inhibitor cocktail set III, A23187 and the detergents: ASB-16 (an amidosulfobetaine) and CHAPS were obtained from Calbiochem (VWR International). EDTA, EGTA, HEPES, dithiothreitol (DTT), Triton X-100, Tween 20, Na^+ orthovanadate, Na^+ β-glycerophosphate, glycine, genistein, staurosporine and Tris base were obtained from Sigma (Poole, UK). Na^+ (meta)-arsenite was from Fluka Chemicals, (Gillingham, UK). Protein G sepharose (Amersham Biosciences, Little Chalfont, UK) was washed 3 times before use. Microcystin-Sepharose was from Upstate (Charlottesville, VA), recombinant N-glycosidase F from Roche Diagnostics (Lewes, UK), and anti-NKCC1 from Alpha Diagnostics International (San Antonio, TX). Bumetanide was a gift from Leo Laboratories Ltd. (Aylesbury, UK).

Ferret basic medium (FBM) comprised (mM): 150 NaCl, 5 KCl, 0.05 EGTA, 10 HEPES, pH 7.5 at 38 °C, adjusted with NaOH. Lysis buffer contained (mM): 10 HEPES, 2 EDTA, 2 Na^+ pyrophosphate, 2 NaF, 1 Na^+ β-glycerophosphate, 1 Na^+ vanadate, pH 7.6 at room temperature. Na^+ vanadate was added from a 200 mM stock just prior to use. The stock was prepared by dissolving Na^+ vanadate in water, adjusting pH to 10 with HCl and then boiling until colourless and then readjusting the pH to 10 [25]. It was frozen until used. Immunoprecipitation buffer (IPB) contained (mM): 150 NaCl, 20 HEPES, 1 EDTA, 2 NaF, 1 Na^+ β-glycerophosphate, pH adjusted to 7.6 at room temperature with NaOH. Tris-buffered saline (TBS) contained (mM): 136 NaCl, 20 Tris base, pH 7.6 adjusted with HCl at room temperature.

2.2. Preparation of erythrocyte suspensions and flux measurements

Blood was taken by cardiac puncture from adult ferrets terminally anaesthetised with Na^+ pentobarbitone (Sagatal, Rhône Mérieux, Harlow, UK, 120 mg kg^{-1}) according to guidance from the British Home Office. Cells were washed four times by centrifugation and resuspension in FBM, care being taken to remove all of the buffy coat. They were stored at 5 °C in FBM containing 22 mM glucose until used (normally within 3 days). All plastics used to handle cells were sterile and all solutions were passed through a 0.2-μm filter before use.

Washed erythrocytes at about 7% hematocrit were incubated at 38 °C for the indicated times in FBM containing 11 mM glucose and the following additions: control (no additions, 20 min), 20–50 nM calyculin A (15 min), 50 μM PP1 (30 min), 2 μM staurosporine (20 min), 0.3 mM genistein (20 min), 1 mM Na^+ arsenite (60 min), 0.008–0.03% gluteraldehyde (5 min), and various combinations of these. Where necessary cell [Mg^{2+}] was reduced to sub micromolar levels by incubating the cells in FBM containing 2 mM EDTA and 10 μM A23187 for 15 min [26].

Cotransporter fluxes were determined by adding ^{86}Rb to aliquots of these suspensions and then measuring the uptake of ^{86}Rb, with and without 10 μM bumetanide, a specific cotransporter inhibitor, as described previously [20].

2.3. Preparation of erythrocyte membranes

Cells were spun out of solution, cooled on ice and then injected into 20 volumes of ice-cold lysis buffer containing 1% protease inhibitor cocktail, and stirred for 10 min on ice. Membranes were washed 3 times by centrifugation (25,000×*g* for 10 min) and resuspension in ice-cold lysis

buffer. Membrane protein concentrations were measured with Coomassie Plus protein assay reagent (Pierce Biotechnology, Rockford, IL) or 2-D Quant (Amersham Biosciences). Samples were stored in liquid nitrogen after adding 2% protease inhibitor cocktail.

Membranes were deglycosylated by incubating them with 1% SDS at 60 °C for 20 min. Samples were then diluted 5-fold into deglycosylation buffer (in mM: 150 NaCl, 20 HEPES, 1 EDTA) containing 1% Triton X-100, 1% CHAPS and 2% protease inhibitor cocktail. Recombinant N-glycosidase F (80–160 units/ml) was added and the tubes were incubated at 37 °C overnight. Inclusion of 2% mercaptoethanol had no effect on results. Membranes were dephosphorylated by treating them with alkaline phosphatase (Promega, Madison, WI) for 1 h at 37 °C.

2.4. Immunoprecipitation of the cotransporter

Cotransporter was immunoprecipitated with T4 (Developmental Studies Hybridoma Bank, University of Iowa), a monoclonal antibody to the C-terminal of the cotransporter [27]. This antibody recognises both NKCC1 and NKCC2 isoforms of the cotransporter in the SDS-denatured state. Membranes were therefore heated to 60 °C in the presence of 1% SDS for 20 min and were then diluted 5-fold with IPB with the following additions: 1 mM Na^+ vanadate, 2% protease inhibitor cocktail, 1 μM microcystin L-R, 1% Triton X-100 and 0.5% ASB-16. The mixture was incubated for 1 h at 4 °C followed by centrifugation at 14,000×*g* for 10 min to remove any precipitate. The supernatant was pre-cleared with protein G sepharose, T4 ascites fluid was added and the tube was incubated at 4 °C for 60 min. The immune complex was precipitated with protein G sepharose and washed 3 times with IPB containing 1% Triton X-100 and 0.5% ASB-16. Cotransporter was eluted by heating the beads to 70 °C for 20 min in ×4 NuPAGE LDS sample buffer (Invitrogen Corporation, Carlsbad, CA) containing 166 mM DTT. The supernatant, diluted 4-fold and with [DTT] made up to 100 mM, was subjected to SDS-PAGE.

2.5. Microcystin pull down assay

Membranes, solubilised in IPB containing 1 mM Na^+ vanadate, 0.5% ASB-16, 1% Triton X-100 and 2% protease inhibitors, were incubated with Microcystin-Sepharose for 1 h at 4 °C. The beads were washed 3 times with IPB containing 0.5% ASB 16 and 0.1% Triton X-100. Proteins were eluted from the beads as described above.

2.6. Gel electrophoresis and Western blotting

We used either 3–8% Tris–acetate or 4–12% bis-tris NuPAGE gels (Invitrogen). Gels were calibrated against Mark 12 and HiMark unstained molecular weight markers (Invitrogen) and a biotinylated protein ladder (Cell Signaling). Membranes and protein samples were heated to 70 °C for 10 min in LDS sample buffer (Invitrogen) containing 100 mM DTT then and centrifuged at 14,000×*g* for 1 min prior to electrophoresis. Protein bands were stained with GelCode Blue, a colloidal Coomassie stain (Pierce).

Proteins were blotted to nitrocellulose in an Xcell II run at 30V for 90 min using a transfer buffer (in mM: 25 bicine, 25 bis-tris, 1 EDTA) containing 0.1% SDS and 10% methanol (Invitrogen). Blots were blocked with TBS containing 0.1% Tween 20 and either 5% dried milk powder, or 5% filtered (0.2 μm) bovine serum albumin (fraction V, ICN Biomedical, Costa Mesa, CA) when phospho-specific antibodies were used. They were then incubated at 4 °C with primary antibodies diluted in blocking buffer, T4 1:5000 for 1 h or rabbit anti-phosphothreonine (Cell Signaling Technology, Beverly MA) 1:2000 overnight. After washing and re-blocking, the blots were treated with horseradish peroxidase-conjugated secondary antibodies (1:10,000, Jackson ImmunoResearch Laboratories, West Grove, PA). Antibody binding was quantified using ECL reagents and Hyperfilm (Amersham Biosciences). Gels and blots were scanned and the images analysed with TotalLab (Non Linear Dynamics, Newcastle, UK).

Most data are expressed as means with standard errors and the significance of differences between means is assessed with two-tailed *t*-tests, the exact value of *P* being stated. Rate constants are given with standard deviations. Lines through data are fitted to specific models using non-linear regression analysis (Prism 4.03, GraphPad Software, San Diego, CA). All experiments were repeated with the blood from at least 3 ferrets. Representative blots are shown.

3. Results

3.1. Measurement of threonine phosphorylation of the cotransporter

Our first aim was to establish a simple robust assay to measure threonine phosphorylation of the cotransporter in ferret erythrocytes using readily available antibodies. Cotransporter was immunoprecipitated with the monoclonal antibody T4 [27]. The immunoprecipitate was then separated into components by SDS-PAGE. The proteins were blotted to nitrocellulose, care being taken to ensure that sufficient time was given for the complete transfer of large proteins, and the presence of phosphorylated threonine residues in the protein bands was detected with an anti-phosphothreonine antibody (Fig. 1). A prominent band covering molecular weights ranging from 140 to 160 kDa was observed in all samples, precisely the place where we would expect to find the cotransporter if its monomeric glycosylated molecular weight is about 150 kDa (see later). The relative intensity of this band depended on how the cells had been treated prior to the preparation of membranes. Treatments that activated cotransport, for instance, incuba-

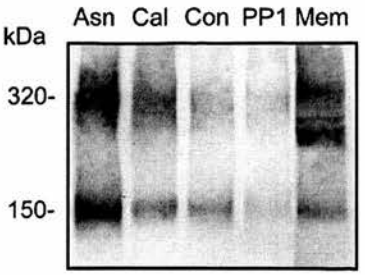

Fig. 1. Threonine phosphorylation of T4 immunoprecipitates. T4 immunoprecipitates were prepared from the membranes of ferret erythrocytes that had been incubated at 38 °C in FBM containing 11 mM glucose and the following additions: none for 30 min (Con), 50 μM PP1 for 30 min (PP1), 20 nM Calyculin A for 15 min (Cal) and 1 mM Na^+ arsenite for 60 min (Asn). Immunoprecipitates were run on a 3–8% Tris-acetate gel together with a sample of control membranes (Mem). The gel was blotted and probed with an antibody to phosphothreonine.

tion with calyculin A or Na^+ arsenite, increased the intensity compared to controls, whereas treatment with PP1, decreased the intensity (Fig. 1). This is consistent with the idea that calyculin or arsenite activate the cotransporter by causing its phosphorylation, whereas PP1 inhibits by reducing its phosphorylation. Usually a second band, covering the range 300–320 kDa (Fig. 1), was also seen in each lane. In some cases, the intensity of this band was similar to the low molecular weight band, though in most it was much lower, and it appeared to depend to some extent on how membrane samples were treated prior to electrophoresis (see later). Some faint bands at intermediate weights were also sometimes visible. Shown on the same blot (Fig. 1) is an example of a membrane sample, separated by SDS-PAGE, and probed with the anti-phosphothreonine antibody. Prominent bands were usually observed at 150, 250, 270 and 300 kDa.

In order to interpret these phosphorylation patterns, we need to know the identity of the proteins immunoprecipitated by T4 and the molecular weights of cotransporter forms found in the membrane or sample buffer.

3.2. Molecular weight of cotransporter complexes

In Western blots of ferret erythrocyte membranes the cotransporter is detected by a variety of cotransporter antibodies as a smear at 140–160 kDa together with high molecular weight complexes, comprising a prominent smear at about 300 kDa and often bands at 400–500 kDa (Fig. 2A). In addition, much sharper bands were seen at about 250 and 270 kDa (Fig. 2A). A similar pattern of bands is seen when T4-immunoprecipitates prepared from erythrocytes are run on SDS gels (Fig. 2B). There are prominent broad bands centred at 150 and 300 kDa, but the bands at 250 and 270 kDa are less conspicuous.

All high molecular weight species were seen despite heating the samples with SDS and reducing agents such as 100 mM DTT or 5 mM tris[2-carboxyethyl]phosphine (TCEP) prior to running gels. The proportion of T4 staining found at high molecular weights increased slowly with the length of time cells were stored (4 °C) before the preparation of membranes, and with the time that membranes were stored frozen (−20 °C) before electrophoresis (data not shown). A possible explanation for the bands at 300 and 500 kDa is that the cotransporter forms homodimers and trimers but we cannot rule out the possibility that it binds to other proteins, and the bands at 250 and 270 kDa may provide evidence for just such interactions. Importantly, SDS-resistant high molecular weight forms of the cotransporter assemble during storage, even in the cold. Variations were minimised by preparing membranes from cells within 3 days of blood collection, and by storing membranes in liquid nitrogen. Despite these precautions, bands at 250, 270 and 300 kDa could be detected even in the freshest samples, suggesting that these forms may normally be present in the membrane under physiological conditions. However, because some of these complexes form during storage or in sample buffer, it is difficult to assess the extent to which the cotransporter exists in these forms in the membrane. To address this issue, we treated cells with low concentrations of gluteraldehyde (0.008–0.03%) to cross-link proteins prior to preparation of membranes. The procedure, which has been used to fix erythrocyte ion transporters in their active or inactive states [28], greatly increased the proportion of transporter found in the 300-kDa form (Fig. 2C), supporting the idea that many cotransporter molecules in erythrocyte membranes are found in dimers, or bound to other proteins.

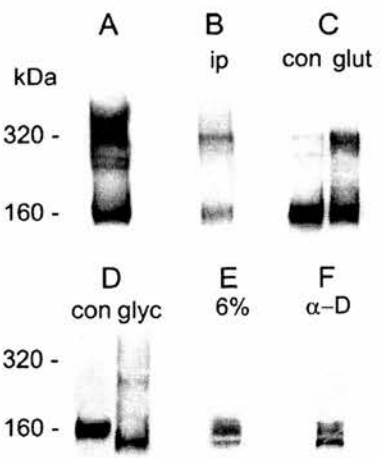

Fig. 2. Cotransporter bands in blots of erythrocyte membranes and T4-immunoprecipitates. Samples were run on: 3–8% Tris-acetate gels (A–D), 6% (E) or 9% (F) tris-glycine gels and probed with T4 (A–E) or an NKCC1-specific antibody from Alpha Diagnostics International (F). A: control membranes showing all the major cotransporter bands seen commonly, B: T4-immunoprecipitate prepared from control membranes. C: con—control membranes, glut—membranes from cells treated with 0.008% gluteraldehyde for 5 min, D: con—control membranes, glyc—membranes treated overnight at 37 °C with N-glycosidase F, E and F: cotransporter seen as clear doublets in control membranes.

The appearance of the cotransporter as a broad, smeared band has been reported for other cell types and species. This smearing is usually attributed to variable N-linked glycosylation of sites in the large extracellular loop of the cotransporter [27,29]. We examined this possibility by treating ferret erythrocyte membranes overnight with recombinant N-glycosidase F. Following treatment the apparent mean molecular weight of the transporter fell by about 25 kDa to 124±1 (n=4) kDa, close to the expected weight of the cotransporter based on its sequence. Unexpectedly, the band remained very smeared (Fig. 2D). Doubling the amount of glycanase did not cause any further change in molecular weight and nor did dephosphorylating the cotransporter with alkaline phosphatase (data not shown). Thus, variable glycosylation or phosphorylation does not explain the wide range of molecular weights the transporter displays. Densitometer scans of the 150-kDa band often showed two peaks suggesting that the band may comprise two components, an idea supported by the finding that it occasionally appeared as a distinct doublet with weights centred on 140 and 160 kDa (e.g. Fig. 2E and F). Doublets have also been observed in T4-immunoprecipitates from endothelial cells [30] and membranes from rat parotid gland [31]. In the latter case, the 140-kDa band was attributed to an unphosphorylated, immature form found in intracellular compartments. Such compartments do not exist in ferret erythrocytes, and the 140-kDa form resides in the plasma membrane like the 160-kDa form. In addition, dephosphorylation (with alkaline phosphatase) made no difference to the apparent molecular weight of the transporter in our studies (data not shown).

T4 interacts with both the NKCC1 and NKCC2 isoforms of the cotransporter [27] which have slightly different molecular weights [2], so a plausible explanation for the doublet at 140–160 kDa is that ferret erythrocytes express both isoforms. Membranes were therefore probed with a variety of antibodies that are specific for NKCC1. The results were similar to those with T4, and importantly, the Alpha Diagnostics antibody (developed to a peptide in the C-terminus) also revealed a doublet at 140–160 kDa (Fig. 2F). Antibodies specific for NKCC2 failed to identify proteins at molecular weights ranging from 120 to 160 kDa, the expected monomeric weight of this transporter (though occasionally there was staining at 240 kDa, data not shown). We also attempted to identify the proteins immunoprecipitated with T4 by MALDI-TOF mass spectroscopy following their digestion with trypsin. We were unable to identify the proteins in the prominent bands even at high yields. This is not an unusual problem with very hydrophobic membrane proteins especially if they have been treated with SDS [32,33] which is necessary when using T4. This technical problem is very disappointing as we had hoped to identify the components of the high molecular weight complexes by mass spectroscopy and thus establish whether the cotransporter dimerizes or binds to other proteins. Thus, although we cannot categorically rule out the possibility that some NKCC2 is expressed in these cells, we can conclude that the vast majority of bands detected by T4 contain NKCC1.

3.3. Relationship between threonine phosphorylation of the cotransporter and transport rate

Resting K^+ fluxes through the cotransporter are high, about 15 mmol l cell^{-1} h^{-1} when ferret erythrocytes are incubated under control conditions, and this is reduced to about 0.5 mmol l cell^{-1} h^{-1} in the presence of 10 μM bumetanide, indicating that over 95% of resting K^+ uptake is via the cotransporter [34]. Fig. 5 shows that fluxes are stimulated 2.6-fold by treating cells with calyculin A or with Na^+ arsenite, are reduced by about 40% when protein kinases are inhibited with PP1, staurosporine, genistein or by reducing cell Mg^{2+} content below 1 μM [20,21]. Figs. 1, 4 and 5 show that these changes in transport rate are paralleled by changes in phosphothreonine levels detected in T4-immunoprecipitates prepared from erythrocyte membranes.

It was necessary to establish a robust protocol to quantify cotransporter phosphorylation. We have seen that cotransporter molecules can be distributed amongst a variety of forms with different molecular weights and that heating samples with SDS and reducing agents do not cause these complexes to break up. It is thus important to include all relevant forms if cotransporter phosphorylation is to be measured accurately. We therefore analysed how normalised total phosphothreonine (all that found in a lane above 140 kDa normalised to the value found in the same region with control cells) correlated with the normalised amount of phosphothreonine found in the bands centred at 150 or 300 kDa under a variety of conditions (Fig. 3). The same relative changes in phosphorylation were found no matter which method of analysis was used. We therefore usually compared phosphorylation in the 150-kDa bands as these were the most prominent. Adding in phosphorylation from faint, ill-defined bands often simply increased the error on the measurements without affecting the ratios. It is also clear from these results that threonine phosphorylation of the cotransporter does not affect the propensity of the transporter to form or separate from the 300-kDa complexes.

Phosphothreonine was clearly detected in T4-immunoprecipitates prepared from all control membranes (e.g. Figs. 1, 4 and 6), consistent with the large resting fluxes found under control conditions. Figs. 1 and 5 show that calyculin increased cotransporter threonine phosphorylation 2.4-fold (±0.3, n=6 ferrets), consistent with PrP-1 being one of the cotransporter's regulatory phosphatases, and Na^+ arsenite increased it 3.1-fold (±0.7, n=5 ferrets). Kinase inhibition by drugs or Mg^{2+}-removal reduced it by about 40%, in line with the changes in transport rate (Figs. 4 and 5).

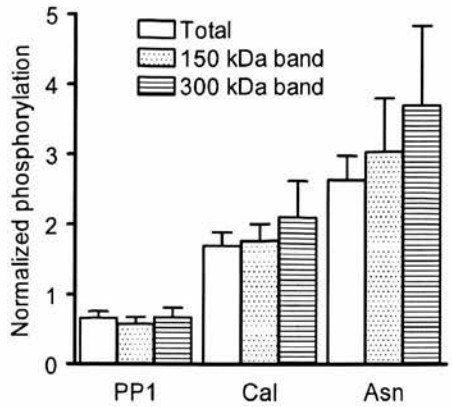

Fig. 3. Similar changes in threonine phosphorylation are seen in both the low and high molecular weight forms of the cotransporter. T4-immunoprecipitates were prepared from the membranes of erythrocytes that had been incubated at 38 °C in FBM containing 11 mM glucose and the following additions: 50 μM PP1 (PP1) for 30 min, 20 nM calyculin A (Cal) for 15 min, or 1 mM Na^+ arsenite (Asn) for 60 min. Control cells were incubated for 30 min in FBM with 11 mM glucose. Immunoprecipitates were run on 3–8% Tris-acetate gels, blotted and probed with an antibody to phosphothreonine. Signal intensity in the lanes at molecular weights above 140 kDa (Total), or in the bands centred on 150 kDa and 300 kDa were measured and expressed as a ratio of the level seen in the same regions on control lanes. Bars represent the mean ratios with their standard errors ($n=5$).

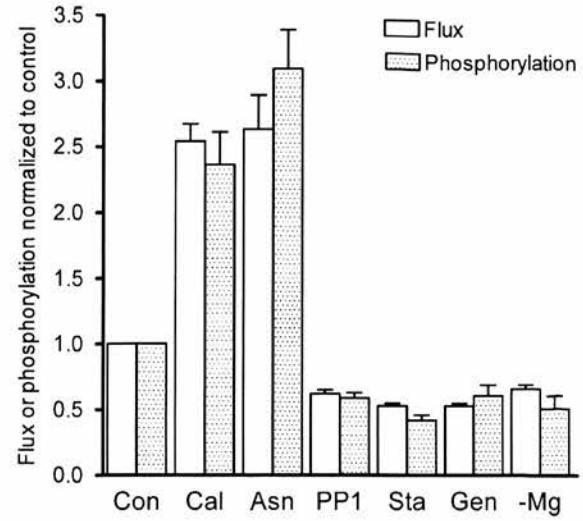

Fig. 5. Comparison of cotransporter threonine phosphorylation with fluxes. Threonine phosphorylation of the cotransporter was detected in T4-immunoprecipitates prepared from ferret erythrocytes that had been incubated at 38 °C in FBM containing 11 mM glucose and the following additions: none for 30 min (Con), 20–50 nM calyculin for 15 min (Cal), 1 mM Na^+ arsenite for 60 min (Asn), 50 μM PP1 for 30 min (PP1), 2 μM staurosporine for 20 min (Sta), 0.3 mM genistein for 20 min (Gen) or 2 mM EDTA and 10 μM A23187 for 15 min (−Mg). Cotransporter rate, measured as ^{86}Rb influx rate constant, was determined under the same conditions. Both phosphorylation and fluxes are normalized to the values seen in controls. Values are given as means with their standard errors.

Importantly, cotransporter threonine phosphorylation was not abolished by any of these procedures.

Stimulation of transport by calyculin A is prevented when cells are pre-treated with PP1, staurosporine, genistein or are Mg^{2+}-depleted [20]. The simplest explanation is that these treatments prevent phosphorylation of the cotransporter itself, though we could not rule out the possibility that they prevented the phosphorylation of a cofactor that is required for full activation of the transporter by protein–protein interactions. Experiments using T4-immunoprecipitates indicate these treatments inhibit transport by preventing phosphorylation of the transporter itself. Non-specific inhibition of kinases by Mg^{2+}-depletion completely prevented any rise in phosphorylation or stimulation of transport when calyculin was added (Fig. 6).

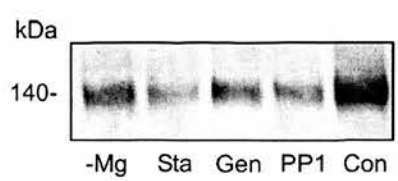

Fig. 4. Kinase inhibition reduces but does not abolish threonine phosphorylation of the cotransporter. T4-immunoprecipitates were prepared from the membranes of ferret erythrocytes that had been incubated at 38 °C in FBM containing 11 mM glucose and the following additions: none (Con), 50 μM PP1 for 30 min (PP1), 0.3 mM genistein for 20 min (Gen), 2 μM staurosporine for 20 min (Sta) or with 2 mM EDTA and 10 μM A23187 for 15 min (−Mg). Immunoprecipitates were run on 3–8% Tris-acetate gels, blotted and probed with an antibody to phosphothreonine.

Inhibition of Src kinases with PP1 also greatly reduced the stimulation of transport and the increase in phosphorylation, though did not completely prevent them (Fig. 6). In both cases, changes in transport parallel changes in phosphorylation.

3.4. Inhibition of transport and phosphorylation by PP1 or Mg^{2+}-removal after stimulation by calyculin

We have previously shown [20], and confirm here (Fig. 6) that Mg^{2+}-removal, or addition of PP1, after cells have been treated with calyculin partially inhibits transport over a 30-min period. Fig. 6 also shows that this reduction in transport is accompanied by a large reduction in threonine phosphorylation. Given the concentrations of calyculin used, this inhibition of transport and phosphorylation was surprising. The simplest explanation is that residual PrP-1 activity is sufficient to dephosphorylate the transporter when kinases are inhibited. If this were true both transport and phosphorylation should eventually fall back to the control level, at a rate that is a function of calyculin concentration, the higher the concentration, the less residual PrP-1 activity and the slower the rate. Fig. 7 shows that cotransport falls back to control at the same rate when PP1 or Mg^{2+}-removal is used to inhibit kinases (Fig. 7A). It also shows (Fig. 7B) that the rate of fall decreases with increasing calyculin concentration. Kinetic experiments on threonine phosphorylation are much harder to carry out,

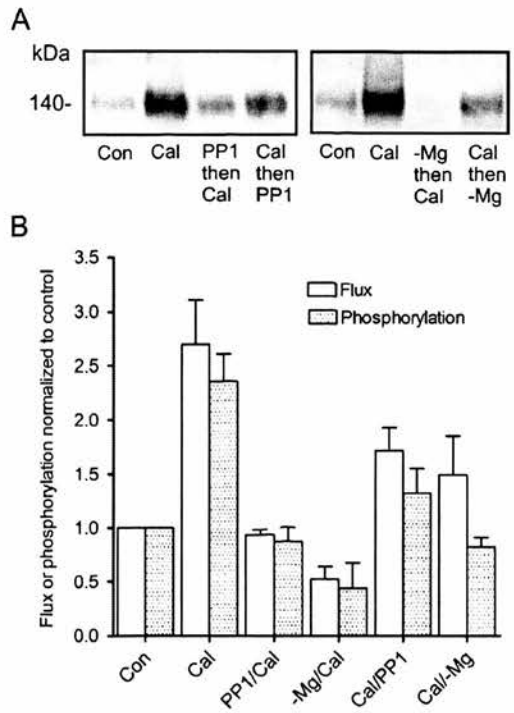

Fig. 6. PP1 or Mg^{2+}-depletion prevents and reverses cotransporter phosphorylation and fluxes stimulated by calyculin. A: T4-immunoprecipitates were prepared from the membranes of ferret erythrocytes that had been incubated at 38 °C in FBM containing 11 mM glucose and the following additions: none (Con), 50 nM calyculin for 15 min (Cal), 50 μM PP1 for 30 min followed by 50 nM calyculin for 15 min (PP1 then Cal), 50 nM calyculin for 15 min followed by 50 μM PP1 for 30 min (Cal then PP1), 2 mM EDTA with 10 μM A23187 for 15 min followed by 50 nM calyculin for 15 min (−Mg then Cal), 50 nM calyculin for 15 min followed by 2 mM EDTA with 10 μM A23187 (Cal then −Mg). Immunoprecipitates were run on 3–8% Tris-acetate gels, blotted and probed with an antibody to phosphothreonine. B: ^{86}Rb uptake was determined under the same conditions. Both phosphorylation and fluxes are normalized to the values seen in controls. Values are given as means with their standard errors.

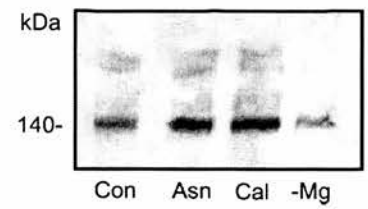

Fig. 8. Microcystin pulls down the cotransporter. Microcystin-Sepharose was used to precipitate proteins from the membranes of ferret erythrocytes that had been incubated at 38 °C in FBM containing 11 mM glucose and the following additions: none (Con), 1 mM Na^+ arsenite for 60 min (Asn), 50 nM calyculin A for 15 min (Cal), or with 2 mM EDTA and 10 μM A23187 for 15 min (−Mg). Eluates were run on 3–8% Tris-acetate gels, blotted and probed with T4.

however, phosphorylation had fallen below control levels in all samples taken 30 min after Mg^{2+} is removed (Fig. 6) and in one third of samples treated with PP1. In the other two thirds, it was about 50% above control, but very much lower that in the presence of calyculin alone.

3.5. Microcystin pull-down is more efficient with phosphorylated cotransporter

In view of the finding that PrP-1 may be one of the cotransporter's regulatory phosphatases we examined whether PrP-1 binds strongly to the cotransporter in ferret erythrocytes, as it does in other species [16]. If this were so, it should be possible to pull down the cotransporter with microcystin, a molecule that binds tightly to PrP-1. This was found to be the case (Fig. 8). Microcystin conjugated to Sepharose pulled down the cotransporter in both its low and high molecular weight forms. Interestingly, the amount of cotransporter pulled down in these assays closely parallels the phosphorylation state of the cotransporter. Thus, pretreatment of cells with calyculin or arsenite increased the

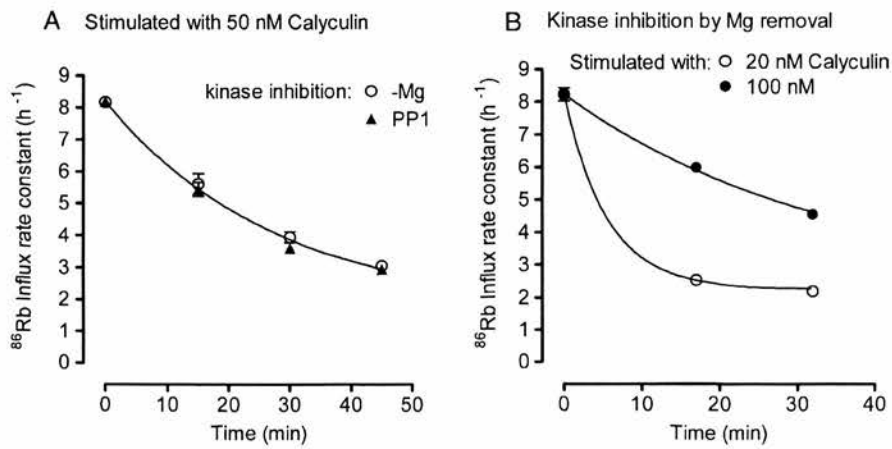

Fig. 7. Cotransport rate returns to normal when kinases are inhibited after calyculin treatment. Cells were incubated at 38 °C in FBM containing 11 mM glucose and the indicated calyculin concentration for 10 min. At this point, either 50 μM PP1 (PP1) or 10 μM A23187 with 2 mM EDTA (−Mg) were added. Samples of the suspension were transferred to separate tubes to which ^{86}Rb was added to measure fluxes over 4 min. Influx rate constants were determined and plotted at the mid point of the flux period timed from the addition of PP1 or A23187. Rate constants are shown with standard deviations if these are larger than point size. Lines are best fits to data, assuming that rate constants fall exponentially with time to the control level. A: comparison of the effects of PP1 or Mg^{2+}-removal on fluxes stimulated with 50 nM calyculin. B: comparison of the effects of Mg^{2+}-removal on fluxes stimulated with 20 or 100 nM calyculin.

amount of cotransporter (1.61±0.1 (n=2) and 2.66±0.84 (n=5) fold, respectively), whereas treatment of cells with PP1, Mg^{2+}-depletion, or genistein all reduced the amount of cotransporter pulled down (to 0.69±0.12 control, n=5).

4. Discussion

We describe a simple assay to measure threonine phosphorylation of the Na–K–2Cl cotransporter in ferret erythrocytes that has permitted us to address a number of ongoing questions about cotransport regulation. The assay is based on the immunoprecipitation of the cotransporter with T4 followed by measurement of threonine phosphorylation with an antibody. Although we cannot entirely rule out the possibility that some NKCC2 is expressed in ferret erythrocytes (though this would be highly unusual), we show that the material detected by T4 in these cells is consistent with it being, or containing, NKCC1. In order to make appropriate measurements of phosphorylation, it was necessary to understand the forms the cotransporter can adopt when isolated from cell membranes.

Ferret erythrocyte Na–K–2Cl cotransporter runs on SDS gels as a prominent broad band at 140–160 kDa. Often an additional broad band is seen at 300–320 kDa together with some sharp bands at intermediate weights. Some very high molecular weight complexes are occasionally seen (Fig. 2). Perhaps, up to half of the cotransporter molecules in the membrane are in high molecular weight complexes as indicated by the cross-linking study with gluteraldehyde (Fig. 2C), and these can survive and also form during sample preparation. The most likely explanation for the 300–320 kDa band is the formation of a dimer, as previously proposed on the basis of cross-linking studies in rat parotid glands [35], though binding to different proteins to form a 300 kDa complex cannot be excluded. All members of the cation-chloride-cotransporter (CCC) family (Na–K–2Cl, K–Cl, Na–Cl cotransporters, and CIP, a regulatory protein), are able to form complexes with themselves and with other members of the family, and the formation of these complexes can affect transport [36–40]. The cotransporter has also been shown to interact with unrelated proteins, for instance the anion-exchanger [41]. It would also appear that NKCC1 is one of the major threonine phosphorylated proteins (>100 kDa) in ferret erythrocyte membranes (Fig. 1).

Figs. 5 and 6 show there is a strong correlation between transport rate and cotransporter threonine phosphorylation in ferret erythrocytes. Calyculin and arsenite, compounds that maximally stimulate cotransport (2.6-fold, means not significantly different, P=0.72), also cause a large increase in threonine phosphorylation, 2.4-fold in the case of calyculin and 3.1-fold for arsenite. Although phosphorylation was almost always higher when cells from a particular ferret were treated with arsenite, this difference was not significant (P=0.09). On the other hand, inhibition of protein kinases with PP1, staurosporine, genistein or by removing intracellular Mg^{2+} reduced both transport and threonine phosphorylation to about 60% control. The correlation between transport and phosphorylation over this wide range of conditions, which includes the minimum and maximum rates of transport in these cells, is striking. However, we must be cautious if attempting to infer phosphorylation levels from transport rates. As discussed, phosphorylation may be higher than predicted when arsenite is used to stimulate transport, but most importantly, we have been unable to detect a significant rise in threonine phosphorylation when transport is maximally stimulated by deoxygenation [42]. We have yet to find a situation where the cotransporter is phosphorylated more than in resting cells without transport being stimulated in ferret erythrocytes.

Our results show that the cotransporter is partially threonine phosphorylated in ferret erythrocytes under resting conditions, and this may account for the high fluxes observed under these conditions. Importantly, we show that the transporter remains partially phosphorylated when cells are treated with kinase inhibitors or when their Mg^{2+} content is drastically reduced. This contradicts the hypothesis that some cotransporter molecules are active when not phosphorylated. It seems more likely that kinase inhibition leaves some cotransporter molecules phosphorylated and active. This may be because the sites are not accessible to phosphatases or that the appropriate phosphatases are not active. Experiments are under way to explore these possibilities.

The data in Fig. 7 show that PrP-1 is highly active in ferret erythrocytes and support the view that it dephosphorylates key threonine residues involved in regulating transport rate. They make less plausible the supposition that calyculin also activates a kinase that phosphorylates the transporter, an alternative explanation for the inhibition of transport by kinase inhibitors in the presence of calyculin. Thus, in the absence of kinase activity, residual PrP-1 can still rapidly dephosphorylate the transporter leading to a reduction in transport rate. With 20 nM calyculin, residual PrP-1 dephosphorylates the cotransporter so transport falls to within 5% of control in 16 min, with 100 nM calyculin this takes 100 min. They are also consistent with an EC_{50} for calyculin of 1–3 nM, values estimated from the amount of calyculin required to activate transport ([20] and Flatman, unpublished). The tight binding of PrP-1 to the cotransporter was exploited to precipitate the cotransporter from membranes with microcystin-sepharose. Unexpectedly, we found that the amount of cotransporter pulled down with microcystin parallels the level of cotransporter threonine phosphorylation. It appears that phosphorylated cotransporter binds PrP-1 more avidly.

In conclusion, the method described for assessing total threonine phosphorylation of the cotransporter provides important information on transporter function that complements that obtained using phospho-cotransporter specific

antibodies which examine the phosphorylation of one out of several threonine residues that can affect transport [31]. The combination of these methods would be particularly useful where it is not possible to make an antibody to a particular phosphorylated residue, as is the case with the cotransporter.

Acknowledgements

We thank staff at the Edinburgh Protein Interactions Centre (EPIC) for help with mass spectroscopy, and the Wellcome Trust and Medical Research Council (UK) for support.

References

[1] J.M. Russell, Sodium-potassium-chloride cotransport, Physiol. Rev. 80 (2000) 211–276.
[2] M. Haas, B. Forbush, III, The Na–K–Cl cotransporter of secretory epithelia, Annu. Rev. Physiol. 62 (2000) 515–534.
[3] P.W. Flatman, Regulation of Na–K–2Cl cotransport by phosphorylation and protein–protein interactions, Biochim. Biophys. Acta 1566 (2002) 140–151.
[4] C. Lytle, Na^+–K^+–$2Cl^-$ Cotransport, in: I. Bernhardt, J.C. Ellory (Eds.), Red Cell Membrane Transport in Health and Disease, Springer, Berlin, 2003, pp. 173–195.
[5] P.W. Flatman, Regulation of Na–K–2Cl cotransport in red cells, Adv. Exp. Med. Biol. 559 (2004) 77–88.
[6] H.C. Palfrey, E.B. Pewitt, The ATP and Mg^{2+} dependence of Na^+–K^+–$2Cl^-$ cotransport reflects a requirement for protein phosphorylation: studies using calyculin A, Pflügers Arch. 425 (1993) 321–328.
[7] J.D. Klein, W.C. O'Neill, Volume-sensitive myosin phosphorylation in vascular endothelial cells: correlation with Na–K–2Cl cotransport, Am. J. Physiol. 269 (1995) C1524–C1531.
[8] M.C. Muzyamba, A.R. Cossins, J.S. Gibson, Regulation of Na^+–K^+–$2Cl^-$ cotransport in turkey red cells: the role of oxygen tension and protein phosphorylation, J. Physiol. (Lond.) 517 (1999) 421–429.
[9] C. Lytle, B. Forbush III, The Na–K–Cl cotransport protein of shark rectal gland. II. Regulation by direct phosphorylation, J. Biol. Chem. 267 (1992) 25438–25443.
[10] M.E. O'Donnell, A. Martinez, D. Sun, Endothelial Na–K–Cl cotransport regulation by tonicity and hormones: phosphorylation of cotransport protein, Am. J. Physiol. 269 (1995) C1513–C1523.
[11] M. Haas, D. McBrayer, C. Lytle, $[Cl^-]_i$-dependent phosphorylation of the Na–K–Cl cotransport protein of dog tracheal epithelial cells, J. Biol. Chem. 270 (1995) 28955–28961.
[12] A. Tanimura, K. Kurihara, S.J. Reshkin, R.J. Turner, Involvement of direct phosphorylation in the regulation of the rat parotid Na^+–K^+–$2Cl^-$ cotransporter, J. Biol. Chem. 270 (1995) 25252–25258.
[13] C. Lytle, B. Forbush III, Regulatory phosphorylation of the secretory Na–K–Cl cotransporter: modulation by cytoplasmic Cl, Am. J. Physiol. 270 (1996) C437–C448.
[14] R.B. Darman, B. Forbush, A regulatory locus of phosphorylation in the N terminus of the Na–K–Cl cotransporter, NKCC1, J. Biol. Chem. 277 (2002) 37542–37550.
[15] C. Lytle, Activation of the avian erythrocyte Na–K–Cl cotransport protein by cell shrinkage, cAMP, fluoride, and calyculin-A involves phosphorylation at common sites, J. Biol. Chem. 272 (1997) 15069–15077.
[16] R.B. Darman, A. Flemmer, B. Forbush, Modulation of ion transport by direct targeting of protein phosphatase type I to the Na–K–Cl cotransporter, J. Biol. Chem. 276 (2001) 34359–34362.
[17] C. Lytle, A volume-sensitive protein kinase regulates the Na–K–2Cl cotransporter in duck red blood cells, Am. J. Physiol. 274 (1998) C1002–C1010.
[18] J.D. Klein, S.T. Lamitina, W.C. O'Neill, JNK is a volume-sensitive kinase that phosphorylates the Na–K–2Cl cotransporter in vitro, Am. J. Physiol. 277 (1999) C425–C431.
[19] K. Piechotta, N. Garbarini, R. England, E. Delpire, Characterization of the interaction of the stress kinase SPAK with the Na^+–K^+–Cl^- cotransporter in the nervous system, J. Biol. Chem. 278 (2003) 52848–52856.
[20] P.W. Flatman, J. Creanor, Regulation of Na^+–K^+–$2Cl^-$ cotransport by protein phosphorylation in ferret erythrocytes, J. Physiol. (Lond.) 517 (1999) 699–708.
[21] P.W. Flatman, J. Creanor, Stimulation of Na^+–K^+–$2Cl^-$ cotransport by arsenite in ferret erythrocytes, J. Physiol. (Lond.) 519 (1999) 143–152.
[22] T. Krarup, L.D. Jakobsen, B.S. Jensen, E.K. Hoffmann, Na^+–K^+–$2Cl^-$ cotransport in Ehrlich cells: regulation by protein phosphatases and kinases, Am. J. Physiol. 275 (1998) C239–C250.
[23] I. Matskevich, D.K. Apps, P.W. Flatman, The Na–K–2Cl cotransporter forms high molecular weight complexes in ferret red blood cell membranes, Pflugers Arch.-Eur. J. Physiol. 443 (2002) S186.
[24] I. Matskevich, P.W. Flatman, Regulation of Na^+–K^+–$2Cl^-$ cotransport by threonine phosphorylation in ferret red cells, J. Physiol. (Lond.) 547.P (2003) C20.
[25] J.A. Gordon, Use of vanadate as protein-phosphotyrosine phosphatase inhibitor, Methods Enzymol. 201 (1991) 477–482.
[26] P.W. Flatman, The effects of magnesium on potassium transport in ferret red cells, J. Physiol. (Lond.) 397 (1988) 471–487.
[27] C. Lytle, J.-C. Xu, D. Biemesderfer, B. Forbush III, Distribution and diversity of Na–K–Cl cotransport proteins: a study with monoclonal antibodies, Am. J. Physiol. 269 (1995) C1496–C1505.
[28] J.C. Parker, Gluteralderhyde fixation of sodium transport in dog red blood cells, J. Gen. Physiol. 84 (1984) 789–803.
[29] J.-C. Xu, C. Lytle, T.T. Zhu, J.A. Payne, E. Benz Jr., B. Forbush III, Molecular cloning and functional expression of the bumetanide-sensitive Na–K–Cl cotransporter, Proc. Natl Acad. Sci. U. S. A. 91 (1994) 2201–2205.
[30] G. Jiang, J.D. Klein, W.C. O'Neill, Growth factors stimulate the Na–K–2Cl cotransporter NKCC1 through a novel Cl-dependent mechanism, Am. J. Physiol., Cell Physiol. 281 (2001) C1948–C1953.
[31] A.W. Flemmer, I. Giménez, B.F.X. Dowd, R.B. Darman, B. Forbush, Activation of the Na–K–Cl cotransporter NKCC1 detected with a phospho-specific antibody, J. Biol. Chem. 277 (2002) 37551–37558.
[32] H. Zischka, C.J. Gloeckner, C. Klein, S. Willmann, M.S. Lange, M. Ueffing, Improved mass spectrometric identification of gel-separated hydrophobic membrane proteins after sodium dodecyl sulfate removal by ion-pair extraction, Proteomics 4 (2004) 3776–3782.
[33] C. Klein, C. Garcia-Rizo, B. Bisle, B. Scheffer, H. Zischka, F. Pfeiffer, F. Siedler, D. Oesterhelt, The membrane proteome of *Halobacterium salinarum*, Proteomics 5 (2005) 180–197.
[34] P.W. Flatman, Sodium and potassium transport in ferret red cells, J. Physiol. (Lond.) 341 (1983) 545–557.
[35] M.L. Moore-Hoon, R.J. Turner, The structural unit of the secretory Na^+–K^+–$2Cl^-$ cotransporter (NKCC1) is a homodimer, Biochemistry 39 (2000) 3718–3724.
[36] L. Caron, F. Rousseau, E. Gagnon, P. Isenring, Cloning and functional characterization of a cation-Cl^- cotransporter-interacting protein, J. Biol. Chem. 275 (2000) 32027–32036.
[37] D.B. Mount, A. Baekgaard, A.E. Hall, C. Plata, J. Xu, D.R. Beier, G. Gamba, S.C. Hebert, Isoforms of the Na–K–2Cl cotransporter in murine TAL I. Molecular characterization and intrarenal localization, Am. J. Physiol. 276 (1999) F347–F358.
[38] C. Plata, D.B. Mount, V. Rubio, S.C. Hebert, G. Gamba, Isoforms of

the Na–K–2Cl cotransporter in murine TAL. II. Functional characterization and activation by cAMP, Am. J. Physiol. 276 (1999) F359–F366.

[39] S. Casula, B.E. Shmukler, S. Wilhelm, A.K. Stuart-Tilley, W. Su, M.N. Chernova, C. Brugnara, S.L. Alper, A dominant negative mutant of the KCC1 K–Cl cotransporter, J. Biol. Chem. 276 (2001) 41870–41878.

[40] C. Plata, P. Meade, A. Hall, R.C. Welch, N. Vázquez, S.C. Hebert, G. Gamba, Alternatively spliced isoform of apical Na^+–K^+–Cl^- cotransporter gene encodes a furosemide-sensitive Na^+–Cl^- cotransporter, Am. J. Physiol., Renal Physiol. 280 (2001) F574–F582.

[41] H. Guizouarn, N. Gabillat, F. Borgese, Evidence for up-regulation of the endogenous Na–K–2Cl co-transporter by molecular interactions with the anion exchanger tAE1 expressed in *Xenopus* oocyte, J. Biol. Chem. 279 (2004) 11513–11520.

[42] P.W. Flatman, Activation of ferret erythrocyte Na^+–K^+–$2Cl^-$ cotransport by deoxygenation, J. Physiol. (Lond.) 563 (2005) 421–431.